The Development of a Model for

Percutaneous Absorption

A Thesis Submitted for the Degree of

Doctor of Philosophy

in

The University of Oxford

by

Jonathan Hadgraft

University College

August 1976

Physical Chemistry Laborator

Oxford.

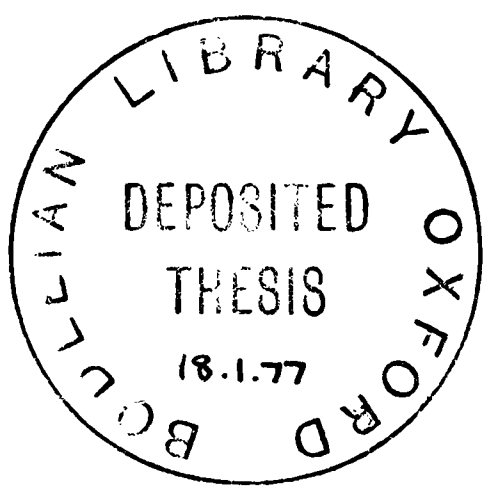

ABSTRACT

A novel piece of diffusion apparatus has been developed which utilizes the well characterized hydrodynamics of a rotating disc. Liquid liquid interfaces may be established on either side of the filter in the cell and the rate at which species are transferred from one phase to the other can be measured. The rates are measured at different rotation speeds and by extrapolation to infinite rotation speed the rate constant for the transfer reaction at the interface can be obtained. These interfacial rate constants have been measured for some carboxylic acids and esters of nicotinic acid. The nicotinates have been chosen since their rate of skin penetration is easily measured.

In order to study the rate of percutaneous absorption, solutions of the nicotinates are applied to the forearm. The material diffuses through the skin and when it reaches the blood vessels a red response develops. By timing the onset of the red response an estimate of the rate of penetration is obtained. Three nicotinates have been chosen to cover a wide range of partition coefficients.

A mathematical model has been developed to describe the transport of drugs across skin. This has been combined with the *in vivo* measurements and the values of the interfacial barriers

determined *in vitro* to provide information about the mechanism of percutaneous absorption. The results indicate that for simple molecules the main route of penetration is via the intercellular channels.

The model has been further applied to results from the literature and has been shown to be satisfactory in explaining the data.

ACKNOWLEDGEMENTS

I am indebted to Dr W.J. Albery for his help and guidance during the course of this work.

I should like to thank:

my father for stimulating discussions and arguments concerning the content of this thesis;

my wife for encouragement and proof reading;

Mrs Elizabeth Price for deciphering and typing the script.

I would also like to express my gratitude to the S.R.C. and Glaxo for financial support.

CONTENTS

CHAPTER I		Introduction	1
	I	Skin Structure	2
		a. The Epidermis	4
		b. The Dermis	6
		c. The Appendages	6
	II	Pathways of Percutaneous Absorption	8
	III	Factors affecting Percutaneous Absorption	11
		i. Drug-skin Interactions	11
		a. Skin hydration	11
		b. Circulatory effects	12
		c. Chemical effects	12
		ii. Vehicle-skin Interactions	13
		a. Hydration effects	14
		b. Temperature effects	14
		c. Solvent effects	15
		iii. Drug-Vehicle Interactions	15
		iv. Drug-Vehicle-Skin Interactions	18
	IV	Measurement of Percutaneous Absorption	19
		a. *In Vitro* Studies	20
		b. *In Vivo* Studies	22
	V	Physicochemical Properties and Percutaneous Absorption	24
		a. Interfacial Barriers	25
	VI	Mathematical Models and correlation of *in vivo* and *in vitro* work	26

CHAPTER II The Measurement of Diffusion Coefficients, Viscosities and Partition Coefficients 29

I Chemicals and Solutions for Experimental Work 29

II Diffusion Coefficients 31

a. Apparatus 31

b. Theory for non steady state and steady state fluxes in the Stokes Cell 37

c. Experimental measurement of the pore area and the cell constant 41

d. Measurement of diffusion coefficients 44

e. Estimation of diffusion coefficients by various techniques 51

III The Measurement of Partition Coefficients 55

CHAPTER III The Rotating Diffusion Cell 59

I Introduction 59

II The Hydrodynamics to a Rotating Disc 61

III Rotating Cell Design 67

a. The Baffle 67

b. Filters 72

c. Millipore MF filter treatment 76

d. Duralon filter treatment 77

i. Blocking using HFP 78

ii. Blocking the pores with cyano acrylate adhesive 79

iii. Blocking the pores with a masking perspex bevel 80

IV Theory 81

i. Single phase experiments 83

ii. Two phase experiments 83

a. Outer 84

b. Inner 84

c. Sandwich 84

V Characterization of the Hydrodynamics 85

1. Single Phase Experiments 85

a. Procedure 86

i. Filter assembly 86

ii. Filling 86

iii. Following the diffusion 87

iv. Rotation speed variation 87

b. Results 88

c. The effect of mass flow on experimental results 90

d. Minimising the effects of mass flow 92

i. The scallop effect 93

ii. The vortexing problem 95

2. Two Phase Experiments 98

i. Interface instability 99

a. Carbon tetrachloride 99

b. Isopropyl myristate 100

ii. Experimental Procedure 100

iii. Results 102

3. Discussion 116

CHAPTER IV The Diffusion of Nicotinic Acid Esters and Betamethasone 17 Valerate Across IPM 118

1 Methyl Nicotinate 119

i. Experimental procedure for pH stat detection of methyl nicotinate 119

ii. Theory for pH stat detection 121

iii. Flux determination by a sampling technique 125

iv. Theory 126

v. Experimental 127

vi. Results 129

a. System I (Methyl Nicotinate in water) 129

b. System Ia (using a bevelled filter holder) 131

c. System II (methyl nicotinate in 60% w/v glycerol) 133

d. System III (methyl nicotinate in 80% w/v glycerol) 136

e. System IV (n-butyl nicotinate in water) 138

f. System V (n-hexyl nicotinate in water) 141

vii. Discussion 141

2 Betamethasone.17.Valerate 144

i. Radioactive Sampling Technique 145

ii. Results 146

iii. Type I Experiments. Aqueous-organic-aqueous 147

iv. Type II Experiments. Organic-aqueous-organic 150

CHAPTER V *In Vivo* Experiments 154

I Theory 155

II Experimental 171

a. Non pulse experiments 171

b. Pulse experiments 172

III Results 174

A. Non pulsed experiments 174

i. Analysis of non pulse results 176

a. The diffusional path length 181

b. Diffusion Coefficient of methyl nicotinate in the skin 182

ii. Analysis of results, showing the effect of concentration depletion 183

B. Pulse Experiments 189

i. Analysis of pulse results 191

a. Empirical relationships between t_1 and t_2 194

b. Values of κ and $K/\sqrt{p}$ 194

c. Calculation of values of u' 199

d. Calculation of the triggering concentration n'_E 206

CHAPTER VI General Discussion 208

Two Phase Studies 209

Interfacial Transfer Terms 211

An *in vitro* model for percutaneous absorption 215

In vivo Results 217

The Final Model 223

Application of the Model 225

General Model for Structure-Activity Relationships 228

Future Developments 230

In Vitro Model 231

APPENDIX 1 233

APPENDIX 2 234

APPENDIX 3 236

APPENDIX 4 240

REFERENCES 241

CHAPTER 1

INTRODUCTION

The study of the penetration of substances through the skin is becoming increasingly important as the public comes into contact with highly potent materials manufactured by the chemical industry. There are many areas of potential danger which receive publicity from time to time; most frequent are reports of poisoning by the careless and indiscriminate use of agrochemicals[1]. Although the physiological actions of the majority of these substances are well known and documented, the basic physical chemistry of skin absorption has been less fully described. The purpose of this work is to provide fundamental data for the processes involved in percutaneous absorption and consequently to identify the kinetic values which control the penetration rate.

The first significant investigation was performed at the turn of the century[2] when it was found that certain drugs applied to the intact human skin could, after a period of time, be detected in the urine. Almost coeval with this the possible toxic effects from the systemic absorption of chemicals were first recognized[3]. Since then much work has been performed into the cataloguing of chemicals which have toxic effects when they are absorbed through the skin. The interest of governments in chemical warfare has led to the identification and indexing of a large number of compounds of actual and potential toxicity. These include sarin and other nerve gases which act by blocking choline esterase in the nerve synapses. The rates at which these compounds are absorbed

percutaneously are well documented[4,5].

One reason for the increase of the available data in this field was the general application of radiochemical methods for following the small concentration changes involved. The application of these elegant techniques to the skin can only yield semi-quantitative information since the skin is one of the most unhomogeneous organs of the body[6]. In order to study the more fundamental processes a skin-like material of well controlled chemical constitution and physical integrity is required. A number of researchers have attempted this approach with limited success[7,8,9], these are discussed more fully in a later section. It is probable that the use of model systems to investigate percutaneous pharmacology will expand significantly in the future, particularly in the study of percutaneous toxicology[10].

I. Skin Structure

The human skin consists of three distinct layers, the epidermis, the dermis, and the subcutaneous fat, some of the more important properties of which are summarized in Figure (1).

Figure 1. Some of the more important properties of the epidermis, dermis and subcutaneous fat.

	Thickness	Water Content	Cellular Activity	Vasculature	Function
EPIDERMIS	0.2 mm	10-25 %	Actively dividing cells	none	Barrier
DERMIS	3-5 mm	<70 %	Mostly non-cellular	blood vessels lymphatics sweat glands	Connective tissue support
SUBCUTANEOUS FAT	Variable	Low	closely packed cells	blood vessels	Thermal insulation

a. The Epidermis

Of the three regions summarized above the epidermis provides the major barrier to drug penetration. Thus it is the nature of the epidermal layer which is most important in any study on percutaneous absorption.

A cross-section through the epidermis is shown in Figure (2), the average thickness being approximately 0.2 mm. The epidermis is a highly organized kinetic system formed mainly from a single basal layer of actively dividing cells. The life history of the epidermal cells has been well studied[11]. As the cells multiply in the stratum germinativum they migrate towards the skin surface and keratinization occurs. During the migration away from the basal layer the cells become remote from the blood supply, their source of nourishment, and they die. Keratinization occurs which is accompanied by a change in cellular dimensions. The cell flattens to become a roughly hexagonal plate which has the approximate dimensions 25 x 0.5 μm.

These flattened cells constitute the stratum corneum. The outer layers of the stratum corneum are less densely packed than those adjacent to the underlying granular layer (the stratum granulosum). The average distance between the cells of the stratum corneum is 0.04 μm and the total quantity of lipid which can be extracted from this cellular region is sufficient to fill the intercellular channels[12,13]. Most of this fat is comprised of glyceride, sterol, wax and hydrocarbon[14].

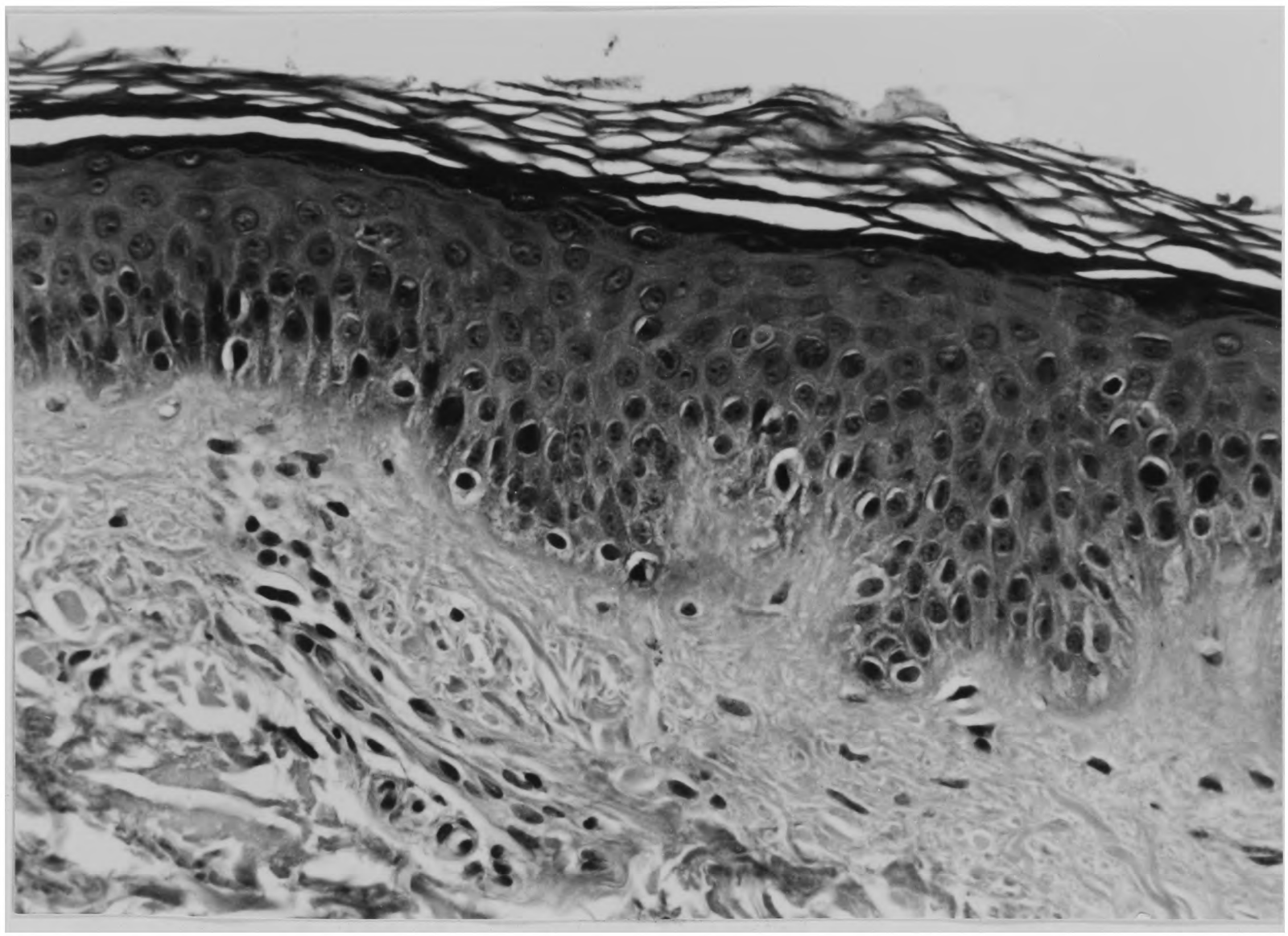

Figure (2). Photomicrograph of a transverse section through the epidermis.

For the purposes of creating a model of the stratum corneum it may be regarded that the intercellular channels occupy 0.4% of the total cross-sectional area of the skin surface (calculated as 0.04 μm channels on an hexagonal 25 μm lattice)[15].

b. The Dermis

The dermis is 20-30 times thicker than the epidermis and is largely aqueous. Its surface at the dermal-epidermal junction is formed into cone-like ridges (papillae) which serve to connect the two layers. Contained in the papillae are capillary loops and nerve endings which are connected to a complex network of blood vessels and nerves lying deeper in the skin. Also penetrating the dermis are the cutaneous appendages i.e. the pilosebaceous follicles and sweat glands.

c. The Appendages

The epidermis is not a homogeneous barrier but is interspersed with hair follicles, sebaceous glands and sweat glands. These appendages are not regularly spaced over the body surface as shown in Table (1)[16]. The sebaceous glands open into the hair follicles and produce sebum which then distributes itself over the skin surface. The thickness of the layer has been estimated as being between 0.4 and 4 μm[17,18,19,20]. Approximate compositions

Table (1). The distribution and the relative areas occupied by the appendages[16].

Appendage	Density/cm^2	Total Fraction Area
Hair Follicles	40 (Abdomen)	1.5×10^{-3}
	100 (Forearm)	3.8×10^{-3}
Sweat Ducts	210 (Abdomen)	8.1×10^{-3} (Surface opening)
	220 (Forearm)	8.4×10^{-3} (Surface Opening)
Stratum Corneum	-	1.00

of sebum have been estimated and the average proportions are:- free fatty acids 28%; triglycerides 40%; higher fatty alcohols 10%; cholesterol 5%; hydrocarbons 17%[21,22].

II. Pathways of Percutaneous Absorption

The penetration of drugs through the skin is slow due to the very effective barrier nature of the epidermis. There are several possible routes by which a drug may pass from the skin surface to the blood vessels and lymphatics in the dermis; these are outlined in Figure (3). The possible routes have been investigated and the data obtained shows that there are many arguments for and against each route[23].

Tregear[15] reviews the literature and states that penetration probably occurs via the cornefied system rather than via an appendageal route. However it is not possible to tell whether the route through the cornefied system is through or around the keratinized cells.

Autoradiographic investigation and staining techniques produce conflicting results for the role of the appendages. The percutaneous absorption of corticosteroids and probably other large molecules may occur by both routes[24]. Surface active agents such as sodium lauryl sulphate are possibly transported across the skin mainly via a follicular route.

In this work a mathematical model has been developed to elucidate whether a small diffusant, e.g. a nicotinate ester, diffuses via an inter- or an intracellular route. It has been stated that penetration is probably via the intercellular channels since no higher alcohols than methanol can pass between the fibrils of a keratin matrix[25]; however higher alcohols do penetrate

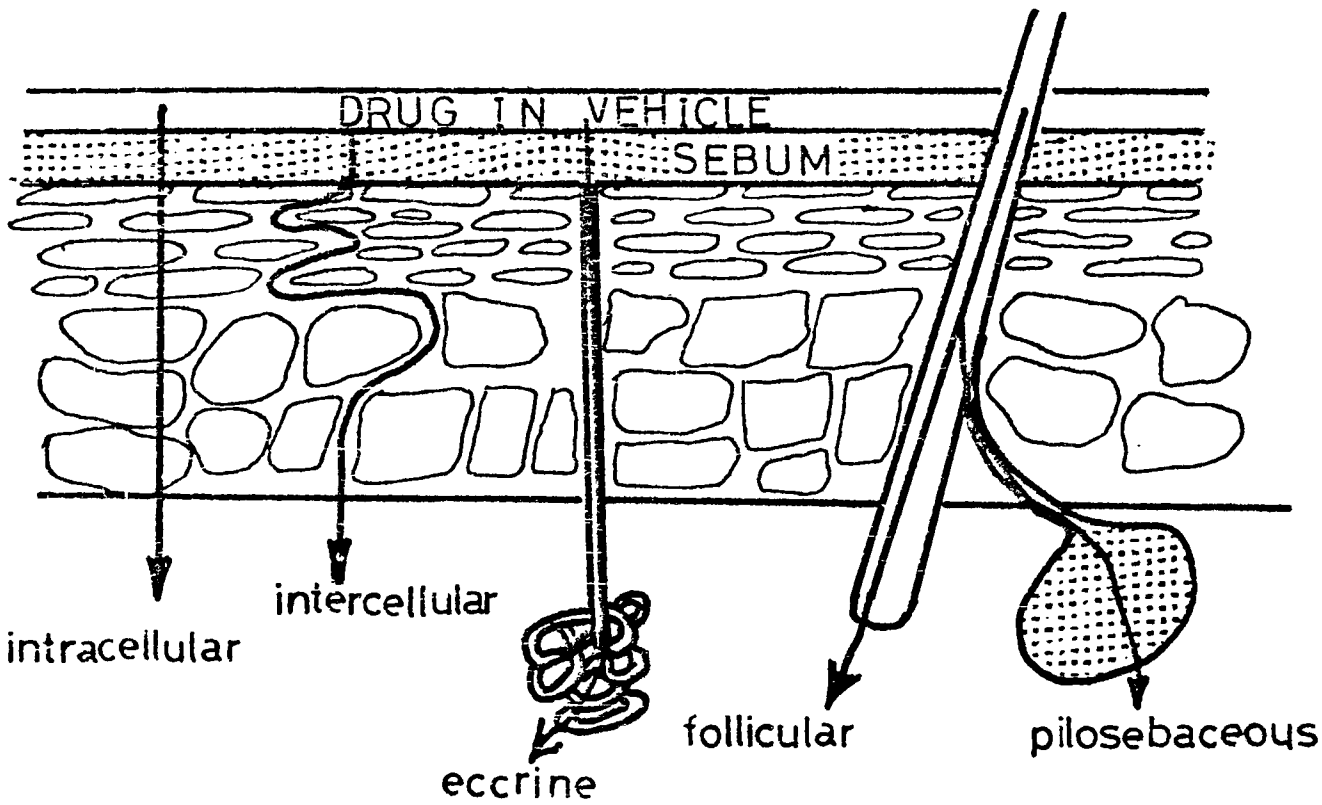

Figure (3). A diagrammatic representation of the skin and the possible routes of penetration.

the skin and at a greater rate than methanol[26].

Whichever route is predominant there remains the problem as to whether or not there is a specific barrier zone located in the epidermis. When the epidermis is progressively stripped with Scotch tape, there is initially little effect on the rate of transepidermal water loss. After twelve to fifteen strippings there is a sudden increase[27]. This led to the supposition that there was a distinct barrier zone which was situated in the lower layers of the cornefied epithelium. However the penetration rate of salicylic acid[28] and some corticosteroids[29] gradually increases with stripping and there is a gradual recovery of impermeability after this type of experiment[30].

For a model system it is probably best to regard the fully formed keratin layer as the main barrier to penetration. The lower layers which are more densely packed than those adjacent to the surface offer the greatest resistance to penetration for some molecules. This is seen to an extreme in the case of water, where it is the lower layers which are entirely responsible for preventing excessive moisture loss.

Another added complication is the possible existence of interfacial transfer rates[31] which could prove to be quite significant in the overall transport process. Interfacial transfer occurs at any phase boundary. The first possible phase boundary encountered by the drug is the vehicle/sebum interface. However it has been shown[18,32,33] that the sebum layer provides no

contribution to the rate determining process. The remaining interfaces are the vehicle/intercellular fluid and the intercellular fluid/dermal fluid boundaries. These transfer processes have been included in the mathematical model and their significance discussed.

III. Factors Affecting Percutaneous Absorption

The principal factors affecting the rate of epidermal penetration are the properties of a) the drug, b) the vehicle, and c) the skin. There are thus four possible interactions between these components[23]:

i Drug x skin

ii Vehicle x skin

iii Drug x vehicle

iv Drug x vehicle x skin.

Some of the more important sub-divisions of these four main interactions will be outlined below.

i. Drug-skin Interactions

a) Skin hydration

The degree of hydration of the skin has a marked effect on the rate of percutaneous absorption[33,34]. The reason for the increase in penetration rate with increasing hydration is not fully understood. It may in part be due to the extra water

increasing the area of the stratum corneum[35]. Some drugs that are applied to the skin may have a pharmacologic action which directly affects the degree of hydration. Pregnenolone acetate has been shown to act in this manner[36]. The hydrating action of many of the drugs used in dermatological preparations has not been investigated in any detail.

b) Circulatory effects

Large increases in penetration rates with increased blood flow are unlikely[15]. It is possible, however, that vasoconstriction does slow down absorption rates. This should manifest itself for the corticosteroids where the blanching effect is thought to be due to constriction of the peripheral blood vessels. When applied to the skin, the steroids may slow their own rate of clearance. A similar effect is observed for the local anaesthetic cocaine which also possesses vasoconstrictor activity[37]. The synthetic local anaesthetics (e.g. lignocaine) do not possess this property and clinically a vasoconstrictor is often added to the preparation. This reduces the rate of clearance and hence prolongs the time of anaesthetic action.

c) Chemical effects

There are two main types of chemical effect; metabolism of the drug as it diffuses across the epidermis and the binding of the drug by the skin. The study of the metabolism of topical

agents has been mainly confined to the corticosteroids[38]. Some work has been conducted on the metabolism and diffusion of the metabolites of the organophosphorus insecticides[39,40].

Due to the complex nature of the skin it is not surprising that many drugs may bind quite strongly to it. Certain unsaturated and 2-hydroxy carboxylic acids are selectively absorbed by powdered human callous tissue[41] and many topical antibacterial agents are thought to bind to keratin[42]. It is possible that the 'reservoir' of corticosteroid[43,44,45] which builds up in the stratum corneum is due to chemical binding with the components of the skin[46].

ii. Vehicle-skin Interactions

Whenever a vehicle (cream, lotion or ointment) is placed on the skin surface, the normal conditions in which the skin exists are altered. The physical properties of the epidermis may change and rates of drug absorption will be accelerated or impeded. The changes induced are most likely due to:

a) Effect of hydration;

b) Effect on skin temperature;

c) Solvent influence on the barrier structure.

a) Hydration Effects

As discussed above, the state of hydration has a considerable effect on percutaneous absorption. A topically applied vehicle may either increase or decrease the hydration of the upper layers of the epidermis[47,48]. In the case of a glycol, water is absorbed from the skin and penetration rates are decreased. Water insoluble substances and water in oil emulsions increase the degree of hydration by preventing or retarding water loss.

The ambient relative humidity will also affect the degree of hydration. When it is low the amount of water diffusing into the stratum corneum from below is insufficient to replace the water lost from the skin surface.

b) Temperature Effects

An occlusive dressing on the skin will tend to increase the surface temperature. However the effect will probably be negligible compared to that of hydration. Investigations show that the penetration rate of methyl nicotinate decreases with a drop in the ambient temperature[49]. It has been calculated[15] that in very cold weather penetration rates could drop by an order of magnitude. For this reason *in vivo* work reported in this thesis has been conducted at relatively constant temperatures.

c) Solvent Effects

There are a number of vehicles which increase the permeability of skin. Some actually damage the cellular structure whereas others act by an ill understood mechanism. The latter group are the more interesting and of these dimethyl sulphoxide (DMSO) is the best known.

DMSO has been shown to enhance the penetration of many different types of drugs both *in vivo* and *in vitro*[50,51]. It is possible that this solvent acts by replacing the water in the epidermis to give a continuous phase through which diffusion occurs more rapidly. Other possible effects are reversible structural changes such as swelling of the stratum corneum. The exact mechanism of action has not yet been resolved.

iii. Drug-Vehicle Interactions

It is possible that the rate of drug release from the applied vehicle is slower than the uptake by the skin. This has been shown for the release of methyl nicotinate from polyethylene glycol 300[49]. Figure (4) shows that when a solution of methyl nicotinate in polyethylene glycol 300 is applied to the skin an erythematous zone is produced which increases and decays as normal. When the erythema has disappeared it may be further induced by agitation of the residual liquid. This indicates that the rate of uptake of the methyl nicotinate is much more rapid than its release rate.

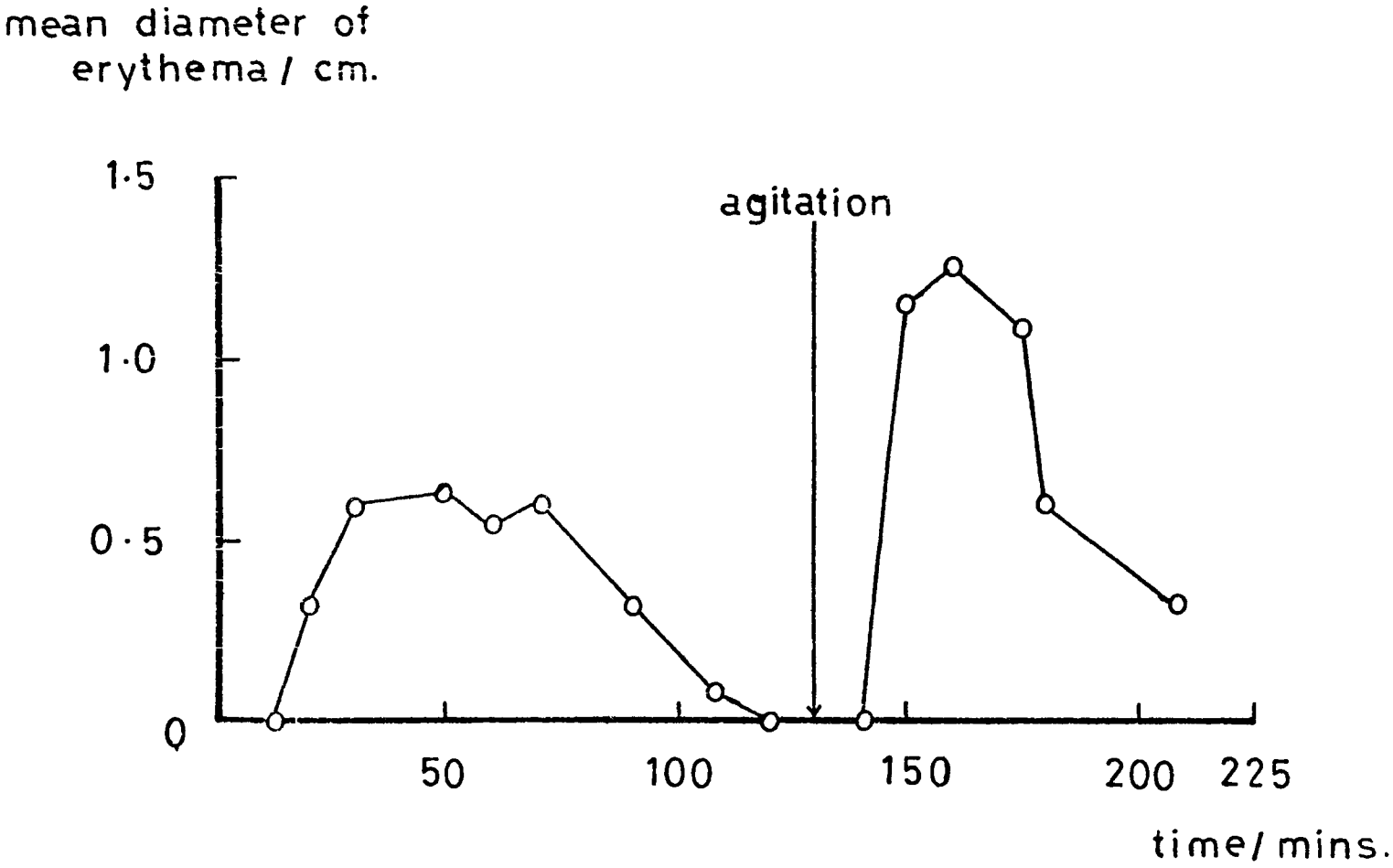

Figure (4). The variation in erythema diameter with time for a solution of methyl nicotinate in polyethylene glycol 300 (from reference 49).

For these conditions the skin may be treated as a perfect sink and the mathematics for this type of diffusion problem has been solved[52]. It is known as semi-infinite linear diffusion and the equation describing the release rate is:-

$$N \sim 2\left(\frac{Dt}{\pi}\right)^{\frac{1}{2}} c_{\infty} \qquad (1.1)$$

where

N is the number of mols diffused in time t per unit area;

D is the diffusion coefficient;

c_{∞} is the bulk concentration.

Thus it follows that the amount of drug released will be in proportion to the square root of time. Such behaviour is found , e.g. the data quoted by Poulsen et al.[53] may be treated using equation 1.1 to give a good linear correlation between N and $t^{\frac{1}{2}}$.

More frequently suspensions or emulsions are used in topical preparations and a similar mathematical formula applies to the release rates[54],

$$N \sim (2c_d Dc_s t)^{\frac{1}{2}} \qquad (1.2)$$

where

c_d is the drug concentration;

c_s is the solubility of the drug in the external phase of the ointment.

This equation has been verified experimentally by several investigators[55].

The diffusion equation will be further complicated if there is a significant interfacial transfer barrier for the transport of the drug between the two phases of the ointment[56]. Also equation 1.2 takes no account of the particle size of the suspended drug. Release rates have been shown to be dependent on particle size for some corticosteroids[57].

iv. Drug-Vehicle-Skin Interactions

The major factors which are involved in this threefold interaction may be seen in equation 1.3. This equation describes the steady state flux, j, of drug crossing a model skin of thickness h:-

$$j = \frac{D_s K_p c_v}{h} \qquad (1.3)$$

where,

D_s is the diffusion coefficient of the drug in the skin;

K_p is the skin-vehicle partition coefficient;

c_v is the drug concentration in the vehicle.

The diffusion coefficient is involved in a threefold interaction since the ratio of the diffusion coefficients of the drug in the skin and in the vehicle determines whether or not depletion of the drug in the vehicle is significant. The mathematical relationship showing this effect will be discussed in a later section.

Not included in the simple expression above is the possibility of an interfacial transfer barrier between the vehicle and the skin. It has been shown that the interfacial barrier for the transfer of p-methyl benzyl chloride across an isopropyl myristate-water interface is fairly large ~ 56 kJ mol^{-1} [31]. Consequently it may be that interfacial barriers for drugs crossing the vehicle/skin interface are large enough to be rate determining. Further analysis of this effect is given later.

IV. Measurement of Percutaneous Absorption

Percutaneous absorption has been studied from many different angles and it is often very difficult to inter-relate the results. The types of approaches that have been used are[23]:

a) skin physiology and biochemistry;

b) general pathways of percutaneous absorption;

c) comparative efficacy of vehicles;

d) drug mechanism of action;

e) dermatology and therapeutics;

f) sensitisation and toxicity;

g) general interfacial transport.

Studies on a large number of very varied compounds have been conducted both *in vivo* and *in vitro*, a comprehensive list has been compiled by Katz and Poulsen.[23]

a. *In vitro* studies

The most useful *in vitro* studies have been conducted using excised human skin[58]. Cell designs for holding the skin specimen have changed over the past years but the most popular is that described by Coldman[59]. The transfer rates can either be measured by the disappearance of the substrate from the donor compartment or by its appearance in the receptor compartment. The technique is of especial use in measuring the transepidermal rates of transfer of highly toxic substances prior to *in vivo* tests.

Experiments using model membranes have been conducted and they provide information about the more fundamental processes involved. Water evaporation from the skin has been simulated in a chamber divided by a Millipore filter which has been saturated with cotton seed oil and cholesteryl palmitate (66:33)[7]. Similarly filter papers have been saturated with isopropyl myristate and used to study the *in vitro* release of betamethasone derivatives from various ointment bases[8]. The results obtained using this model correlated favourably with *in vivo* vasoconstrictor results.

Materials also used in simulation work include cuprophane and silicone rubber sheeting. The release of hydrocortisone from aqueous creams through a cuprophane sheet has been shown to be affected by the addition of tetrahydrofurfuryl alcohol[60]. The results correlated with *in vivo* studies. More recently the use of silicone rubber sheeting has gained popularity. Reported

experimental work has tended to be in the simulation of gastro-intestinal absorption[61], although some work is being conducted using it in the simulation of skin absorption. The major advantage of using this type of membrane is that its area and thickness are well defined[62,63]. Rigorous diffusion studies have been conducted using silicone rubber sheeting with various substrates in order to gain a better understanding of some of the more fundamental physicochemical concepts involved[64,65,66].

Another piece of apparatus which has been developed is the Schulman type *in vitro* cell[67]. The cell contains two aqueous phases separated by a third liquid lipid phase simulating the biomembrane. The disadvantage of this type of design is that the interfacial areas are not well defined. However some useful semi-quantitative results have been obtained, e.g. the effect of lipid polarity on the transport of salicylic acid[68].

A simplification often employed is to study the drug release rates from ointments directly into isopropyl myristate. The isopropyl myristate is of sufficient volume to act as a sink. The release of fluocinonide from various ointment bases has been studied and the results compare favourably with *in vivo* vasoconstrictor assays[69]. Isopropyl myristate has been used as a receptor phase in several studies[8,53,70] and the results indicate that this solvent simulates the lipids present in the epidermis quite effectively.

"*In vitro* methods, as yet, have only a limited practical application, their results may point the way to further *in vivo* work. If their outcome supports animal and human experimental findings, they may have a useful place in the screening of new products without the difficulties which *in vivo* methods usually involve."[71]

b. *In vivo* Studies

Many methods have been devised for studying the *in vivo* transepidermal rates of drug absorption[23]. The most important of these are summarized in Table (2).

The method chosen to study *in vivo* penetration rates of nicotinate esters in this thesis utilizes their ability to cause dilation of the peripheral blood vessels[73]. The vasodilation is caused by a local action of the ester on the vessel walls and nerve mechanisms[74]. The dilation of the blood vessels after application of the ester is clearly seen as a red area known as erythema.

The nicotinates have been used several times to assess the effect of vehicle formulation on percutaneous absorption[49,75,76] and also to study some of the more basic physical chemistry involved[77,78]. They are convenient to use and reproducible results are obtained when the time of onset of erythema is taken as a measure of the rate of penetration.

The major problem involved in *in vivo* work is the assessment

Table (2) Methods of Measuring Percutaneous Absorption[72]

In Vivo	
1) Histological studies	e.g. keratolysis from salicylic acid
2) Use of Tracers	a) Dyes b) Fluorescent Compounds c) Radioactive tracers i direct surface counting ii autoradiography iii isotope measurement in body
3) Measurement of physiological response	e.g. vasodilation, vaso-constriction, anaesthesia
4) Analysis of tissues	e.g. skin, blood, urine
5) Loss of penetrating substance from surface	
6) Animal models	

of the degree of percutaneous absorption. Allowance must be made for the inherent biological variation[79,80]. Such variations may be due to:

a) skin age and site;

b) skin temperature and peripheral circulation;

c) the state of the skin (normal, abraded, diseased);

d) the relative humidity and degree of skin hydration.

By using one subject for the *in vivo* work in this thesis, the biological variations are minimized and quantitative analysis of the data is simplified.

V. Physicochemical Properties and Percutaneous Absorption

Recent advances in percutaneous absorption have been made by investigating the basic physical chemistry of the process. Until the fundamental concepts are understood it will not be possible to deliver drugs reliably via a transepidermal route[81]. The advantages of transdermal therapeutic systems have been outlined[82] and it seems probable that some drugs will be administered more efficiently by this technique. It is thus important to study the basic transport properties of model systems and to try and apply the results to the *in vivo* situation.

a. Interfacial Barriers

In two phase systems of biological and industrial interest, it has usually been assumed that a rapid concentration equilibrium is established at the interface. However it has been shown that in some systems there is very slow interfacial transfer[31].

The theoretical implications of slow interfacial transfer for diffusion in emulsions have been considered[83,84,85,86]. However in this field very few instances of interfacial barriers have been found. One case reported is the transport of diethylphthalate across a hexadecane-water interface[87]. The transport rate is markedly reduced when gelatin is adsorbed on the interfacial surface. The effect was studied by observing the release rate of the diethylphthalate from an emulsion, the particle size distribution of which was measured using a Coulter counter.

A new technique has been developed for studying transport in two phase systems[31]. The interface is located on the surface of a glass sinter in a modified Stokes diffusion cell. The interfacial area is then accurately defined by the surface pore area of the glass sinter which can be measured[88] and will not alter appreciably during fairly vigorous stirring. Applying this technique an appreciable interfacial barrier for the transport of p-methyl benzyl chloride across two organic-aqueous interfaces was demonstrated. For the transport of methyl nicotinate across a water-isopropyl myristate interface only limits could be found for the value of the interfacial term.

In order to study the generality of interfacial transfer barriers and to see how they may be applied to a biological system a new piece of apparatus was constructed[90,91]. The filter in the new apparatus must be thin so that the diffusion across it is not rate determining. For such a thin filter the diffusion layers on either side of it will be of a similar thickness and could contribute significantly to the overall rate process[89].

Using conventional stirring techniques the diffusion layer thicknesses are neither well defined nor calculable. However stirring in the new apparatus relies on rotation of the filter and transport to and from the filter is controlled by rotating disc hydrodynamics. The thicknesses of the diffusion layers are thus controlled by varying the rotation speed[92]. In this apparatus all the transport parameters are accurately defined and thus the various contributions to the transport process may be separated. Consequently interfacial transfer processes may be studied over an extended range.

VI. Mathematical Models and Correlation of *in vivo* and *in vitro* work

Many researchers have attempted to produce theoretical equations describing the steady state penetration rates involved in skin absorption. The problems involved (e.g. the ill understood pathway of penetration) create many difficulties and the equations produced are only more or less successful. If the route of penetration is

included in the model, the mathematics becomes very complex and for some treatments it is more convenient to regard the epidermis as a homogeneous biophase[93].

Although the mechanisms of penetration have not been fully identified, Higuchi has shown that there are some relationships which are valid irrespective of the complexity of the chosen model. The penetration rates from vehicles in which a drug is present at the same thermodynamic activity should be equal[54]. This has been verified experimentally for a simple system. The rates of penetration of methyl nicotinate from simple aqueous-glycerol mixtures are the same for solutions of equal chemical potential[78].

Various theories for describing transepidermal transfer rates in terms of simple physicochemical properties have been described[15]. Each theory is partially successful but it is impossible to elucidate which component of the tissue is the diffusional barrier.

Vasoconstrictor assays for numerous corticosteroids have been combined with Higuchi's theories[54] and a simple formula for the rate of absorption deduced[94]. A correlation between the relative absorption of the steroids and the simple properties of solubility and partition coefficient has been shown.

The relationship between permeation rates and lipophilic nature has been studied by multiple regression analysis[95]. The results indicate that it may be possible to predict the relative degree of drug absorption through skin from the physicochemical

constants of a series of compounds and the absorption data of a few parent molecules. Although the results are promising, this type of analysis does not lead to an understanding of the basic transport properties involved.

Consequently theoretical predictions are possible relating the change in penetration rate to chemical structure. By slight modification of the side chains of certain molecules the partition coefficient may be altered considerably giving a marked increase or decrease in percutaneous activity. The rate of penetration of ethyl nicotinate is thus 37,000 times faster than nicotinic acid[96].

In this work a mathematical model has been developed to analyze the *in vivo* data on the esters of nicotinic acid. Using the model, the relative effects of the following properties may be predicted:

1) route of penetration;
2) interfacial barriers;
3) depletion of the drug in the vehicle.

By combining the *in vivo* results with the *in vitro* results from the rotating diffusion cell and analyzing them with the mathematical model, a better understanding of the fundamental transport processes involved in percutaneous absorption has been established.

CHAPTER II

THE MEASUREMENT OF DIFFUSION COEFFICIENTS, VISCOSITIES AND PARTITION COEFFICIENTS

I. Chemicals and Solutions for Experimental Work

All chemicals were of Analar Grade and were used without further purification except the following:-

^{3}H-Betamethasone-17-Valerate was supplied by Glaxo Research Laboratories. The chemical structure of betamethasone-17-valerate is

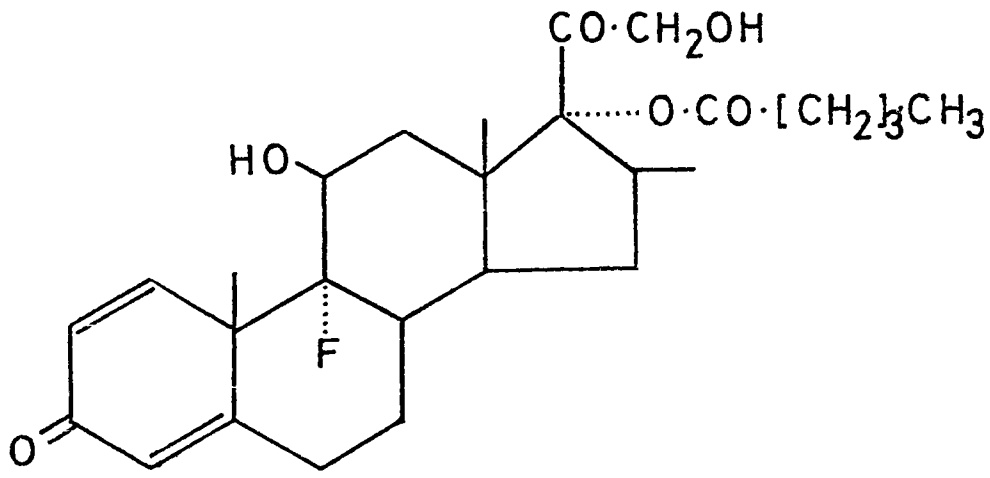

The tritium label is on the valerate side chain and the compound has a specific activity of 15 µCi/mg. The radiochemical purity was checked in conjunction with Glaxo using thin layer chromatography on a silica gel plate. The solvent system used was chloroform: ethyl acetate (2:1) and the spot was found to be monodisperse with an R_f value the same as a known pure sample of unlabelled betamethasone-17-valerate.

n-butyl nicotinate. This ester was not available commercially and was prepared from n-butanol and nicotinic acid[96,97]. 41g nicotinic acid, 83 cm^3 butan-1-ol and 40 cm^3 concentrated sulphuric acid were heated for 4 hours on a steam bath. The resulting solution was allowed to cool and then poured onto 200 g crushed ice. Sufficient ammonia was added to make the solution strongly alkaline. The mixture was then extracted with 4 x 25 cm^3 diethyl ether and dried overnight with anhydrous magnesium sulphate. The ether was distilled off and the remaining liquid distilled under reduced pressure. The required ester distilled over at 117°C and 10 mm pressure[98]. The resultant clear liquid had a refractive index of 1.495 which agrees with published values[96].

Ethanol. The ethyl alcohol used for ultra-violet spectrophotometry was Absolute Alcohol supplied by James Burroughs Ltd.

^{3}H-n-hexadecane. Supplied by The Radiochemical Centre, Amersham as a tritium standard. The standard contained 2.27 μCi per gram on 1st December 1973.

n-hexyl nicotinate. Supplied by Fluka A.G. Its refractive index agreed with quoted values and was not purified further[96].

Isopropyl Myristate. Supplied by Bush, Boake and Allen. Its refractive index agreed with quoted values[99] and it was not purified further. Its purity was within the limits specified by the British Pharmaceutical Codex[100].

Methyl Nicotinate was obtained puriss grade from Koch-Light and was purified by distillation at 87-89°C and 15 mm pressure. The white crystals produced had a melting point of 38°C and gave a monodisperse spot of the correct R_f value when subjected to thin layer chromatography (alumina stationary phase with benzene: methanol 9:1 solvent system)[101].

Repelcote is 2% dimethyldichlorosilane in carbon tetrachloride (Hopkin and Williams Ltd) and is used in the treatment of Millipore filters to render them water repellent.

Scintillation Fluid. Two commercial scintillation fluids were used. Both were manufactured by Koch Light. These are the general purpose fluids KL401 and KL402 used for aqueous and organic samples respectively.

Water. The water used throughout was demineralised water which was then doubly distilled from an all glass still.

II. Diffusion Coefficients

The integral diffusion coefficients required for the analysis of later experimental data were measured using a modified Stokes diffusion cell[88].

a) Apparatus

Modified Stokes Diffusion Cell

The modified Stokes Cell is shown in figures 5 and 6. It is divided into two distinct regions, the upper and the lower

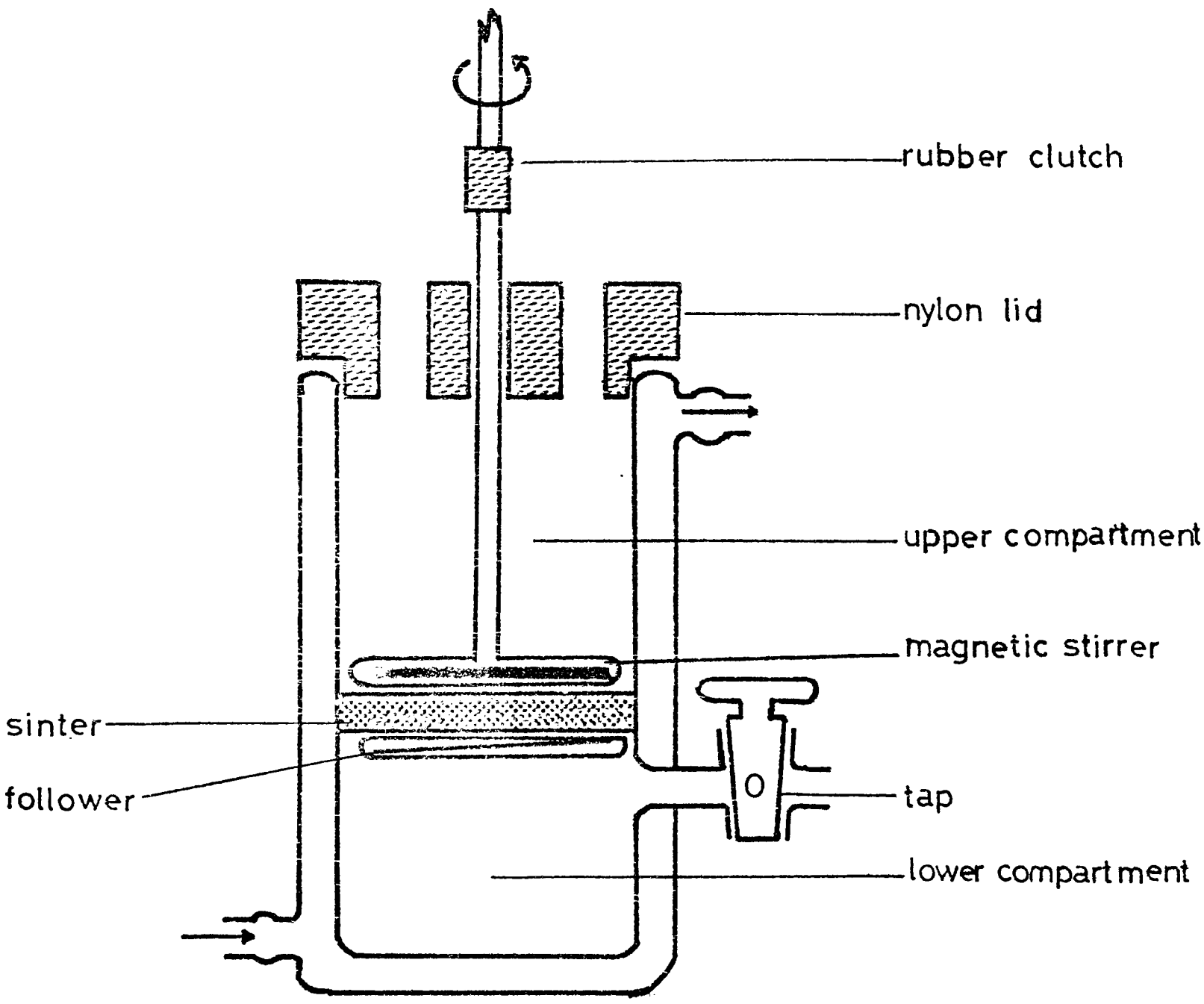

Figure (5). Diagram of the Modified Stokes Diffusion Cell.

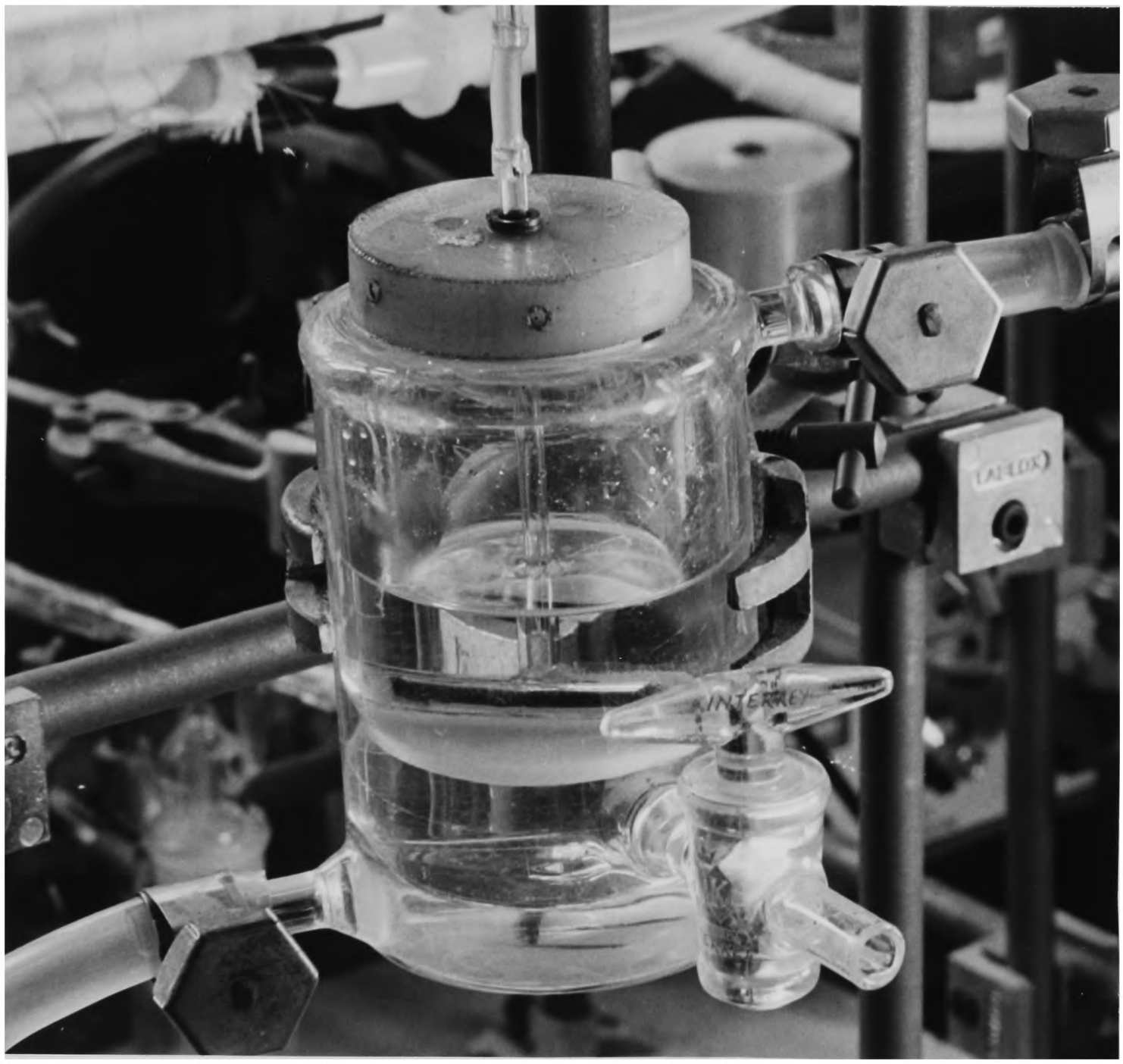

Figure (6). Photograph of the modified Stokes' Diffusion Cell.

compartments, the capacities of which are approximately 50 cm^3 and 29 cm^3 respectively. The two sections are separated by a homogeneous porous glass sinter, the pores of which have a diameter less than 2.5 μm. The top is closed with a nylon lid and cork sealing ring. Holes drilled into the lid support the glass and calomel electrodes, stirrer shaft, nitrogen supply tube and alkali delivery tube. The cell is surrounded by a thermostatting jacket through which water is circulated to maintain the cell contents at the desired temperature. The lower compartment is accessible via a glass inlet port which passes through the thermostatting jacket.

Stirring

The stirring of the two compartments is very important since it is necessary to prevent the formation of stagnant layers on either side of the glass sinter. If stagnant layers were present they would provide an additional diffusion process, the magnitude of which could not be calculated. It has been shown that for this apparatus the flux of material diffusing across the sinter is independent of the rotation speed of the stirrer in the region from 1.5 to 6 Hz[102]. At stirrer speeds less than 1.5 Hz the observed flux is decreased due to the presence of stagnant layers. For rotation speeds greater than 6 Hz the increased flux is probably caused by the stirring affecting the liquid contained inside the glass sinter.

The stirrer used for the system is shown in figures (5) and (6). The top compartment contains a glass encapsulated magnet attached via a thin glass rod and a rubber clutch to a pulley. Attached

to the magnet is a polythene skirt which sweeps the top surface of the sinter. The lower compartment is stirred by a floating glass tube which contains a length of iron wire and thus follows the magnetic stirrer above it.

Titration

The cell is characterised by the area (A) and length (ℓ) of the pores, the ratio of these being the cell constant (B). The values of these constants are most conveniently measured using a titration technique[88]. The pH stat used in this work consists of:

a) a Radiometer TTT2 titrator;

b) a Radiometer ABU11 autoburette;

c) a Radiometer SBR3 recorder.

The titrator unit is especially designed for automatic end point titrations and automatic pH stat work with curve recording. The drift of the meter is less than 0.002 pH unit per 24 hours which makes it especially reliable for monitoring diffusion experiments which last 2 or 3 days. An additional feature of the unit is that the titrant delivery rate is controlled and will be proportionally slowed down near the end point. This minimises the risk of overshooting the end-point. The accuracy of the end-point setting is ±0.1 pH unit.

The autoburette driven by the titrator delivers up to 2.5 cm^3 of titrant with an accuracy of ± 0.5%. It can deliver very small volumes (~ 0.002 cm^3). The accuracy and reproducibility along the length of the burette was checked by ejecting volumes of double distilled water from the apparatus into

preweighed dry glass vials. It is possible to continuously vary the flow rate from the burette in the range 0.5 to 5 cm^3 min^{-1}. This in conjunction with the proportional band control on the titrator provides a sensitive means for producing smooth pH stat curves.

The recorder is mechanically linked to the autoburette and has a scale expansion to give a full scale deflection (25 cm) corresponding to 1 cm^3 of titrant. The chart speed is variable from 1 second to 2 hours per centimetre which allows accurate determination of both slow and fast diffusion fluxes.

The alkali supply connected to the autoburette was stored in a glass flask fitted with an absorption tube filled with self-indicating "carbosorb" granules. Since barium hydroxide was used as the alkali in all the pH stat work, any carbon dioxide entering the system manifests itself by the production of a white precipitate of barium carbonate.

Nitrogen Supply

The fluxes of acid diffusing during an experiment are very small and consequently it is necessary to reduce the amount of carbon dioxide entering the system to a negligible level. Carbon dioxide effects are particularly noticeable when the solution is being statted to a high pH (~ 10). At this pH the flux of carbon dioxide entering the system can be comparable to the flux of diffusing acid.

To prevent excessive carbon dioxide from entering the system, nitrogen from a cylinder is blown through the liquid in the upper compartment of the cell. In order that evaporation caused by this flow is minimised, the gas is presaturated by passage through a wash bottle of distilled water. Any carbon dioxide in the gas supply is removed by a large tube of self indicating "carbosorb" granules. To ensure that no excess pressure builds up in the apparatus, the supply line includes a back pressure ediometer filled with mercury.

b) Theory for non steady state and steady state fluxes in the Stokes Cell.

The characterisation of the cell constant B and area A of the Stokes Cell involves the measurement of fluxes of acetic acid across the sinter[83]. Acetic acid has been chosen as the diffusant since its diffusion coefficient over a range of concentrations is well known[103].

The concentration profiles existing in the cell at different stages of an experiment are shown in figure 7. Initially the sinter is full of acid (profile t_o) at concentration C^o_{HA}. As the sinter is depleted, the rate of depletion is described by the solution of Fick's second law of diffusion for the case of semi-infinite linear diffusion[52]. The solution given below in equation 2.1 is valid in the region from t_o to t_1 (figure 7). In this time period about 20% of the acetic acid contained in the sinter has diffused into the upper compartment.

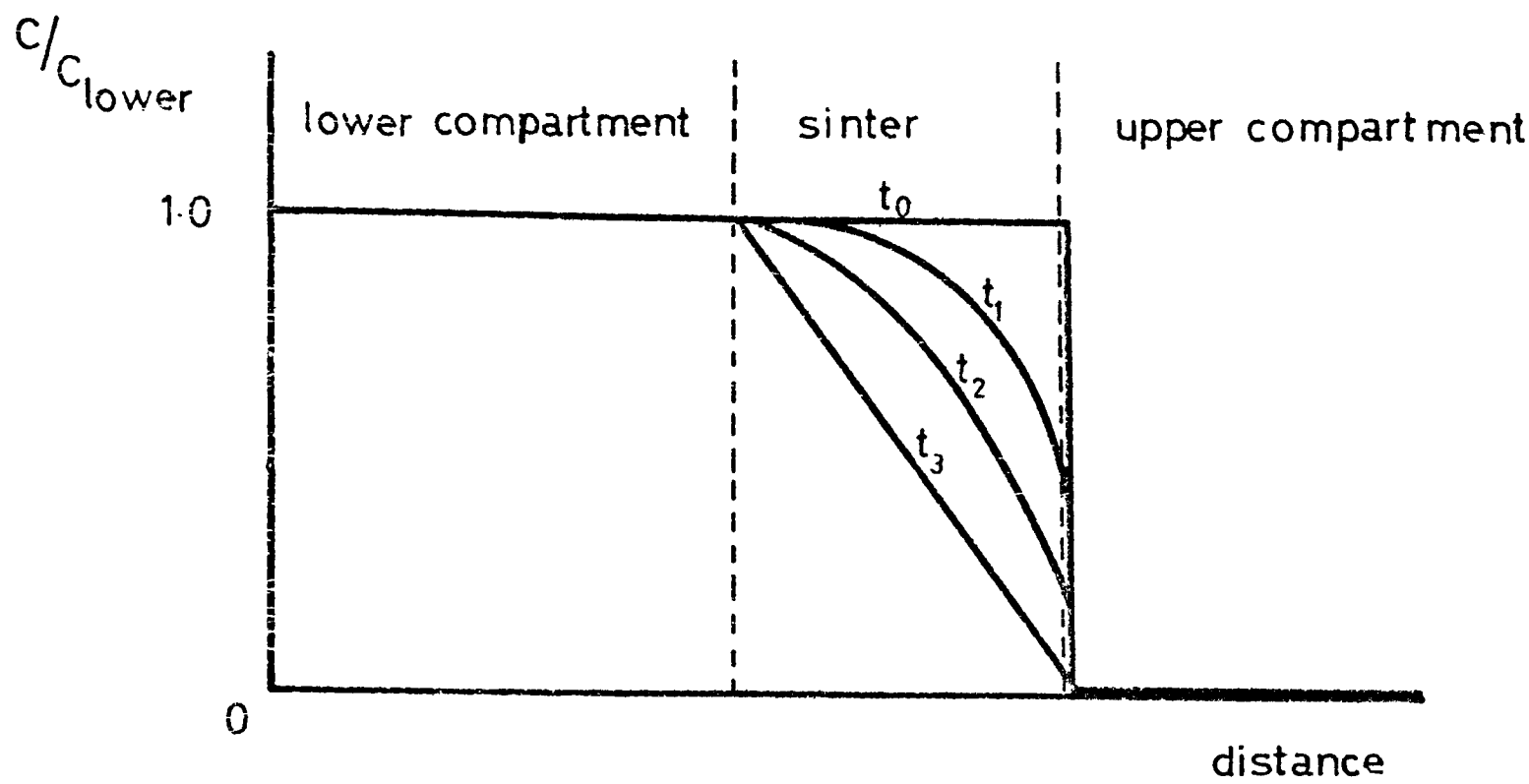

$$t_0 = 0 < t_1 < t_2 < t_3$$

Figure (7). Concentration profiles at different time intervals for a diffusion experiment in the Stokes Cell.

When t, the time from the start of diffusion is small, the number of mols of acid, N, which have diffused at time t is given by:

$$N = 2 \times 10^3 \, A \, c^o_{HA} \left(\frac{Dt}{\pi}\right)^{0.5} \qquad (2.1)$$

where:

A/mm^2	is the pore area;
$D/m^2 s^{-1}$	is the diffusion coefficient;
c^o_{HA}/M	is the bulk acid concentration;
t/s	is the time.

It is interesting to note that this equation is analogous to that predicting the release rates of drugs from ointments[69].

By using the solution for semi-infinite linear diffusion, where the rate of diffusion depends on the pore area, it is possible to obtain an accurate determination of A[88].

From time t_1 to t_2 (figure 7) there is deviation from the $\sqrt{t}$ dependence shown above and at t_3 a linear concentration gradient is produced. The flux (J $mol.s^{-1}$) of acid diffusing down this linear concentration gradient is given by Fick's 1st Law of Diffusion:

$$J = BD_{HA}c^o_{HA} \qquad (B = A/\ell) \qquad (2.2)$$

where:

B/mm	is the cell constant;
ℓ/mm	is the length of the pores in the sinter;
$D_{HA}/m^2.s^{-1}$	is the diffusion coefficient of acetic acid.

For acetic acid there will be slight dissociation and the flux may be more accurately described:

$$J = B(D_{HA}c_{HA} + D_{H^+}c_{H^+}) \qquad (2.3)$$

In this expression the liquid junction potential effect on H^+ has been ignored, its significance in this type of experiment being negligible[88]

The dissociation constant, K_a, for acetic acid varies with ionic strength and can be found at the appropriate ionic strength[104]. The following relationships are then used in the calculation of the cell constant

$$c_{H^+} = \frac{K_a c_{HA}}{c_{Ac^-}} \qquad (2.4)$$

$$c_{HA} = c^{o}_{HA} - c_{H^+} \qquad (2.5)$$

The value of D_{H^+} can be calculated at infinite dilution from the Nernst relationship:

$$D_{H^+} = \left(\frac{RT}{F^2}\right) \lambda^{\infty}_{H^+} \qquad (2.6)$$

Substitution of a value of $\lambda^{\infty}_{H^+}$ of 349.82 Ω^{-1} $m^2.mol^{-1}$ [105] into the above expression gives

$$D_{H^+} = 9.31 \text{ m}^2 \text{ Gs}^{-1} \qquad (2.7)$$

The diffusion coefficient of acetic acid varies with concentration and may be calculated by an empirical relationship[103]

$$D_{HA}/m^2Gs^{-1} = 1.201 - 0.55\ c_{HA} \qquad (2.8)$$

In calculating D_{HA}, c_{HA} is taken as the concentration of acid half way through the sinter ($c^o_{HA}/2$).

c) Experimental Measurement of the pore area and cell constant.

The filling procedure and setting up for experimentation is well documented[106,107]. Acetic acid is drawn through the sinter by applying a vacuum to the tap in the lower compartment. The most important aspect of the filling operation is to ensure that no air bubbles become trapped in the sinter; this would produce false values for the cell constant.

The pore area is measured by following the non steady state flux. Figure 8 shows the way in which the flux of acetic acid varies with time; the graph has been continued into the steady state region. From equation 2.1 it is seen that the pore area may be obtained by plotting the number of mols of acid diffused in time t against $\sqrt{t}$ (fig. 9). The gradient of the graph is then:-

$$2\pi^{-\frac{1}{2}}A.D^{\frac{1}{2}}.c_{HA} \quad .$$

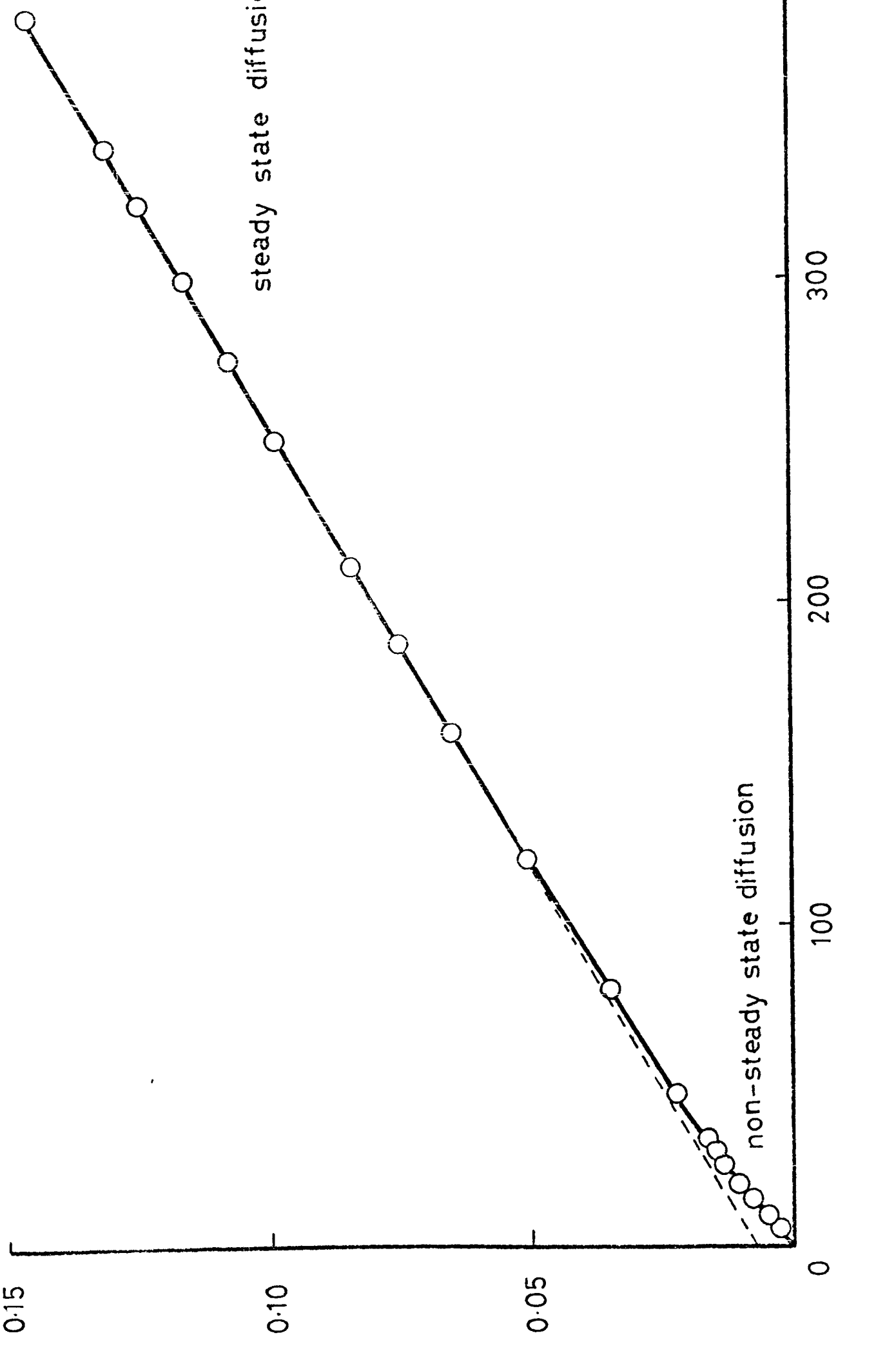

Figure (8). The number of mols (N) of acetic acid diffused as a function of time (t) showing the gradual build up to steady state conditions in the Stokes Cell.

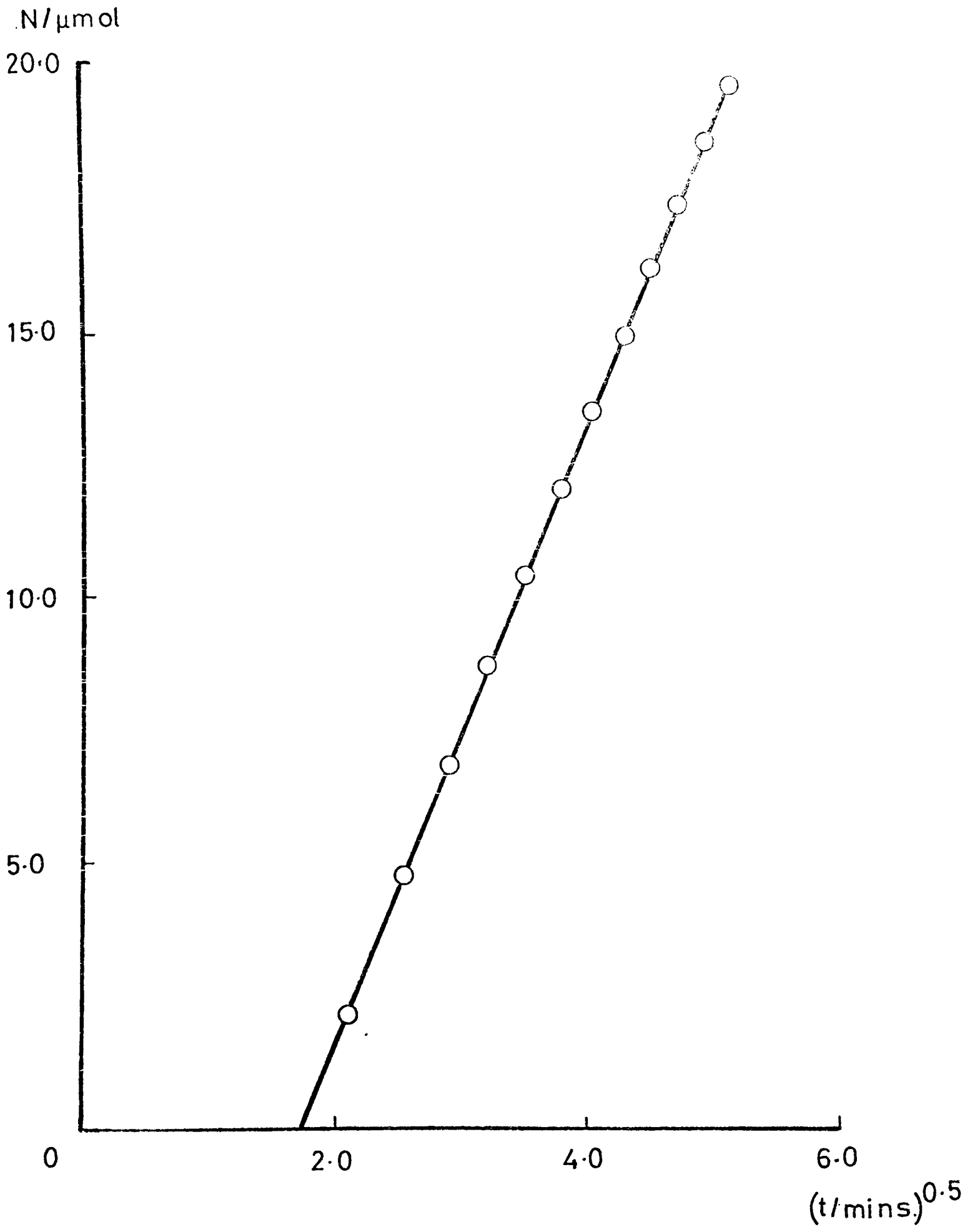

Figure (9). Typical results for a non-steady state experiment.

From the five experiments conducted:

$$A/mm^2 = .182 \pm 6$$

where the error given is the probable error on the mean. These limits will be used for further experimental data.

The cell constant, B, is obtained from the steady state fluxes which are of the order 5 mol.Gs^{-1}. Five experiments measuring the cell constant gave a value

$$B/mm = 32.3 \pm 0.6$$

These experiments were conducted before, during and after the cell had been used to measure diffusion coefficients. No noticeable deterioration of the sinter with time was observed.

From the values of B and A a value of ℓ, the pore length may be calculated

$$\ell/mm = 5.6 \quad .$$

Visual observation of the sinter gives an estimated length of approximately 4 mm. The difference is attributable to the tortuosity of the pores.

d) Measurement of Diffusion Coefficients

Once the Stokes' Cell has been calibrated, it may be used to measure integral diffusion coefficients. Since it was not possible to measure the flux of the diffusants through the sinter

continuously by a pH stat technique, samples were removed periodically from the upper compartment and assayed. Theory was developed to calculate the diffusion coefficients from these measurements. The samples removed were analysed using a Unicam SP500 spectrophotometer.

Ultra Violet Spectra of methyl, butyl and hexyl nicotinates.

The absorption maxima and molar extinction coefficients were found for methyl, butyl and hexyl nicotinates and are reported in table (3). Solutions of different concentrations were used and the results found to be in accordance with the Beer-Lambert Law.

Table (3)

Molar Absorbances of the different nicotinates in water and ethanol

Substrate	λ_{max}/nm	ε_{max}	
		water	ethanol
methyl nicotinate	263	3096	2822
n-butyl nicotinate	264	2880	2640
n-hexyl nicotinate	264	2780	2550

Theory of sampling technique

The experimental data give the concentration of diffusant in the upper compartment as a function of time. The concentration change during the experiment is not a linear function of the diffusion coefficient since volume changes occur in the upper compartment due to the sampling process. The complete experiment is divided into a series of sub-experiments lasting from time (t_o) to ($t_o + t_*$), each providing an estimate of the integral diffusion coefficient.

Diagrammatically the system may be represented:-

Time/s	Lower Compartment		Upper Compartment	
	Concentration/M	Volume/dm^3	Concentration/M	Volume/dm^3
t=0	$c^o_{\ell o}$	v_ℓ	0	v^o_u
t=t	c_ℓ	v_ℓ	c_u	v_u
$t=t_o$	$c_{\ell o}$	v_ℓ	c_{uo}	v_u
$t=t_o+t_*$	$c_{\ell *}$	v_ℓ	c_{u*}	v_u

If $D/m^2 s^{-1}$ is the diffusion coefficient,

B/mm is the cell constant,

the flux $j/mol\ s^{-1}$ is given by:

$$j = DB(c_\ell - c_u) = v_u\left(\frac{dc_u}{dt}\right) = -v_\ell\left(\frac{dc_\ell}{dt}\right) \qquad (2.9)$$

By mass balance throughout a sub-experiment,

$$c_{\ell o} v_\ell + c_{uo} v_u = c_\ell v_\ell + c_u v_u \qquad (2.10)$$

and

$$c_\ell = c_{\ell o} + \frac{v_u}{v_\ell} (c_{uo} - c_u) \quad . \qquad (2.11)$$

Substituting

$$\frac{dc_u}{dt} = \frac{DB}{v_u} \left\{ c_{\ell o} - \frac{v_u}{v_\ell} - c_u \left(1 + \frac{v_u}{v_\ell}\right) \right\} \qquad (2.12)$$

Integration and application of the boundary conditions,

at the start of a sub-experiment $t = t_o$ $c_u = c_{uo}$,

at the end of a sub-experiment $t = t_o + t_*$ $c_u = c_{u*}$,

gives:

$$DB \left(\frac{1}{v_u} + \frac{1}{v_\ell} \right) t_* = -\ell n \left[1 - \left(\frac{c_{u*} - c_{uo}}{c_{\ell o} - c_{uo}} \right) \left\{ 1 + \frac{v_u}{v_\ell} \right\} \right] \quad (2.13)$$

$c_{\ell o}$ may be calculated from

$$v_u c_{uo} + \sum_n v_n c_n + v_\ell c_{\ell o} = v_\ell c^o_{\ell o} \qquad (2.14)$$

where $\sum_n v_n c_n$ is the sum of the products of the volumes and concentrations of the samples removed from the upper compartment.

Due to the form of the final equation, it is unnecessary to calculate the actual concentrations c_{u*}, c_{uo} and $c_{\ell,o}$ by substituting the molar extinction coefficient. Once the optical

densities of the samples have been established, the only operation required is to multiply by the dilution. Hence in tables where concentrations are given, the results are given in optical density units which are the actual concentrations divided by the molar extinction coefficient.

Experimental Procedure

A typical run is that to measure the diffusion coefficient of methyl nicotinate in isopropyl myristate. The cell is washed through thoroughly with acetone to remove any traces of water from the sinter. Care is taken not to expose the upper surface of the frit to air, since any air bubbles trapped in the pores would alter the cell constant. Isopropyl myristate is drawn several times through the sinter using a water pump. The cell is flushed through several times with 0.3 M methyl nicotinate in isopropyl myristate and finally filled with this solution. The upper compartment is emptied and 40 cm^3 fresh isopropyl myristate introduced by pipette. The time is noted, the stirrer (2Hz) started and any holes in the cell lid sealed.

At known time intervals samples are removed and diluted with ethanol. The optical densities of these samples are measured using a Unicam SP500 spectrophotometer.

Results

Typical results are shown for the diffusion of methyl nicotinate in water at 37°C. These are given in Table (4). The diffusion coefficients measured by this technique are given in Table (6) along with estimated diffusion coefficients which are required for later work.

Table (4)

Typical experimental results for the diffusion of methyl nicotinate in water at 37° C

c_{uo}/ε_{max}	c_{u*}/ε_{max}	t*/ks	$c_{\ell o}/\varepsilon_{max}$	D/m^2s^{-1}
13.5	10.85	14.16	255.31	0.91
26.4	13.5	56.52	252.18	1.17
29.4	26.4	15.48	236.08	1.05
33.1	29.4	13.14	233.26	1.53
46.1	33.1	63.84	229.76	1.18

The Determination of the diffusion coefficient of acetic acid in isopropyl myristate

When acetic acid dissolves in isopropyl myristate it is possible for dimerisation to occur. An equilibrium will be established between the two species which is concentration dependent

$$\begin{array}{ccccc} M & + & M & \underset{k_{-b}}{\overset{k_b}{\rightleftharpoons}} & B \\ m & & m & & b \end{array} \qquad (2.15)$$

Diffusion of both dimer and monomer is possible and the simple equations derived in the earlier text do not adequately describe the system. The steady state transport equations applying to the two species are:-

$$D_M(\partial^2 m/\partial z^2) - 2k_b m^2 + 2k_{-b} b = 0 \qquad (2.16)$$

$$D_B(\partial^2 b/\partial z^2) + k_b m^2 - k_{-b} b = 0 \qquad (2.17)$$

To measure the diffusion coefficient, a two phase experiment is conducted in the Stokes Cell. It has been shown that a stable interface can be established on the upper surface of the glass sinter in a Stokes Cell[31]. For this experiment the lower compartment of the cell is filled with a solution of acetic acid in IPM (0.298 M) and the top compartment is filled with 40 cm^3 water. The flux of acid diffusing is monitored using the pH stat which maintains a pH of 7 in the upper compartment.

Since the pH in the aqueous phase is kept at 7 both m and b tend to zero at z = 0 (the top surface of the frit). Also as m and b tend to zero b << m. Multiplication of equation (2.17) by 2, addition to equation (2.16) and integration between z = 0 and z = ℓ gives

$$D_M m + 2D_B b = (D_M m + 2D_B b)_{z=\ell}(z/\ell) \qquad (2.18)$$

thus $$j = D_M \left(\frac{dm}{dz}\right)_{z=0} = (D_M m + 2D_B b)_{z=\ell}/\ell$$

$$= \frac{D_M (m+2b)_{z=\ell}}{\ell} \cdot f \qquad (2.19)$$

where $$f = \frac{1 + 2D_B K_b m_\ell / D_M}{1 + 2K_b m_\ell} \qquad (2.20)$$

Interfacial transfer terms do not have to be included since they may be shown to be negligible for this system.

Values of j are found from the pH stat trace, ℓ is the thickness of the glass frit and (m+2b) is the total acid concentration (= 0.298 M). The function f can be calculated from a known value of K_b (page 57). The ratio D_B/D_M may be estimated from the dependence of the diffusion coefficients of carboxylic acids on molal volume [108]. Assuming the dimer to occupy twice the molal volume of the monomer the ratio is simply $2^{-0.6}$.

Using this technique the diffusion coefficient of the monomeric form at 298°K is found to be 0.48 $m^2\ Gs^{-1}$. Consequently the dimeric species has an estimated diffusion coefficient of 0.32 $m^2\ Gs^{-1}$. The measured monomeric diffusion coefficient is in good agreement with a calculated value (Table (6)).

e) Estimation of Diffusion Coefficients by Various Techniques

Some diffusion coefficients are difficult to determine and estimates for these have been made by three techniques,

(a) the ratio method;

(b) the molal volume method;

(c) the Stokes-Einstein equation.

The Ratio Method

The diffusion coefficient of a species (A) is known in one solvent, D_k^A, and an estimate is required in another solvent D_u^A. If for a species (B) we know the ratio of the diffusion coefficients in the two solvents D_k^B/D_u^B , then we may calculate,

$$D_u^A = D_k^A \times \left(\frac{D_u^A}{D_k^A} \right) \qquad (2.22)$$

The Molal Volume Method

This method has been used for two diffusion coefficients, butyl and hexyl nicotinate in water. It was difficult to measure values for these because of their very low solubility in water. Estimates for them have been calculated by the ratio method and the two different approaches give values which are in good agreement.

Diffusion coefficients may be related to molal volumes [109]

$$D/m^2Gs^{-1} = \frac{4.95}{V^{1/3}} \qquad (2.23)$$

where $V/cm^3\ mol^{-1}$ is the molal volume.

Using the diffusion coefficient of methyl nicotinate in water the molal volume may be calculated:

$$V = 75.7 \ .$$

For each $-CH_2-$ group added, the molal volume is increased by 16.2 [109]. This gives molal volumes of 124.3 and 156.7 for n-butyl and n-hexyl nicotinate respectively. Substitution back into the equation gives values for the diffusion coefficients. These are reported in Table (6).

The Stokes-Einstein Equation

The Stokes-Einstein equation states that the diffusion coefficient in a liquid is proportional to the temperature and inversely proportional to the viscosity of the liquid:

$$D \ \alpha \ \frac{T}{\nu}$$

Consequently viscosity measurements are needed to estimate diffusion coefficients by this method. In addition some viscosities are

required for the treatment of later data, these will also be reported here.

Viscosities were measured using an Ostwald viscometer. The viscometer was thermostatted at the required temperature and calibrated using water, the viscosity of which was known [110]. The results are given in Table (5).

Table (5)

Viscosities of liquids used in experiments measured using an Ostwald viscometer

Liquid	Temperature/^{o}K	Viscosity/m^2Ms^{-1}
water	298	0.89 [110]
water	310	0.68 [110]
isopropyl myristate	298	5.8
isopropyl myristate	310	4.23
60% w/v glycerol	310	6.597
80% w/v glycerol	310	28.4

Using these viscosities in the Stokes-Einstein equation, estimates of diffusion coefficients show self-consistencies with experimental results (Table (6)).

Table (6)

Diffusion Coefficients measured and estimated by the techniques described. Values from previous work show the reference number.

Diffusant	Solvent	Temp/^{o}K	$D/m^2\ Gs^{-1}$			
			'experimental'	'ratio'	'molal volume'	'Stokes-Einstein'
acetic acid	water	298	1.2(±.05)[103]	-	-	-
acetic acid	IPM	298	0.48[a]	0.45 (±.02)	-	-
acetic acid	IPM	298	-	-	0.32[b]	-
hexoic acid	water	298	0.78(±.03)[108]	-	-	-
methyl nicotinate	water	298	0.39±.01	-	-	-
methyl nicotinate	water	310	1.17±.07	-	-	1.17(±.07)
methyl nicotinate	60% glycerol	310	-	-	-	0.12(±.01)
methyl nicotinate	80% glycerol	310	-	-	-	0.029(±.002)
methyl nicotinate	IPM	310	0.51±.03	-	-	0.56(±.03)
butyl nicotinate	water	310	-	0.99 (±.06)	0.99 (±.06)	-
butyl nicotinate	IPM	310	0.43±.01	-	-	-
hexyl nicotinate	water	310	-	0.92 (±.05)	0.92 (±.05)	-
hexyl nicotinate	IPM	310	0.40±.03	-	-	-

(a) diffusion coefficient of monomer

(b) diffusion coefficient of dimer

III. The Measurement of Partition Coefficients

Analysis of the two phase experiment and the *in vivo* work reported later requires the measurement of several partition coefficients. The partition coefficients determined have all been obtained by using the following technique.

The substrate is dissolved in either the organic or the aqueous phase. Five cm^3 of both phases are placed in a sealed glass tube and shaken in a thermostatted tank for at least 24 hours. When equilibration has occurred, the layers are separated and either or both assayed. The method of assay, either u.v. spectrophotometry or pH titration, depends on the nature of the substrate.

Dimerisation of the carboxylic acids

In the case of the carboxylic acids, dimerisation is possible and the effective partition coefficients are concentration dependent. For monomer M and dimer B, the following equilibria are possible:

$$\underset{m_\phi}{M_{aqueous}} \overset{K_m}{\rightleftharpoons} \underset{m_*}{M_{organic}} \overset{K_b}{\rightleftharpoons} \underset{b_*}{\tfrac{1}{2}B_{organic}} \qquad (2.24)$$

The total concentration of acid present in the organic phase is thus:-

$$c_* = 2b_* + m_* \qquad (2.25)$$

Using the equilibrium constants above:

$$b_* = K_b^2 m_*^2 \qquad (2.26)$$

$$c_* = 2K_b^2 m_*^2 + m_* \qquad (2.27)$$

$$c_\phi = m_\phi = m_* \; K_m \qquad (2.28)$$

Therefore:

$$\frac{c_*}{c_\phi} = \frac{1}{K_{eff}} = \frac{1}{K_m} + \frac{2K_b^2 c_\phi}{K_m^2} \quad . \qquad (2.29)$$

By measuring the ratio c_*/c_ϕ at different aqueous acid concentrations, separation of K_b and K_m is possible. Figure (10) shows a graph for acetic acid partitioning between isopropyl myristate and water with values of K_b and K_m given.

Figure (11) shows a graph of c_*/c_ϕ against c_ϕ for n-hexoic acid partitioning between hexane and water. Since the intercept is so close to zero, separation of the K_b and K_m parameters is not possible. For this system values of K_{eff} have been used in subsequent calculations.

The results of the other partition coefficients measured are given in Table (7). There is close correlation between the values measured for these nicotinates and previously determined ether-water partition coefficients [121].

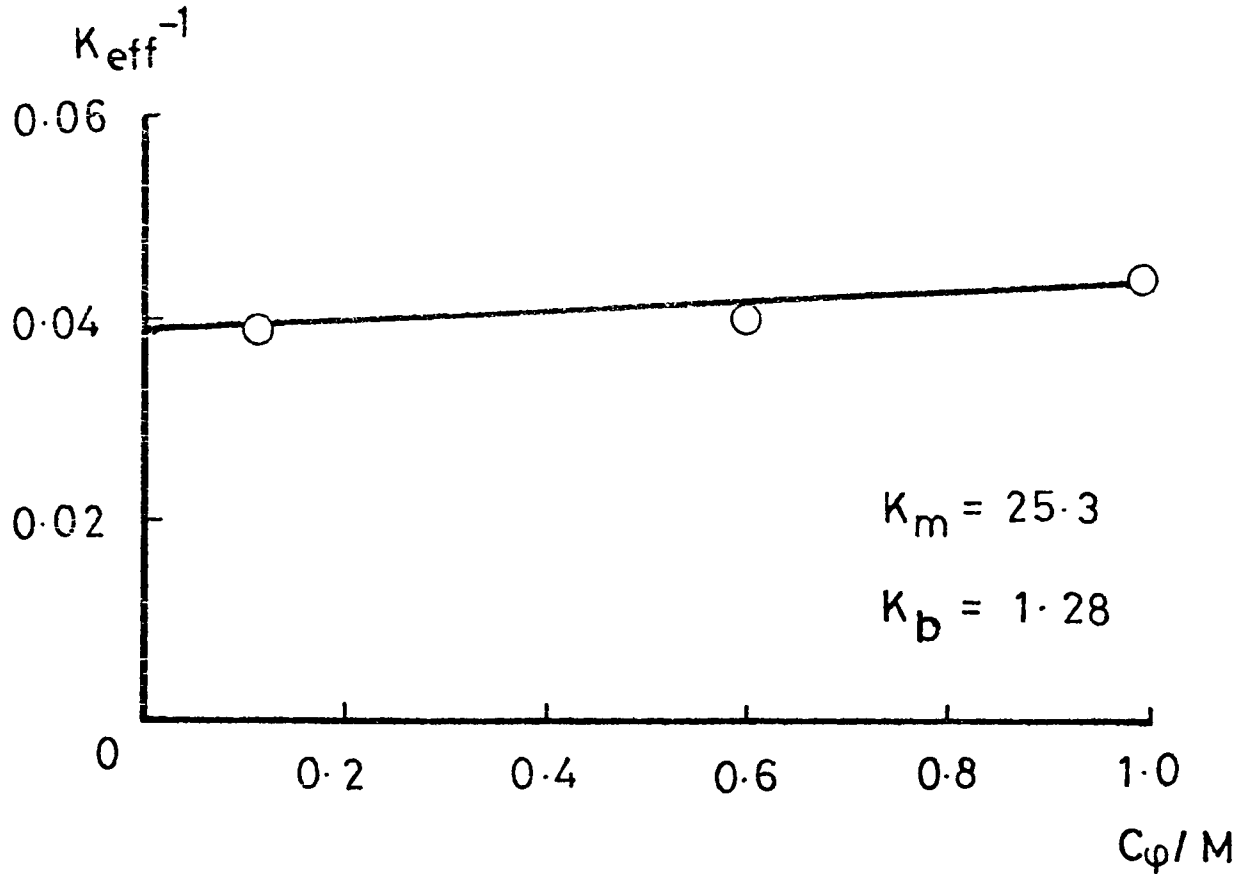

Figure (10). Variation of the partition coefficient with aqueous concentration for acetic acid between isopropyl myristate and water.

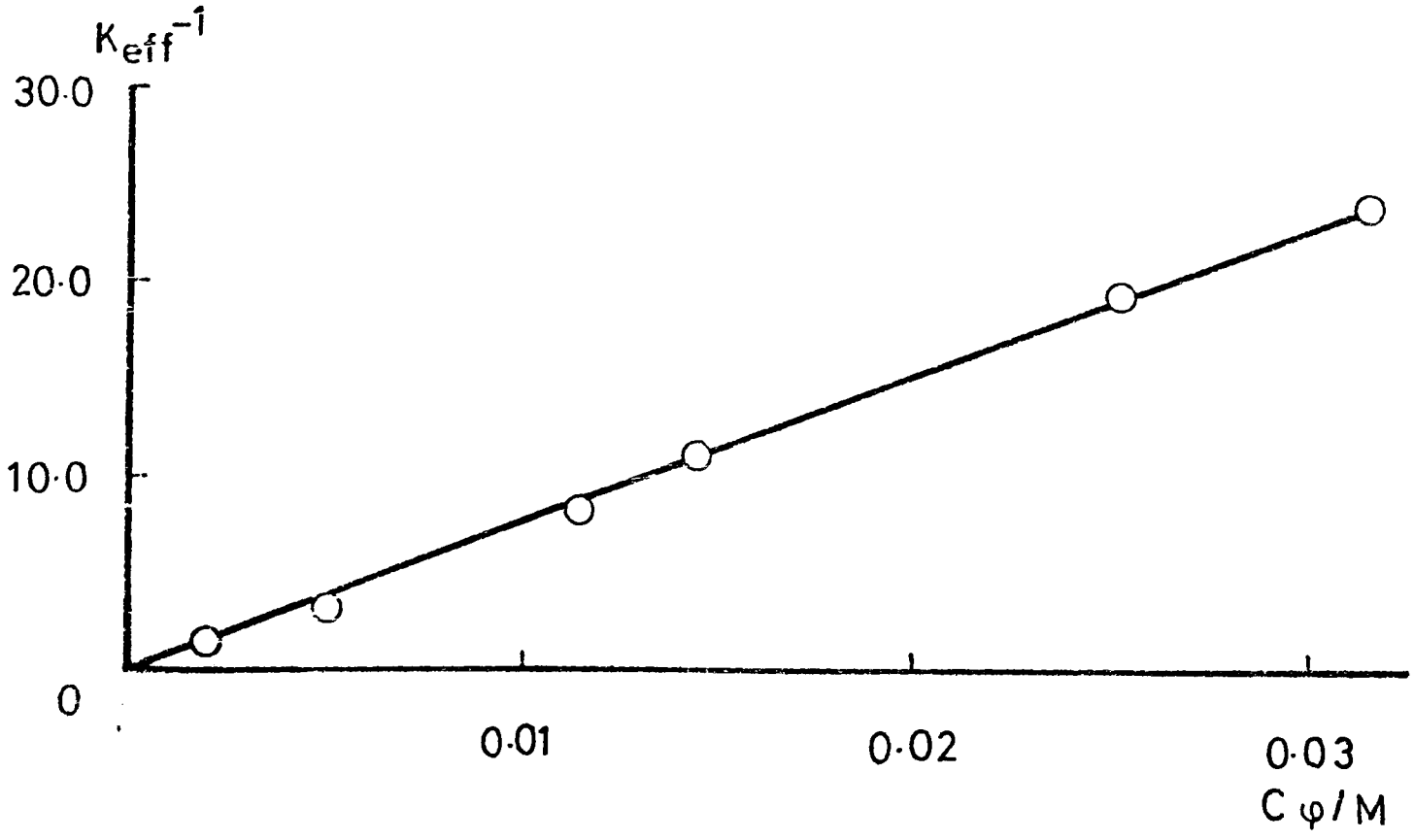

Figure (11). Variation of the partition coefficient with aqueous concentration for hexoic acid between hexane and water.

Table (7)

The partition coefficients for nicotinate esters between various aqueous phases and isopropyl myristate at 298°K[77] and 310°K.

Phase	Methyl Nicotinate		n-butyl nicotinate	n-hexyl nicotinate
	298°K[77]	310°K	310°K	310°K
Water	0.305	0.394	0.026	0.014
40% w/v glycerol	0.328	0.401	0.028	0.015
60% w/v glycerol	0.362	0.52	-	-
80% w/v glycerol	0.442	0.60	-	-
100% w/v glycerol	0.935	-	-	-

CHAPTER III

THE ROTATING DIFFUSION CELL

I. Introduction

In the conventional Stokes Cell the thickness of the glass frit is approximately 3 mm. Consequently a long time elapses before steady state fluxes are established. If a much thinner filter could be used, e.g. a Millipore filter (~ 150 μm), the time to establish steady state conditions would be reduced to a matter of seconds. Experimental data could be accumulated much more rapidly.

The Stokes Cell has been used to study the transport of various species across the interface between two liquid phases[31]. Transport to the interface is controlled by diffusion across the sinter and the total transfer process, provided no chemical reaction occurs, can be controlled either by this diffusion process or by slow transfer across the interface. The relative importance of these two processes depends on the magnitude of $10^{-3}/DB$ compared to $1/Ak_I$[31]

where

D/m^2s^{-1}	is the diffusion coefficient of the species in the filter
B/mm	is the cell constant
A/mm^2	is the pore area
k_I/ms^{-1}	is the interfacial rate constant.

For the detection of interfacial barriers

$$\frac{1}{k_I} > \frac{10^{-3}}{\ell D}$$

and thus by making ℓ as small as possible, the range over which k_I may be studied is considerably extended.

A piece of apparatus was designed in which very thin filters could be used in place of the glass frit. In the Stokes Cell, mechanical stirrers are used to sweep the upper and lower surfaces of the sinter. This serves to prevent the formation of stagnant diffusion layers and to maintain a uniform concentration distribution in the two compartments. Mechanical stirring of very thin filters is not practicable since they are so fragile. Ideally a design is required in which the solution in the two compartments is stirred and the thicknesses of the diffusion layers on either side of the filter are accurately known.

Part of the solution to the problem is provided by using the hydrodynamics to a rotating disc electrode. Diffusion layers for rotating disc electrodes have been well characterised [111,112], and the rotation ensures good stirring of the bulk solution. However in any apparatus incorporating a rotating filter the correct hydrodynamics have to be established on both sides of the filter. Thus the design of the apparatus incorporates a special baffle to impose the correct hydrodynamics to the inner surface of the filter.

II. The Hydrodynamics to a Rotating Disc

The rotating diffusion cell relies on the hydrodynamics produced when a planar disc is rotated in a fluid. The properties of the flow patterns produced have been described in detail[92,111]. Mathematically it is more convenient to express the flow velocities (v) in terms of cylindrical polar co-ordinates (figures (12) and (13)).

At $z = 0$, $v_\phi = r\omega$ and $v_r = v_z = 0$ (ω/radians.s^{-1} is the rotation speed). As z increases the radial force imposed on the fluid drives liquid outwards from the centre, and v_r rises accordingly. Concomitantly the velocity component v_ϕ tends to fall as the rotational force is viscously damped. The velocity component in the z direction is caused since fluid flung out radially needs to be replenished from the bulk solution; as z increases this reaches a limiting value.

The velocity components may be described in terms of a non-dimensional distance function γ,[113,114] where

$$\gamma = \left(\frac{\omega}{\nu}\right)^{\frac{1}{2}} z = \frac{z}{z_H} \qquad (3.1)$$

ν is the kinematic viscosity and z_H ($= (\frac{\nu}{\omega})^{\frac{1}{2}}$) is the thickness of the hydrodynamic layer. The velocity components are then given by the following equations:

$$v_\phi = r\omega\, G(\gamma) \qquad (3.2)$$

$$v_r = r\omega\, F(\gamma) \qquad (3.3)$$

$$v_z = -(\omega\nu)^{\frac{1}{2}} H(\gamma) \quad . \qquad (3.4)$$

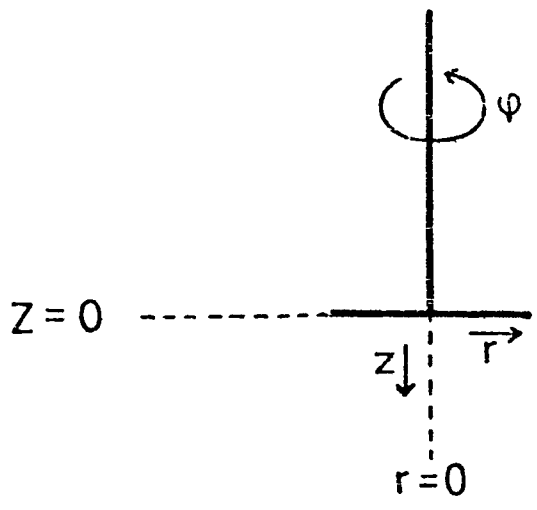

Figure (12). Co-ordinates for the rotating disc system.

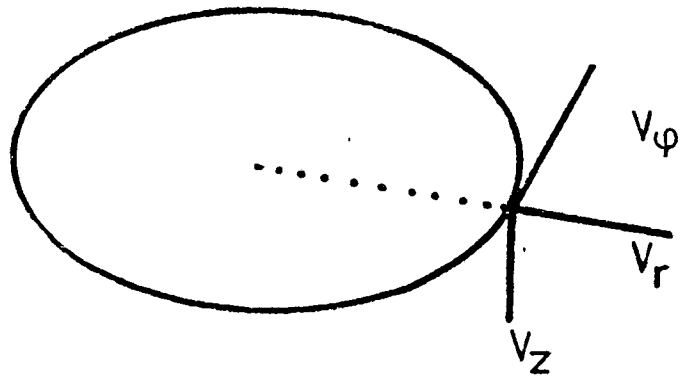

Figure (13). Velocity Components for the rotating disc system.

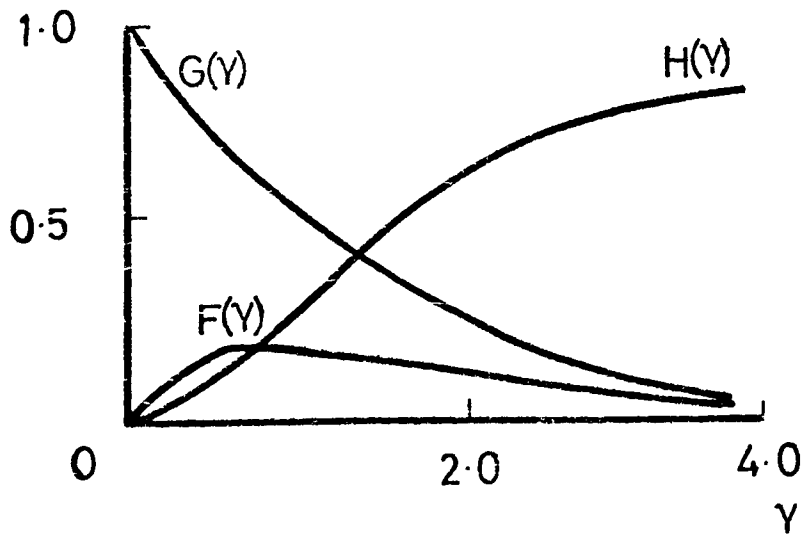

Figure (14). Variation of the velocity components $F(\gamma)$, $G(\gamma)$ and $H(\gamma)$ with γ at a rotating disc.

The way in which the functions F, G, and -H vary with γ is shown in figure (14).

The last equation shows that the flow towards the disc is independent of r and thus in any plane parallel to the disc surface v_z is constant. The flow patterns imposed by a rotating disc are represented pictorally in figure (15).

The Diffusion Layer

When studying diffusion problems regional variations in concentration are important. By solving the mathematics for a rotating disc electrode, it can be shown that the fluid is divided into two regions. The two regions are a well stirred region where convection is predominant, and a stagnant layer of thickness Z_D. In the latter region diffusion is the main transport process. A concentration profile in the solution is given in figure (16).

The thickness (Z_D) of the diffusion layer is given by the Levich equation[92]

$$Z_D = 0.643\, \nu^{1/6} D^{1/3} W^{-\frac{1}{2}} \qquad (3.5)$$

where $\nu/m^2 s^{-1}$ is the kinematic viscosity;

$D/m^2 s^{-1}$ is the diffusion coefficient;

W/Hz is the rotation speed.

In this thesis preliminary work is conducted using substrates with known diffusion coefficients to verify that the hydrodynamics produced in the apparatus are those described by the above equation.

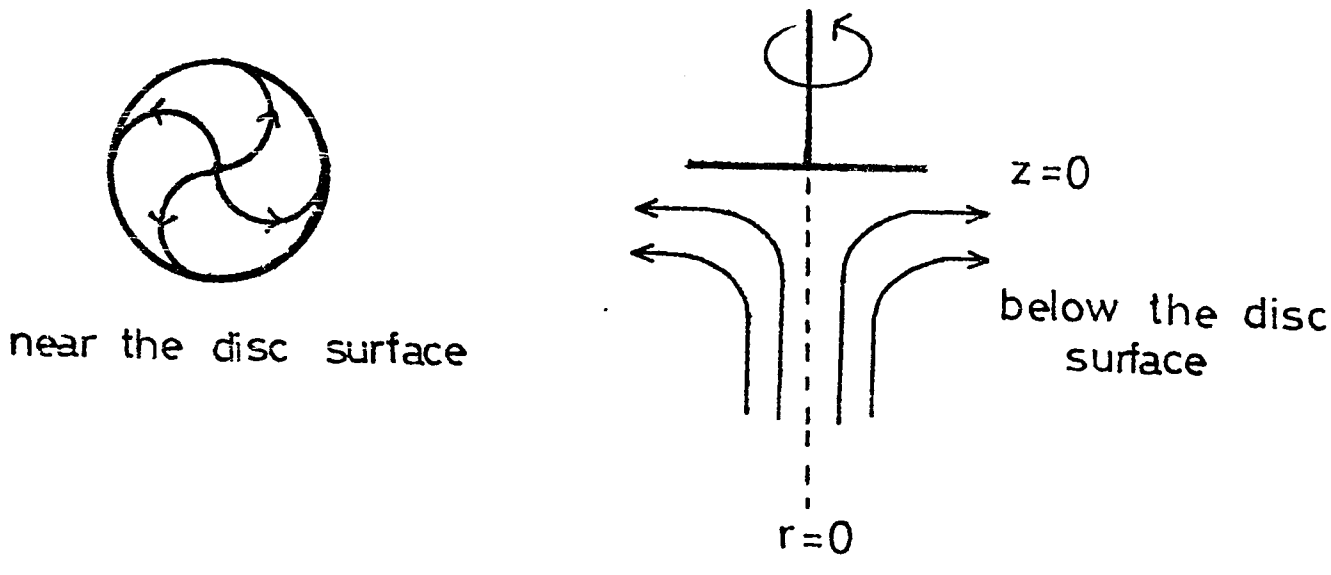

Figure (15). Schematic flow patterns at a rotating disc.

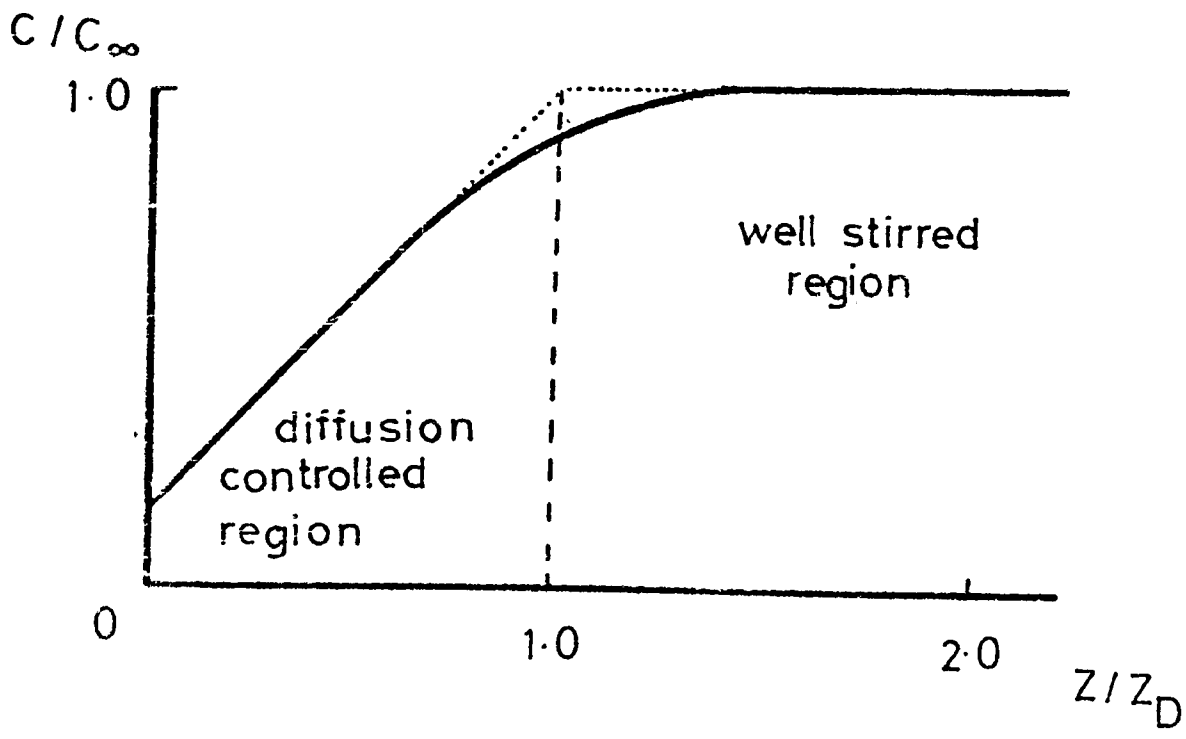

Figure (16). Concentration profile for transport to a rotating membrane.

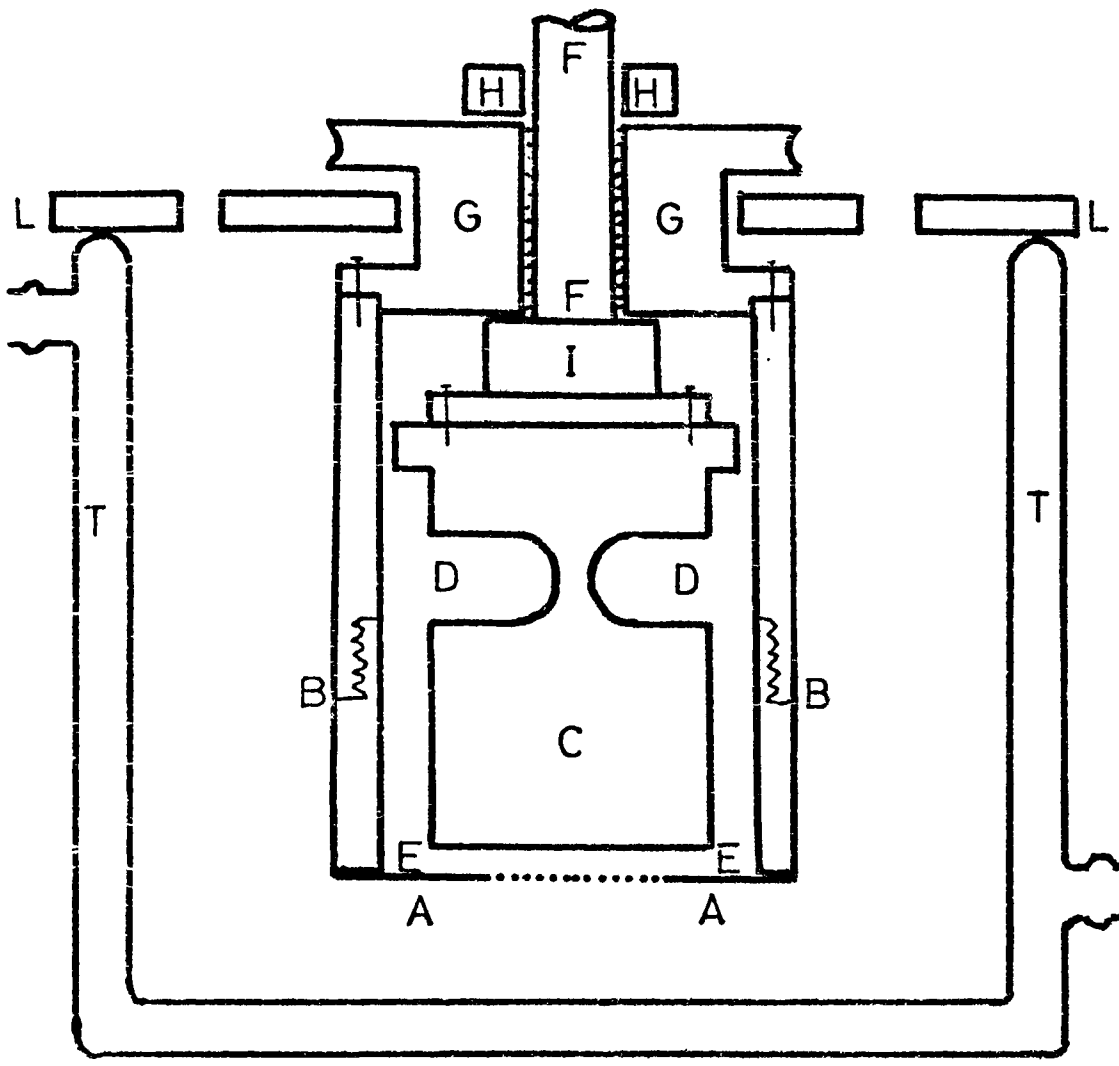

Figure (17). Cross sectional diagram of the Rotating Diffusion Cell.



Figure (18). The Assembled Rotating Diffusion Cell, showing the treated Millipore Filter.

III. Rotating Cell Design

Figures (17,18) show a cross sectional diagram and a photograph of various parts of the cell. The apparatus ready for use is shown in figures (19, 20). Figure (20) shows a view of all the diffusion apparatus used.

A Millipore filter (A) divides the apparatus into an inner and an outer compartment. The filter is treated so that only a central region remains permeable. It is mounted onto a rotating perspex cylinder (B) of diameter and length approximately 50 and 100 mm respectively. The lower part of the cylinder is designed so that it may be easily detached by unscrewing it from the main unit. This removable part and the associated filter is known as the filter assembly.

(a) The Baffle

Inside the rotating cylinder is a stationary cylindrical baffle (C) made of P.T.F.E. The diameter of the baffle is approximately 28 mm and it has two large slots (D) milled into it 25 mm distant from its lower edge. The construction of the apparatus is such that there is a 2 mm gap (E) between the lower edge of the baffle and the Millipore filter.

The purpose of the baffle is to impart the correct hydrodynamic flow above the inside surface of the filter. The solutions to the hydrodynamic equations for the rotating disc[92] assume an infinite disc diameter. In the absence of a baffle the rotating cylinder (B) would interfere with the flow pattern generated by

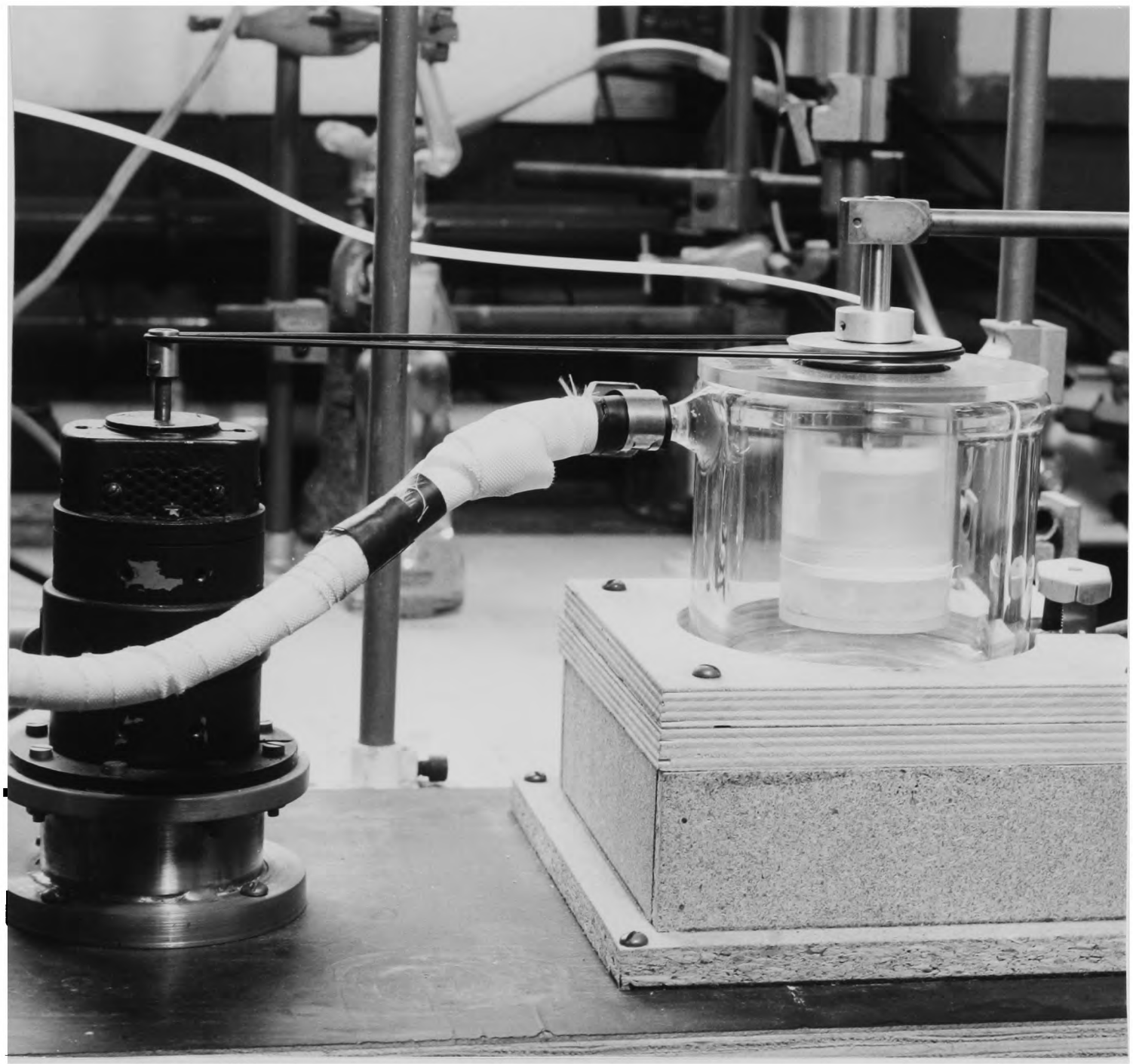

Figure (19). The Rotating Diffusion Cell in position for an experimental run.

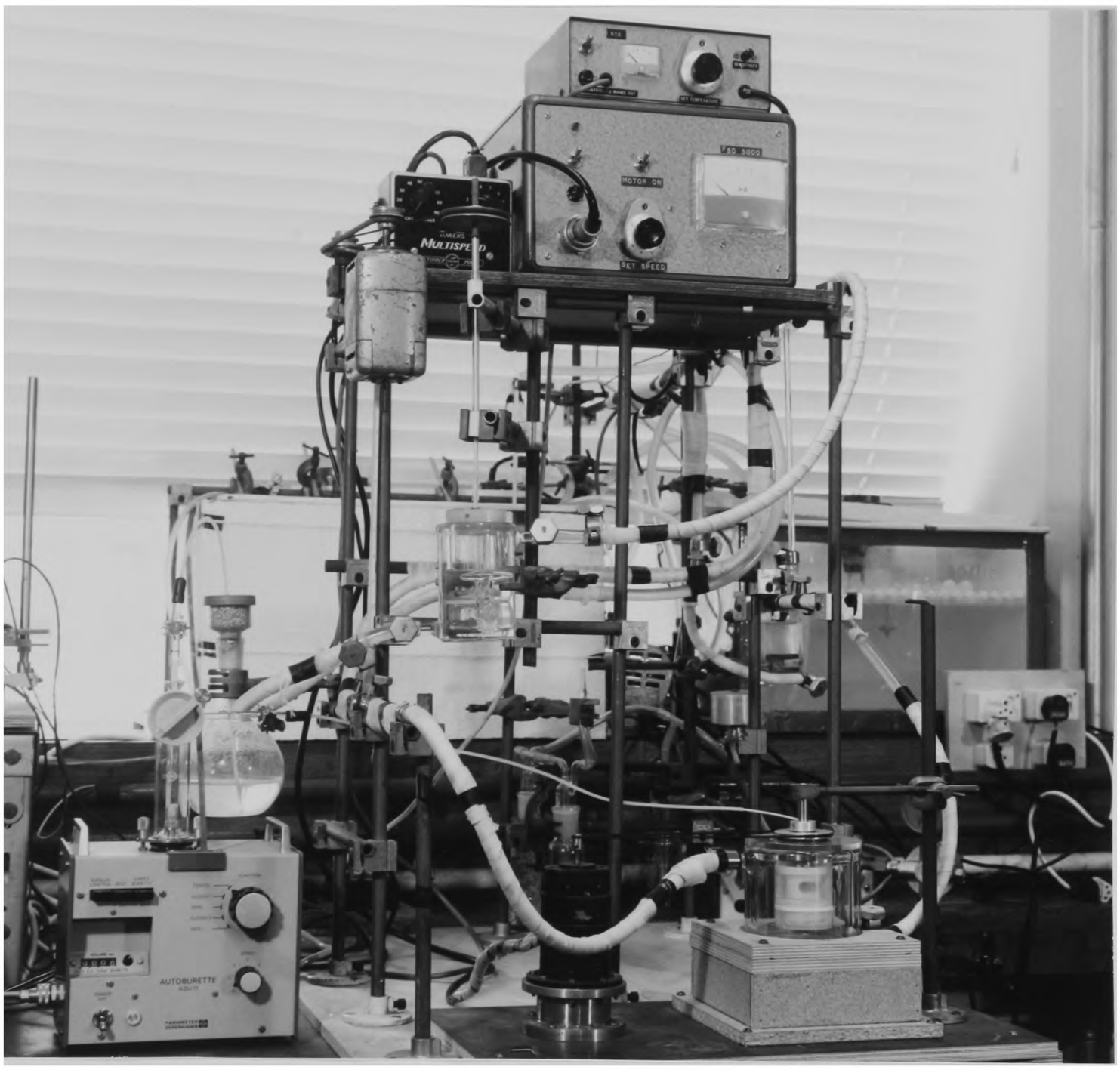

Figure (20). The Apparatus used for diffusion work showing, in addition, the pH stat, the motor controller and the thermostatting.

the rotating filter and the Levich equation would not be applicable. The baffle is designed to shield the central region of the disc from the convective transport created by cylinder (B) without impeding the main flux of material towards the filter. Thus with the present design at distances greater than 2 mm the flow imposed by the filter is the same as that to a normal rotating disc; i.e. it is towards and normal to the plane of rotation. Under these conditions the Levich equation is applicable. The hydrodynamic flow lines are shown diagrammatically in figure (21). Inside the baffle the solution travels towards the disc, it is flung centrifugally through the gap (E) and returns through the slots (D).

The rotary properties of the two cylinders are achieved by attaching the parts to a stainless steel bearing block (G) which contains a push fit roller bearing. The outer cylinder (B) is attached to the bearing block which has also been designed to act as a pulley. The pulley, bearing block, outer cylinder and filter assembly rotate freely about a central stainless steel inlet tube (F) which is bolted to the P.T.F.E. baffle. Vertical movement of the inner cylinder is prevented by the mantle (I) and a removable locking collar (H).

The complete assembly is placed in a double walled thermostatted vessel (T) with a perspex lid (L) which prevents excessive evaporation. The lid is drilled to accept electrodes for pH monitoring and nitrogen and alkali delivery tubes similar to those for the conventional Stokes Cell.

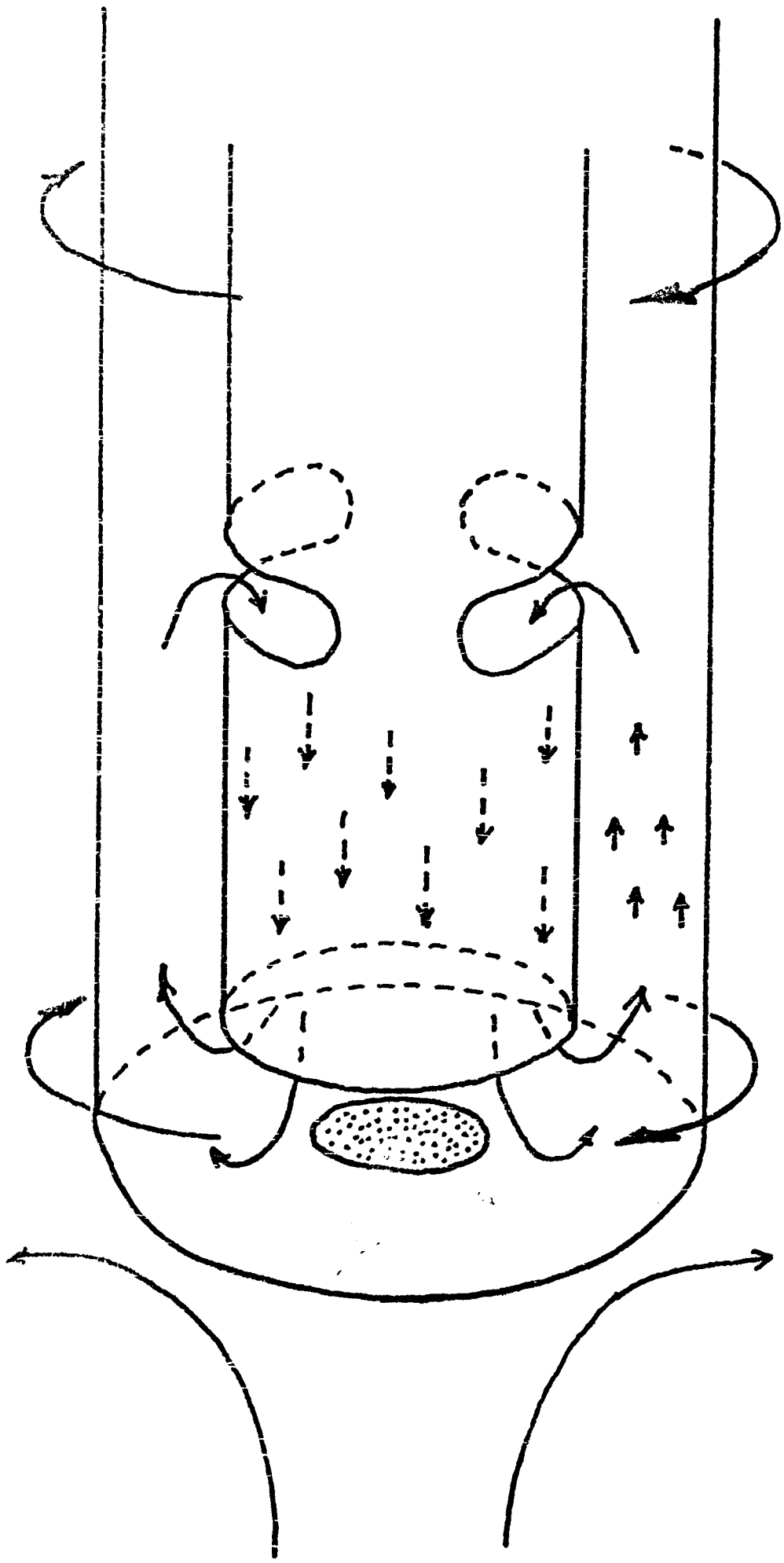

Figure (21). Schematic representation of the flow patterns in the rotating diffusion cell.

The cell is driven via a rubber drive band by an Adenco velodyne motor. Figure (22) shows schematically how this system operates. Calibration of the rotation speeds was performed using a transistorised counting unit. The rotation speed can be set accurately using a potentiometer on the control box. A calibration curve of rotation speed plotted against potentiometer setting is shown in figure (23).

(b) Filters

Two types of Millipore filters were used, MF filters composed of mixed cellulose esters and Duralon filters composed of nylon. The characteristics of the filters are given in Table (8). Initial results were obtained with MF filters which are stuck to the outer cylinder and the outer region rendered impermeable. The treated filter and filter assembly is shown in figure (24), the filter on the right-hand side is untreated and the left-hand one is fixed to a P.T.F.E. support ready for use. The following methods are adopted for preparation of the filters.

Table (8)

Characteristics of Millipore Filters[115,116]

Type	Pore Size/μm	Quoted Porosity	Measured[116] porosity	Thickness/μm
MF	5.0	84	80	130
MF	1.2	82	82	150
MF	0.8	82	-	150
Duralon	1.0	63	-	140

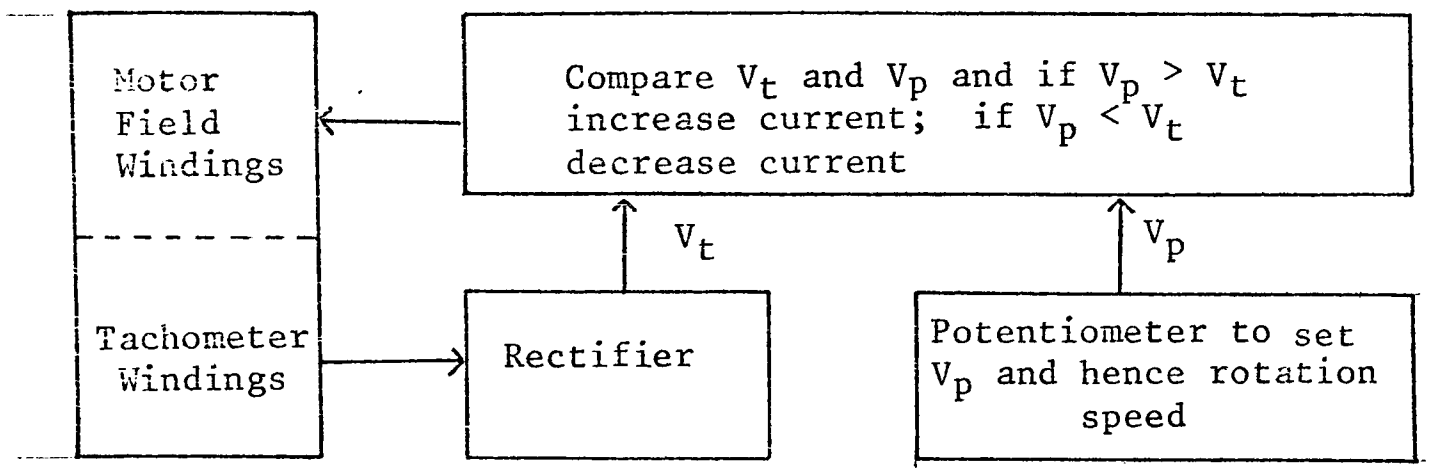

Figure (22). Schematic representation of Velodyne motor and motor controller.

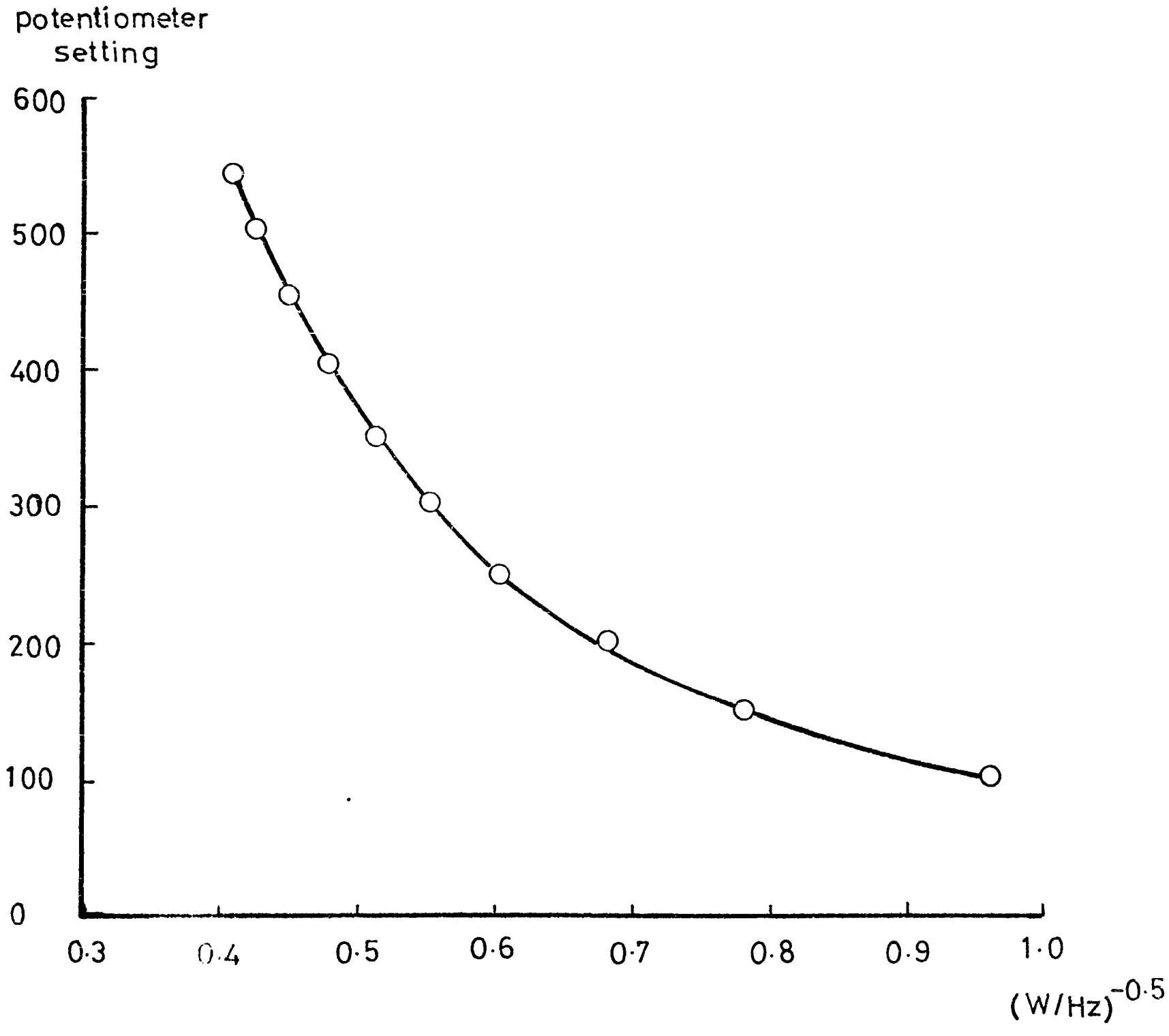

Figure (23). Rotation speed calibration curve.

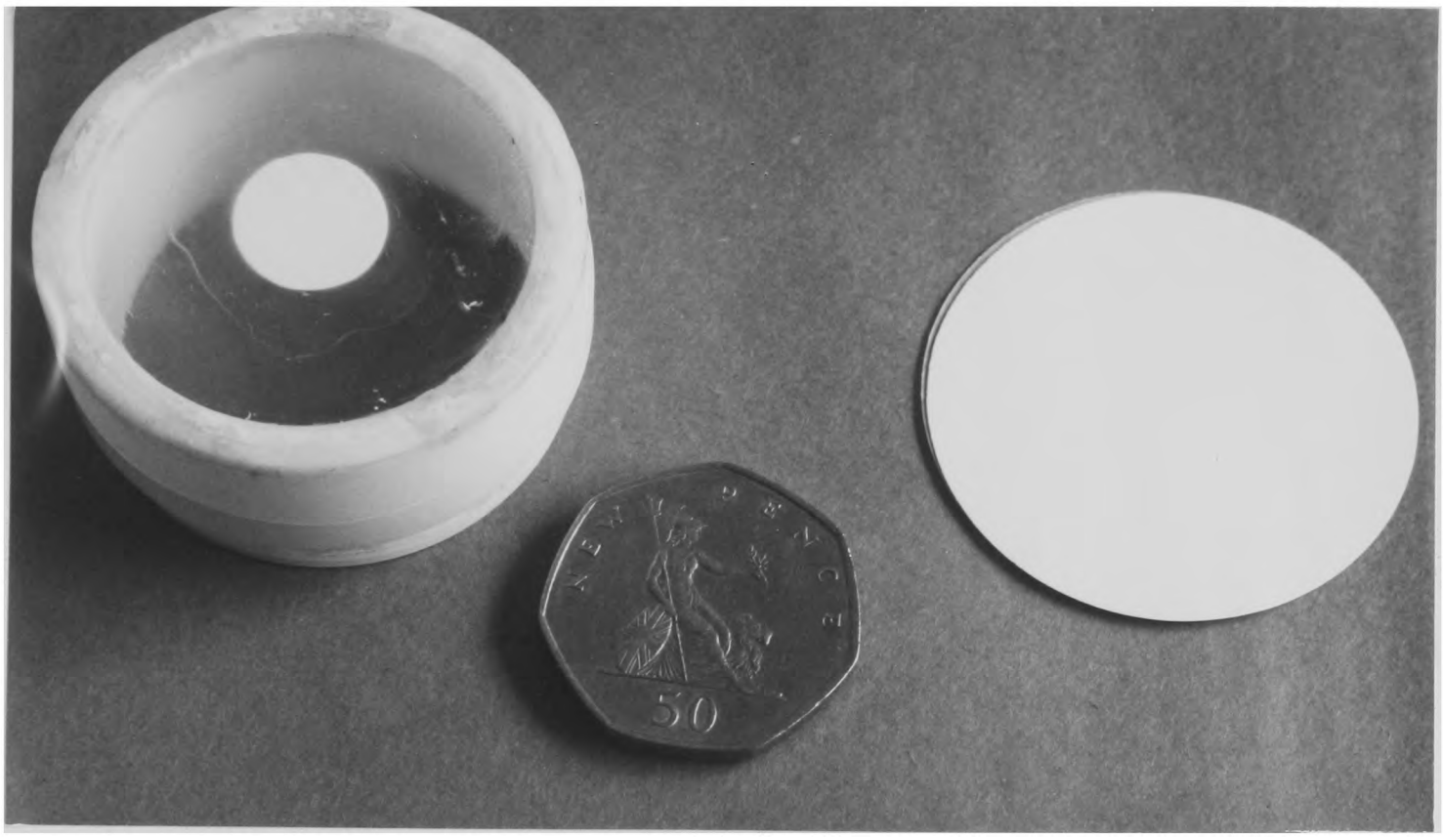

Figure (24). The Filter Assembly. The left-hand illustration shows a treated MF filter fixed to a teflon support with cyanoacrylate adhesive. The right-hand illustration is an untreated filter.

(c) Millipore MF Filter Treatment

The filter is glued to the perspex ring (B) using Millipore MF cement. If a P.T.F.E. assembly is used a cyano-acrylate adhesive produces a strong enough bond between the filter and the P.T.F.E. to allow experiments to be conducted[117]. When the filter has been firmly attached to the support the assembly is placed in a special template in which a centrally drilled hole is positioned directly above the centre of the assembly. It is thus possible to place a drop of glycerol onto the centre of the filter. The template is then removed. The glycerol spreads radially outward, the high viscosity making this conveniently slow. If a large masked area is required more glycerol is added until the desired diameter is produced. The unmasked pores are then collapsed by careful application of clearing solution. Clearing solution has the formula, by volume[118],

dioxane	33
hexane	33
dichloroethane	33
water	1

This leaves the unmasked area impermeable to fluid.

When the clearing solution is applied, the filter immediately becomes translucent and flexible to the extent of being somewhat elastic. The filter tends to sag in the centre due to the weight of glycerol it is supporting.

It is thus important to apply the fluid from the centre radially

outwards. If this procedure is not followed the glycerol tends to run along the surface of the filter and a porous region is produced which is neither circular nor concentric. As soon as the solvent evaporates, the filter becomes transparent, taut and rather brittle. The strength of the filter depends to a certain degree on the pore size. Three pore sizes were investigated (5.0, 1.2 and 0.8 μm). The 5.0 μm filters were the strongest and the 0.8 μm filters were extremely fragile.

In work on interfacial transfer, a stable interface is required which is best produced by using a small pore size. A compromise between maximum interface stability and filter strength was achieved by using 1.2 μm filters and these were used for the majority of the work.

When the clearing solution solvents have completely evaporated the filter is washed through several times with distilled water to remove the glycerol. This process also removes the surfactant Triton-X-100 incorporated into the filter to improve the flow characteristics for commercial purposes[118].

In some instances it is possible to repair filters that split round the edge of the perspex. This is achieved by patching with spare filter material and perspex cement.

(d) Duralon Filter Treatment

When nylon filters are used several modifications to the above procedure are adopted. The duralon filters are stuck to the perspex assembly using a cyanoacrylate adhesive. (Millipore MF cement does not produce a strong enough bond, nor does perspex

cement.) The second problem is that the filter material is slightly attacked by glycerol and thus it cannot be used as the masking liquid. A suitable alternative was found to be polyethylene glycol 400 (PEG) which has a similar viscosity to glycerol.

The major problem encountered when using duralon filters is the method of rendering the periphery of the filter impermeable. Three methods were adopted.

(i) Blocking using hexafluoroisopropanol (HFP). The first method resembles that for MF filters and relies on the ability of a mild solvent to collapse the pore structure. The solvent used for this is hexafluoroisopropanol[119]. The action of this liquid is rather too vigorous and results in many failures; however, if a successful filter is made it is far more durable than its MF counterpart. The properties of the HFP which make it a less successful collapsing agent than clearing fluid are:-

a) its strong attacking power;

b) its low volatility.

The strong attacking power results in an immediate collapse of the pore structure and then it is difficult for the solvent to spread over the rest of the filter. Since it cannot spread and it has a low volatility, the solvent remains in contact with one region of the filter which it dissolves completely.

Various techniques were developed to improve even application. An atomiser was used to spray the neat solution onto the filter; this was unsuccessful as was trying to dilute the attacking power of the

HFP with cosolvents (water, carbon tetrachloride and dioxane were investigated).

(ii) Blocking the pores with cyanoacrylate adhesive.

Cyanoacrylate adhesives were applied to the unmasked area and allowed to spread into the filter until they reached the P.E.G. The polymerisation of cyanoacrylates is catalysed by the OH groups[120] in the P.E.G. and consequently as soon as the adhesive had spread over the filter and come into contact with the P.E.G. hardening occurred. The unmasked area was rendered impermeable by physical obstruction. However, when polymerisation occurred, heat was evolved which reduced the surface tension of the adhesive. The excess adhesive then flowed over the P.E.G. and polymerised producing an ill defined permeable area. Some successful filters were produced by this technique but they were surprisingly brittle.

(iii) Blocking the pores with a masking perspex bevel.

This method involves the physical obstruction of the pores with a perspex template. A disc of perspex 47 mm in diameter and 2.6 mm thick has a hole drilled in its centre 20 mm in diameter. The remaining annulus has a 10° bevel cut across one face. The filter is stuck to the plane face as shown in figure (25). The bevel with filter is then glued to the end of the filter assembly.

By employing this blocking technique it is possible to experiment with different types of membrane. One such example is silicone rubber sheeting*. This was stuck to the perspex bevel

---

* Silastic sheeting manufactured by Dow Corning and supplied by Lepetit Pharmaceuticals.

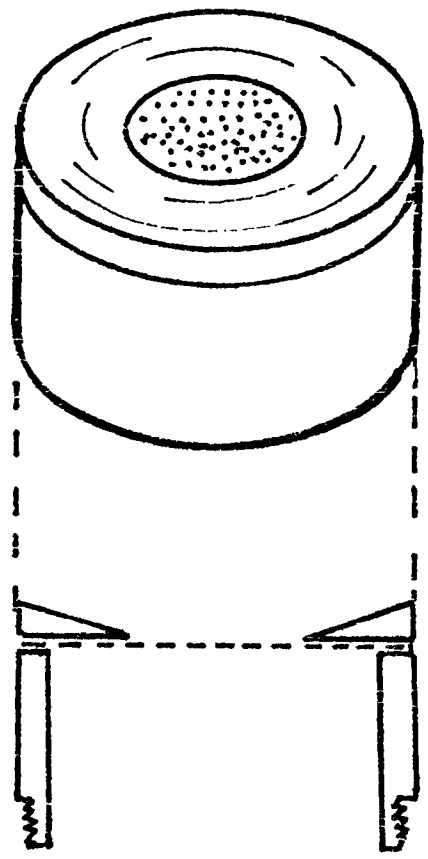

Figure (25). Diagram of filter assembly with the perspex bevel.

using a silicone rubber adhesive.

IV. Theory

The most general case is examined first and then equations applicable for the different types of experiment conducted are derived from the general solution.

Interfaces may be established on both sides of the filter and the general system may be described:-

	inner	interface	filter	interface	outer
length:	$-Z_{D,I}$ →	←	ℓ →	←	$Z_{D,o}$
area:	A	αA	αA	αA	A
diffusion coefficient	D_I		D_F		D_o
partition coefficients	1		K_F		K_o
rate constants		$\underset{k_1/K_F}{\overset{k_1}{\rightleftharpoons}}$		$\underset{k_2K_F/K_o}{\overset{k_2}{\rightleftharpoons}}$	

The partition coefficients describe the partitioning with respect to the inner phase. The distances Z_D describe the lengths of the diffusion layers produced by the rotating disc hydrodynamics and are given by the Levich equation:

$$Z_D = 0.643\ \nu^{1/6}\ D^{1/3} W^{-\frac{1}{2}}$$

The concentration of the diffusing compound is maintained at zero in the bulk of the outer compartment when the pH stat technique is used[88]. Extending the equations previously derived[31],

the measured flux J/mol. s^{-1} is given by:-

$$J = \vec{k}Ac_I \qquad (3.6)$$

where

$$\frac{1}{\vec{k}} = \frac{Z_{D,I}}{D_I} + \frac{1}{\alpha k_1} + \frac{\ell}{\alpha D_F K_F} + \frac{1}{\alpha k_2 K_F} + \frac{Z_{D,o}}{D_o K_o} \qquad (3.7)$$

A is the measured filter area

α is the ratio of the pore area to the measured filter area

c_I is the concentration of diffusant in the bulk of the inner compartment.

The different terms in equation (3.7) describe the possible rate determining processes for transport of the diffusant from the inner to the outer compartment.

The different types of experiment conducted in the cell are:-

(i) single phase, in which there are no interfaces;

(ii) outer, in which a single interface is located on the outside surface of the filter;

(iii) inner, in which a single interface is located on the inside surface of the filter;

(iv) sandwich, in which a sandwich is formed with two interfaces and the same phase in both inner and outer compartments.

In the different experiments conducted, aqueous and organic liquids have been used denoted by the subscripts ϕ and * respectively.

(i) Single Phase Experiments

In these, only aqueous systems were studied, there are no interfaces and hence no terms in k_1 and k_2. $K_F = K_o = 1$ and thus equation (3.7) reduces to

$$\frac{1}{\vec{k}} = \frac{Z_{D,I}}{D_I} + \frac{\ell}{\alpha D_F} + \frac{Z_{D,o}}{D_o} \qquad (3.8)$$

$$= \frac{2Z_{D,\phi}}{D_\phi} + \frac{\ell}{\alpha D_\phi} \qquad (3.9)$$

Substituting the Levich equation

$$\frac{1}{\vec{k}} = 1.286\ \nu^{1/6}\ D_\phi^{-2/3} W^{-\frac{1}{2}} + \alpha \frac{\ell}{D_\phi} \qquad (3.10)$$

and a graph plotted of $\frac{1}{\vec{k}}$ vs $W^{-\frac{1}{2}}$ should have a gradient $1.286\ \nu^{1/6}\ D^{-2/3}$ and intercept $\frac{\ell}{\alpha D_\phi}$.

(ii) Two Phase Experiments

For the two phase experiments, in the following equations K_p, k_I and k_{-I} have the following significance

Organic Aqueous

$$c_* \underset{k_{-I}}{\overset{k_I}{\rightleftharpoons}} c_\phi \qquad K_p = \frac{k_I}{k_{-I}} = \frac{c_\phi}{c_*}$$

The experiments may be divided into various categories depending on the position of the organic aqueous interface.

a) Outer

The organic/aqueous interface is located on the outer surface of the filter. In equation (3.7) k_1 has no significance, $D_I = D_F = D_*$, $K_F = 1$, $k_2 = k_I$, $K_o = K_p$ and

$$\frac{1}{\vec{k}} = \frac{Z_{D_*}}{D_*} + \frac{\ell}{\alpha D_*} + \frac{1}{\alpha k_I} + \frac{Z_{D_\phi}}{D_\phi K_p} \qquad (3.11)$$

b) Inner

The organic/aqueous interface is located on the inner surface of the filter. In equation (3.7) $D_I = D_*$, $k_1 = k_I$, $D_F = D_o = D_\phi$, $K_F = K_o = K_p$, and k_2 has no significance.

Thus

$$\frac{1}{\vec{k}} = \frac{Z_{D_*}}{D_*} + \frac{1}{\alpha k_I} + \frac{\ell}{\alpha D_\phi K_p} + \frac{Z_{D_\phi}}{D_\phi K_p} \qquad (3.12)$$

c) Sandwich

There are two sub-divisions, an aqueous/organic/aqueous sandwich (i), and an organic/aqueous/organic sandwich (ii) may be established.

(i)

$$D_I = D_o = D_\phi,\ k_1 = k_{-I},\ D_F = D_*,\ K_F = \frac{1}{K_p},\ k_2 = k_I, K_o = 1$$

Thus

$$\frac{1}{\vec{k}} = \frac{2Z_{D_\phi}}{D_\phi} + \frac{2}{\alpha k_{-I}} + \frac{\ell K_p}{\alpha D_*} \qquad (3.13)$$

(ii)

$$D_I = D_o = D_*,\ k_1 = k_I,\ D_F = D_\phi,\ K_F = K_p,\ k_2 = k_{-I},\ K_o = 1$$

Thus

$$\frac{1}{\vec{k}} = \frac{2Z_{D_*}}{D_*} + \frac{2}{\alpha k_I} + \frac{\ell}{\alpha D_\phi K_p} \qquad (3.14)$$

V. Characterisation of the hydrodynamics

The apparatus has been designed to produce known, reproducible hydrodynamics in the fluid on either side of the Millipore filter. It is, however, necessary to examine experimentally whether or not the hydrodynamics expected are produced. By introducing some dye into the inner compartment when the apparatus is rotating, it is possible to see that the flow patterns are those shown in figure (21). The dye passes down the centre of the P.T.F.E. baffle and is then forced by convection up the gap between the perspex and P.T.F.E. cylinders.

1. Single Phase Experiments

The initial experiments conducted in the rotating diffusion cell paralleled those measuring the cell constant of a Stokes

Cell[88]. The diffusion of acetic acid from the inner to the outer compartment was followed using a pH stat technique.

(a) Procedure

i) Filter Assembly. The filter is washed thoroughly with water until no air bubbles remain pocketed in the porous matrix. Air bubbles can be seen as white patches in a translucent grey background(where the filter is impregnated with water). P.T.F.E. tape is placed on the screw thread of the filter assembly to ensure a water-tight fit with the rest of the perspex cylinder. The assembled apparatus is placed in the thermostatted pot and clamped into position.

ii) Filling. Background electrolyte (5 mM barium acetate) is added to the outer compartment until the level just reaches the lower surface of the Millipore filter. Acetic acid (0.1 M) is introduced into the inner compartment using a 50 cm^3 syringe. Simultaneously background electrolyte is added to the outer compartment, maintaining, as far as possible, a negligible hydrostatic pressure difference between the two levels. The total volumes of solutions used are:-

inner compartment:	40 cm^3
outer compartment:	180 cm^3

Usually air bubbles become trapped on the under surface of the filter and are held there by surface tension.

These may be removed either by increasing the rotation speed suddenly or by sweeping them off using a specially designed L shape wire. This is covered in nylon to prevent damage to the filter.

iii) Following the diffusion. When the levels are equal the glass and calomel electrodes are introduced through the perspex lid. The alkali delivery tube is placed into the outer compartment and a steady stream of presaturated nitrogen allowed to bubble through the solution. The inner compartment is sealed by means of a rubber bung placed in the stainless steel inlet shaft. The pH stat is switched on and set to maintain a pH of 7. Traces are produced by the recorder plotting the volume of alkali added against time.

Blank runs were conducted to ensure that there was no appreciable flux caused by the absorption of carbon dioxide from the air.

iv) Rotation speed variation. The range of rotation speed used is found to be most convenient in the region 1 to 7 Hz. At rotation speeds less than 1 Hz the thickness of the hydrodynamic layer becomes too large and at these low speeds stirring of the bulk solution is not very efficient. This results in a stepped trace from the pH stat. At very high rotation speeds, since the cylinder is quite large, the solution in the outer compartment tends to be flung out of the thermostatted pot.

(b) Results

Equation (3.9) shows that for a single phase experiment

$$\frac{Ac_\infty}{J} = \frac{1}{\vec{k}} = \frac{2ZD_\phi}{D_\phi} + \frac{\ell}{\alpha D_\phi}$$

Rearranging

$$\frac{D_\phi c_\infty}{J} = \frac{1}{\beta} = \frac{2ZD_\phi}{A} + \frac{1}{B}$$

where B is the cell constant (A/ℓ) of the filter.

A simple computer program (Appendix 1) was written which calculates the value β from the fluxes given by the pH stat trace. It allows for depletion of the bulk concentration and considers the dissociation of the acetic acid. Sequences of points are taken such that about ten values of β for each rotation speed are obtained. A mean value for β is taken and its reciprocal plotted against $W^{-\frac{1}{2}}$. The intercept of the graph gives $\frac{1}{B}$ and the gradient should be $2 \times 0.643\ \nu^{1/6} D^{1/3}\ A^{-1}$.

Several experiments were conducted using this technique and the results are plotted in figure (26). As can be seen there is little correlation between the theoretical gradient and the experimental points. This is caused by mass flow through the filter when the levels in the two chambers are not equal.

Modified filling procedure. The following method was employed to ensure that there was no hydrostatic pressure difference between the two compartments. Both compartments are filled with

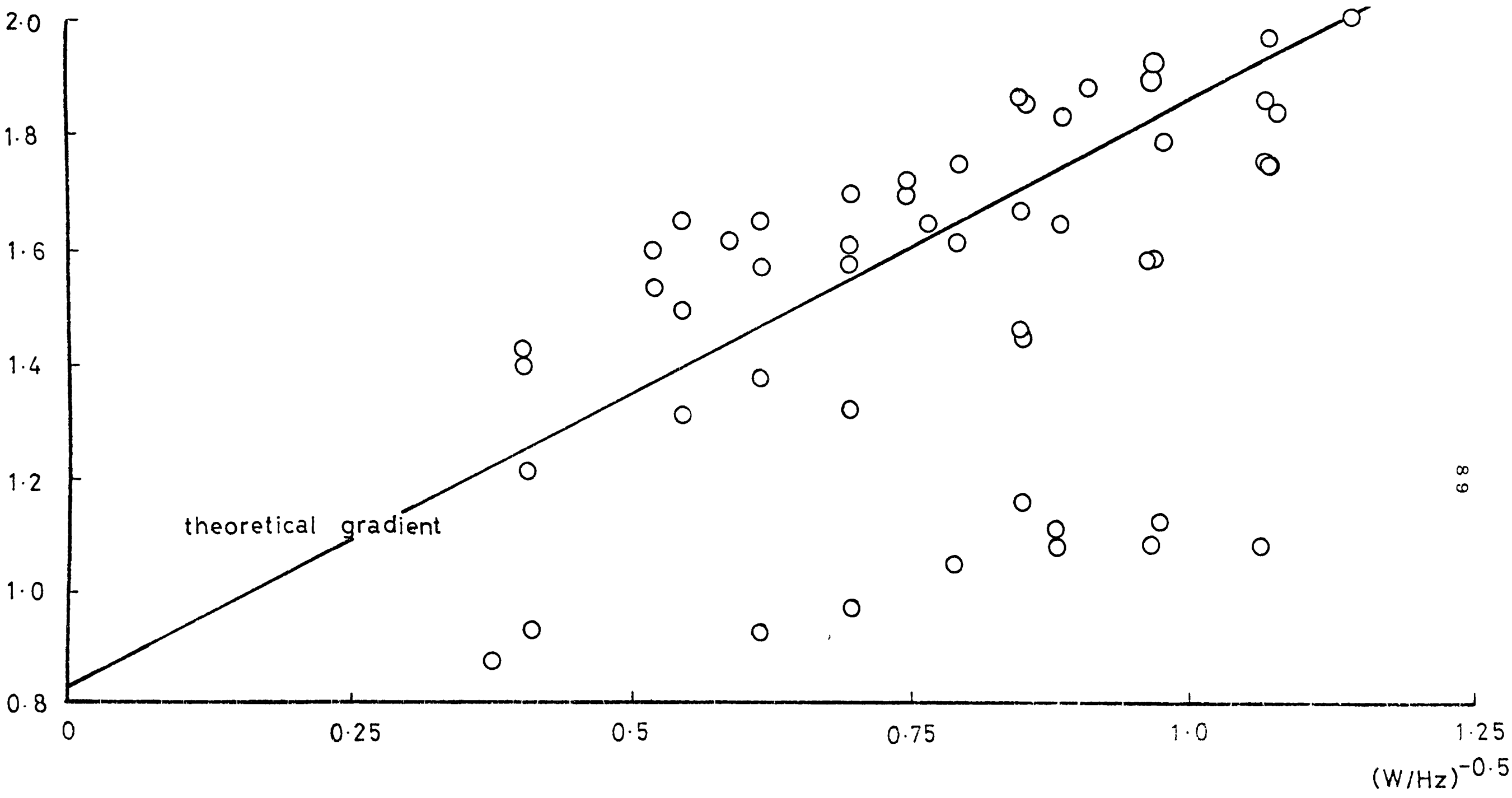

Figure (26). Some single phase experiment results.

background electrolyte and left for a couple of hours for the levels to equilibrate. Glacial acetic acid is then injected into the inner compartment. The volume, 250 μℓ is negligible compared to the 40 cm^3 capacity of the inner compartment, and this increase in volume should not result in any significant mass flow through the filter. The bulk acid concentration is measured by titration of a sample of the inner compartment solution at the end of the experiment and allowance made for the acid titrated away by the pH stat. The results could not be correlated with the theoretical equations which was attributed to the constant addition of alkali to the outer compartment causing mass flow into the inner compartment.

(c) The effect of mass flow on experimental results

For a mass flow, velocity v, Fick's 2nd law of diffusion will have a correction term:

$$\left(\frac{\partial c}{\partial t}\right) = D\left(\frac{\partial^2 c}{\partial z^2}\right) - v\left(\frac{\partial c}{\partial z}\right) \qquad (3.15)$$

For steady state conditions

$$D\left(\frac{\partial^2 c}{\partial z^2}\right) - v\left(\frac{\partial c}{\partial z}\right) = 0 \qquad (3.16)$$

Integrating

$$D\left(\frac{\partial c}{\partial z}\right) - vc = a \qquad (3.17)$$

therefore

$$\left(\frac{\partial c}{\partial z}\right) - \left(\frac{v}{D}\right)c = \frac{a}{D} \qquad (3.18)$$

Integrating further

$$e^{-\frac{vz}{D}} c = a' e^{-\frac{vz}{d}} + b' \qquad (3.19)$$

where $a' = -\frac{a}{v}$

Applying the boundary conditions

At $z = 0$, $c = 0$

$z = \ell$, $c = c_\infty$

$$a' = -\frac{c_\infty}{\left(e^{\theta}-1\right)} \quad \text{and} \quad b' = \frac{c_\infty}{\left(e^{\theta}-1\right)} \qquad (3.20)$$

where $\theta = v\ell/D$

The flux of material is given by equation (3.17)

$$\text{Flux} = \frac{vc_\infty}{\left(e^{\theta}-1\right)} = \frac{Dc_\infty}{\ell}\left\{\frac{\theta}{\left(e^{\theta}-1\right)}\right\} \qquad (3.21)$$

which tends to $\frac{Dc_\infty}{\ell}$ when $\frac{v\ell}{D} << 1$.

Expanding e^{θ}

$$\text{Flux} \quad \sim \quad \frac{Dc_{\infty}}{\ell} \left\{ \frac{1}{1 + \frac{1}{2}\theta} \right\} \qquad (3.22)$$

In the single phase experiments alkali is continuously added as the flux of acid is being monitored. It is this volume addition that is causing mass flow through the filter. To see if this is significant, a value of θ must be estimated. The flow velocity may be estimated since 1 cm^3 of alkali is added in approximately three hours; the area of the filter is 2 cm^2:

$$v = \frac{0.50}{3 \times 60 \times 60} \quad \text{cm. } s^{-1}$$

$$\ell \sim 3 \times 10^{-2} \text{ cm}$$

$$D \sim 10^{-5} \text{ cm}^2 \text{ s}^{-1}$$

$$\theta = \frac{v\ell}{D} = .14$$

Thus θ is not very much smaller than 1. Although small volumes are being added over a fairly long period of time the effect of mass flow is significant because diffusion processes are very slow.

(d) Minimising the effects of mass flow

In order to prevent mass flow occurring a constant head device was designed. In essence this removes an equivalent volume of solution from the outer compartment as soon as it has been added from the autoburette.

The first design for keeping the outer compartment volume constant involved the immersion of a drawn out glass tube into the apparatus. The tip of the tube just touched the liquid surface and the other end was connected to a vacuum pump. Thus as alkali was added the excess fluid was sucked away by the vacuum. Two problems arose in this type of experiment.

i) The Scallop Effect. At low rotation speeds there is no turbulence on the surface of the liquid in the outer compartment. As a result of this the liquid level varies between narrow limits even though excess added fluid is being continuously removed. The variation is a result of a surface tension effect. When the vacuum tube just touches the surface, liquid is drawn away to a lower level depending on the degree of surface tension. This is shown diagrammatically in figure (27). In case (a) liquid is just being sucked away; case (b) shows that the fluid will drop to a level dependent on the surface tension strength. As soon as the surface tension is not sufficiently strong to support the weight of water the tube will stop sucking (c). Case (c) will then build up to case (a) as alkali is added. The hydrostatic pressure difference thus alters by an amount Δx. In case (a) the observed flux will be less than case (c). Since a cyclical process is happening a "scalloping" effect is seen in the alkali added/time plots (figure (28)). At high rotation speeds, there is turbulence on the liquid surface which tends to break the surface tension effect and case (b) never arises. At these speeds the scalloping on the alkali/time traces is not observed.

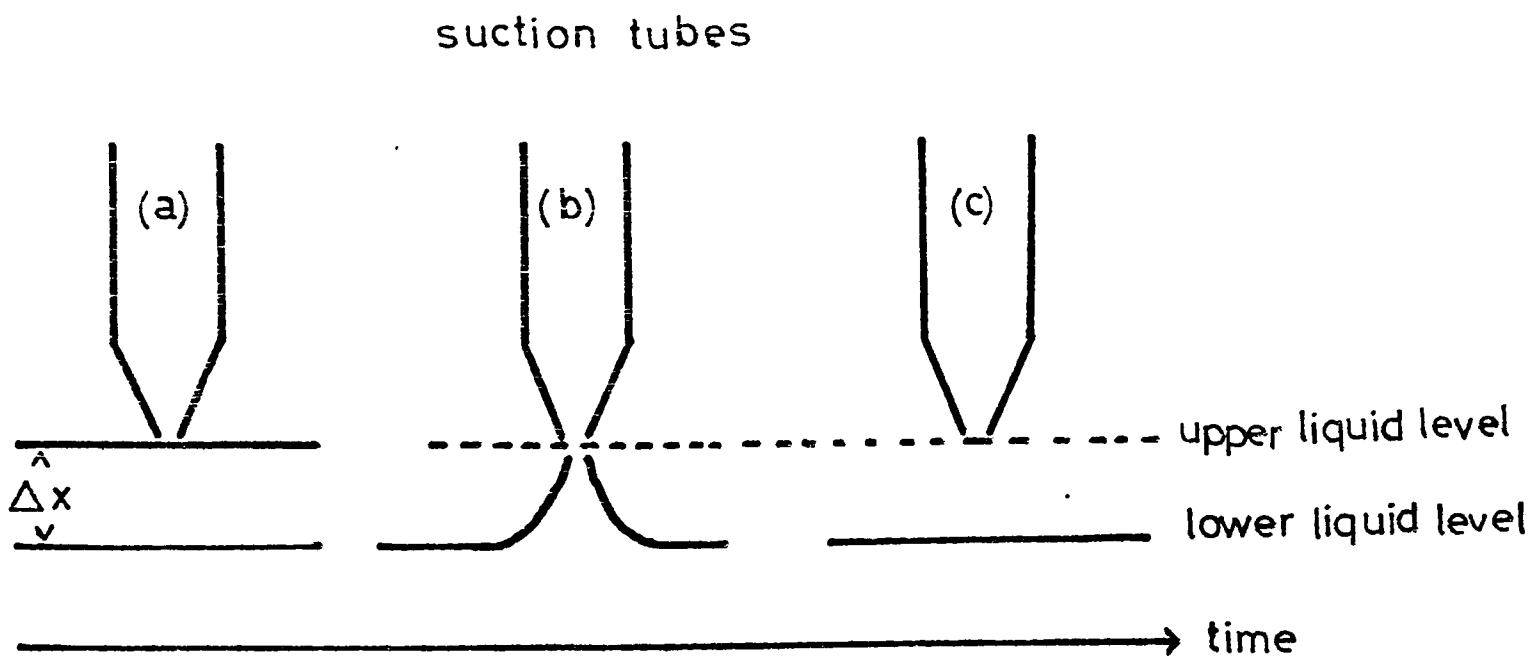

Figure (27). Changes in liquid levels to cause scalloping effect.

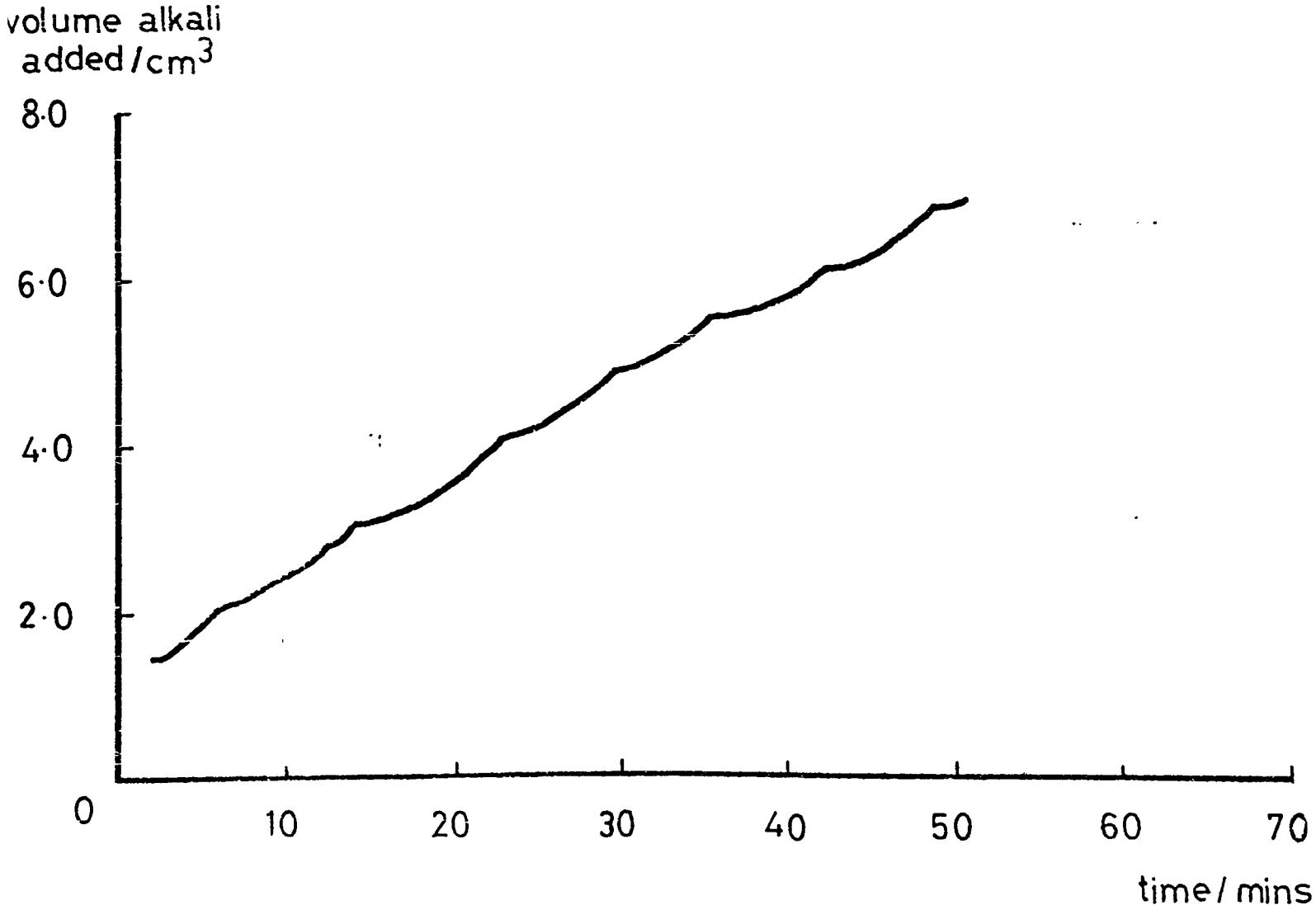

Figure (28). Flux trace showing scalloping effect.

ii) The vortexing problem. The two extreme cases are shown in figure (29). At low rotation velocities the liquid level is maintained by the inserted vacuum tube. At increased speeds the liquid in the outer compartment tends to vortex as shown in case II. When this happens the tube will not suck any fluid away. Liquid will flow from the outer compartment to the inner compartment due to the increased hydrostatic pressure as alkali is added. After some time a steady state situation will arise when the liquid level has risen and added fluid is again sucked away ($t+\delta t$). When this has occurred the bulk concentration in the inner compartment will have been decreased by a non calculable amount.

If the apparatus is again slowed down, the liquid level will now be above the tube (case I, $t+\delta t$). The fluid will be removed to the old level (t) and an excess hydrostatic pressure exists in the inner compartment. Mass transfer occurs from the inner to the outer compartment until the level reaches the original one and a new steady state exists.

Various suction tubes were designed to try and minimise the scalloping effect. In order to prevent the vortexing problem, the experiment was always conducted such that if there was any mass transfer it was from the inner to the outer compartment. Thus when the new steady state is established, the bulk concentration in the inner compartment can still be calculated. Any mass transfer in the opposite direction renders calculation of the bulk concentration impossible. Some of the designs of the

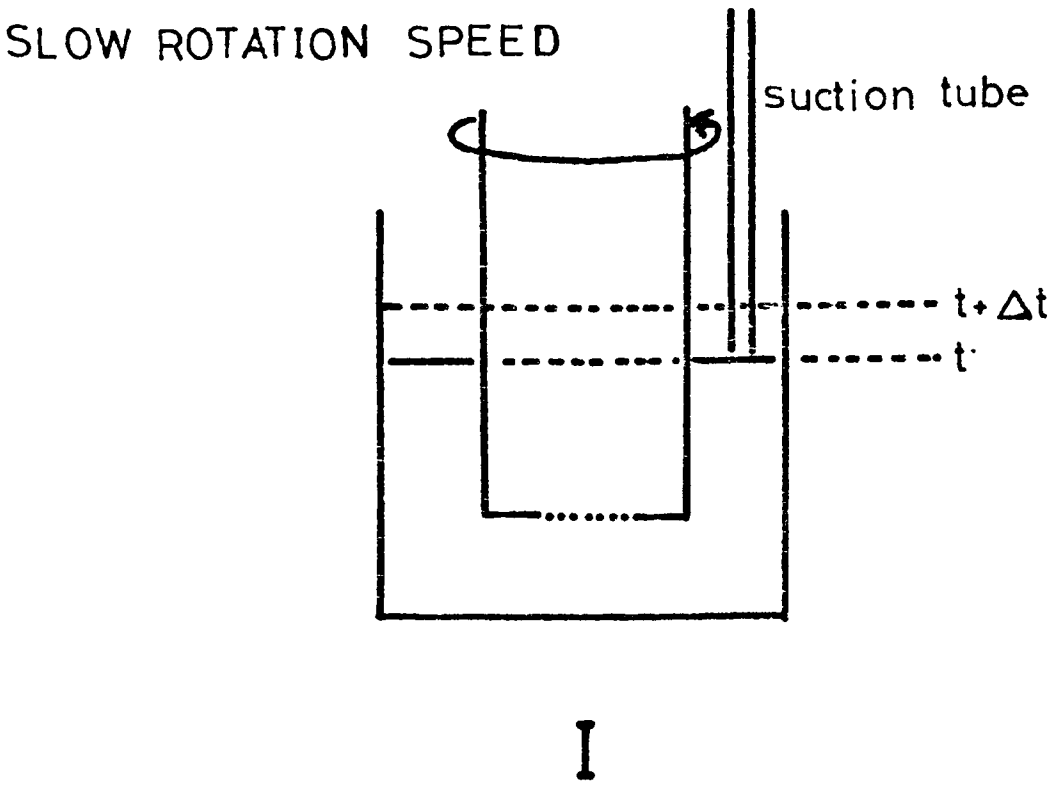

Figure (29). The Vortexing Problem.

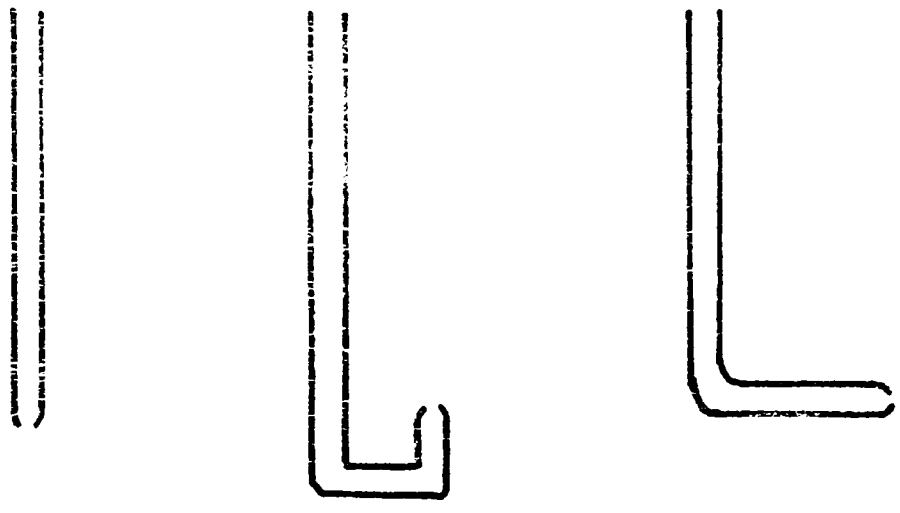

Figure (30). Designs of various suction tubes used for the single phase experiments.

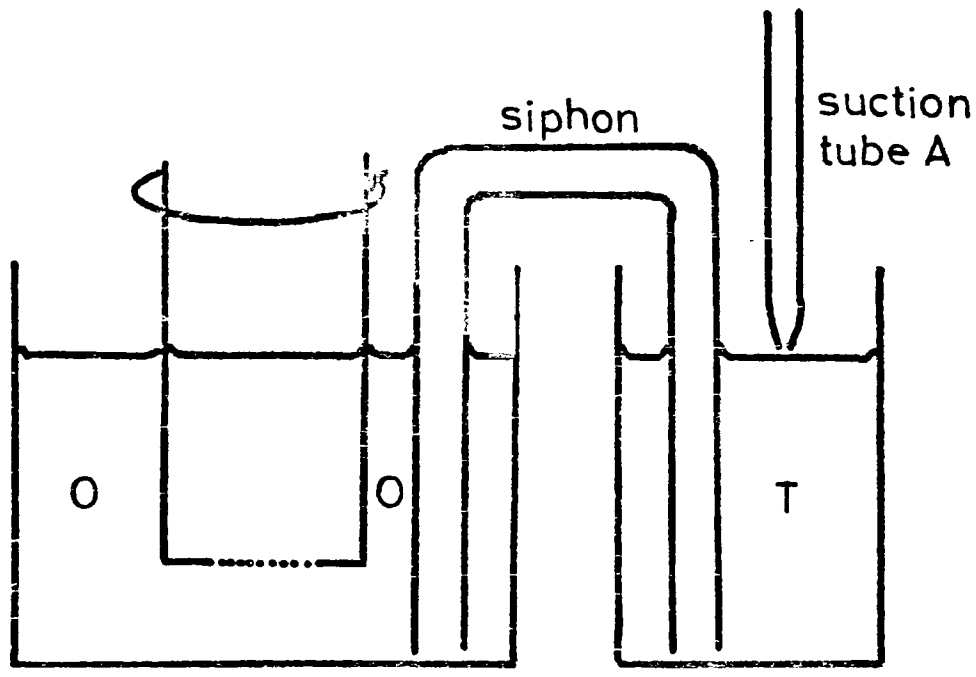

Figure (31). The rotating diffusion cell with siphon inserted to maintain a constant level in the outer compartment O.

suction tubes are shown in figure (30). For these designs and others no accurate reproducible relationship between $1/\beta$ and $W^{-\frac{1}{2}}$ could be found and one last attempt was made to maintain a constant liquid level in the outer compartment.

A siphon, figure (31), was introduced into the outer compartment (O) and registered the change in pressure by siphoning liquid into or out of the side tube (T). The level in the side tube was kept constant using a tube (A) connected to a vacuum pump. The vortexing problem is prevented by this technique and it was hoped that there may be sufficient damping in the siphon to cut down the scalloping effect. Again the scalloping effect was observed which shows how sensitive the system is to mass flow. No reproducible results were obtained from the runs performed.

It was obvious at this stage that in order to produce any consistent results the problem of mass transfer had to be overcome. In order to achieve this no simple method could be thought of whilst keeping to a single phase system.

2. Two Phase Experiments

In a two phase experiment the interfacial surface tension should locate the interface accurately on the surface of the filter and should be sufficient to maintain small hydrostatic pressure differences. The pressure supported by an interface is given by the following equation

$$P = 2\gamma/r \qquad (3.23)$$

where γ is the interfacial surface tension and r is the pore size of the filter. For Millipore filters $r < 5$ μm and for a carbon tetrachloride/water interface, $\gamma = 45$ mN m^{-1} [110].

$$P = 18 \times 10^3 \text{ Nm}^{-2} \text{ or } \sim 0.2 \text{ atmospheres.}$$

A pressure as large as this should be sufficient to maintain liquid levels in the rotating diffusion cell and thus prevent mass flow occurring.

(i) Interface Stability

The organic fluids used in the two phase experiments described previously[31] were carbon tetrachloride and isopropyl myristate. Experiments were conducted to determine the stability of interfaces formed on Millipore filters between these two organic solvents and water.

(a). Carbon Tetrachloride. If the levels in the inner compartment (organic phase) and outer compartment (aqueous phase) are equal, the interface formed on the lower surface of the Millipore filter is not stable. Carbon tetrachloride flows through the filter and collects in the outer compartment. This flow may be prevented by maintaining the aqueous level several centimetres above that of the organic phase. Some two phase kinetic studies have been studied using this technique[117]. The instability is attributed to the high density of the carbon tetrachloride.

(b) Isopropyl myristate. Isopropyl myristate has a density less than 1 and consequently should be more stable in the inner compartment than carbon tetrachloride. Experiments showed that the interface formed was remarkably stable. The stability of the interface was improved if the filter was pretreated with repelcote. This pretreatment renders the filters water repellent and any tendency for the water to 'creep' into the filter is minimised. In subsequent experiments where the filter is saturated with an organic phase it has always been pretreated with repelcote.

(ii) Experimental Procedure

The most satisfactory method of filling the rotating diffusion cell for a two phase experiment is as follows:-

(a) The filter is impregnated with the phase it is to contain. Any excess fluid present is removed with absorbent tissue.

(b) The apparatus is assembled in position and the motor switched on.

(c) The aqueous phase is added to the outer compartment until its level just reaches the lower surface of the filter.

(d) Both compartments are then filled simultaneously.

(e) The flux of diffusant is monitored.

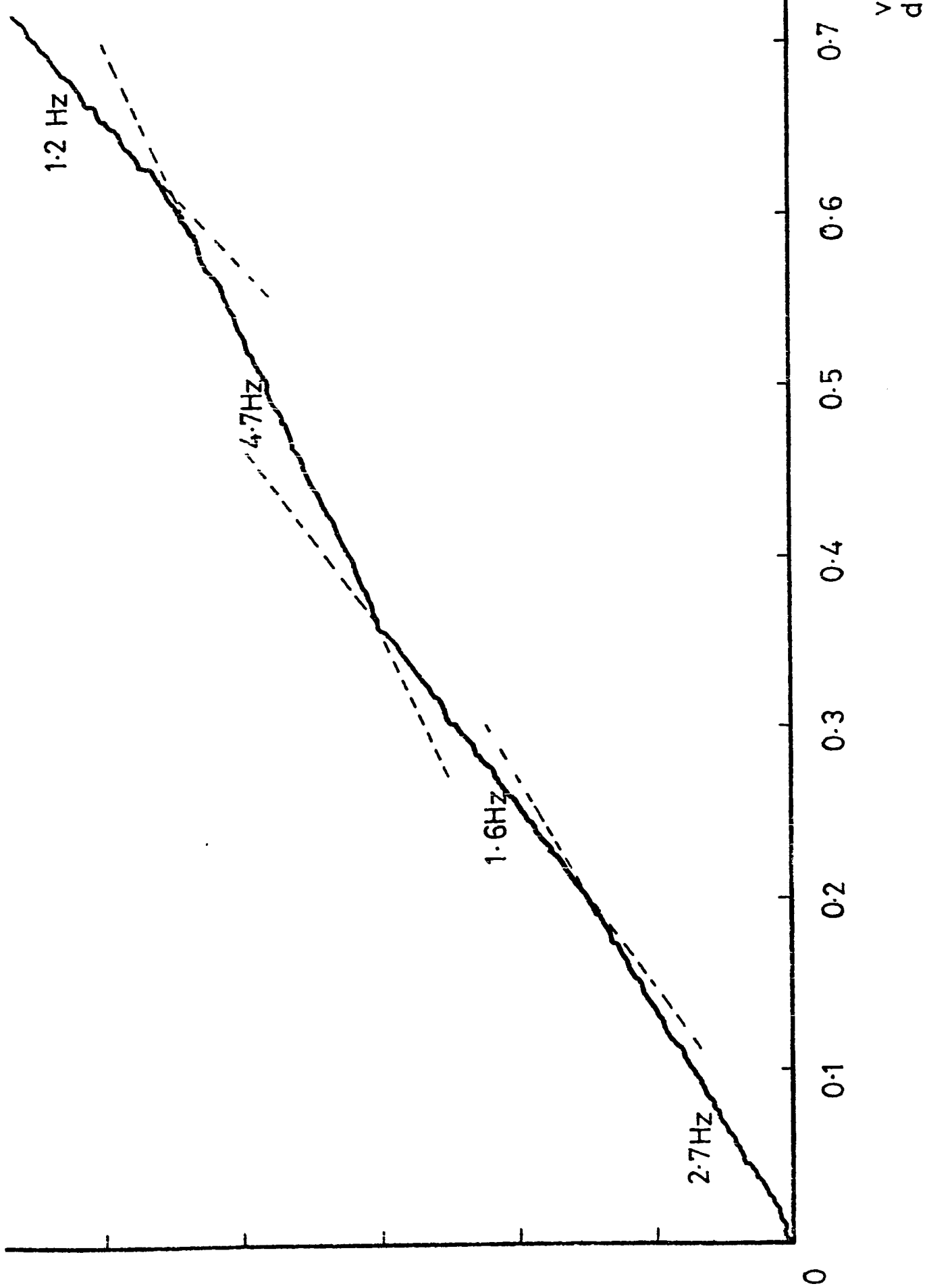

Figure (32). Typical experimental trace for sandwich experiment using hexoic acid diffusing across a hexane sandwich.

(iii) Results

The transport of various carboxylic acids was investigated since a continuous monitor of their flux may be achieved using the pH stat technique[88]. All the results obtained were at 298°K. Figure (32) shows a typical pH stat trace for a two phase experiment. The rapid response for the thin filter is clearly seen when the rotation speed is changed. Steady state conditions will be established in ~ 20 seconds whereas the conventional Stokes Cell requires several hours[88].

The systems studied to characterise the hydrodynamics will be dealt with in turn. In all cases the experimental points are plotted on a graph and the theoretical gradient from the Levich equation forced through them. This produces an estimate for the intercept which describes the diffusion through the filter and any interfacial rate processes which are significant. The test for good hydrodynamics is that the experimental points lie on the line predicted by the Levich equation.

System I. Substrate, acetic acid; phases isopropyl myristate/water.

(a) Outer

The IPM/water interface is located on the outer surface of the filter and

$$\frac{1}{\vec{k}} = \frac{Z_{D*}}{D_*} + \frac{\ell}{\alpha D_*} + \frac{1}{\alpha k_I} + \frac{Z_{D_\phi}}{D_\phi K_p} \qquad (3.11)$$

In this experiment $K_p = 25.3$ and $\frac{Z_{D*}}{D_*} > \frac{Z_{D_\phi}}{D_\phi K_p}$. The experiment is thus testing the hydrodynamics in the inner compartment.

There is a further complication to equation (3.11) caused by the dimerisation of the acetic acid in the isopropyl myristate . From equation (2.19) page (50) a correction f to account for dimerisation is needed. Equation (3.11) corrected becomes

$$\frac{f}{\vec{k}} = \frac{Z_{D_m}}{D_m} + \frac{\ell}{\alpha D_m} + \frac{f}{\alpha k_I} \qquad (3.24)$$

where

$$f = \frac{1 + 2D_B K_b m_e / D_m}{1 + 2K_b m_e} = 0.88 \qquad (3.25)$$

and

D_m is the diffusion coefficient of acetic acid monomers [Table (6) page (54)]

D_B is the diffusion coefficient of acetic acid dimers [Table (6) page (54)]

K_b is the monomer/dimer equilibrium constant [Figure (10) page (57)]

m_e is the monomer concentration in the bulk organic phase.

The concentration of acetic acid used in these experiments was 0.298 M. This is the same concentration that was used in the Stokes Cell experiment and thus there is a comparable degree of dimerisation in both sets of experiments. A 5mM solution of barium acetate was used as the background electrolyte in the outer compartment.

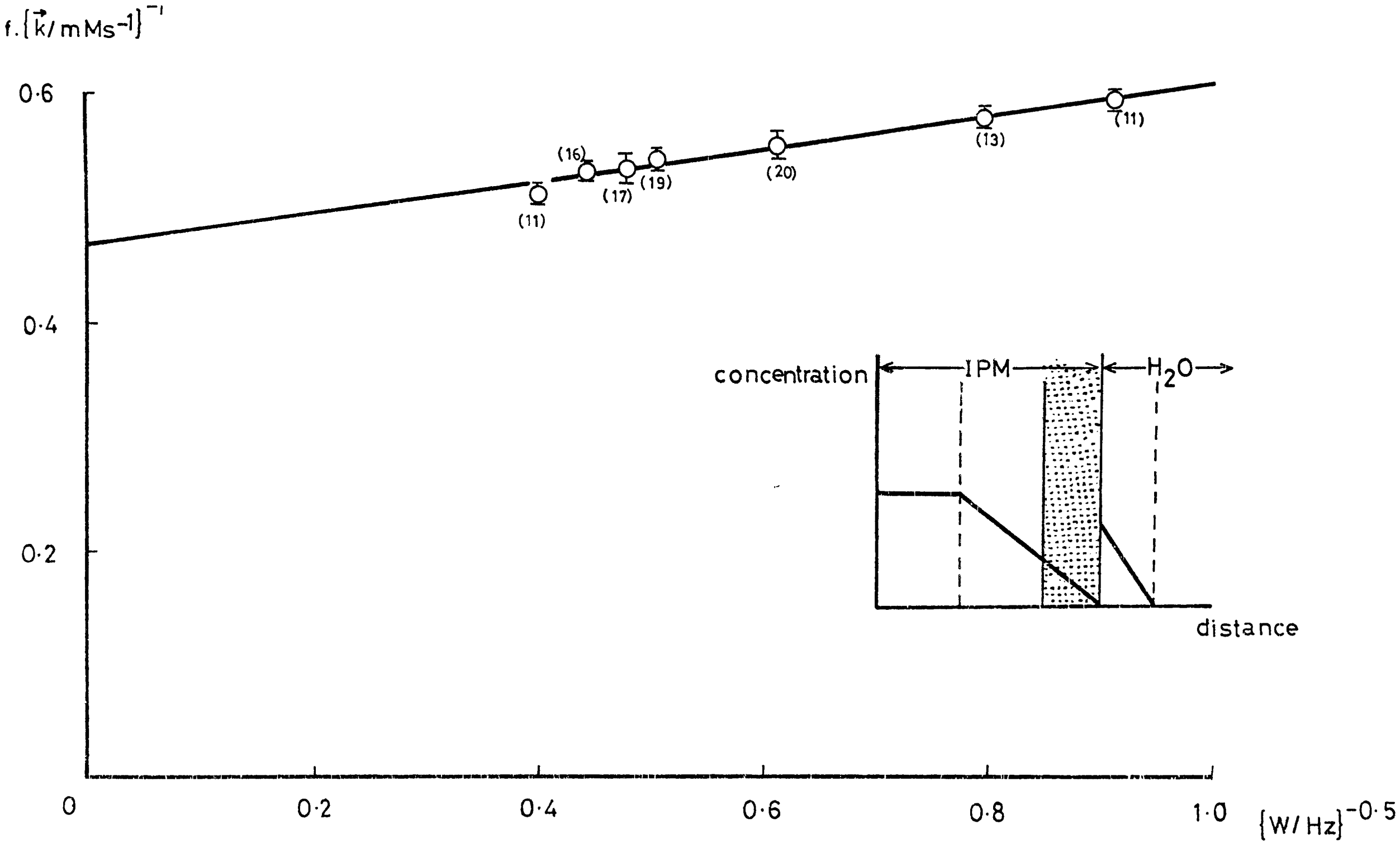

Figure (33). $f.(\vec{k})^{-1}$ vs $W^{-\frac{1}{2}}$ plot for acetic acid in IPM/H_2O outer experiment. The figures in parentheses show the number of determinations performed at that point.

Five experiments were conducted on this system. In each experiment the flux of acetic acid diffusing was measured at seven rotation speeds, the speeds being varied over the range 1 to 7 Hz. During the experiment the rotation speeds are chosen at random, each being selected three times. The mean flux is then calculated for each rotation speed. A value for $(f/\vec{k})$ is estimated which is plotted as a function of the rotation speed in figure (33). The insert in figure (33) shows diagrammatically the concentration profile for the system. The straight line drawn through the points in figure (33) is the theoretical gradient predicted by the Levich equation. From equation (3.24) the theoretical gradient is given by expanding the term Z_{D_m}/D_m

$$\begin{aligned} &= 0.643\ \nu^{1/6}\ D_m^{-2/3} \\ &= .141\ \text{Ms}\ \text{m}^{-1}\ \text{Hz}^{\frac{1}{2}} \end{aligned} \qquad (3.26)$$

where ν is the kinematic viscosity of IPM at 298°K (Table (5) page (53)).

Since the experimental points lie on the theoretical line, the hydrodynamic flow achieved in the inner compartment is correct and is accurately described by the Levich equation.

The intercept generated by the experimental points and the theoretical gradient corresponds to diffusion through the filter and to the interfacial transfer process (the last two terms in equation (3.24)). The term for diffusion through the

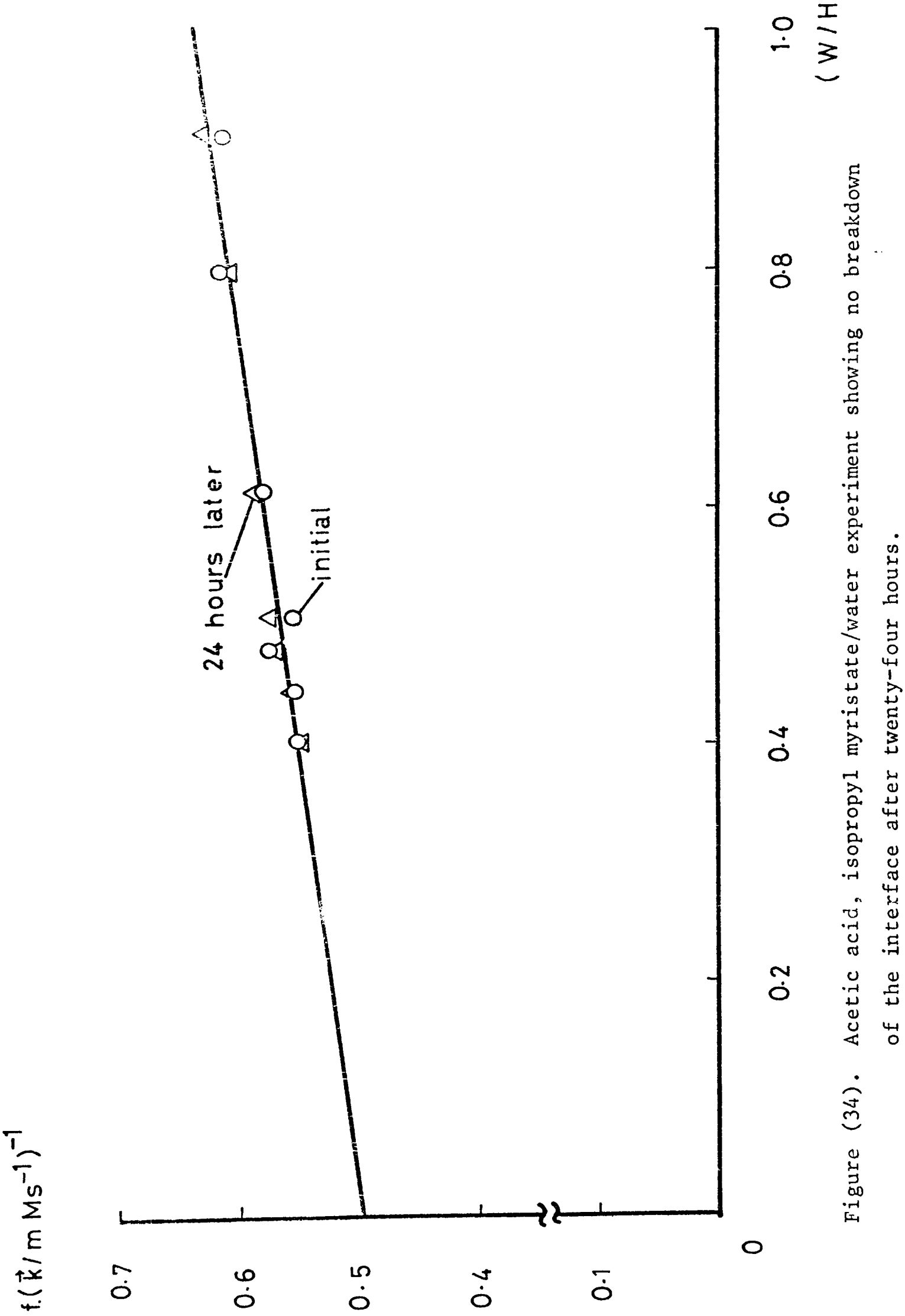

Figure (34). Acetic acid, isopropyl myristate/water experiment showing no breakdown of the interface after twenty-four hours.

filter can be calculated. In these experiments 5 μm MF filters were used the α and ℓ values for which are given in Table (8) (page 72). Thus a value for k_I ,the interfacial term,may be calculated

$$k_I/m\ Ms^{-1} = 7.18 \pm 0.3$$

$$k_{-I}/m\ Ms^{-1} = 0.28 \pm 0.02$$

The value for k_{-I} has been calculated by using the monomeric partition coefficient since experiment showed that there was very little dimerisation in this system.

Interface Stability. In order to test the stability of the interface, an experiment was left overnight and flux measurements resumed after 24 hours had elapsed. The results are shown in figure (34). The gradients obtained on the successive days and the reproducibility of the fluxes indicate that the interface has remained intact.

(b) Sandwich

A sandwich of IPM is placed between two aqueous phases. Two interfaces are established, one on the inner surface and one on the outer surface of the 1.2 μm MF filter. The experiment was performed to investigate the stability of this type of system. Sandwich experiments are particularly important since these are to be used later as the models for percutaneous absorption.

The rate constant, $\vec{k}$, for the transfer process is given by equation (3.13)

$$\frac{1}{\vec{k}} = \frac{2Z_{D_\phi}}{D_\phi} + \frac{2}{\alpha k_{-I}} + \frac{\ell K_p}{\alpha D_*} \qquad (3.13)$$

Allowing for dimerisation in the organic phase

$$\frac{1}{\vec{k}} = \frac{2Z_{D_\phi}}{D_\phi} + \frac{2}{\alpha k_{-I}} + \frac{\ell K_p}{f\alpha D_m} \qquad (3.27)$$

where f in this case is 0.98, the larger value of f is due to the decreased acetic acid concentration.

Two experiments were conducted with flux measurements being determined at three rotation speeds. The concentration of acetic acid used was 0.1 M and 5 mM barium acetate was used as the background electrolyte. The observed fluxes were very small ~ 1 mol. Gs^{-1} and no marked variation of flux with rotation speed was observed. The results are given in table (9).

Table (9). Results for the acetic acid, IPM sandwich experiment.

Rotation Speed /Hz	Flux/mol.Gs^{-1}	$(\vec{k}/m.Ms^{-1})^{-1}$	Calculated Intercept/ $Ms.m^{-1}$
3.34	1.1	18.27	18.21
4.48	1.08	18.61	18.56
5.64	1.1	18.27	18.22

The calculated intercepts were obtained by forcing the theoretical gradient through the experimental points. The theoretical gradient from the Levich equation and equation (3.13) is

$$2 \times 0.643\ \nu^{1/6}\ D^{-2/3} = 0.11\ \text{Ms}\ \text{m}^{-1}\ \text{Hz}^{\frac{1}{2}} \qquad (3.14)$$

An estimate for k_{-I} can be calculated since the intercept is the sum of the two final terms in equation (3.13).

$$k_I/\text{m Ms}^{-1} = 7.27 \pm 0.3$$

therefore $$k_{-I}/\text{m Ms}^{-1} = 0.29 \pm 0.02\ .$$

These values compare very well with those obtained in the outer experiment described previously.

Interfacial Stability of the Organic Sandwich. The interface stability was very good. A large pressure difference could be maintained over a twenty-four hour period with no apparent mass transfer. Breakdown of the interface may be detected visually by inspecting the filter after the experiment. When the filter is impregnated with IPM it appears translucent, any water which permeates the filter renders it white. No white patches could be seen after a sandwich experiment had been left for three days.

The strength of the interfacial tension may also be demonstrated by lifting the inner compartment out of the liquid in the outer compartment. For some time the aqueous solution

in the inner compartment will remain in the inner compartment, the weight being supported by the interfacial surface tension.

System II. Substrate n-hexoic acid, phases hexane/water.

(a) Outer

Equation (3.11) is the appropriate solution for this system

$$\frac{1}{\vec{k}} = \frac{Z_{D*}}{D_*} + \frac{\ell}{\alpha D_*} + \frac{1}{\alpha k_I} + \frac{Z_{D_\phi}}{D_\phi K_p} \qquad (3.11)$$

In this experiment $K_p = 9.7 \times 10^{-2}$ and $D_* > D_\phi$ thus

$$\frac{Z_{D_\phi}}{D_\phi K_p} > \frac{Z_{D_*}}{D_*}$$

The experiment is thus testing the hydrodynamics in the outer compartment. Although dimerisation occurs significantly in this system the diffusion processes in the organic layers are not rate determining and hence no correction has to be made.

The concentration of hexoic acid in hexane used for the experiments was 0.2 M and 5 mM potassium chloride was used as the background electrolyte. Two experiments were conducted and the results are shown in figure (35). The insert in the figure is a diagrammatic representation of the concentration profile in the system. The lines drawn on the graph are the

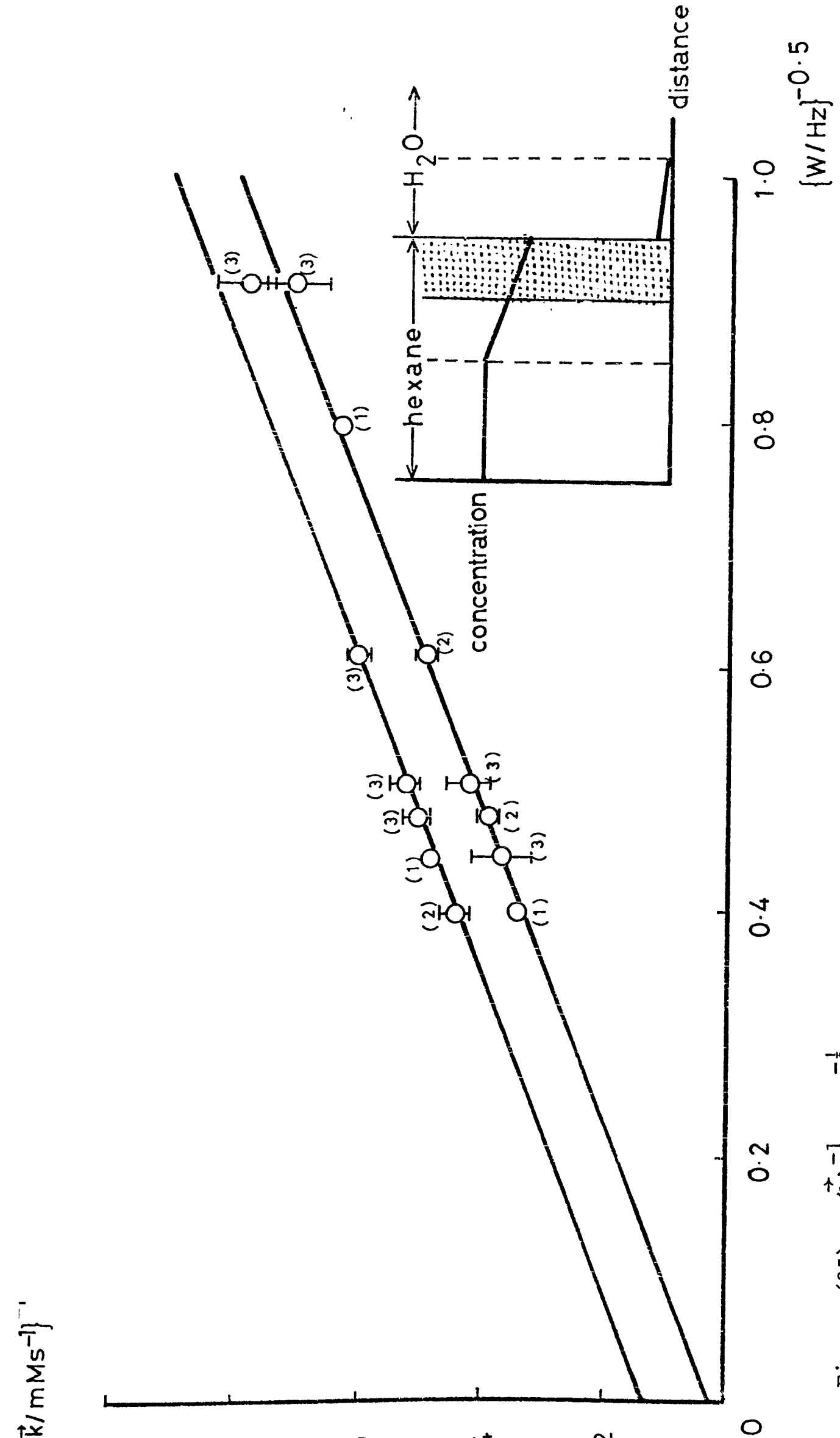

Figure (35). $(\vec{k})^{-1}$ vs $W^{-\frac{1}{2}}$ plot for hexoic acid in hexane/H_2O outer experiment.

theoretical gradients predicted by the Levich equation. The good correlation shows that the hydrodynamics produced in the outer compartment is described accurately by the Levich equation.

Hexane has a high volatility and evaporation of the solvent causes the length 'ℓ' of the impregnated filter to vary. Because of this variation of ℓ, the interfacial terms cannot be separated out and no estimates for k_I and k_{-I} for this system can be made.

(b) Sandwich

The hydrodynamics on both sides of the filter may be tested in a sandwich type experiment where solution of the flux equations give

$$\frac{1}{\vec{k}} = \frac{2Z}{D_\phi} + \frac{2}{\alpha k_{-I}} + \frac{\ell K_p}{\alpha D_*} \qquad (3.13)$$

Hexoic acid is not very soluble in water and the bulk concentration used (0.02 M) is a factor of one hundred lower for these experiments. Potassium chloride is used as the background electrolyte. Four experiments were completed, the results are shown in figure (36). The theoretical gradient has been forced through the points, the good agreement shows that the hydrodynamics on both sides of the filter are those predicted by the Levich equation.

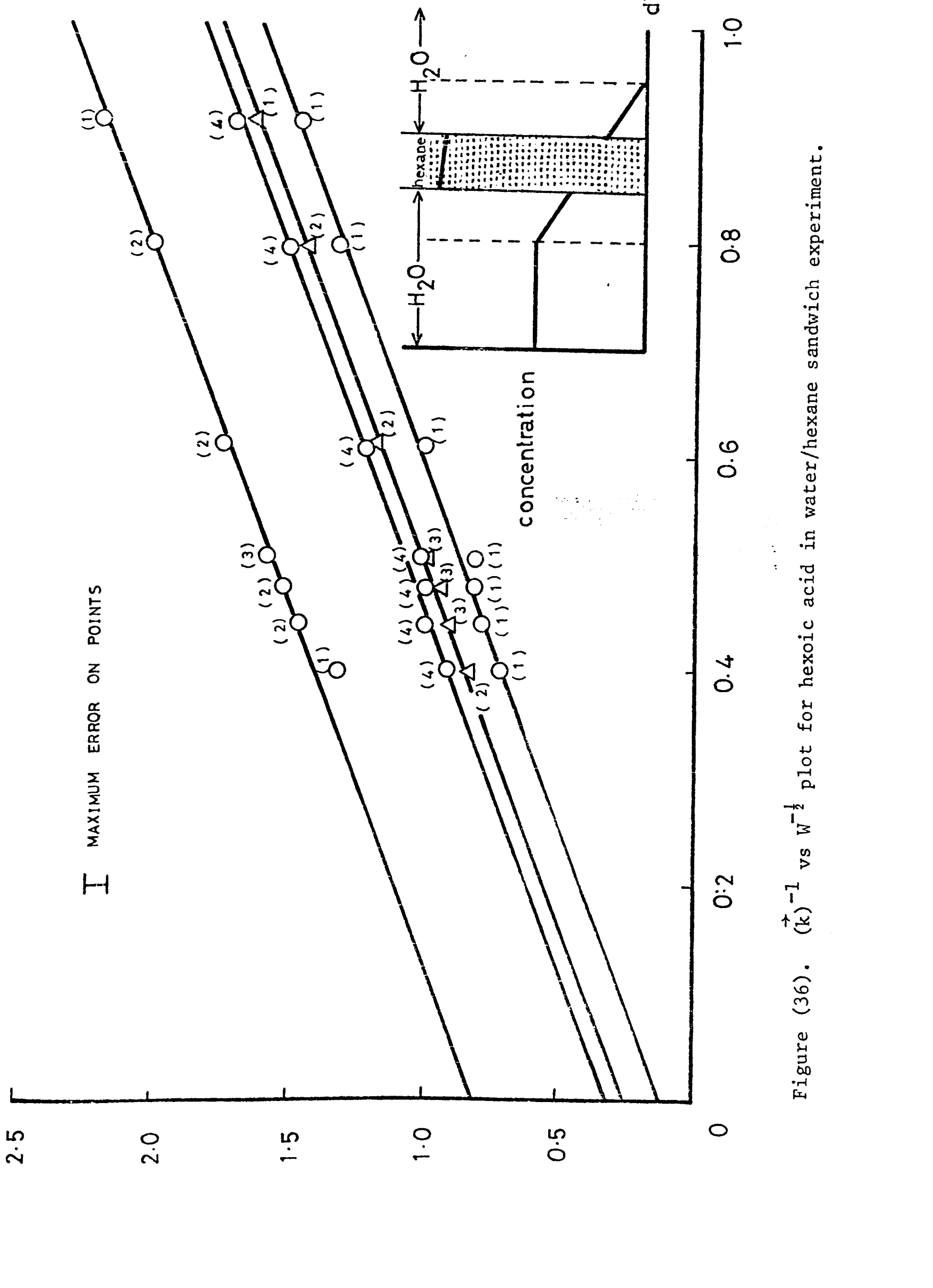

Figure (36). $(\vec{k})^{-1}$ vs $W^{-\frac{1}{2}}$ plot for hexoic acid in water/hexane sandwich experiment.

Again, the intercept variation between experiments has been caused by solvent evaporation during impregnation of the filter. No determination of the interfacial transfer coefficients was possible for this system.

(c) Inner

This experiment with the interface located on the inner surface of the filter was performed to investigate if this type of system was stable. There was no pretreatment of the filter with repelcote since the filter was impregnated with an aqueous phase. The solutions used were the same as those for the 'outer' experiment.

The equation describing the transport processes is

$$\frac{1}{\vec{k}} = \frac{Z_{D_*}}{D_*} + \frac{1}{\alpha k_I} + \frac{\ell}{\alpha D_\phi K_p} + \frac{Z_{D_\phi}}{D_\phi K_p} \qquad (3.12)$$

Since $K_p = 9.7 \times 10^{-2}$ at the acid concentration used and $D_* > D_\phi$

$$\frac{Z_{D_\phi}}{D_\phi K_p} > \frac{Z_{D_*}}{D_*}$$

and the experiment tests the hydrodynamics in the outer compartment. There is no difficulty with solvent evaporating from the filter and a value for the interfacial transfer term may be obtained.

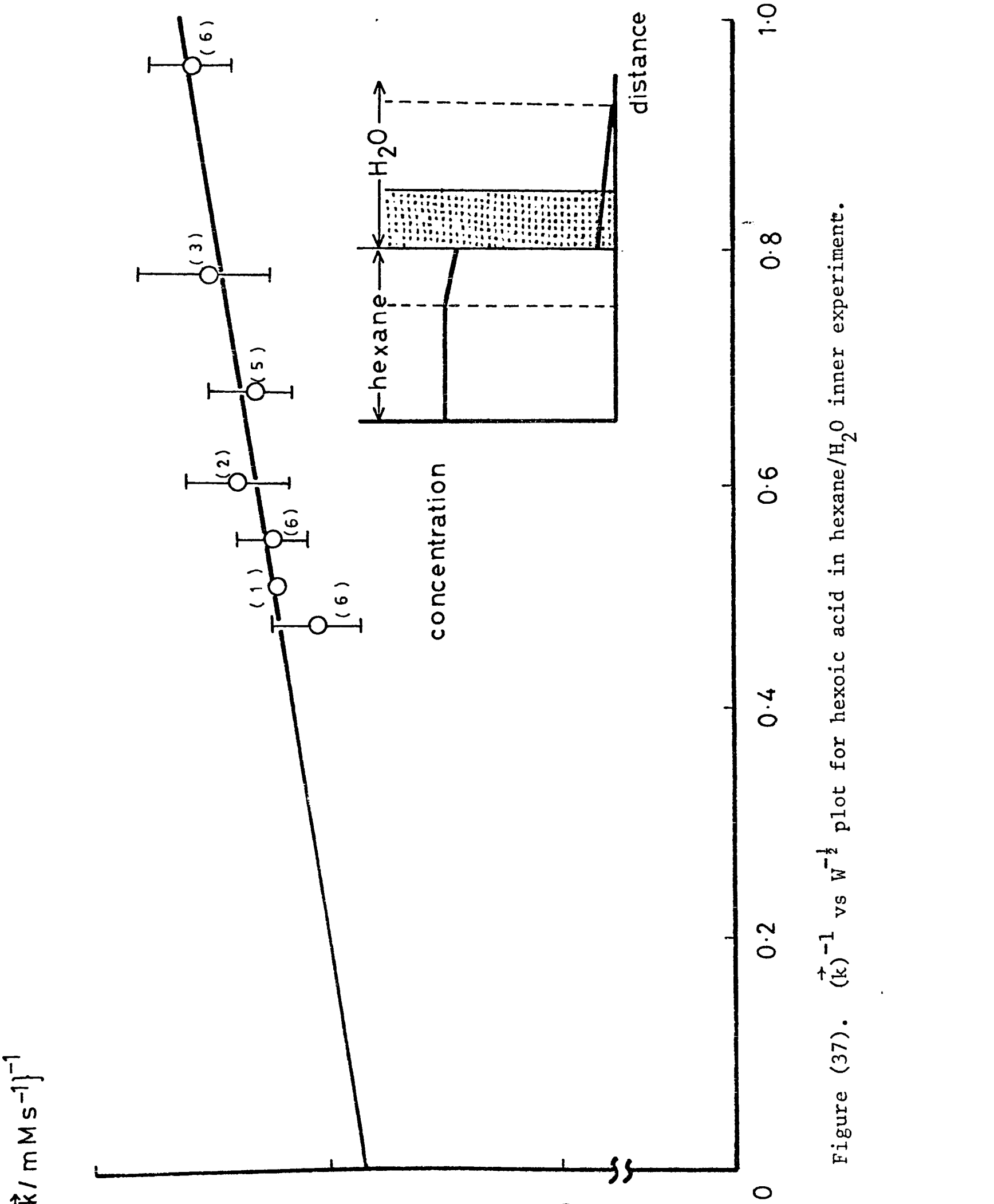

Figure (37). $(\vec{k})^{-1}$ vs $W^{-\frac{1}{2}}$ plot for hexoic acid in hexane/H_2O inner experiment.

Using the theoretical gradient of 0.767 Ms m^{-1} $Hz^{\frac{1}{2}}$ and the experimental points from four experiments (figure (37)) a value for the intercept at infinite rotation speed may be calculated.

$$\frac{1}{\vec{k}} = 2.87 \pm .02 \text{ Ms } m^{-1}$$

The contribution towards this intercept from the diffusion process through the filter is

$$\frac{150 \times 10^{-6}}{0.82 \times 0.78 \times 10^{-9} \times 9.7 \times 10^{-2}} = 2.42 \text{ Ms. } m^{-1}$$

Thus for this system k_I and k_{-I} may be calculated.

$$k_I/m \text{ Ms}^{-1} = 2.7 \pm 0.2$$
$$k_{-I}/m \text{ Ms}^{-1} = 28 \pm 1.6$$

3. Discussion

The systems studied are summarised in Table (10). Five different systems have been chosen to characterise the hydrodynamics in both the inner and the outer compartment. In all cases the experimental points agree extremely well with the theoretical gradients predicted by the Levich equation. The good agreement between theory and experiment shows that the correct hydrodynamic conditions for controlled transport have been achieved both inside and outside the disc for all systems studied. Further verification

Table (10) Two Phase Systems Studied

	Substrate	Inner Phase	Filter[(a)]	Outer Phase	Size of Z_D term[(b)]
1	acetic acid	IPM	IPM *	water	inner
2	acetic acid	water *	IPM *	water	both
3	hexoic acid	hexane	hexane *	water	outer
4	hexoic acid	water *	hexane *	water	both
5	hexoic acid	hexane *	water	water	outer

(a) Asterisks indicate position of interface(s)

(b) The dominant Z_D term in the different flux equations.

is obtained in further experiments conducted on various esters of nicotinic acid.

The interfacial transfer coefficients obtained will be discussed later.

CHAPTER IV

THE DIFFUSION OF NICOTINIC ACID ESTERS & BETAMETHASONE.17.VALERATE ACROSS ISOPROPYL MYRISTATE

IPM has been used by various researchers as a model for skin. *In vivo* and *in vitro* correlation shows that the choice of IPM for this purpose is quite successful. By studying the transfer of physiologically active substances across a water/IPM interface in the rotating diffusion cell it may be possible to obtain information about the fundamental processes involved in percutaneous absorption.

In order to simulate skin a sandwich experiment is used where IPM is the organic phase contained in the pores of a millipore filter. The use of this three compartment model is analogous to the *in vivo* situation of drug in vehicle; skin; aqueous sink. In these preliminary experiments only very simple systems have been studied. Transport phenomena across interfaces are poorly described in the literature and usually the more simple the system chosen, the easier it is to separate and understand the different fundamental steps involved.

The physiologically active substrates chosen for the experiments are three esters of nicotinic acid: methyl, n-butyl and n-hexyl. These have been chosen since the rate of percutaneous absorption is easily measured by their ability to cause vasodilation[73]. The esters cover a wide range of ether/water partition coefficients[125] which should be reflected in their transport properties.

I. Methyl Nicotinate

The transport of the methyl ester across a water/IPM interface has been previously studied in a conventional Stokes Cell[31]. In this case no interfacial barrier could be detected since the rate determining process was the diffusion across the impregnated glass sinter. The nicotinate flux was followed by a pH stat technique. At pH 10 the hydrolysis rate constant is 5.05 Ms^{-1} (298°K) which is fast enough to allow the diffusion process to be monitored.

A similar technique was adopted in the rotating diffusion cell. The main problem encountered when using this method is the large absorption of carbon dioxide at pH 10. The rotating diffusion cell has a loose fitting lid and the passage of nitrogen through and over the liquid in the outer compartment was insufficient to prevent carbon dioxide absorption.

i. Experimental Procedure for pH stat detection of methyl nicotinate

In order to minimise the absorption of carbon dioxide a perspex box was constructed around the rotating cell and motor. The joints between the perspex sheets were sealed with perspex cement and other holes in the box where thermostatting pipes etc. entered were filled with silicone rubber. The lid was made as tight fitting as possible. 'Carbosorb' was placed in a petri dish in the box and nitrogen was flushed through the box as well as over the surface of the liquid in the cell. Blank runs were

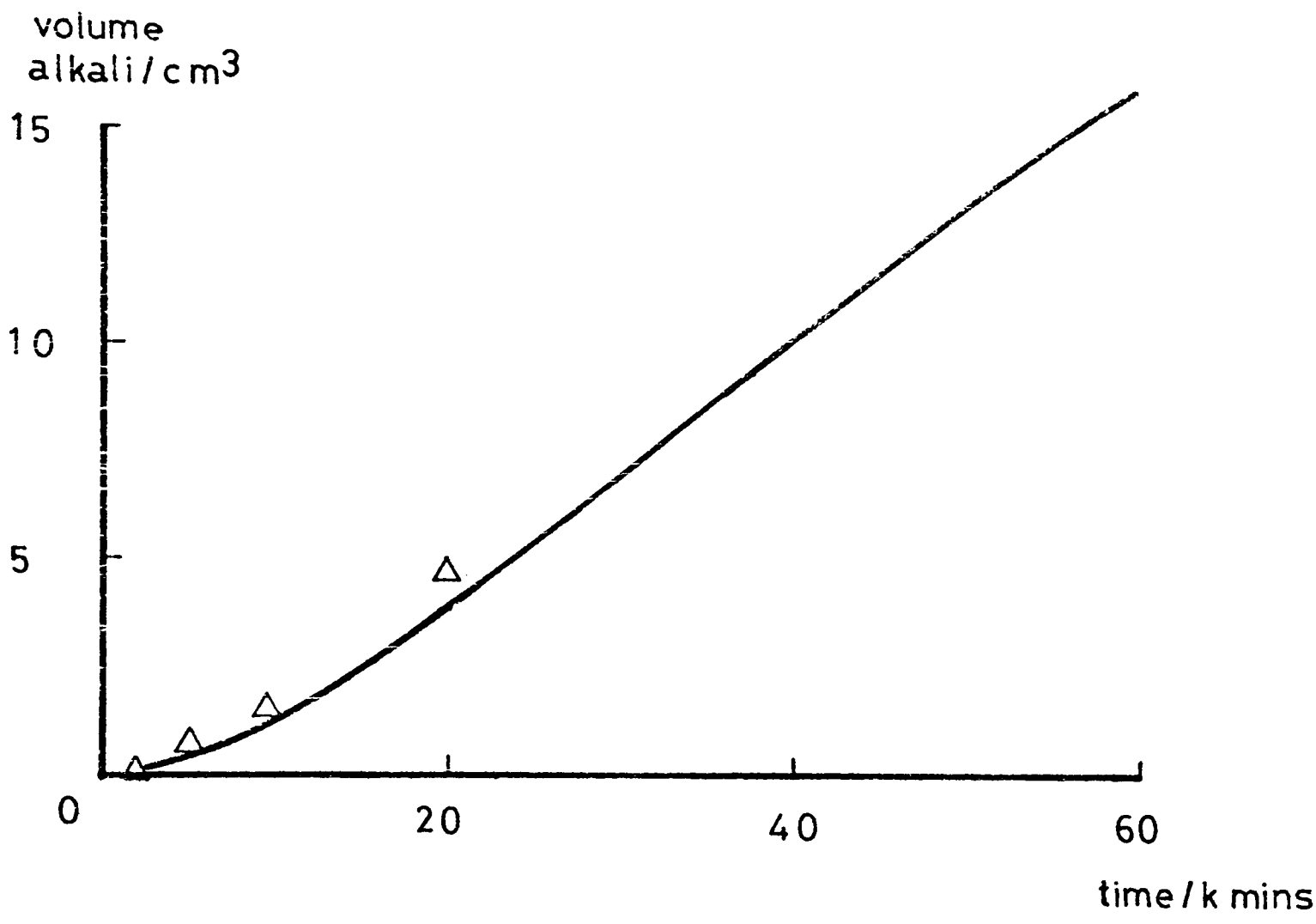

Figure (38). Theoretical curve for detection of methyl nicotinate as it diffuses and is hydrolysed at pH 10. The triangles represent some experimental points.

conducted and it was found that for short periods of time (2 - 3 hours) the flux due to the absorption of carbon dioxide at pH 10 could be kept below 0.4 mol Gs^{-1}.

Normal filling procedures were employed. Repelcoted 1.2 μm Millipore MF filters were used; 5 mM KCℓ was used as background electrolyte and 0.1 M methyl nicotinate was used in the inner compartment.

Some experimental points are shown in figure (38). The initial flux is slow whilst the concentration of the ester in the outer compartment builds up. After a while the trace straightens. At this stage it was found that variation of the rotation speed did not appear to change the flux significantly. This type of behaviour is expected when the theory for the experiment is examined.

ii. Theory for pH stat detection of methyl nicotinate

A sandwich experiment may be defined:-

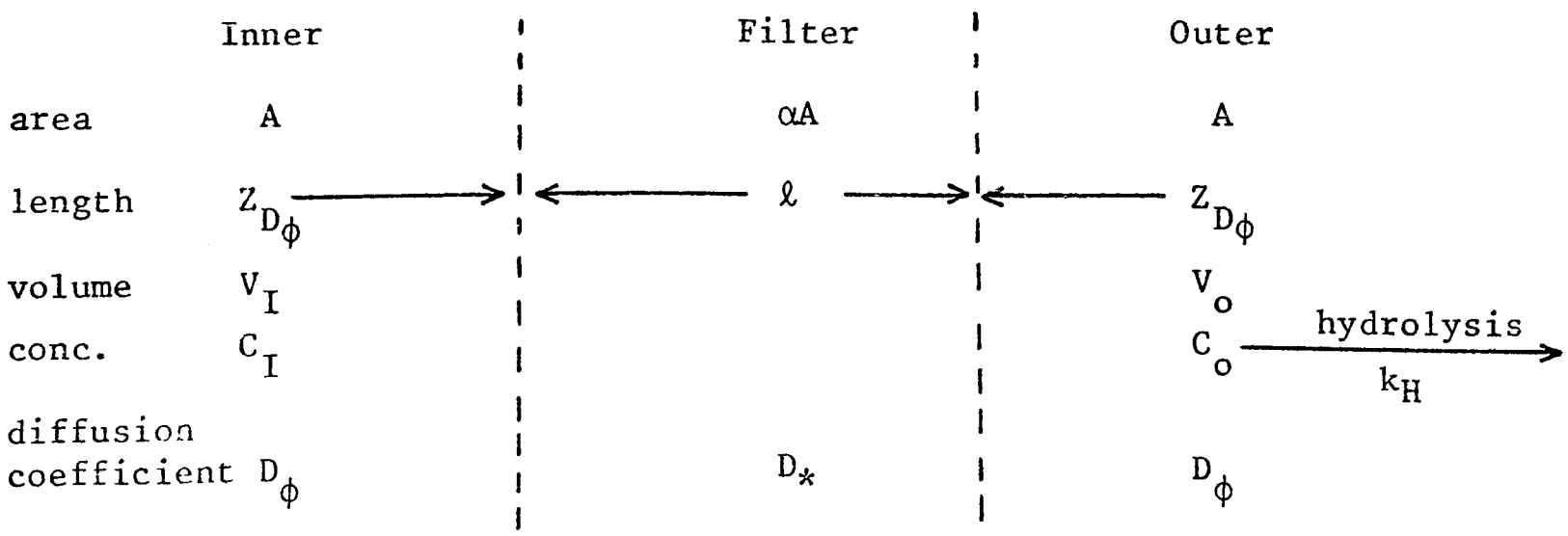

At time $t = 0$. $C_o = 0$. $C_I = C_{I,o}$.

Then

$$J = \vec{k}A\ (C_I - C_o) \tag{4.1}$$

Where $\vec{k}$ has been defined in equation (3.13)

$$\frac{1}{\vec{k}} = \frac{2Z_D\phi}{D_\phi} + \frac{2}{\alpha k_{-I}} + \frac{K_p \ell}{\alpha D_*} \tag{3.13}$$

and $$V_o\left(\frac{\partial C_o}{\partial t}\right) = J - k_H V_o C_o \tag{4.2}$$

$$J = -V_I\left(\frac{\partial C_I}{\partial t}\right) \tag{4.3}$$

Laplace transforming equations (4.1), (4.2), (4.3)

$$\bar{J} = \vec{k}A\ (\bar{C}_I - \bar{C}_o) \tag{4.4}$$

$$V_o s\bar{C}_o = \bar{J} - k_H V_o \bar{C}_o \tag{4.5}$$

$$\bar{J} = -V_I(s\bar{C}_I - C_{I,o}) \tag{4.6}$$

From equations (4.3, 4.4) and (4.5)

$$\bar{C}_I = \frac{\bar{J}}{A\vec{k}} + \bar{C}_o \tag{4.7}$$

$$\bar{J} = V_o\bar{C}_o(s + k_H) \tag{4.8}$$

$$\bar{C}_I = \frac{V_I C_{I,o} - \bar{J}}{V_I s} \tag{4.9}$$

From equations (4.7) and (4.9)

$$\overline{J}\left(\frac{V_I s}{A\vec{k}} + 1\right) + s\overline{C}_o V_I = V_I C_{I,o} \qquad (4.10)$$

Substituting equation (4.8)

$$V_o\overline{C}_o(s + k_H)\left(\frac{V_I s}{A\vec{k}} + 1\right) + s\overline{C}_o V_I = V_I C_{I,o} \qquad (4.11)$$

Therefore

$$V_o\overline{C}_o\left[(s + k_H)(s + k_*) + \frac{sV_I k_*}{V_o}\right] = V_I C_{I,o} k_* \qquad (4.12)$$

where

$$k_* = \frac{A\vec{k}}{V_I}$$

$$\text{therefore} \quad \overline{C}_o = \frac{V_I C_{I,o} k_*}{V_o\left[(s+k_H)(s+k_*) + \frac{sV_I}{V_o} k_*\right]} \qquad (4.13)$$

Separating into roots

$$\overline{C}_o = \frac{V_I C_{I,o} k_*}{V_o[(s+a)(s+b)]} \qquad (4.14)$$

$$\text{where} \quad a+b = k_H + k_*\left(1 + \frac{V_I}{V_o}\right) \qquad (4.15)$$

$$ab = k_H k_* \qquad (4.16)$$

But $k_H > k_*$ and both are very small ($\sim 10^{-5} s^{-1}$) thus the following approximations may be used to find values for k_H and k_*:

$$a = k_*(1 + \alpha) \qquad (4.17)$$

$$b = k_H(1 - \beta) \qquad (4.18)$$

For α and β small

$$\alpha \simeq \beta$$

Substituting equations (4.17) and (4.18) into equation (4.15) and since $\alpha k_* << \beta k_H$

$$\beta = - \frac{k_* V_I}{k_H V_o}$$

therefore

$$a = k_* \left(1 - \frac{k_* V_I}{k_H V_o} \right) \qquad (4.19)$$

$$b = k_H \left(1 + \frac{k_* V_I}{k_H V_o} \right) \qquad (4.20)$$

Inverting equation (4.14)

$$C_o = \frac{V_I C_{I,o} k_*}{V_o} \left\{ \frac{e^{-at} - e^{-bt}}{b - a} \right\} \qquad (4.21)$$

However the solution in which we are interested concerns the volume (V_{OH}) of alkali (concentration C_{OH}) added as a function of time.

$$C_{OH}\left(\frac{\partial V_{OH}}{\partial t}\right) = k_H V_o C_o \qquad (4.22)$$

Therefore
$$C_{OH}V_{OH} = \frac{V_I C_{Io}\, k_* k_H}{(b-a)} \int_o^t (e^{-at} - e^{-bt})dt \qquad (4.23)$$

$$= \frac{V_I C_{Io}\, k_* k_H}{(b-a)}\left[\left(\frac{1-e^{-at}}{a}\right) - \left(\frac{1-e^{-bt}}{b}\right)\right] \qquad (4.24)$$

$$= \frac{V_I C_{Io}\, k_* k_H}{ab}\left[\frac{b(1-e^{-at}) - a(1-e^{bt})}{(b-a)}\right] \qquad (4.25)$$

Substitution of equation (4.16) gives

$$V_{OH} = \frac{V_I C_{Io}}{C_{OH}}\left[1 - \left(\frac{be^{-at} - ae^{-bt}}{b-a}\right)\right] \qquad (4.26)$$

Thus the volume of alkali added as a function of time is given by a double exponential, equation (4.26). From the experimental trace it is very difficult to separate 'a' and 'b' to give an accurate measure of k_{-I}, the interfacial transfer coefficient. By choosing suitable values for 'a' and 'b' in equation (4.26) it is possible to see that the equation does predict the form of the experimental trace (Figure (38)).

Since separation of the transport parameters is difficult using this pH stat technique a sampling technique was developed. This sampling technique is applicable to all the esters used.

iii. Flux determination by a sampling technique

In this technique volumes of liquid are removed at known time intervals from the outer compartment and are analyzed

spectrophotometrically. A value for $\vec{k}$ is obtained by a more direct route and separation of the various transport processes is simplified.

iv. Theory

Sandwich experiments are conducted and $\vec{k}$ has the same significance as k in equation (3.13); similar notation has been used for concentrations and volumes as used in the previous piece of theory on pages 121-122 . The theory is similar to that for sampling in the Stokes Cell (pages 46 - 47).

$$J = A(\vec{k}C_I - \overleftarrow{k}C_o) \tag{4.27}$$

$$= V_o\left(\frac{dC_o}{dt}\right) \tag{4.28}$$

$$= -V_I\left(\frac{dC_I}{dt}\right) \tag{4.29}$$

Differentiation of equation (4.27) with respect to t and substitution of equations (4.28) and (4.29) gives

$$\frac{dJ}{dt} = -kJ \tag{4.30}$$

where $$k = A(\vec{k}/V_I + \overleftarrow{k}/V_o) \tag{4.31}$$

By mass balance $$V_I C_{It} = V_I C_{Io} - (V_o C_{ot} - V_o C_{oo}) \tag{4.32}$$

Integration of equation (4.30) and substitution into equations (4.27) and (4.32) gives:-

$$\frac{(C_{ot} - C_{oo})(1 + K_o V_o/V_I)}{K_o C_{Io} - C_{oo}} = 1 - \exp(-kt) \qquad (4.33)$$

where

$$K_o = \frac{\vec{k}}{\overleftarrow{k}}$$

In the sandwich experiments $\vec{k}$ is equal to $\overleftarrow{k}$ and K_o is thus unity.

From equation (4.31)

$$\vec{k} = \frac{k}{A(1/V_o + 1/V_I)} \qquad (4.44)$$

Hence $\vec{k}$ can be determined and separated as before into the various transport terms.

v. Experimental

The experimental details for all the experiments involving the nicotinates are essentially identical. The rotating diffusion cell is filled in the normal manner and is thermostatted at 37°C. The volumes contained in the inner and outer compartments are 40 and 180 cm^3 respectively. The various concentrations and filters used are summarised in Table (11).

Table (11). Conditions for the experiments with the different esters of nicotinic acid.

System	ester	Composition of inner compartment	Composition of outer compartment	Filter
I	methyl	0.1M in water	water	1.2μm MF repelcoted
Ia	methyl	0.1 M in water	water	1.0μm Duralon in bevel
II	methyl	0.1 M in 60% w/v glycerol	60% w/v glycerol	1.2μm MF repelcoted
III	methyl	0.1 M in 80% w/v glycerol	80% w/v glycerol	1.2μm MF repelcoted
IV	n-butyl	8 mM in water	water	1.0μm Duralon
V	n-hexyl	0.8mM in water	water	1.0μm Duralon
Va	n-hexyl	0.8mM in water	water	1.0μm Duralon in bevel

Experiments were allowed to run for one day at one rotation speed. During this time approximately eight samples were removed from the outer compartment and analyzed in a Unicam SP500 spectrophotometer. From the measurements a mean value for $\vec{k}$ was calculated at each rotation speed.

vi. Results

(a) System I (Methyl nicotinate in water)

Six experiments were conducted to measure the flux of methyl nicotinate across a Millipore filter impregnated with IPM. Typical results from a day's experiments are shown in Table (12).

Table (12). Typical results for measuring $(\vec{k})^{-1}$ at one rotation speed.

C_{ot}/mM	C_{oo}/mM	t/ks	C_{Io}/mM	$(\vec{k}/\text{mM s}^{-1})^{-1}$
1.49	0	3.72	82.36	0.277
1.91	1.49	0.9	75.68	0.228
3.07	1.91	2.7	74.02	0.239
4.59	3.07	3.6	69.32	0.226
5.88	4.59	3.6	63.45	0.246
7.33	5.88	4.5	58.83	0.250
8.43	7.33	3.6	53.95	0.244
9.21	8.43	3.7	50.75	0.246

Figure (39) shows the mean values of $\vec{k}^{-1}$ from the six experiments plotted as a function of the rotation speed. The theoretical gradient has been calculated from the Levich equation and forced through the six points to give a value for the intercept.

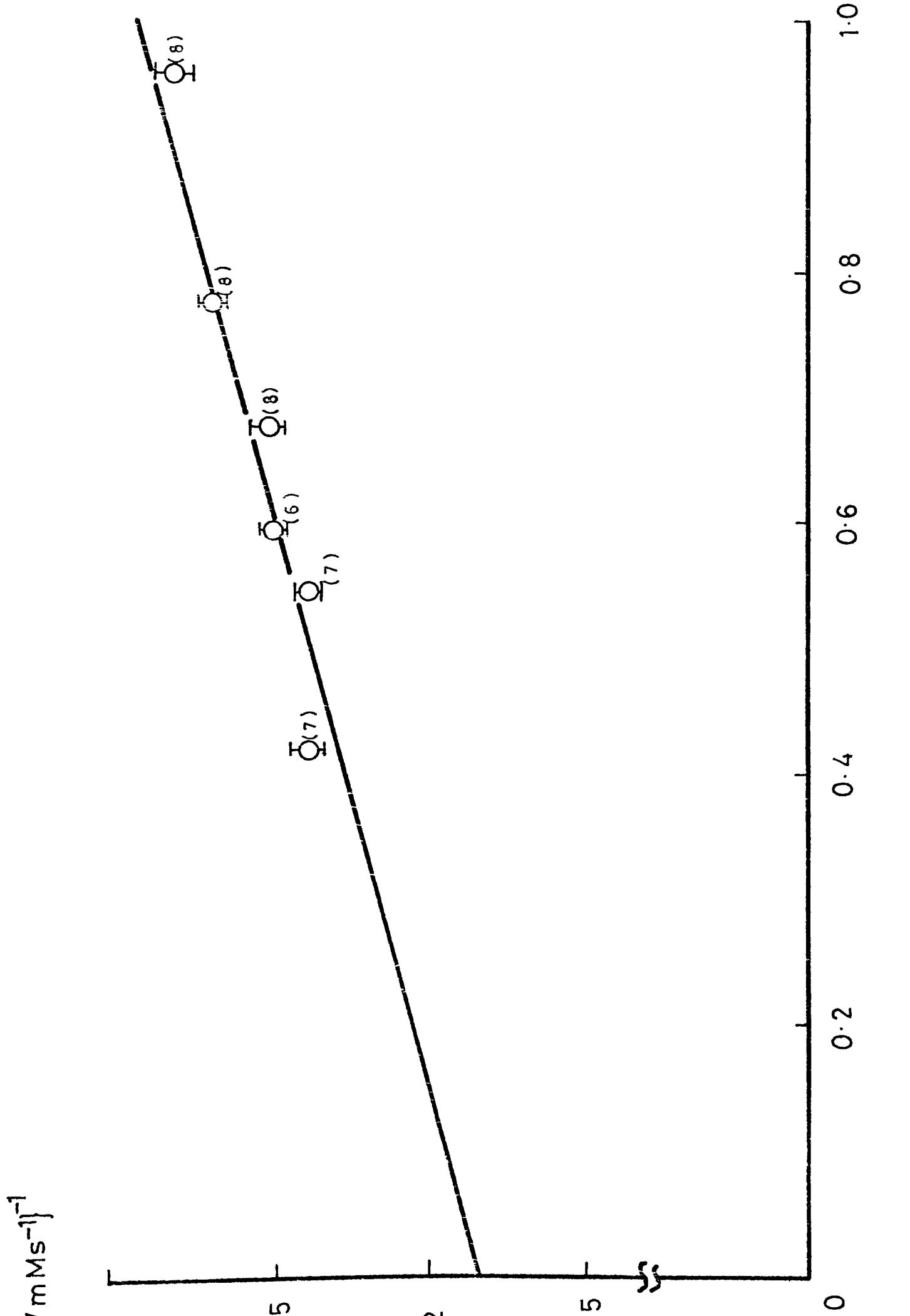

Figure (39). $(\vec{k})^{-1}$ vs $W^{-\frac{1}{2}}$ plot for methyl nicotinate in water/IPM sandwich experiment (no bevel).

The value obtained for the intercept is

$$(\vec{k}/m\ Ms^{-1})^{-1} = 0.184 \pm .002$$

But $$(\vec{k}^{-1})_{W\to\infty} = \frac{\ell K_p}{\alpha D_*} + \frac{2}{\alpha k_{-I}}$$

Using measured values for K_p and D_*, k_{-I} may be calculated

$$k_{-I}/mMs^{-1} = 46.0 \pm 2.8$$

and since $$K_p = k_I/k_{-I}$$

$$k_I/mMs^{-1} = 18.1 \pm 1.0$$

(b) System Ia (using a bevelled filter holder).

Further experiments on the methyl nicotinate /IPM system were performed using a nylon filter, the outer annulus of which was blocked using a perspex bevel. This technique has been described in more detail in the Introductory section on the design of the apparatus (page 79). Experiments were repeated on this system to ensure that the good hydrodynamics were not affected significantly in the presence of the bevel. The solution to the hydrodynamic equations assumes a planar disc surface and thus it was necessary to determine experimentally if there were any adverse effects caused by the modified filter holder.

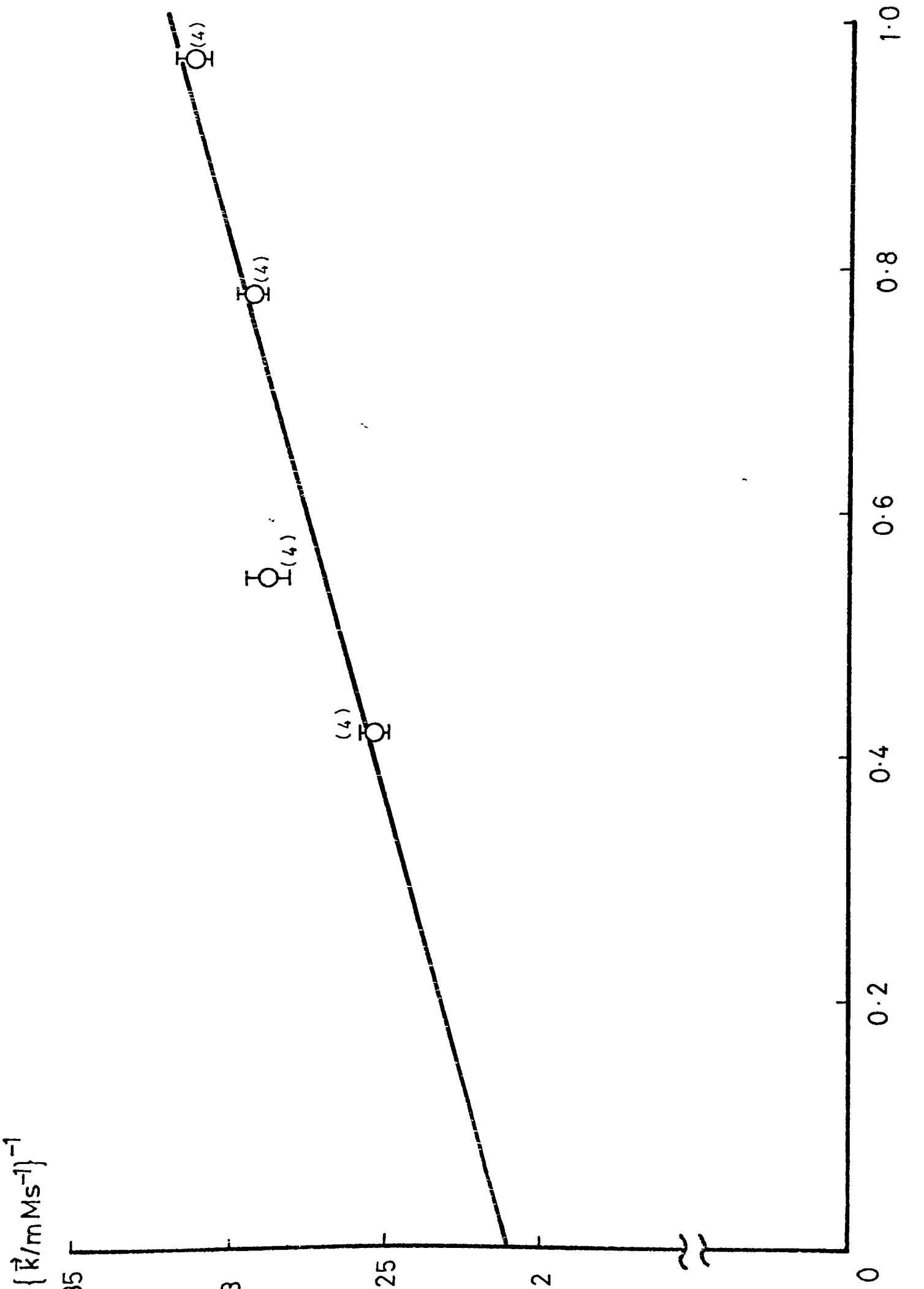

Figure (40). $(\vec{k})^{-1}$ vs $W^{-\frac{1}{2}}$ plot for methyl nicotinate in water/IPM sandwich experiment (with bevel).

Filling the apparatus is identical to that for a normal filter. It is important to make sure that there are no air bubbles trapped under the bevel. The only satisfactory method of removing any trapped air bubbles is to release the cell from its support and tilt it.

Four experiments were conducted and the results are shown in Figure (40). The theoretical gradient has again been forced through the experimental points and the good agreement between experiment and theory shows that the perspex bevel has not interfered significantly with the hydrodynamics.

The calculated intercept is

$$(\vec{k}/\text{m Ms}^{-1})^{-1} = 0.213 \pm 0.004$$

which gives a value of k_{-I}

$$k_{-I}/\text{m Ms}^{-1} = 58.7 \pm 3 \quad .$$

This is larger than the value using the Millipore-MF filters but nevertheless is within reasonable agreement considering the experimental errors involved.

(c) System II. Methyl nicotinate in 60% w/v glycerol

The '*in vivo*' effect of the addition of glycerol to aqueous solutions containing methyl nicotinate has been studied[77]. By obtaining data about the fundamental transport processes involved in these experiments, it is hoped to correlate *in vivo*

and *in vitro* results. The addition of glycerol considerably increases the viscosity of the phases in the two compartments and the experiments will additionally show how reproducible the rotating diffusion cell is with more viscous solutions.

Seven experiments were conducted at five different rotation speeds. The results are shown in Figure (41) with a theoretical gradient forced through the experimental points. The good agreement between the experimental points and the theoretical line shows that controlled transport has been achieved even at this relatively high viscosity.

The calculated intercept is

$$(\vec{k}/m\ Ms^{-1})^{-1} = 0.218 \pm 0.015$$

which gives a value of k_{-I}

$$k_{-I}/m\ Ms^{-1} = 66.1 \pm 4.0$$

and since the partition coefficient $K_p = 0.52$

$$k_I/m\ Ms^{-1} = 34.4 \pm 1.8\ .$$

The values of these interfacial transfer coefficients will be discussed in a later section.

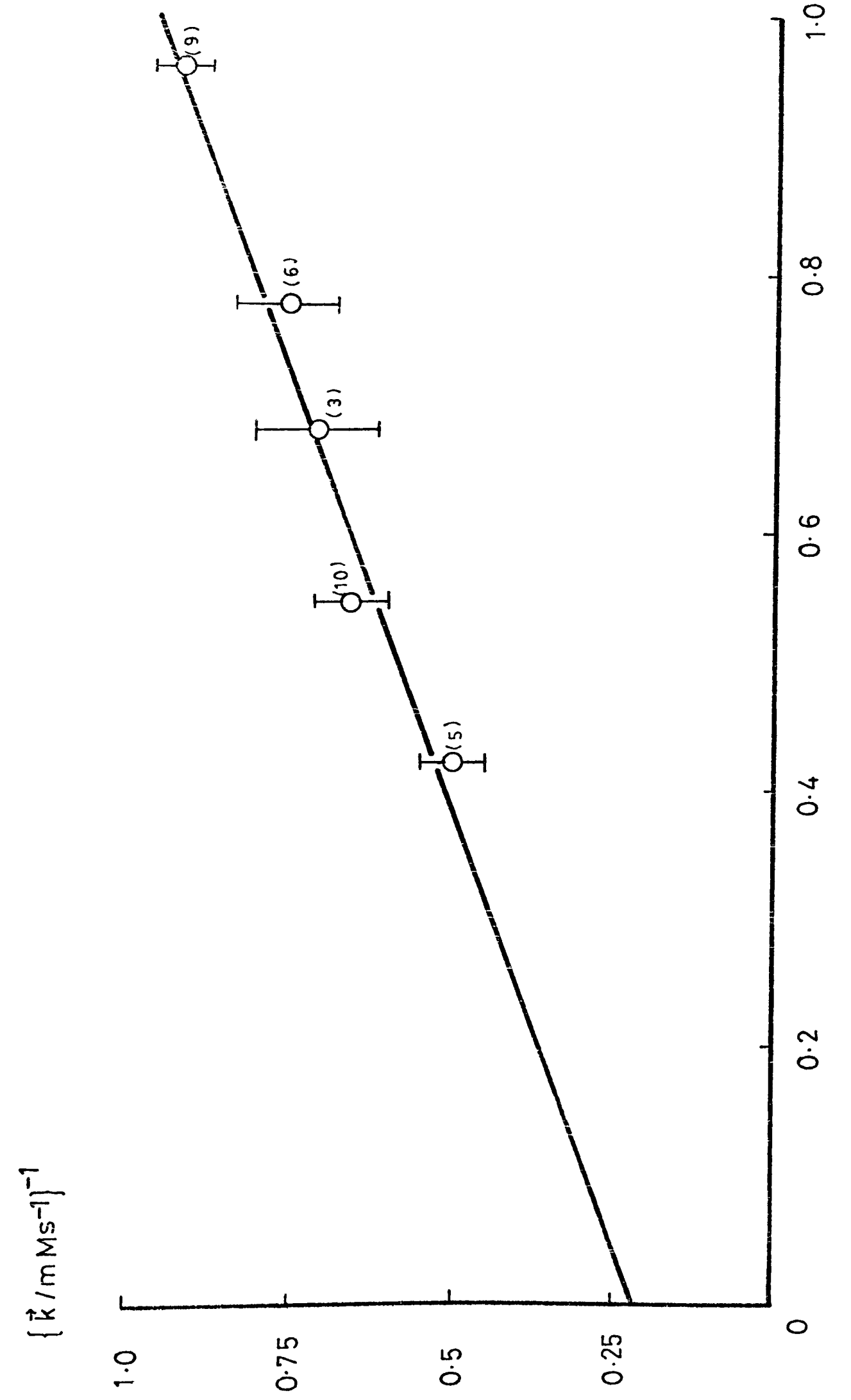

Figure (41). $(\vec{k})^{-1}$ vs $W^{-\frac{1}{2}}$ plot for methyl nicotinate in 60% w/v glycerol/IPM sandwich experiment.

(d) System III. Methyl nicotinate in 80% w/v glycerol.

Addition of more glycerol, at these concentrations, increases the solution viscosity very rapidly. It was doubtful that any useful data could be obtained using such a viscous solution. A calculated value for the diffusion layer thickness for 80% w/v glycerol at 2 Hz is

$$Z_D/\text{mm} = 0.024$$

From the value of Z_D it is possible to calculate the hydrodynamic layer thickness Z_H

$$Z_D/Z_H = (D/\nu)^{1/3} \quad 112$$

therefore $Z_H/\text{mm} = 2.4$.

Consequently the hydrodynamic layer is of the same order of magnitude as the distance between the baffle and the upper edge of the filter (~ 2.5 mm). The hydrodynamic flow in the inner compartment may not be well controlled for these experiments.

Three experiments were conducted and the results are shown graphically in Figure (42), the theoretical gradient has been forced through the points.

The calculated intercept is

$$(\vec{k}/\text{m Ms}^{-1})^{-1} = 0.63 \pm .14 .$$

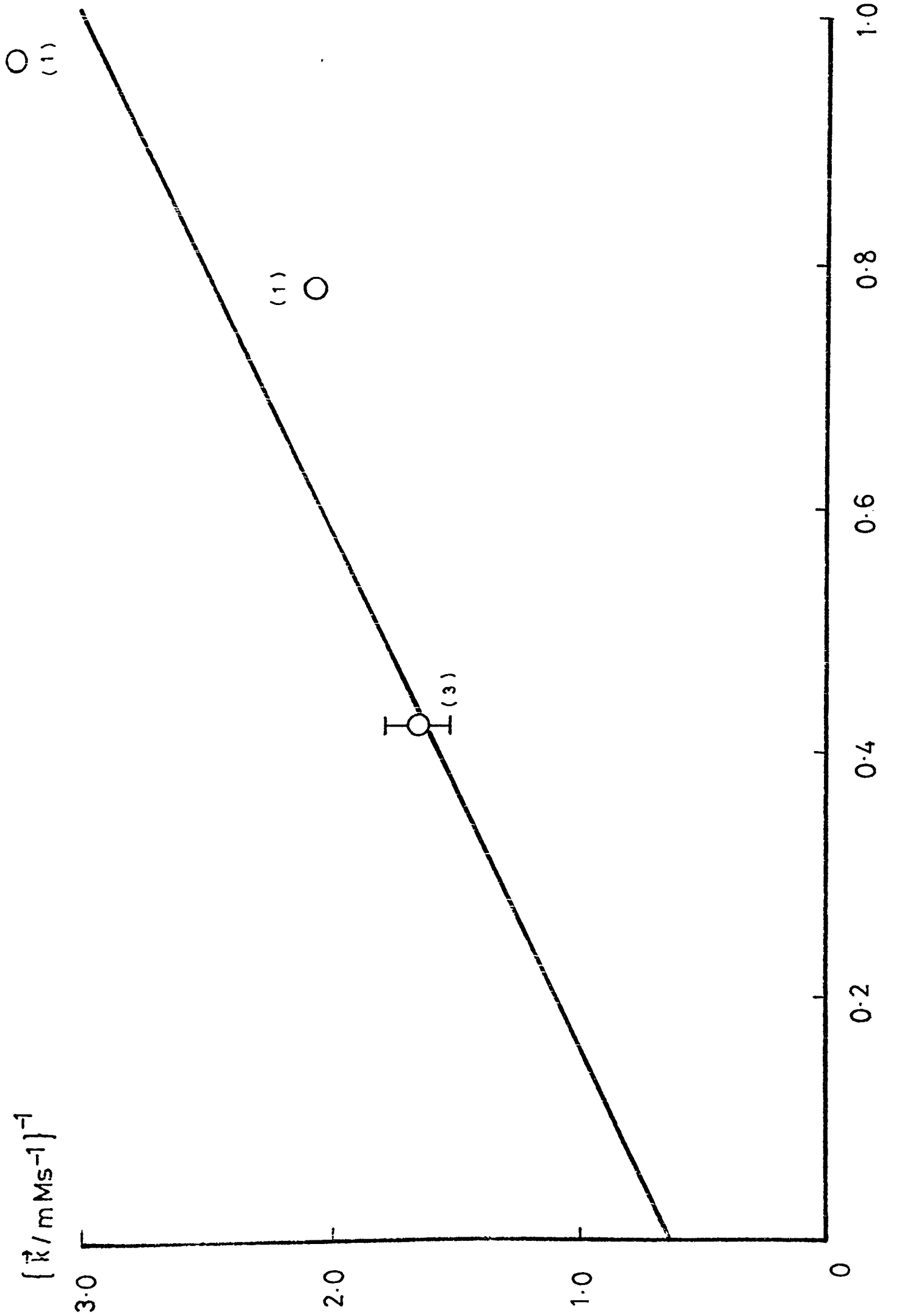

Figure (42). $(\vec{k})^{-1}$ vs $W^{-\frac{1}{2}}$ plot for methyl nicotinate in 80% w/v glycerol/IPM sandwich experiment.

The increased error shows that the well controlled transport properties are beginning to break down.

From the intercept ,values of k_I and k_{-I} may be calculated

$$k_I/m\ Ms^{-1} = 3.5 \pm 1$$

$$k_{-I}/m\ Ms^{-1} = 5.9 \pm 2 \quad .$$

These two interfacial transfer coefficients are of doubtful accuracy but are included for completeness.

(e) System IV. n-butyl nicotinate in water

n-butyl nicotinate even at the low concentrations used (~ 8 mM) was found to attack Millipore MF filters. Duralon filters were used for these experiments and were found to be suitable. As described in the introductory section two techniques were used to block the outer annulus of the filter. The fluxes obtained when the filters were blocked with cyano-acrylate adhesives were found to be abnormally slow. This was attributed to some of the adhesive spreading over the masked area during preparation. Some of the pores in the central region would then be blocked rendering the effective area less than expected. In a few cases the nylon filters were pretreated with repelcote.

Nine successful experiments were completed at six different rotation speeds. Several unsuccessful runs were caused by splits forming in the filter during the run. The splits are only visible

when the apparatus is dismantled and the associated high fluxes only detected after the samples have been assayed. Another cause of failure in an experiment results from interface instability. Again this is only detectable after completion of the experiment by inspection of the filter. If water permeates the filter to a large extent, mass flow can occur and the observed flux will be markedly increased or decreased depending on the relative liquid levels in the inner and outer compartments.

The results of the nine successful experiments are shown in Figure (43). The two points labelled c are those with pores blocked with cyanoacrylate adhesive. As can be seen a much lower flux was observed in these two experiments.

The value for the intercept when the theoretical gradient is forced through the experimental points is:

$$(\vec{k}/m\ ks^{-1})^{-1} = 26.7 \pm 1.8$$

which gives values for the interfacial transfer coefficients:

$$k_I/m\ Ms^{-1} = 5.8 \pm 0.5$$

$$k_{-I}/m\ Ms^{-1} = 223 \pm 19$$

which will be discussed later.

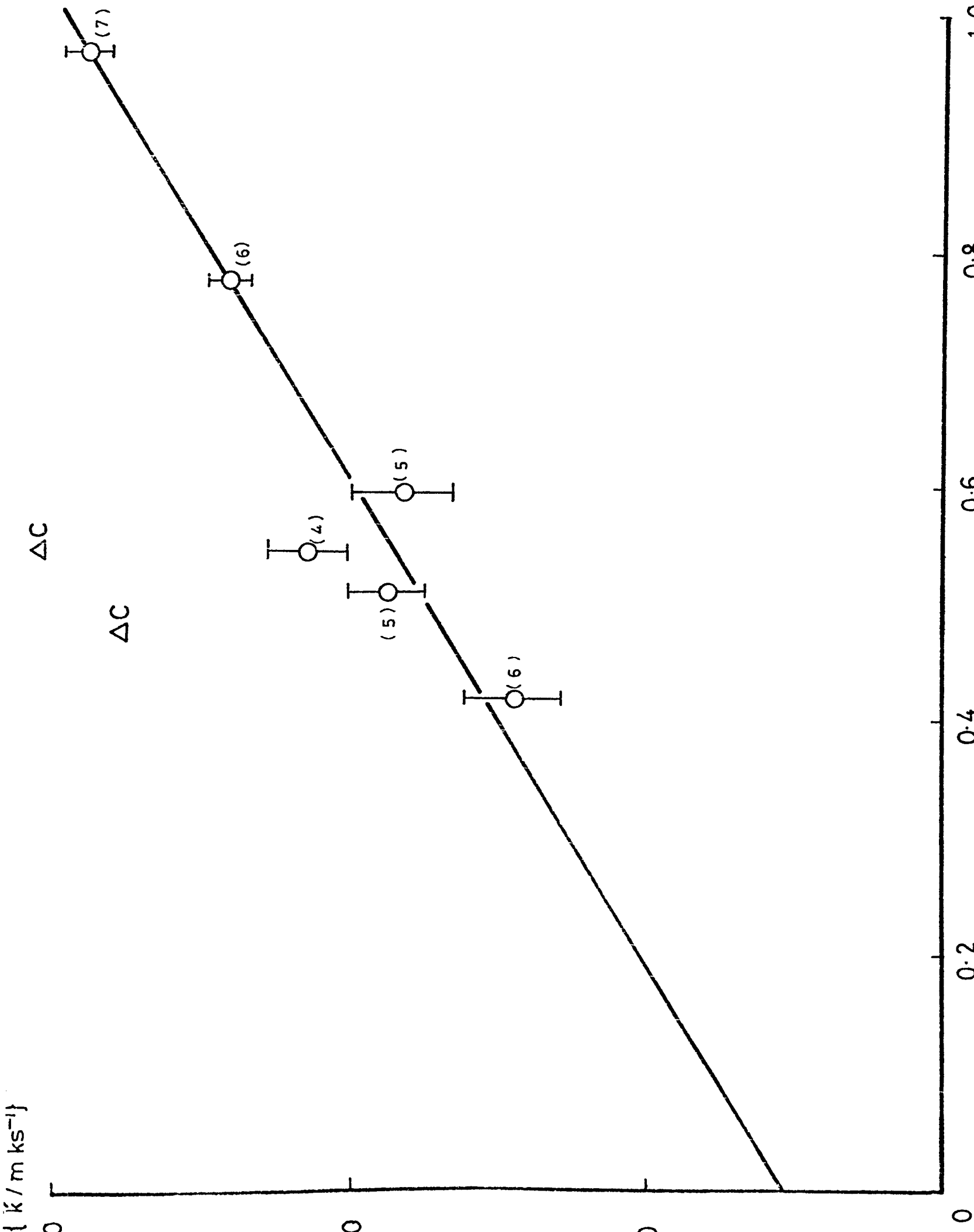

Figure (43). $(\vec{k})^{-1}$ vs $W^{-\frac{1}{2}}$ for n-butyl nicotinate in water/IPM sandwich experiment.

(f) System V. n-hexyl nicotinate in water.

Duralon filters have to be used for these experiments since MF filters are attacked by this ester. The problems involved are the same as described for the n-butyl ester. Filters were used having their outer pore area collapsed with hexafluoroisopropanol and also some which were mounted onto the perspex bevel. The results are combined in Figure (44).

The intercept obtained by forcing the theoretical gradient through the experimental points is:

$$(\vec{k}/m\ Ms^{-1})^{-1} = 0.195 \pm .008$$

Giving for the interfacial transfer coefficients

$$k_I/m\ Ms^{-1} = 0.237 \pm .02$$

$$k_{-I}/m\ Ms^{-1} = 16.9 \pm 1.1 \quad .$$

vii. Discussion

The correlation between the experimental data and the theoretical gradients predicted by the Levich equation confirms that the apparatus produces well characterized hydrodynamics. It is possible to use the present design with solutions having viscosities up to 28 $m^2\ Ms^{-1}$. By altering the baffle design and increasing the distance between the base of the baffle and the filter it is probable that more viscous solutions could be studied.

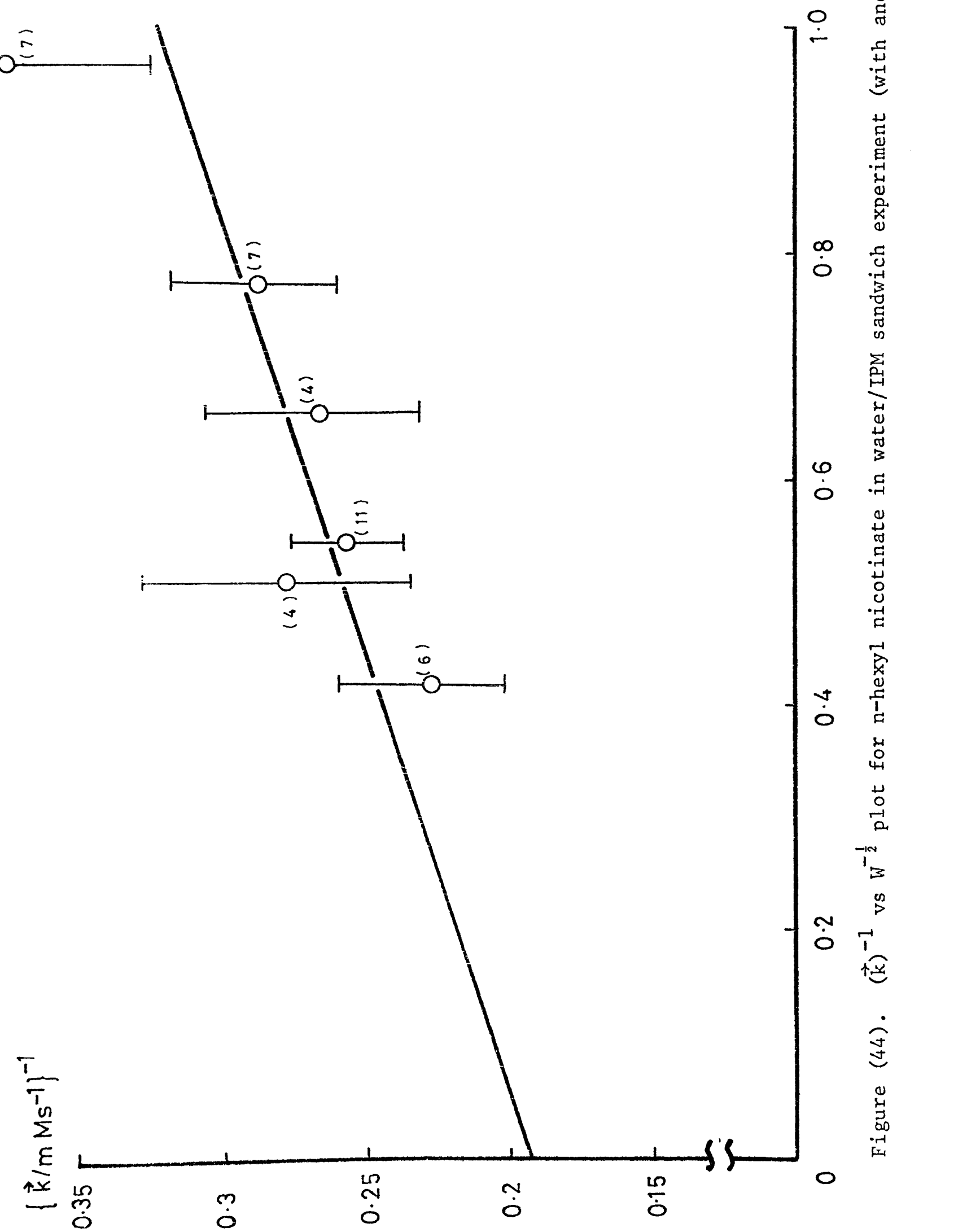

Figure (44). $(\vec{k})^{-1}$ vs $W^{-\frac{1}{2}}$ plot for n-hexyl nicotinate in water/IPM sandwich experiment (with and without bevel).

The interfacial transfer coefficients for the nicotinates studied are summarized in Table (13).

Table (13). Summary of interfacial transfer coefficients for the nicotinates studied.

System	k_I/m Ms^{-1}	k_{-I}/m Ms^{-1}	K_p
methyl nicotinate/water	18.1	46.0	0.39
methyl nicotinate/60% glycerol	34.4	66.1	0.52
methyl nicotinate/80% glycerol	3.5	5.9	0.6
n-butyl nicotinate/ water	5.8	223	2.6×10^{-2}
n-hexyl nicotinate/ water	0.24	16.9	1.4×10^{-2}

With these few results no particular trend is obvious. The interfacial transfer coefficients for all the systems studied will be collated and compared in a later section.

2. Betamethasone-17-Valerate (B.17.V).

The major advance in the field of dermatology over the past decade has probably been the development of topical corticosteroids. The use of these potent drugs is widespread in the treatment of many diseases of the skin. Although much research has been conducted into the release of steroids from different formulations very little is known about their mode of penetration.

It has been shown that propylene glycol at high concentrations decreases the permeability of skin to fluocinolone acetonide and fluocinonide, two topical steroids[69]. The reasons for this decrease in permeability are not understood. It seems probable that it could be caused by a change in the interfacial transfer coefficient and for this reason experiments were conducted to determine the magnitude of the interfacial energy barriers involved when a steroid crosses an aqueous/organic interface.

A typical topical corticosteroid, betamethasone-17-valerate (B.17.V) was studied. Many investigations have been conducted both *in vivo* and *in vitro* on the properties of this steroid. Isopropyl myristate was chosen as the 'model skin' and experiments in the rotating diffusion cell were conducted in a similar way to those described for the nicotinates.

(i) Radioactive Sampling Technique

B.17.V. is very insoluble in water, a saturated solution at room temperature being 3.5×10^{-5} M. Consequently the maximum fluxes obtainable in the rotating diffusion cell are of the order of moles per terasecond. The associated concentration changes are too small to be followed spectrophotometrically but they may be monitored by a radio chemical technique. The B.17.V. used for these experiments has a tritium label in the valerate side chain, the specific activity of which is 15 μCi/mg.

Two commercial Koch Light liquid scintillators were used, KL401 for aqueous samples and KL402 for organic samples. Samples of 1 cm^3 from the outer compartment of the diffusion cell are placed in a counting vial and 10 cm^3 of the appropriate scintillator added. The vials are left overnight in a refrigerator and are then counted in a Beckmann DPM-100 liquid scintillation counter. The counting time of 5 to 10 minutes gives a counting accuracy between 1 and 2 percent.

Since the efficiency of counting varies between vials, a technique of 'spiking' the samples is used to determine the counting efficiency (E). After a batch of vials has been counted, 50 μℓ of a tritium standard (the spike) are added to each vial and the tubes are recounted.

Then $E\% =$

$$100 \times \frac{\text{counts per minute of spiked sample-counts per minute of unspiked sample}}{\text{disintegrations per minute of added spike}}$$

The standard tritium source used was ^{3}H-n-hexadecane from the Radiochemical Centre (Amersham). The spike was added to the sample using a 50 µℓ syringe which was shown to deliver

$$39.4 \pm .07 \text{ mg of n-hexadecane.}$$

Thus the disintegrations per minute of the added spike is known more accurately than the counting accuracy of the machine.

A simple conversion is then performed to give the original sample counts per minute as total disintegrations per minute which is directly proportional to the concentration of the steroid in the sample. The average value for the counting efficiency for the samples was 25%.

Analysis of the results is analogous to that described in the section on the sampling technique for the nicotinates.

(ii) Results

Two types of experiment were conducted, both of the sandwich variety. In the first set of experiments the conventional aqueous/organic/aqueous system was studied and in the second series an organic/aqueous/organic arrangement was used. Both series were performed at 310°K and Millipore-MF 1.2 µm filters were used throughout. In the second series of the experiments the filters were not pretreated with repelcote.

(iii) Type I Experiments. Aqueous-organic-aqueous

Successful experiments of this type were achieved when one rotation speed was maintained for one day. During this period an average of six samples were withdrawn from the outer compartment and assayed. Several experiments were conducted with shorter sampling times with several rotation speed changes per day but in general these were unsuccessful because the concentration changes involved are very small.

The results of the successful experiments are given in Figure (45) and a least mean squares line has been drawn through the points. The theoretical gradient cannot be forced through the experimental points because the value of the aqueous integral diffusion coefficient for B.17.V. is not known.

The gradient and intercept given are

$$\text{Gradient/ks.m}^{-1}\ \text{Hz}^{\frac{1}{2}} = 227 \pm 22$$

$$\text{Intercept/ks.m}^{-1} = 13. \pm 1.3 \ .$$

From the known partition coefficient of B.17.V. between water and isopropyl myristate[122]

$$K_p = 7.5 \times 10^{-3}$$

the gradient of the line gives a determination of the aqueous integral diffusion coefficient:

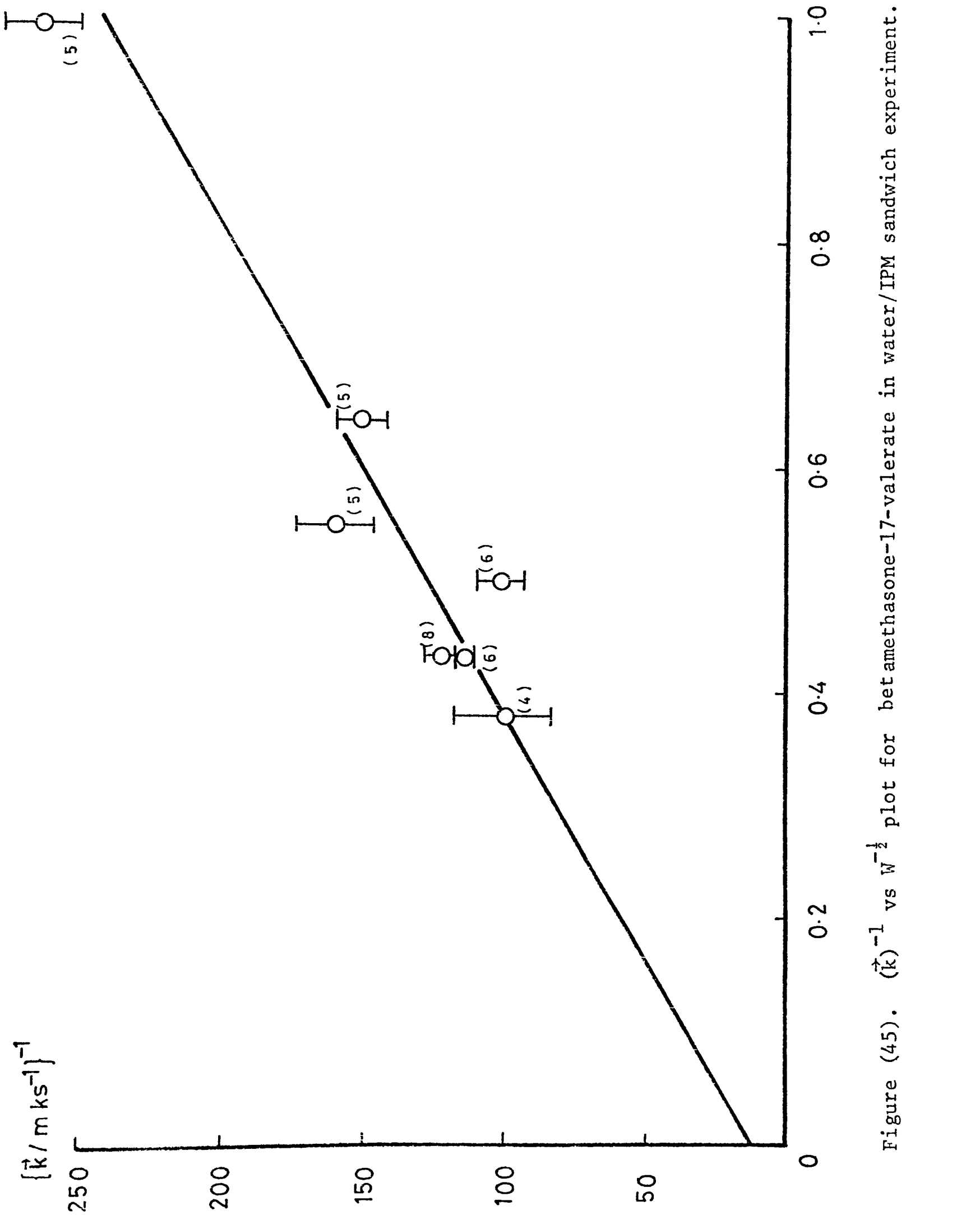

Figure (45). $(\vec{k})^{-1}$ vs $W^{-\frac{1}{2}}$ plot for betamethasone-17-valerate in water/IPM sandwich experiment.

$$D_{\phi}/m^2\ Gs^{-1} = 0.39 \pm 0.04 .$$

Experiments showed that when this type of experiment was left running for periods exceeding twenty-four hours, an equilibrium was established. The relatively rapid equilibration is caused by the large solubility of B.17.V. in isopropyl myristate compared to that in water. In an experiment the total B.17.V. present is 8.4×10^{-7} mols and the solubility of B.17.V. in isopropyl myristate is 4×10^{-3} mol.ℓ^{-1} . Thus the volume of isopropyl myristate required to completely dissolve the available B.17.V. is 0.02 cm^3. The filter contains approximately 0.03 cm^3 of isopropyl myristate which is quite adequate to dissolve the B.17.V. present.

One problem encountered in radioactive tracer work is the lability of the label. In order to ensure that the label remained in position, samples from the outer compartment were placed on a silica gel thin layer chromatography plate. The plates were developed in Chloroform: ethyl acetate (2:1) and dried. They were then scanned for radioactivity. It was found that essentially all the activity was concentrated in a region corresponding to the correct R_f value for B.17.V. A very small spot corresponding to the 21-valerate was just detectable. This is reasonable since the transfer of the valerate side chain from the 17 to the 21 position is well known. However the amount of 21-valerate present compared to the 17-valerate was negligible.

(iv) Type II Experiments. Organic:aqueous:organic

This type of experiment was left running for a period of one week at one rotation speed. Two or three samples are removed during the day and assayed. Three experiments were conducted and the results are given in Figure (46).

The least mean squares gradient and intercept of the line are:-

$$\text{Gradient/Ms.m}^{-1}\ \text{Hz}^{\frac{1}{2}} = 0.458 \pm 0.07$$

$$\text{Intercept/Ms. m}^{-1} = 1.53 \pm 0.05 \ .$$

Visual inspection of the filters after the experiment indicated some interfacial breakdown although no mass flow was apparent. For this reason no reliance is put on the intercept of the graph.

From the gradient the integral diffusion coefficient of B.17.V. in isopropyl myristate may be calculated

$$D_*/m^2\ Gs^{-1} = 0.21 \pm .01 \ .$$

This value of the diffusion coefficient in isopropyl myristate enables us to analyze the intercept in the aqueous:organic: aqueous experiments. The interfacial transfer coefficients can be calculated:-

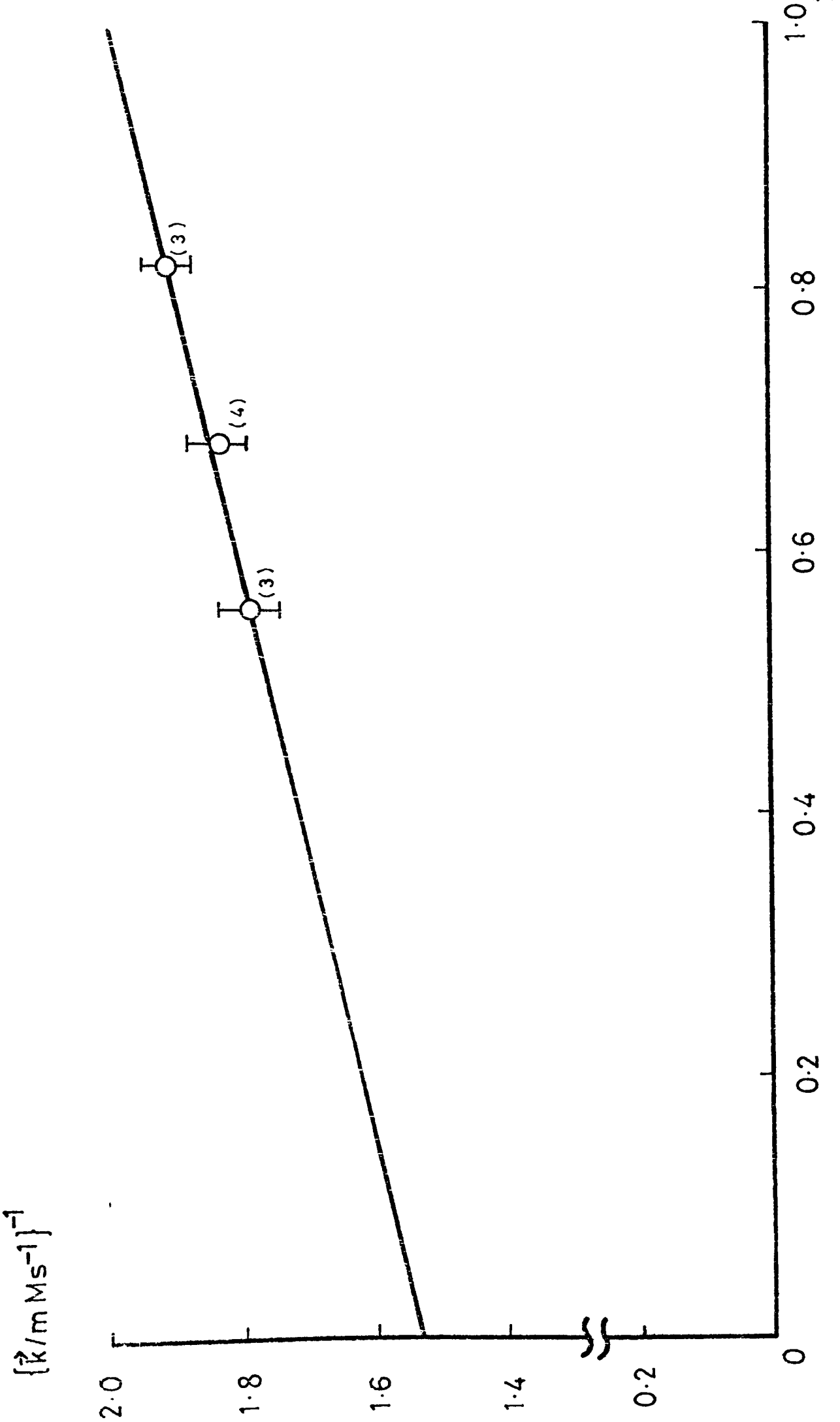

Figure (46). $(\vec{k})^{-1}$ vs $W^{-\frac{1}{2}}$ plot for betamethasone-17 valerate in IPM/water sandwich experiment.

$$k_I/m.\ Ms^{-1} = 2.6 \pm 0.3$$

$$k_{-I}/m.\ Ms^{-1} = 344 \pm 35 \quad .$$

These values will be discussed later.

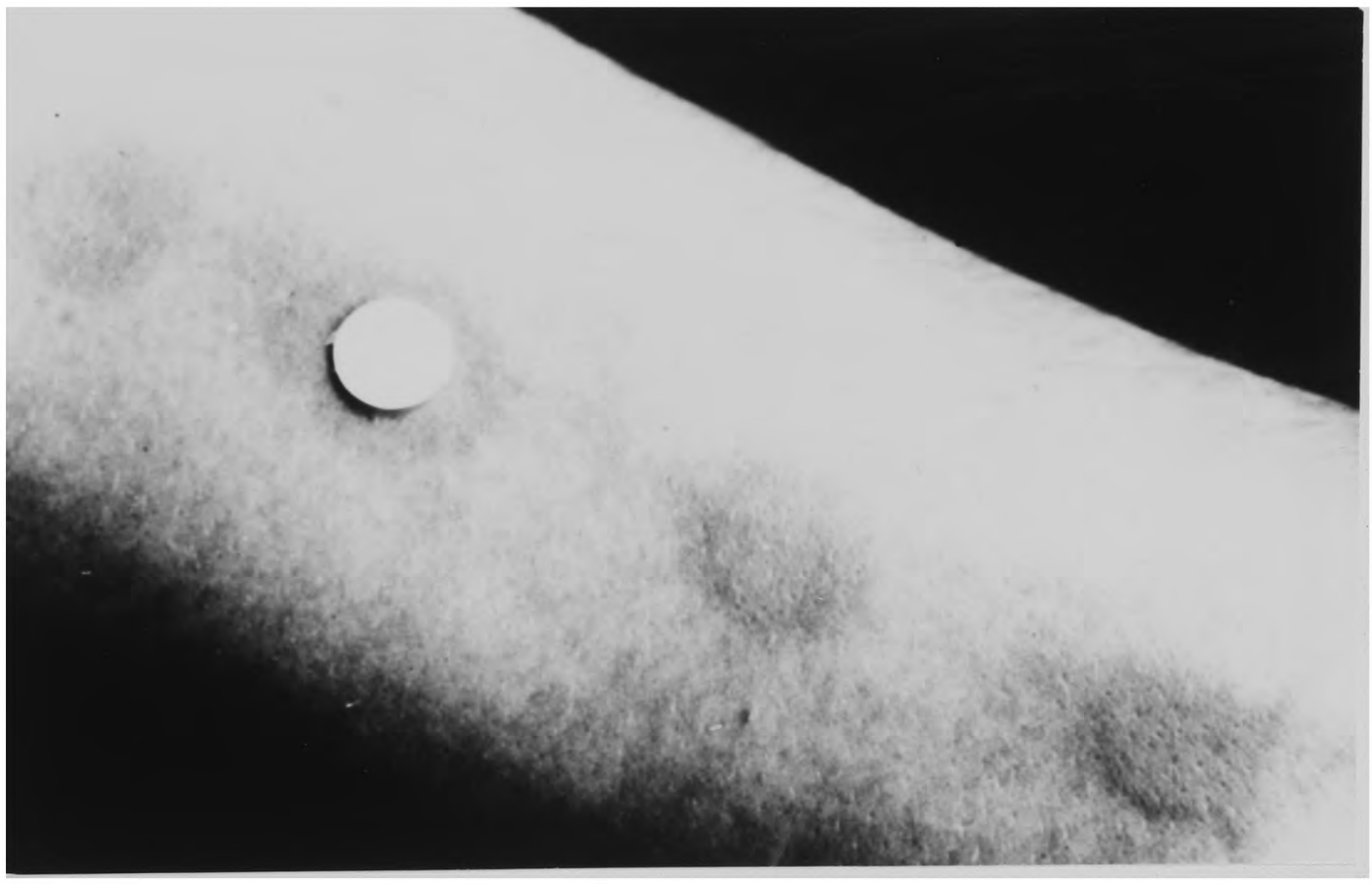

Figure (47). Photograph showing a test patch and erythema induced by an aqueous solution of methyl nicotinate.

CHAPTER V

IN VIVO EXPERIMENTS

Percutaneous absorption has been studied *in vivo* using aqueous solutions of three esters of nicotinic acid, methyl, n-butyl, and n-hexyl. These compounds readily penetrate the skin and, after a few minutes, produce a noticable erythema[73]. The erythema is caused by the local action of the nicotinates on the blood vessel walls and associated nerve mechanisms[74]. Since the blood vessels and nerves are located at the dermal-epidermal junction, the diffusion process involved is across the entire epidermis. Consequently the time of onset of erythema has been taken as a good measure of the rate of skin penetration and reproducible results have been obtained by independent workers[49,75-78,121].

Two types of experiment have been performed which are referred to as pulsed and non-pulsed experiments. Previous experiments have been of the non-pulsed type in which the solution remains in contact with the skin for the duration of the experiment. In the new type of experiment the solution is removed from the skin surface before the onset of erythema. For these there are two characteristic times; the application time, and the time of onset of erythema.

Interpretation of the results of the pulsed experiments is more complex, but this type of experiment allows calculation of

parameters for butyl and hexyl nicotinate which could not have been obtained by other means.

In order to analyze the results of the two types of experiment the diffusion equations describing transport across the epidermis have been solved. The theory includes terms describing the effect of interfacial barriers and concentration depletion in the applied solution.

I. Theory

Figure (48) shows a typical concentration profile for a substance diffusing from a vehicle across the epidermis. In this case steady state conditions have not been established.

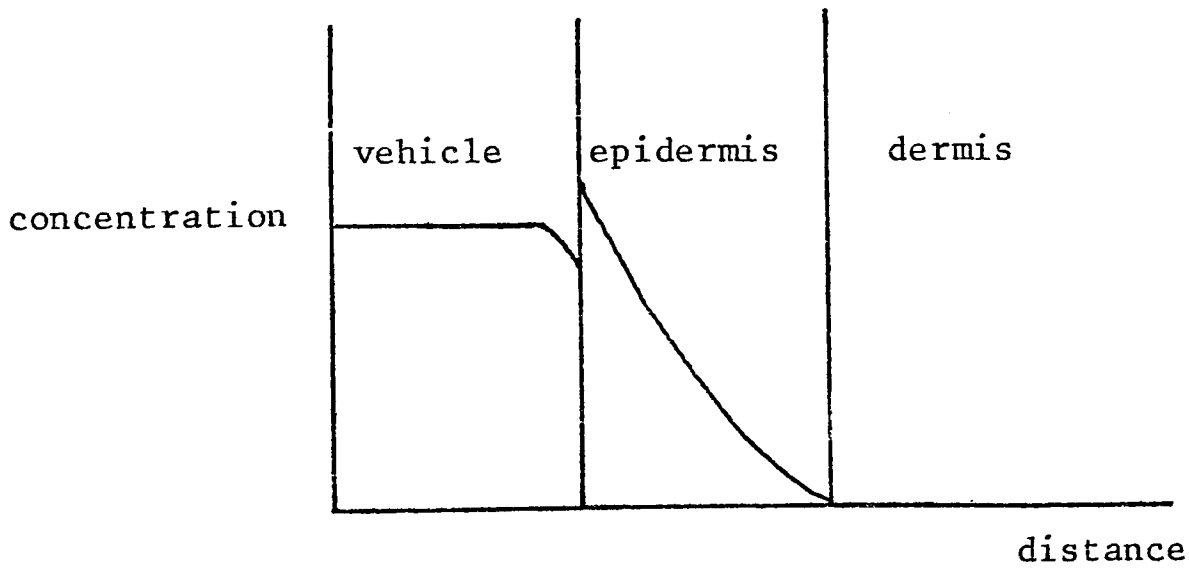

Figure (48)

It is this concentration profile that must be described mathematically. The percutaneous absorption of a substance c may be described by considering diffusion through a barrier of thickness ℓ with the parameters shown:

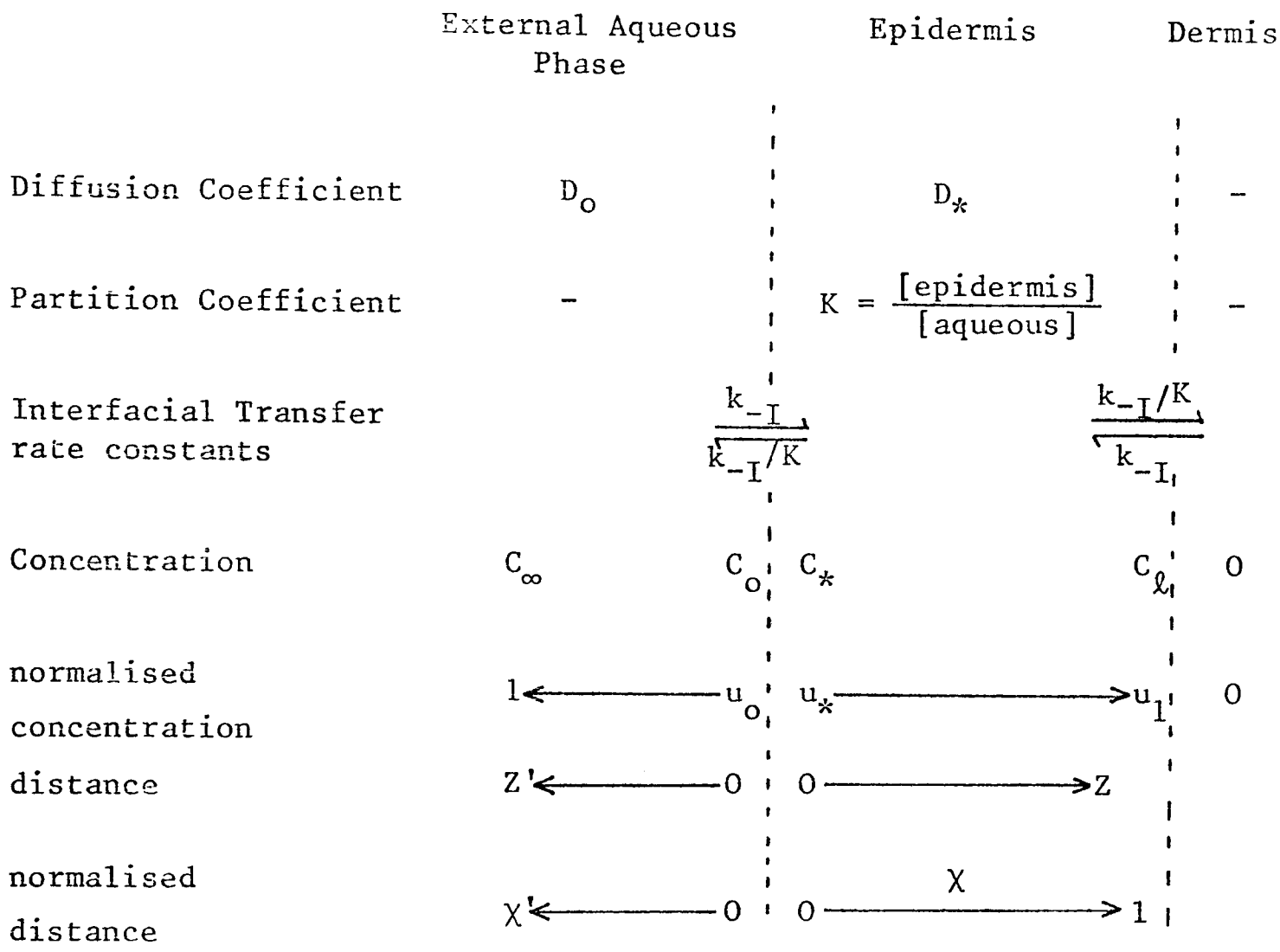

To facilitate solution of the differential equations the following normalizing procedures are adopted:

distance $\chi = z/\ell$

$\chi' = z'/\ell$

time $\tau = tD_*/\ell^2$

concentration $u = c/c_\infty$

interfacial transfer $\kappa = k_{-I}\ell/K\ D_*$

and $p = D_o/D_*$.

The following differential equations then apply:-

In the external aqueous phase:

$$\left(\frac{\partial u}{\partial \tau}\right) = p\left(\frac{\partial^2 u}{\partial \chi'^2}\right) \tag{5.1}$$

At the external interface:

$$p\left(\frac{\partial u}{\partial \chi'}\right)_o = \kappa(K u_o - u_*) = -\left(\frac{\partial u}{\partial \chi}\right)_o \tag{5.2}$$

In the epidermis

$$\left(\frac{\partial u}{\partial \tau}\right) = \left(\frac{\partial^2 u}{\partial \chi^2}\right) \tag{5.3}$$

At the internal interface

$$-\left(\frac{\partial u}{\partial \chi}\right)_1 = \kappa u_1 \tag{5.4}$$

The various boundary conditions for these equations are:

At $\tau = 0$

external aqueous phase $u = 1$

elsewhere $u = 0$

and as $\chi' \to \infty$ $u \to 1$

and in the dermis $u = 0$.

Looking at the concentration profile in the external aqueous phase and taking the Laplace Transform of equation (5.1)

$$s_1\bar{u} - 1 = p\left(\frac{\partial^2\bar{u}}{\partial\chi'^2}\right) \tag{5.5}$$

The solution of this differential equation may be found by using the particular integral

$$\bar{u} = \frac{1}{s_1} \tag{5.6}$$

and by solving the complementary function

$$\left(\frac{\partial^2\bar{u}}{\partial\chi^2}\right) - \frac{s_1\bar{u}}{p} = 0 \tag{5.7}$$

therefore $$\bar{u} = A\, e^{-\sqrt{\frac{s_1}{p}}\,\chi'} + B\, e^{\sqrt{\frac{s_1}{p}}\,\chi'} \tag{5.8}$$

Since $u \to 1$ as $\chi' \to \infty$

$$1 = B\, e^{\sqrt{\frac{s_1}{p}}\,\chi'} \tag{5.9}$$

and the second term in B vanishes. The constant A may be found by differentiating equation (5.8), ignoring the term in B:

$$\left(\frac{\partial\bar{u}}{\partial\chi'}\right) = -\sqrt{\frac{s_1}{p}}\; A\, e^{-\sqrt{\frac{s_1}{p}}\,\chi'} \tag{5.10}$$

At $\chi' = 0$

$$A = -\sqrt{\frac{p}{s_1}}\left(\frac{\partial\bar{u}}{\partial\chi'}\right)_o e^{-\sqrt{\frac{s_1}{p}}\,\chi'} \tag{5.11}$$

Thus the general solution of equation (5.5) is:

$$\bar{u} = \frac{1}{s_1} - \sqrt{\frac{p}{s_1}} \left(\frac{\partial \bar{u}}{\partial \chi'}\right)_o e^{-\sqrt{\frac{s_1}{p}}\chi'} \qquad (5.12)$$

In the epidermal barrier the concentration profile is described by the solution of equation (5.3). Taking the Laplace Transform of this equation

$$s_1 \bar{u} = \left(\frac{\partial^2 \bar{u}}{\partial \chi^2}\right) \qquad (5.13)$$

The general solution of this equation is:-

$$\bar{u} = A \cosh \sqrt{s_1}\chi + B \sinh \sqrt{s_1}\chi \qquad (5.14)$$

therefore $$\left(\frac{\partial \bar{u}}{\partial \chi}\right) = \sqrt{s_1} A \sinh \sqrt{s_1}\chi + \sqrt{s_1} B \cosh \sqrt{s_1}\chi \qquad (5.15)$$

Using the boundary condition

$$\chi = 0 \qquad u = u_*$$

$$\bar{u} = u_* \cosh(\sqrt{s_1}\chi) + \frac{1}{\sqrt{s_1}} \left(\frac{\partial \bar{u}}{\partial \chi}\right)_o \sinh(\sqrt{s_1}\chi) \qquad (5.16)$$

From these equations it is possible to express $\bar{u}$ in terms of κ, K, $\sqrt{p}$, s_1 and χ.

Equation (5.16) gives, when $\chi = 1$,

$$\bar{u}_1 = \bar{u}_* \cosh \sqrt{s_1} + \frac{1}{\sqrt{s_1}} \left(\frac{\partial \bar{u}}{\partial \chi}\right)_o \sinh \sqrt{s_1} \qquad (5.17)$$

Differentiating:

$$\left(\frac{\partial \bar{u}}{\partial \chi}\right)_1 = \bar{u}_* \sqrt{s_1} \sinh \sqrt{s_1} + \left(\frac{\partial \bar{u}}{\partial \chi}\right)_o \cosh \sqrt{s_1} \qquad (5.18)$$

Combining equations (5.4, 5.17, 5.18) and rearranging

$$\left(\frac{\partial \bar{u}}{\partial \chi}\right)_o = - \frac{u_* \left(\kappa + \sqrt{s_1} \tanh \sqrt{s_1}\right)}{\left(1 + \frac{\kappa}{\sqrt{s_1}} \tanh \sqrt{s_1}\right)} \qquad (5.19)$$

From equations (5.2) and (5.19)

$$\left(\frac{\partial \bar{u}}{\partial \chi'}\right)_o = \frac{u_* \left(\kappa + \sqrt{s_1} \tanh \sqrt{s_1}\right)}{p\left(1 + \frac{\kappa}{\sqrt{s_1}} \tanh \sqrt{s_1}\right)} \qquad (5.20)$$

$$\bar{u}_o = \frac{\bar{u}_*}{K} \left\{ 1 + \frac{\kappa + \sqrt{s_1} \tanh \sqrt{s_1}}{\kappa\left(1 + \frac{\kappa}{\sqrt{s_1}} \tanh \sqrt{s_1}\right)} \right\} \qquad (5.21)$$

However from equation (5.12)

$$\bar{u}_o = \frac{1}{s_1} - \sqrt{\frac{p}{s_1}} \left(\frac{\partial \bar{u}}{\partial \chi'}\right)_o \qquad (5.22)$$

Substituting equation (5.20)

$$\bar{u}_o = \frac{1}{s_1} - \sqrt{\frac{p}{s_1}} \left\{ \frac{u_* \left(\kappa + \sqrt{s_1} \tanh \sqrt{s_1}\right)}{p\left(1 + \frac{\kappa}{\sqrt{s_1}} \tanh \sqrt{s_1}\right)} \right\} \qquad (5.23)$$

Equating equations (5.21) and (5.23) gives an expression for $\bar{u}_*$

$$\bar{u}_* = \frac{K\left(1 + \frac{K}{\sqrt{s_1}} \tanh \sqrt{s_1}\right)}{s_1\left[1 + \frac{K}{\sqrt{s_1}} \tanh\sqrt{s_1} + \left(1 + \frac{\sqrt{s_1}}{K} \tanh\sqrt{s_1}\right)\left(1 + \frac{KK}{\sqrt{ps_1}}\right)\right]} \tag{5.24}$$

Combining equations (5.16) and (5.19)

$$\bar{u} = \bar{u}_* \left\{ \cosh\sqrt{s_1}\chi - \frac{1}{\sqrt{s_1}} \sinh\sqrt{s_1}\chi\left[\frac{K + \sqrt{s_1}\tanh \sqrt{s_1}}{1 + \frac{K}{\sqrt{s_1}} \tanh\sqrt{s_1}}\right]\right\} \tag{5.25}$$

Substitution of equation (5.24) into (5.25) gives

$$\bar{u} = \frac{K\left(\cosh\sqrt{s_1}\chi\left(1 + \frac{K}{\sqrt{s_1}} \tanh\sqrt{s_1}\right) - \sinh\sqrt{s_1}\chi\left(\frac{K}{\sqrt{s_1}} + \tanh\sqrt{s_1}\right)\right)}{s_1\left[1 + \frac{K}{\sqrt{s_1}} \tanh \sqrt{s_1} + \left(1 + \frac{\sqrt{s_1}}{K} \tanh \sqrt{s_1}\right)\left(1 + \frac{KK}{\sqrt{ps_1}}\right)\right]} \tag{5.26}$$

which simplifies to:

$$\bar{u} = \frac{K\left[\left(1 + \frac{\sqrt{s_1}}{K\tanh \sqrt{s_1}}\right) \cosh\sqrt{s_1}\chi - \left(1 + \frac{\sqrt{s_1}\tanh\sqrt{s_1}}{K}\right) \frac{\sinh\sqrt{s_1}\chi}{\tanh\sqrt{s_1}}\right]}{s_1\left\{1 + \frac{2\sqrt{s_1}}{K\tanh\sqrt{s_1}} + \frac{s_1}{K^2} + \frac{K}{\sqrt{p}\tanh\sqrt{s_1}} + \frac{\sqrt{s_1}K}{\sqrt{p}K}\right\}} \tag{5.27}$$

which is an expression describing the concentration distribution in the epidermis as a function of distance χ and of the Laplace time variable s_1.

Erythema is assumed to be triggered when the number of mols of ester per unit area in the dermal side of the epidermal-dermal junction (n') has reached a critical value (n'_E).

$$n' = \int_o^t \left(\frac{k_{-I}}{K_s}\right) c_\ell dt \qquad (5.28)$$

$$= \ell c_\infty u' \qquad (5.29)$$

where

$$u' = \int_o^\tau \kappa u_1 d\tau \qquad (5.30)$$

and therefore:

$$\bar{u}' = \frac{\kappa \bar{u}_1}{s_1} = \bar{f}\,(s_1) \qquad (5.31)$$

From equation (5.27), using $\chi = 1$

$$\bar{f} = \frac{K}{s_1^{3/2} \sinh\sqrt{s_1} \left\{1 + \frac{2\sqrt{s_1}}{\kappa \tanh\sqrt{s_1}} + \frac{s_1}{\kappa^2} + \frac{K}{\sqrt{p}\tanh\sqrt{s_1}} + \frac{K\sqrt{s_1}}{\kappa\sqrt{p}}\right\}} \qquad (5.32)$$

The inversion of $\bar{f}$ to find how u' varies with τ is complex due to the presence of the hyperbolic functions. Expression (5.32) may be simplified for the cases where $s_1 >> 1$ and $s_1 << 1$; the hyperbolic terms may be approximated and the bracketed term expressed as factors of the form ($\sqrt{s} + a$). The whole expression

may then be split into partial fractions and standard inverse transforms used[125]. However the complete expression obtained is still very complicated and further approximations may be made to provide simpler solutions. These solutions are given in Table (14), they cover all cases where the critical parameters as given in the table differ by at least one order of magnitude.

Table (14)

The simpler solutions to equation (5.32) showing how u' varies with τ

<table>
<tr><td rowspan="2"></td><td colspan="2" rowspan="2">$\kappa^2\tau >> 1$</td><td colspan="2">$\kappa^2\tau >> 1$</td></tr>
<tr><td>$p/K^2 << \kappa^2\tau$</td><td>$p/K^2 >> \kappa^2\tau$</td></tr>
<tr><td>$\tau^2 << 1$</td><td colspan="2">$\frac{8K\tau^{3/2}}{\sqrt{\pi}(1+K/\sqrt{p})} \exp(-1/4\tau)$</td><td>$\frac{16\sqrt{p}K\tau^{5/2}}{\sqrt{\pi}} \exp(-1/4\tau)$</td><td>$\frac{32\kappa^2K\tau^{7/2}}{\sqrt{\pi}} \exp(-1/4\tau)$</td></tr>
<tr><td>Class</td><td colspan="2">IA(1 and 2)</td><td>IB1</td><td>IB2</td></tr>
<tr><td></td><td colspan="2">$\kappa^2\tau^2 >> 1$</td><td colspan="2">$\kappa^2\tau^2 << 1$</td></tr>
<tr><td rowspan="2">$\tau^2 >> 1$</td><td>$\frac{p}{K^2} << \frac{\kappa^2\tau}{(2+\kappa)^2}$</td><td>$\frac{p}{K^2} >> \frac{\kappa^2\tau}{(2+\kappa)^2}$</td><td>$\frac{p}{K^2} << \kappa\tau$</td><td>$\frac{p}{K^2} >> \kappa\tau$</td></tr>
<tr><td>$\frac{2\sqrt{p}\tau^{\frac{1}{2}}}{\sqrt{\pi}}$</td><td>$\frac{\kappa K\tau}{2+\kappa}$</td><td>$\frac{4\sqrt{p}\kappa\tau^{3/2}}{3\sqrt{\pi}}$</td><td>$\frac{\kappa^2K\tau^2}{2}$</td></tr>
<tr><td>Class</td><td>IIA1</td><td>IIA2</td><td>IIB1</td><td>IIB2</td></tr>
</table>

Certain resemblances between the different solutions in Table (14) may be seen. All the Class I solutions are instances where the concentration distribution in the epidermis is far from the steady state. For all the Class II solutions the relaxation time for establishing a linear concentration gradient in the skin is short compared to the time of the experiment. All the Class A solutions (except IIA2) are cases where the interfacial transport is rapid enough not to be rate determining, while the reverse is true for all the Class B solutions. In all Class I solutions there is significant depletion in the external aqueous phase. The rate determining processes are transport in the aqueous phase together with a possible interfacial barrier at the outer interface. Class 2 solutions show processes where there is slow uptake and hence no depletion term is included.

The mathematical treatment so far has been for cases where the external aqueous phase has been in continuous contact with the skin. For the 'pulse' experiments conducted this is not the case. However, the results obtained in Table (14) are used to describe the concentration distribution at the moment when the patch containing the ester is removed (time t_1). The onset of erythema occurs at time t_2 after the removal of the patch i.e.

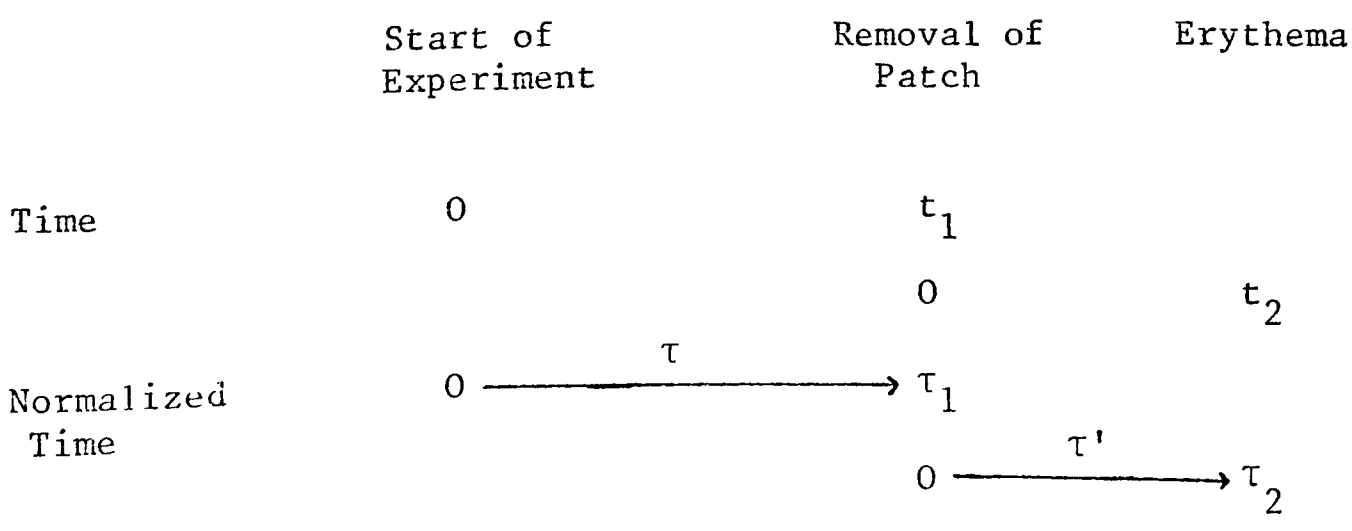

To describe the concentration distribution after the patch has been removed the solution to the following differential equation is required:

$$\left(\frac{\partial u}{\partial \tau'}\right) = \left(\frac{\partial^2 u}{\partial \chi^2}\right) \tag{5.33}$$

Transforming with respect to τ

$$\left(\frac{\partial \bar{u}}{\partial \tau'}\right) = \left(\frac{\partial^2 \bar{u}}{\partial \chi^2}\right) \tag{5.34}$$

and with respect to τ'

$$s_2 \bar{\bar{u}} - \bar{u}_\dagger = \left(\frac{\partial^2 \bar{\bar{u}}}{\partial \chi^2}\right) \tag{5.35}$$

where $\bar{u}_\dagger$ is the value of $\bar{u}$ at $\tau' = 0$ or $\tau = \tau_1$.

At the internal interface:

$$-\left(\frac{\partial \bar{\bar{u}}}{\partial \chi}\right)_1 = \kappa \bar{\bar{u}}_1 \tag{5.36}$$

and at the external interface

$$\left(\frac{\partial \bar{\bar{u}}}{\partial \chi}\right)_o = 0 \tag{5.37}$$

For the "pulse" experiments the number of mols of ester triggering the response is given by equation (5.29) where now:

$$u' = \int_o^{\tau_1} \kappa u_1 d\tau + \int_o^{\tau_2} \kappa u_1 d\tau' \tag{5.38}$$

Therefore

$$u' = \mathcal{L}_2^{-1}\mathcal{L}_1^{-1}\,(\bar{\bar{u}}')_{\substack{\tau=\tau_1\\ \tau'=\tau_2}} \tag{5.39}$$

where $$\bar{\bar{u}}' = \frac{\bar{f}}{s_2} + \frac{\kappa\bar{\bar{u}}_1}{s_2} \tag{5.40}$$

Thus the solution of equation (5.35) with the boundary conditions (5.36, 5.37) and substitution into equation (5.39) is required.

$\bar{u}_+$ and $\bar{\bar{u}}$ will have the following forms:

$$\bar{u}_+ = A\cosh\sqrt{s_1}\chi + B\sinh\sqrt{s_1}\chi \tag{5.41}$$

$$\bar{\bar{u}} = A'\cosh\sqrt{s_1}\chi + B'\sinh\sqrt{s_1}\chi + C'\cosh\sqrt{s_2} + D'\sinh\sqrt{s_2}\chi \tag{5.42}$$

Differentiation of equation (5.42) and substitution of the result along with equation (5.41) into equation (5.35) gives an expression which by applying the boundary conditions gives a solution for u' (Appendix 3)

$$\bar{\bar{u}}' = \bar{f}\,\bar{\bar{g}} \tag{5.43}$$

where

$$\bar{\bar{g}} = \frac{1}{s_2 - s_1}\left[1 - \frac{s_1}{s_2}\left(\frac{\cosh\sqrt{s_1} + \sqrt{s_1}\sinh\sqrt{s_1}/\kappa}{\cosh\sqrt{s_2} + \sqrt{s_2}\sinh\sqrt{s_2}/\kappa}\right)\right] \tag{5.44}$$

As in the inversion of $\bar{f}$, $\bar{\bar{g}}$ can be more readily inverted by choosing values for s_1 and s_2 which differ by more than an

order of magnitude. The conditions chosen are shown in Table (15) in which the values of $\bar{g}$ are given in terms of τ' and the Laplace time variable s_1.

Table (15). Expressions for $\bar{g} = \mathcal{L}_2^{-1} \bar{\bar{g}}$ from equation (5.44)

$\tau' << 1$		$\tau' >> 1$	
$\tau_1 << \tau'$	$\frac{1}{2}\exp\{\sqrt{s_1}(1+\frac{\sqrt{s_1}}{K})\}.g'(\tau')^*$	$\tau_1 << 1$	$\frac{1}{2}\exp\{\sqrt{s_1}(1+\frac{\sqrt{s_1}}{K})\}(1-\exp(-K\tau'))$
$\tau_1 >> \tau'$	$1 + s_1\tau'$	$\tau_1 >> 1$	$1 + \frac{s_1}{K}\{1-\exp(-K\tau')\}$

* $g'(\tau') = \dfrac{8K(\tau')^{3/2}}{\sqrt{\pi}(1+2K\tau')} \exp(-\dfrac{1}{4\tau'})$

In order to obtain the complete expression for the pulse experiments the values given in Table (15) are multiplied by $\bar{f}$ given in equation (5.32) and inverted with respect to s_1.

Solutions to the top row of table (15) may be expressed in more simple terms.

$$f' = \mathcal{L}_1^{-1} \tfrac{1}{2}\exp\left\{\sqrt{s_1}(1+\frac{\sqrt{s_1}}{K})\right\} \bar{f} \qquad (5.45)$$

For $K^2\tau >> (1 + K/\sqrt{p})^{-2}$

$$f' = \frac{2K\tau_1^{\frac{1}{2}}}{\sqrt{\pi}(1+\frac{K}{\sqrt{p}})} \qquad (5.46)$$

and for $\kappa^2\tau \ll (1 + \frac{K}{\sqrt{p}})^{-2}$

$$f' = K\kappa\tau \tag{5.47}$$

These more simple solutions of f' compared to the complex exponential expressions in the top row of Table (14) arise due to the condition $\tau_1 \ll 1$, i.e. the patch is applied to the skin for a very short time compared to the other characteristic times of the experiment.

Turning to solutions in the bottom row of Table (15), the term in unity when multiplied by $\bar{f}$ and inverted gives the answers in Table (14) with $\tau = \tau_1$. This term describes the material that accumulates while the patch is applied. For the second term expressions for f" are needed; where

$$f'' = \int_1^{-1} s\bar{f} = \left(\frac{\partial u'}{\partial \tau}\right)_{\tau=\tau_1} \tag{5.48}$$

The values of f" are given in Table (16) where the numbering of the different cases is identical to that used in Table (14).

Table (16) Values of f'' from equation (5.48)

IA (1 and 2)		IB1	IB2
$\frac{2K\tau_1^{-\frac{1}{2}}}{\sqrt{\pi}(1+K/\sqrt{p})}\ \exp(-1/4\tau_1)$		$\frac{4\sqrt{pK}\tau_1^{\frac{1}{2}}}{\sqrt{\pi}}\exp(-1/4\tau_1)$	$\frac{8K^2K\tau_1^{3}{}^{2}}{\sqrt{\pi}}\ \exp(-1/4\tau_1)$
IIA1	IIA2	IIB1	IIB2
$\frac{\sqrt{p}\tau_1^{-\frac{1}{2}}}{\sqrt{\pi}}$	$\frac{\kappa K}{2+\kappa}$	$\frac{2\sqrt{pK}\tau_1^{\frac{1}{2}}}{\sqrt{\pi}}$	$\kappa^2 K\tau$

The different solutions for u' and how they vary with the relative magnitudes of τ_1 and τ_2 are shown in Figure (49).

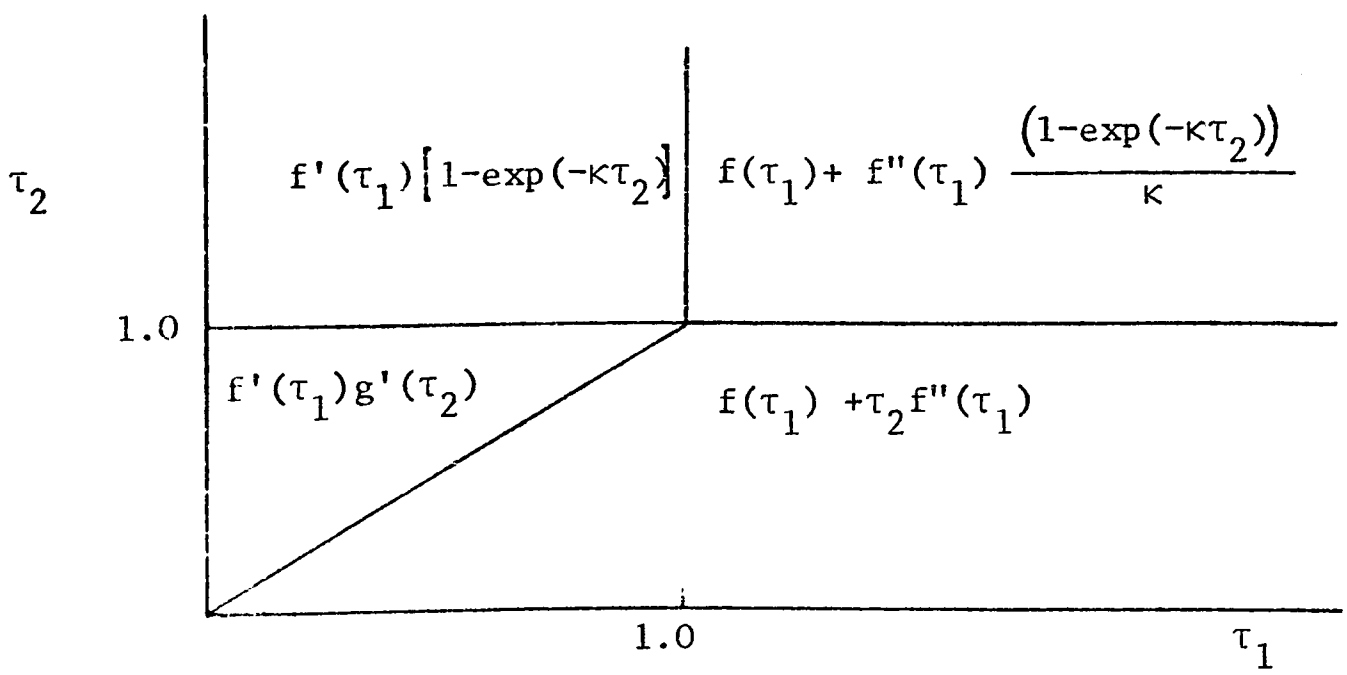

Figure (49). Regions where different approximate solutions for u' for the pulse experiments are found. Values for f, g', f'' and f' are given respectively in Tables 14, 15, 16, and equations (5.46) and (5.47).

Summary of solutions for u' given in Figure (49)

The solution in the bottom right hand corner is where most of the material accumulates in the dermis during the time the patch is applied [$f(\tau_1)$]. A small amount accumulates after the patch has been removed (given by $\tau_2(\partial f/\partial \tau_1)$); in this region the removal of the patch makes no difference to the time of onset of erythema.

In the top half of the figure τ_2 is long enough for the ester accumulated in the epidermis during τ_1 to diffuse to the dermis. The exponential expression arises from the inclusion of interfacial barriers in the model. If $K\tau_2 << 1$ the material will not be transported from the epidermis to the dermis. As $K\tau_2$ becomes large the solutions became independent of τ_2 and all the material accumulated in τ_1 diffuses into the dermis.

The left hand side of the figure shows solutions for short application times. The functions $f'(\tau_1)$ describe how much ester gets into the epidermis during relatively short applications of the patch. Depending on the size of τ_2 this quantity of ester has plenty of time to diffuse across the epidermis or its transport into the dermis is controlled by interfacial transfer at the epidermal-dermal junction described by the complicated function $g'(\tau_2)$.

II. Experimental

The method of application of the solution is the same for both types of experiment. The solutions were applied to the flexor aspect of the forearm of one subject. In order to prevent the solution running and spreading over the skin surface, Astra Hewlitt Al Test Patches were saturated with the solution and placed on the arm[77,78]. When saturated the patches contain 55 $\pm$ 0.5 µl of solution. These absorbent discs were chosen since they are free from skin sensitizers.

Eight discs were placed on each forearm and in a series of experiments the different solutions were applied to each of the available sites. Thus if there was any site variation, each set of results is equally weighted. In all experiments the skin was not pretreated or cleansed in any way. The investigation was conducted in a room where the temperature and humidity remained reasonably constant.

(a) Non pulse experiments

Methyl nicotinate was dissolved in water, 60% w/v glycerol, and glycerol to produce solutions with a concentration range 0.7-120 mM. The solutions were placed on the forearm using the absorbent discs and the times of onset of erythema recorded. The onset of erythema was taken to be the appearance of a red halo around the edge of the paper disc.

In order to minimise evaporation a piece of aluminium foil was left on the outer surface of the absorbent disc.

(b) Pulse Experiments

In this type of experiment, methyl, n-butyl, and n-hexyl nicotinate were dissolved in 40% w/v glycerol. This concentration of glycerol does not significantly alter the partition coefficient and serves to prevent problems caused by solvent evaporation. The saturated discs are placed on the forearm as before but are removed from the skin before the onset of erythema. Any excess solution left on the skin is carefully removed with an absorbent tissue.

Since erythema develops after the discs have been removed a timing standard has to be chosen. The time of onset of erythema could be taken immediately a red area appears or when a standard area of erythema has developed. Several experiments were conducted measuring the time of onset of erythema by both methods. After redness becomes first apparent the erythematous zone spreads very rapidly (figure (50)) and the most reproducible technique was found to be to time the first appearance of redenning.

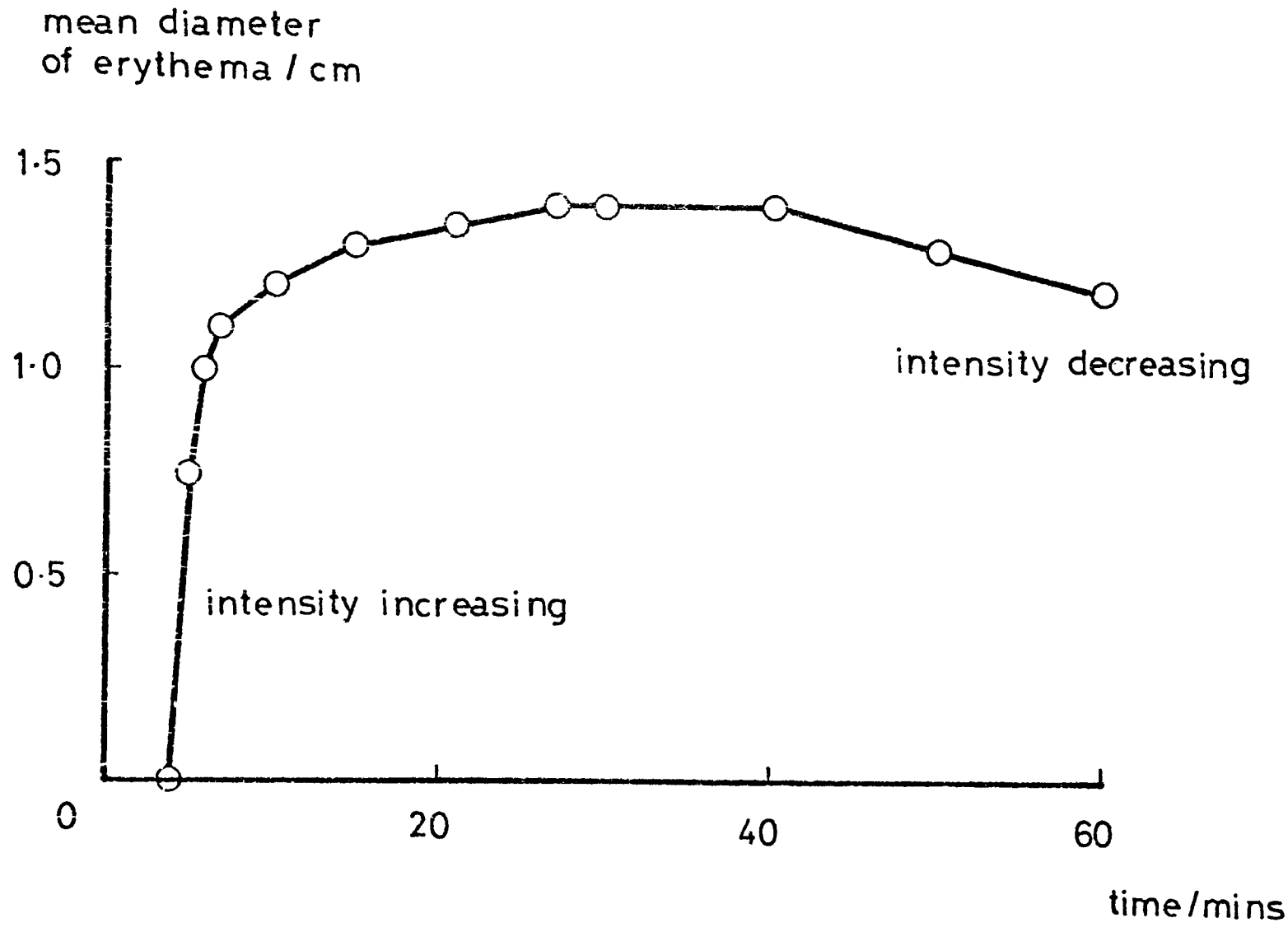

Figure (50). The development of an erythematous zone after the application of a solution of methyl nicotinate (75 mM) to the forearm.

III. Results

A. Non-pulsed experiments

The effect of concentration on the time of onset of erythema for the various aqueous solutions is shown in Table (17).

Table (17)

Methyl Nicotinate Concentration mM	Time of Onset of Erythema mins.	
0.729	10.7 ± 0.2	(16)
3.65	6.5 ± 0.1	(16)
7.29	4.7 ± 0.1	(16)
36.5	4.1 ± 0.1	(16)

Table (17) shows the effect of concentration of methyl nicotinate in water on the time of onset of erythema. The figures in parentheses are the number of determinations.

Table (18)

Methyl Nicotinate Concentration mM	Time of onset of Erythema mins	
0.876	13.7 ± 0.4	(24)
4.38	11.8 ± 0.2	(24)
8.76	6.8 ± 0.1	(24)
43.8	4.9 ± 0.1	(24)

Table (18) shows the effect of concentration of methyl nicotinate in 60% w/v glycerol on the times of onset of erythema. The figures in parentheses show the number of determinations.

Table (19)

Methyl Nicotinate Concentration mM	Time of onset of Erythema mins	
11.24	13.2 ± 0.1	(12)
56.2	8.8 ± 0.3	(12)
112.4	5.9 ± 0.1	(24)

Table (19) shows the effect of concentration of methyl nicotinate in 100% w/v glycerol on the times of onset of erythema. The figures in parentheses show the number of determinations.

Additional results relevant to this section have been obtained in previous work[77,78] and are shown in Table (20).

Table (20)

Methyl nicotinate mM	Time of onset of erythema/mins				
	0%	40%	60%	80%	100%
36.5	4.3 ± 0.1	4.7 ± 0.2	4.8 ± 0.1	6.2 ± 0.3	11.5 ± 0.4
70	4.0 ± 0.1	.	.	.	.
80	.	.	4.2 ± 0.1	.	.
100	.	.	.	4.3 ± 0.1	.
200	.	.	.	.	4.7 ± 0.1

Table (20) from references (77) and (78) shows the effects of increasing concentrations of glycerol and methyl nicotinate on the times of onset of erythema.

(i) Analysis of non-pulse results

From equation (5.29), the number of mols (n'_E) of ester per unit area required to trigger erythema is given by

$$n'_E = \ell . c_\infty . u' \qquad (5.29)$$

where ℓ is the diffusion path length, c_∞ is the concentration of nicotinate in the applied solution, and u' is given, for these continuous application results, in Table (14).

Using equation (5.29) and the functions from Table (14) it is possible to determine which expression best fits the data for the solutions containing no glycerol (Table (17) and the first column in Table (20)).

Starting with the bottom row of Table (14), the relationship between n_E' and t is of the form:

$$\left(\frac{n_E'}{\ell}\right) \cdot \frac{1}{c_\infty} = \Lambda t^{m/2} \qquad (5.49)$$

where Λ is a constant for any one set of conditions, t is the time of onset of erythema, and m takes the values 1, 2, 3, 4. A graph of $-\log c_\infty$ against $\log t$ is shown in figure (51). The points do not lie on a very good straight line but a least squares analysis gives a gradient of 4.3, i.e. m = 8.6. Thus none of the expressions in the lower row of Table (14) fits the data. This implies that $\tau \ll 1$ and the concentration distribution in the epidermis has not reached a steady state.

The remaining equations, in the top line of Table (14), are of the form:

$$\left(\frac{n_E'}{\ell}\right) \cdot \frac{1}{c_\infty} = \Lambda' t^{m/2} \exp(-1/4t) \qquad (5.50)$$

where m = 3, 5 or 7.

Taking logarithms:

$$\log_e\left(\frac{n_E'}{\ell}\right) = \log_e \Lambda' + \log_e(c_\infty t^{m/2}) - 1/4t \qquad (5.51)$$

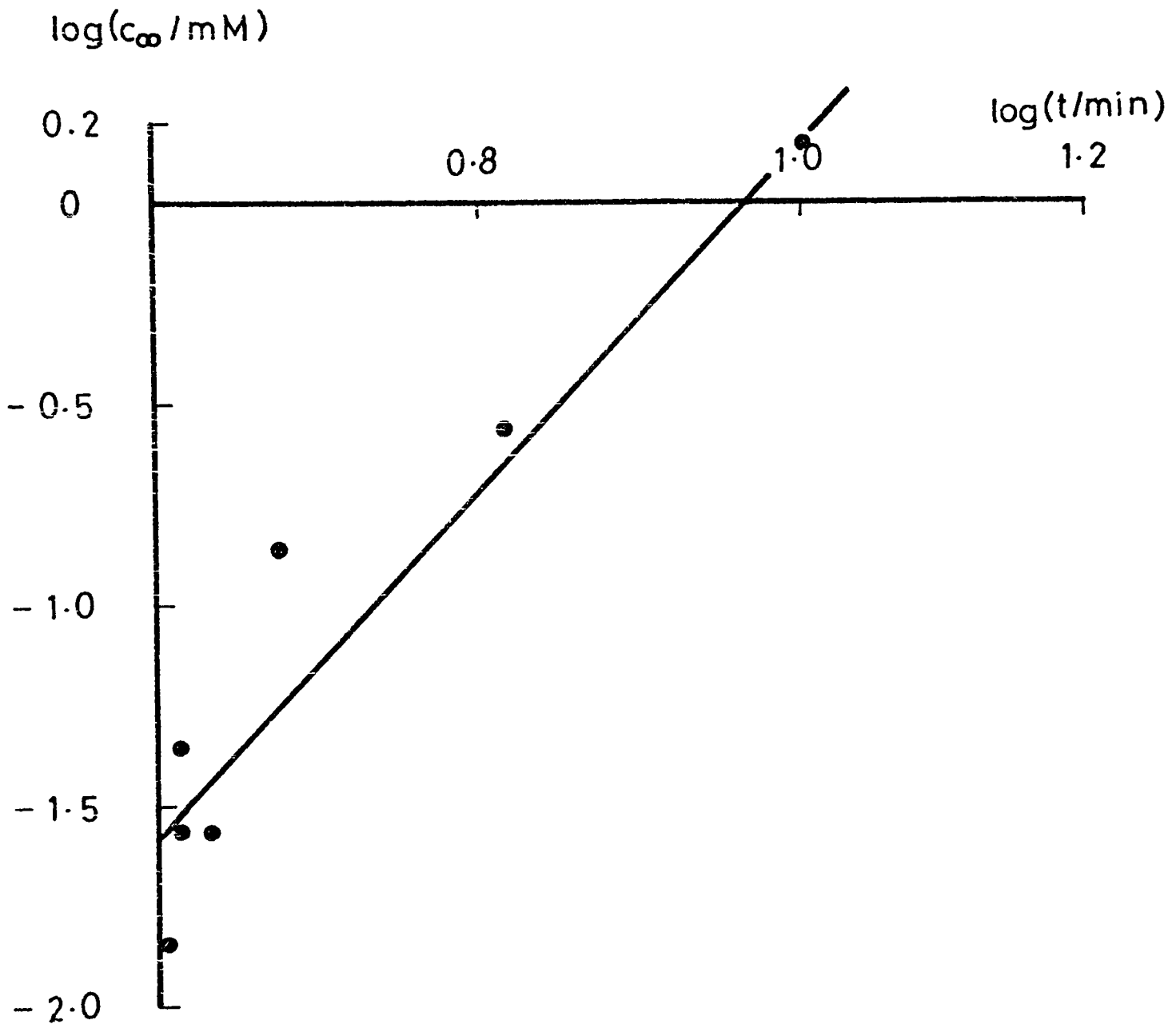

Figure (51). The relationship between log c_∞ and log t for solutions of methyl nicotinate.

Figure (52) shows graphs of $\log(c_\infty t^{m/2})$ plotted against 10/t. Linear regression analysis on the points gives the following results:

Value of m	Gradient	Intercept	Correlation Coefficient
3	0.78 ± 0.11	0.6 ± 0.2	0.921
5	0.51 ± 0.12	1.85± 0.24	0.827
7	0.24 ± 0.12	3.11± 0.26	0.550

The solution for m = 3 gives the best fit and thus for the penetration of methyl nicotinate, interfacial terms are not significant. However the Class IA solution does contain corrections for the effect of concentration depletion in the applied phase.

Concentrating in more detail on the Class IA result:

$$\log\left(\frac{n'_E}{\ell}\right) = \log(c_\infty t^{3/2}) + \log\left\{\frac{8K}{\sqrt{\pi}(1+K/\sqrt{p})}\cdot\left(\frac{D}{\ell^2}\right)^{3/2}\right\} - \frac{\ell^2}{4x2.303\ Dt} \quad (5.52)$$

and from the gradient:

$$\frac{\ell^2}{4 \times 2.303D} = 7.78$$

therefore

$$\frac{D}{\ell^2} = 1.4 \times 10^{-2}\ \text{min}^{-1}$$

$$= 2.33 \times 10^{-4}\ \text{s}^{-1}$$

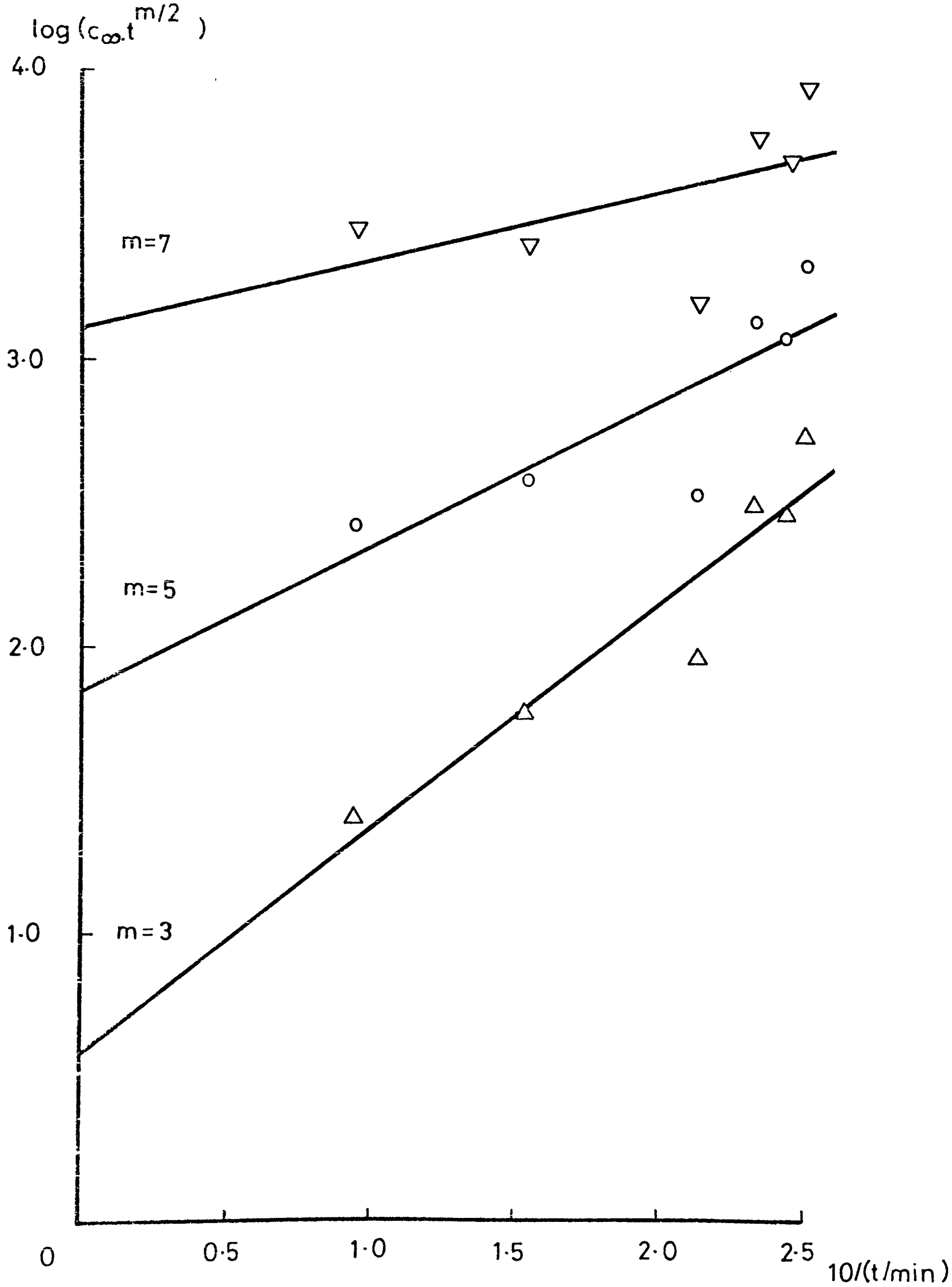

Figure (52). The relationship between $\log(c_\infty t^{m/2})$ and 10/t for aqueous solutions of methyl nicotinate.

With a knowledge of the value of ℓ, the diffusion coefficient could be calculated.

(a) The diffusional path length (ℓ). The stratum corneum provides the principal barrier to drug permeation through the skin and estimates of the diffusional path length are based on the structure of this layer. An idealized model of the stratum corneum has been postulated[124] and is shown in Figure (53).

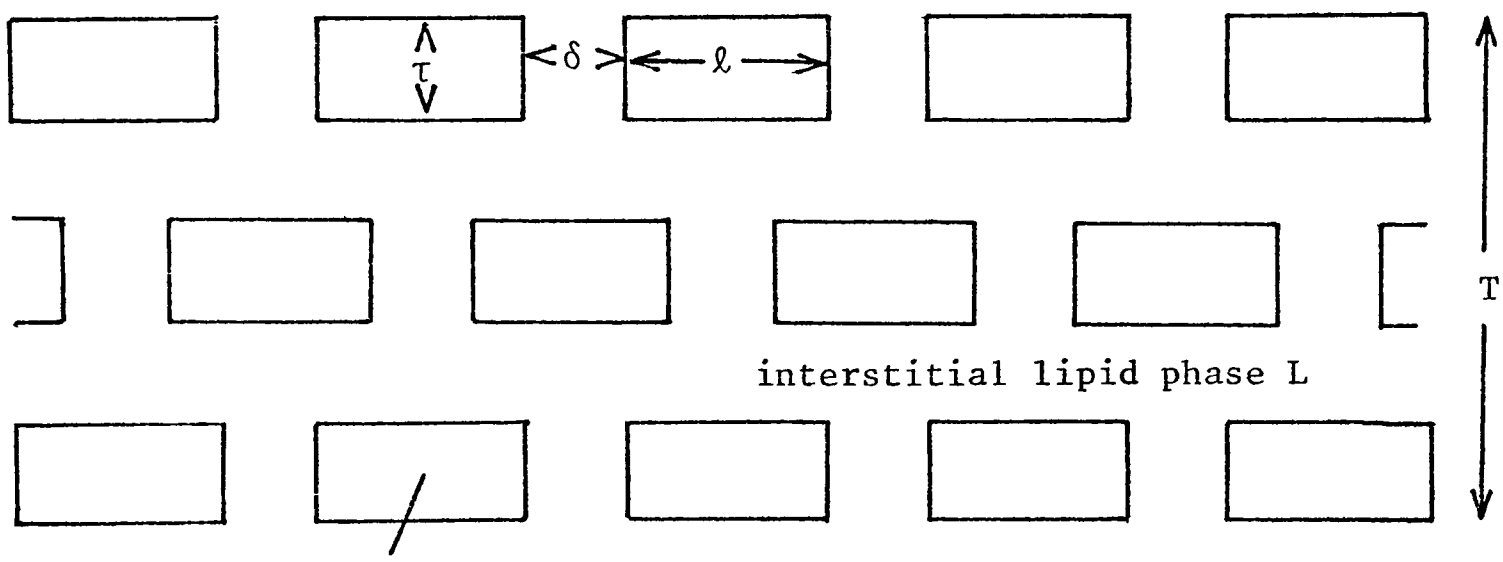

T - average thickness of stratum corneum

τ - average plate thickness

ℓ - average plate length

δ - average thickness of interstitial layer.

Figure (53). An Idealized Model of the Stratum Corneum.

From reference (124):

$$\alpha = \ell/\tau$$

$$\beta = \delta/\tau$$

$$\frac{\phi_L}{\phi_P} = \text{volume fraction ratio (lipid/proteinaceous)}$$

$$\frac{\phi_L}{\phi_P} = \frac{\beta}{\alpha}(\alpha + 2)$$

Area fraction of lipid phase at skin surface = $2\beta/\alpha$

Path length for transport round cells = $\left(1 + \left\{\frac{\alpha+\beta}{2(1+\beta)}\right\}\right).\ T = \lambda.T$

Typical values of τ, ℓ, ϕ_L/ϕ_P and T are respectively 0.5 μm, 25 μm, 0.176 and 15 μm[126,15,23]. Using these values the area fraction is 6.79×10^{-3} (cf. 4×10^{-3} from reference (15)) and the diffusional path length is:

i) 15 μm through the cells;

ii) 337 μm round the cells.

(b) Diffusion coefficient of methyl nicotinate in the skin. Using the two diffusional path lengths, two values for the diffusion coefficient of methyl nicotinate in the stratum corneum may be calculated.

For a path length of 15 μm:

$$D_T = 5.25 \times 10^{-14}\ m^2\ s^{-1}.$$

For a path length of 337 μm:

$$D_R = 2.65 \times 10^{-11}\ m^2\ s^{-1}.$$

The value of D_R for the longer path length is about a factor of ten lower than IPM which may be attributed to the presence of higher molecular weight species (e.g. sterols) in the skin lipids.

(ii) Analysis of results, showing the effect of concentration depletion

Equation (5.52) may be rewritten to give a form in which c_∞ can be corrected to take into account concentration depletion in the applied solution:

$$\log\left(\frac{n'_E}{\ell}\right) = \log\left[F.c_\infty.t^{3/2}\right] + \log\left\{\frac{8}{\pi^{\frac{1}{2}}}\left(\frac{D}{\ell^2}\right)^{3/2}\right\} - \frac{\ell^2}{4 \times 2.303Dt} \qquad (5.53)$$

where $$F = K/(1 + K/\sqrt{p}) \qquad (5.54)$$

$$p = D_{aq}/D_{skin}$$

The solution in immediate contact with the skin surface has been estimated to be at a temperature of 30°C. The diffusion coefficients of methyl nicotinate in the aqueous glycerol mixtures (Table (21)) have been estimated from the viscosities of the glycerol solutions at 30°C [110]. Values of the IPM/Solution partition coefficients (K) are used to calculate F in Table (21).

Two values of the correcting function F, F_R and F_T are given, these correspond to the two proposed mechanisms of penetration. If diffusion is assumed to be through the cells, a

smaller skin diffusion coefficient is used and values of F_T are correspondingly higher than those of F_R.

Table (21). Values of correcting functions (F) to allow for concentration depletion in the applied solution.

Glycerol % w/v	D_{aq}/m^2Gs^{-1}	K	Through Cells		Round Cells	
			$\sqrt{p_T}$	F_T	$\sqrt{p_R}$	F_R
0	1.0	3.28	138	3.2	6.2	2.15
10	0.77	3.13	121	3.05	5.44	1.99
40	0.29	3.05	74.3	2.93	3.34	1.59
60	0.11	2.76	45.8	2.60	2.06	1.18
80	0.02	2.27	19.5	2.03	0.88	0.63
90	0.007	1.9	11.5	1.63	0.52	0.41
100	1.31×10^{-3}	1.07	4.99	0.88	0.22	0.19

Figure (54) shows $\log(K\, c_\infty t^{3/2})$ plotted against 10/t for the values of c_∞ and t given in Tables (17,18,19 and 20). A straight line of gradient 0.78 (from Figure (52)) has been forced through the points. Figure (55) shows how the correcting factors F_T and F_R improve the straight line.

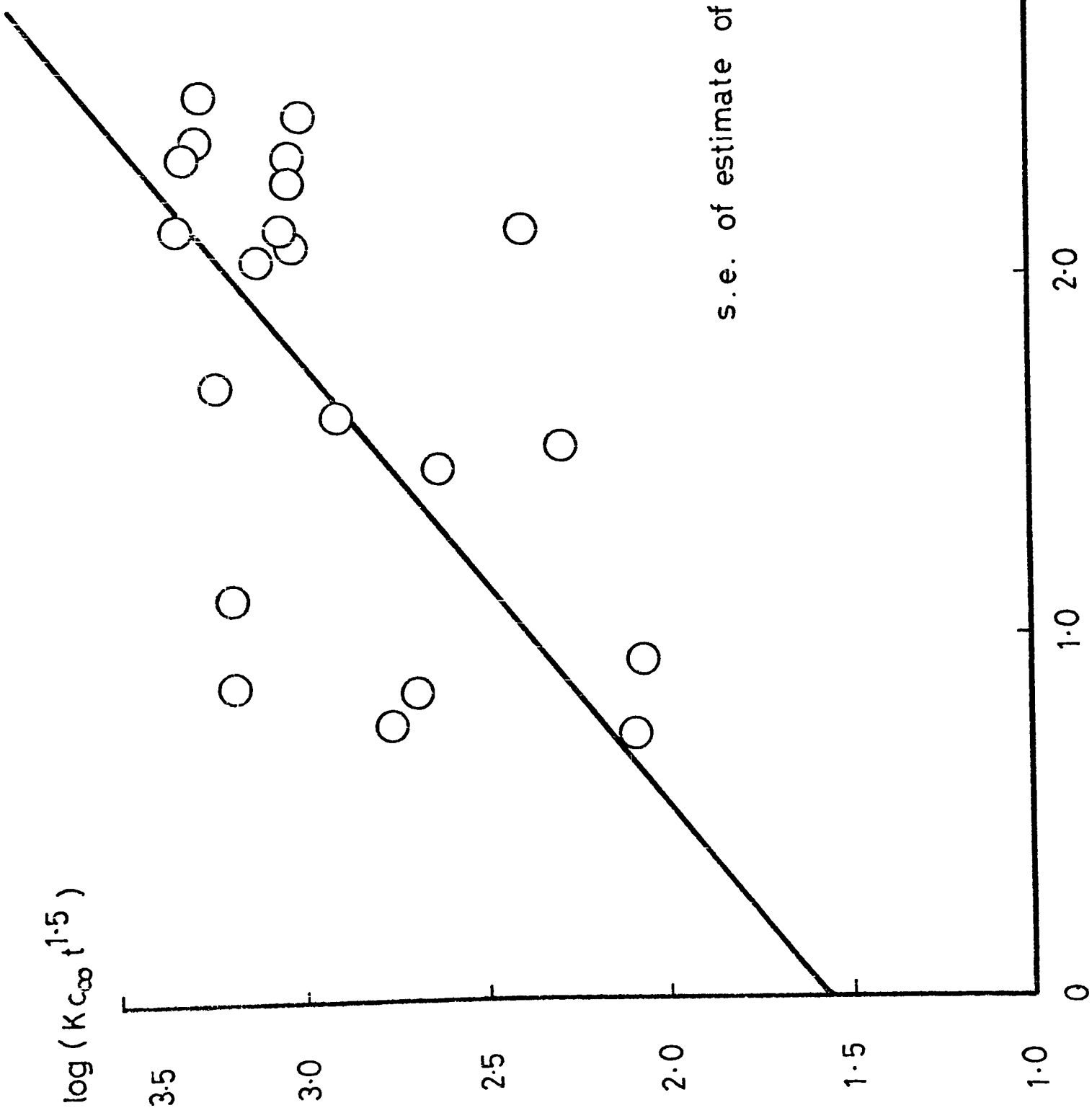

Figure (54). Relationship between log(K $c_\infty t^{3/2}$) and 10/t for aqueous glycerol solutions of methyl nicotinate.

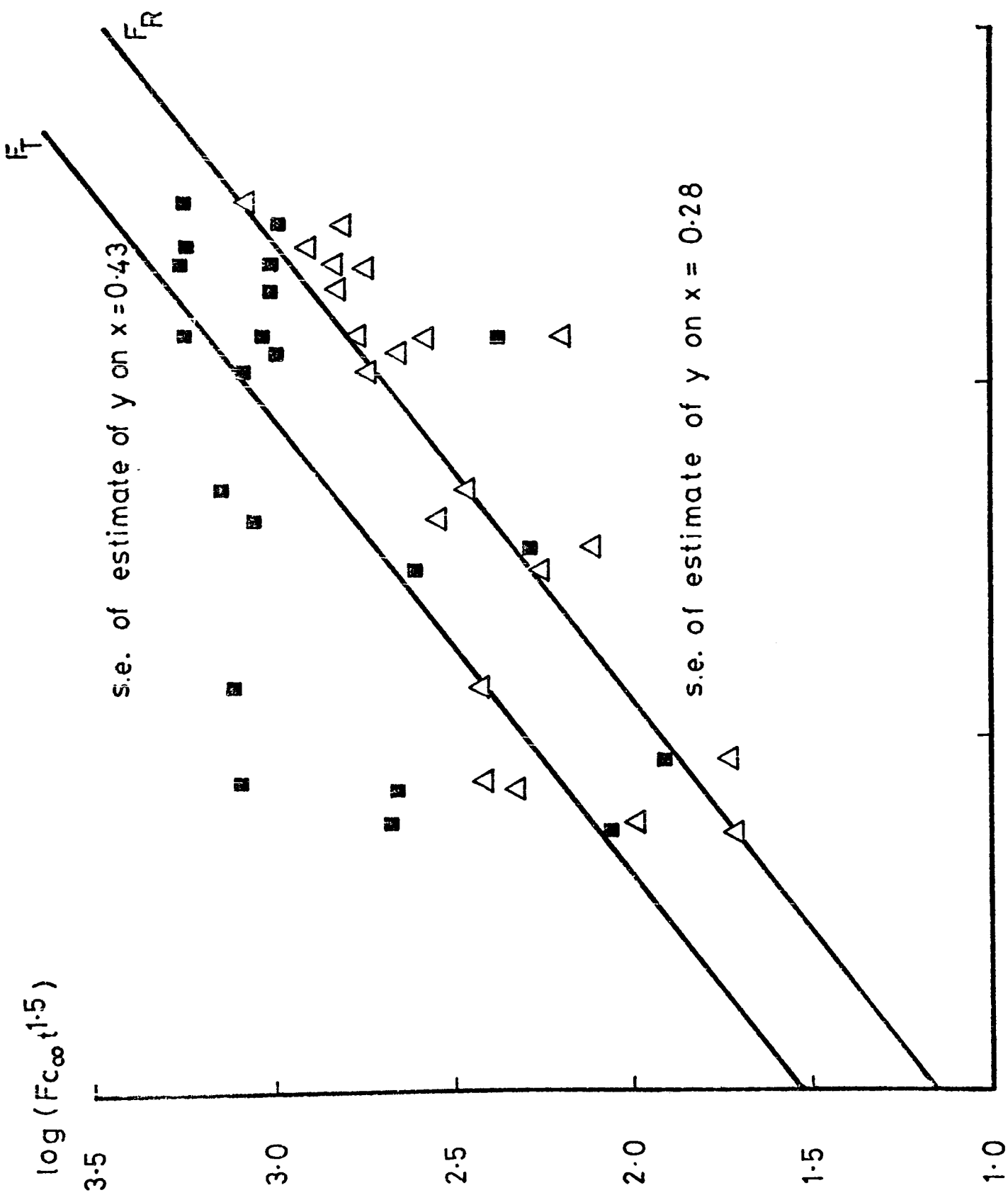

Figure (55). Relationship between $\log(Fc_\infty t^{3/2})$ and 10/t showing how F_R reduces the scatter of the experimental points.

The scatter of the points in figures (54) and (55) has been markedly reduced when the correcting factor F_R has been used. This suggests that the route of penetration of methyl nicotinate through the skin is via the lipid rich intercellular channels.

The triggering concentration (n'_E) of methyl nicotinate.

From equation (5.53), when 10/t is zero

$$\log(n'_E/\ell) = \log(F.c_\infty t^{3/2}) + \log\left\{\frac{8}{\pi^{\frac{1}{2}}}\left(\frac{D}{\ell^2}\right)^{3/2}\right\} \qquad (5.55)$$

and from the intercepts of Figure (55), estimates of (n'_E/ℓ) can be obtained.

Route of penetration through the cells. For penetration through the cells the correcting factor F_T is used. The intercept of the appropriate line in Figure (55) is:

$$\log(F_T.c_\infty.t^{3/2})_{[10/t=0]} = 1.52 \pm 0.06$$

Therefore, using equation (5.55), with a value of (D/ℓ^2) of 1.4×10^{-2} min^{-1}, and expressing c_∞ in mol. cm^{-3} rather than mM

$$\log(n'_{E,T}/\ell) = 1.52 + (-2.13) + (-6)$$

$$n'_{E,T}/\ell = 2.48 \times 10^{-7} \text{ mol. cm}^{-3}$$

therefore $$n'_{E,T} = 3.71 \times 10^{-10} \text{ mol.cm}^{-2}$$

The number of mols per cm^2 of methyl nicotinate required to trigger erythema assuming the route of penetration to be through the cells of the stratum corneum is 3.7×10^{-10}.

Route of penetration via the intercellular channels. For penetration round the cells, the correcting factor F_R is used and the intercept of the appropriate line in Figure (55) is:

$$\log(F_R . c_\infty . t^{3/2})_{[10/t=0]} = 1.14 \pm 0.04$$

Calculating as in the previous section:

$$n'_{E,R}/\ell = 1.03 \times 10^{-7} \text{ mol. cm}^{-2}$$

$$n'_{E,R} = 3.47 \times 10^{-9} \text{ mol. cm}^{-2} .$$

From this calculation it is seen that approximately ten times more methyl nicotinate is required to trigger erythema if the route of penetration is via the intercellular channels.

Since the absolute quantity of methyl nicotinate required to trigger erythema is unknown, it is not possible to tell from the calculated values of n'_E which route of penetration is favoured. However, since the best straight line was obtained when the correcting factor F_R was used it seems probable that the predominant route is via the lipid rich intercellular channels.

B. Pulsed Experiments

The concentrations of the esters used in these experiments were:-

methyl	75 mM
n-butyl	5.3 mM
n-hexyl	0.92 mM

Solutions of n-butyl and n-hexyl nicotinate could not be made more concentrated than this and therefore the effect of concentration on the time of onset of erythema, for these two esters, could not be studied.

In some experiments the erythematous zone did not remain circular. This was attributed to smearing the solution after the patch had been removed. Consequently some solution must have remained in contact with the skin after the patch had been taken away and when this irregularity was noticed the results were rejected. The results of the successful applications are shown in Table (22).

Table (22) shows the results for the pulsed experiments on methyl, n-butyl and n-hexyl nicotinate. The figures in parentheses are the number of determinations.

Table (22)

Application Time mins	Time of Onset of Erythema/mins		
	Methyl Nicotinate	Butyl Nicotinate	Hexyl Nicotinate
0.33	5.3 ± 0.1 (80)	-	-
0.58	5.2 ± 0.1 (80)	6.8 ± 0.1 (80)	-
1.0	4.4 ± 0.1 (80)	5.9 ± 0.1 (80)	-
2.0	3.7 ± 0.1 (80)	5.2 ± 0.1 (80)	-
3.0	3.9 ± 0.1 (80)	5.1 ± 0.1 (80)	12.4 ± 0.5 (16)
5.0	-	-	10.1 ± 0.2 (16)
7.0	-	-	9.4 ± 0.2 (16)
8.0	-	-	8.9 ± 0.1 (16)

The results for the pulsed experiments can be tabulated further. The experiment can be regarded in two parts, the first where the solution is in contact with the skin (time t_1) and the second where the solution has been removed up to the time of onset of erythema (time t_2). Schematically:-

Application Removal of Solution Erythema

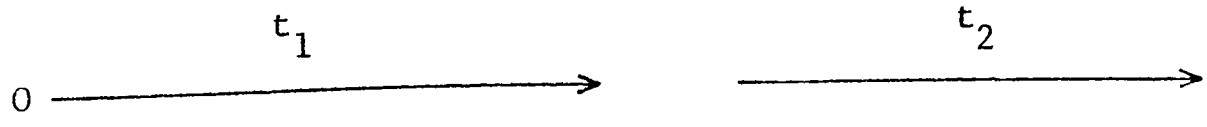

For the pulsed experiments times t_1 and t_2 are separated in Table (23).

Table (23)

Methyl Nicotinate (75mM)		Butyl Nicotinate (5.3mM)		Hexyl Nicotinate (0.92mM	
t_1/min	t_2/min	t_1/min	t_2/min	t_1/min	t_2/min
0.33	5.0	-	-	-	-
0.58	4.6	0.6	6.3	-	-
1.0	3.4	1.0	4.9	-	-
2.0	1.7	2.0	3.2	-	-
3.0	0.9	3.0	2.1	3.0	9.4
-	-	-	-	5.0	5.1
-	-	-	-	7.0	2.4
-	-	-	-	8.0	0.9

Table (23) shows the values of t_1 and t_2 (see text) for the pulsed experiments for the different nicotinates.

(i) Analysis of pulse results

For the pulse experiments, u' is given by equation (5.43)

$$\frac{u'}{s_1 s_2} = \bar{\bar{u}} = \bar{f}\,\bar{\bar{g}} \qquad (5.43)$$

Solutions for $\bar{f}$ and $\bar{\bar{g}}$ have been given in Tables (14) and (15), however these solutions only apply when s_1 and s_2 differ by at least an order of magnitude. The values of t_1 and t_2 in Table (23) show that for this set of experiments t_1 and t_2 and consequently s_1 and s_2 are of the same order of magnitude.

Values of t_1 and t_2 are approximately 3 minutes, therefore using the value of 1.4×10^{-2} min^{-1} for D/ℓ^2:

$$\tau \sim 3 \times 1.4 \times 10^{-2}$$
$$\sim 4 \times 10^{-2}$$

and both s_1 and s_2 will be greater than 1.0. Using the conditions that $s_1 \sim s_2 > 1$ simplifies the expression for u'

$$u' = s_1 s_2 \bar{f} \bar{\bar{g}} \qquad (5.56)$$

Substituting equations (5.32) and (5.44) for $\bar{f}$ and $\bar{\bar{g}}$ and simplifying the hyperbolic functions since s_1 and s_2 are large gives:-

$$u' = \frac{2Ks_2 e^{-\sqrt{s_1}}}{s_1^{\frac{1}{2}}\left[1 + \frac{\sqrt{s_1}}{K}\right]\left[1 + \frac{\sqrt{s_1}}{K} + \frac{K}{\sqrt{p}}\right]} \frac{1}{(s_2 - s_1)} \left\{1 - \left(\frac{s_1(e^{\sqrt{s_1}} + \sqrt{s_1} e^{\sqrt{s_1}/K}}{s_2(e^{\sqrt{s_2}} + \sqrt{s_2} e^{\sqrt{s_2}/K}}\right)\right\} \qquad (5.57)$$

This expression cannot be transformed to give a value of u' in t_1 and t_2 and a different analytical procedure is adopted to interpret these results.

The following flow diagram explains the new procedure:

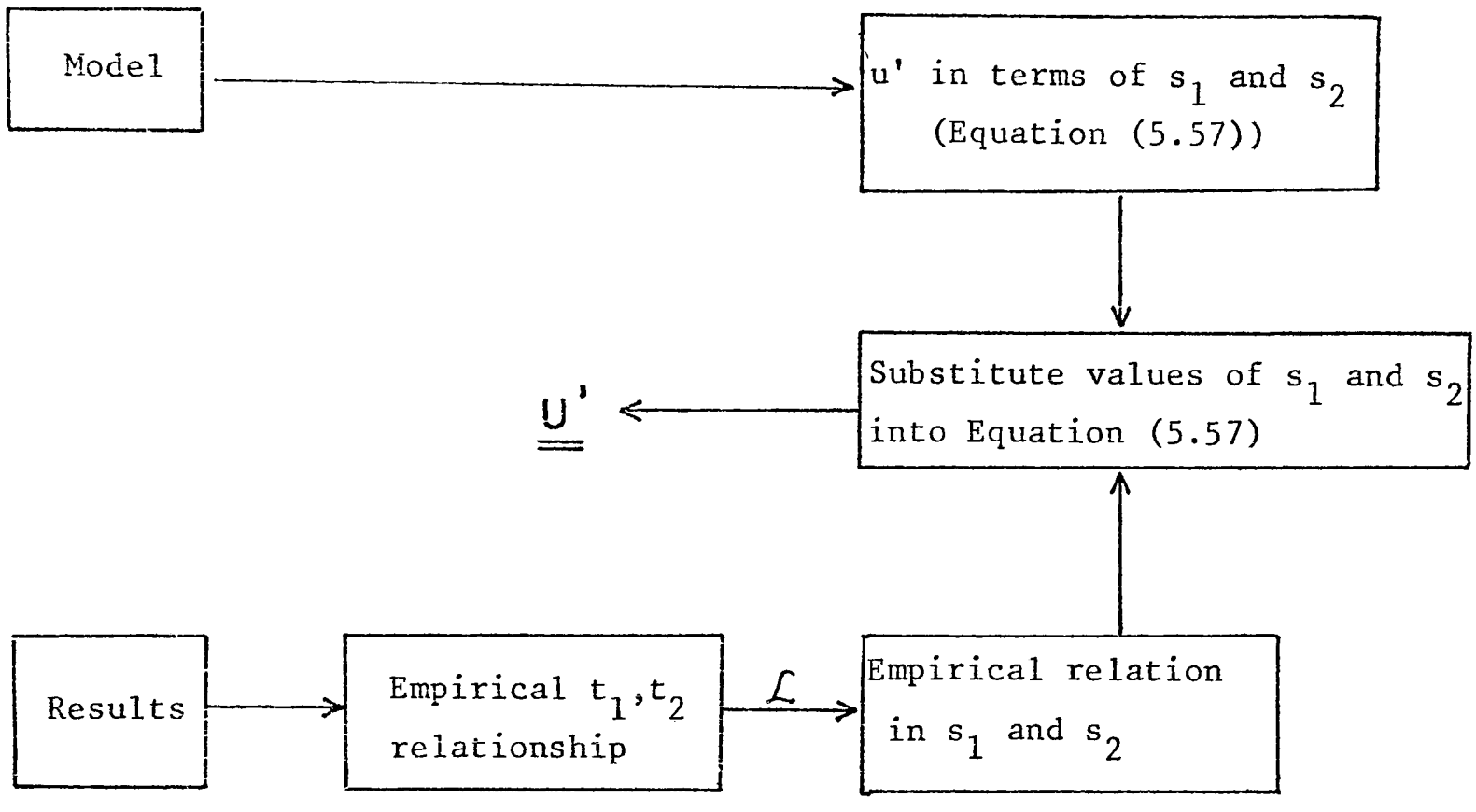

From the results an empirical relationship between t_1 and t_2 is found. The equation describing this relationship is transformed to give a relationship between s_1 and s_2. Values of s_1 and s_2 can then be calculated which are in the correct range and then substituted into equation (5.57) giving values of u'. The values of u' generated by substituting s_1 and s_2 should be constant over the chosen range.

A computer program, given in Appendix (4), has been written which calculates u' for different values of s_1, s_2, κ and $K/\sqrt{p}$.

(a) Empirical relationships between t_1 and t_2. For methyl and n-butyl nicotinate, linear relationships are found between $1/t_1$ and t_2^3. The straight line graphs obtained are shown in Figure (56) and the corresponding equations are:-

$$\text{methyl:} \qquad 1/t_1 = 0.018\ t_2^3 + 0.329 \qquad (5.58)$$

$$\text{n-butyl:} \qquad 1/t_1 = 5.83 \times 10^{-3}\ t_2^3 + 0.298 \qquad (5.59)$$

In the case of n-hexyl nicotinate the best fit is found for a relation between $1/t_1$ and $t_2^{1.91}$ (Figure (57)). The equation relating these two variables is:

$$1/t_1 = 2.85 \times 10^{-3}\ t_2^{1.91} + 0.127 \qquad (5.60)$$

(b) Values of κ and $K/\sqrt{p}$ for obtaining u' . The other variables required to estimate u' from equation (5.57) are the normalized interfacial rate constant, κ, and the depletion factor $K/\sqrt{p}$.

Normalized interfacial rate constants. From the theory section:

$$\kappa = \frac{k_{-I} \cdot \ell}{K \cdot D}$$

Values of k_{-I} are those measured for crossing a water/isopropyl myristate boundary and the values of K used are the isopropyl myristate - water partition coefficients. The values of ℓ and D taken will depend on the route of penetration and two values

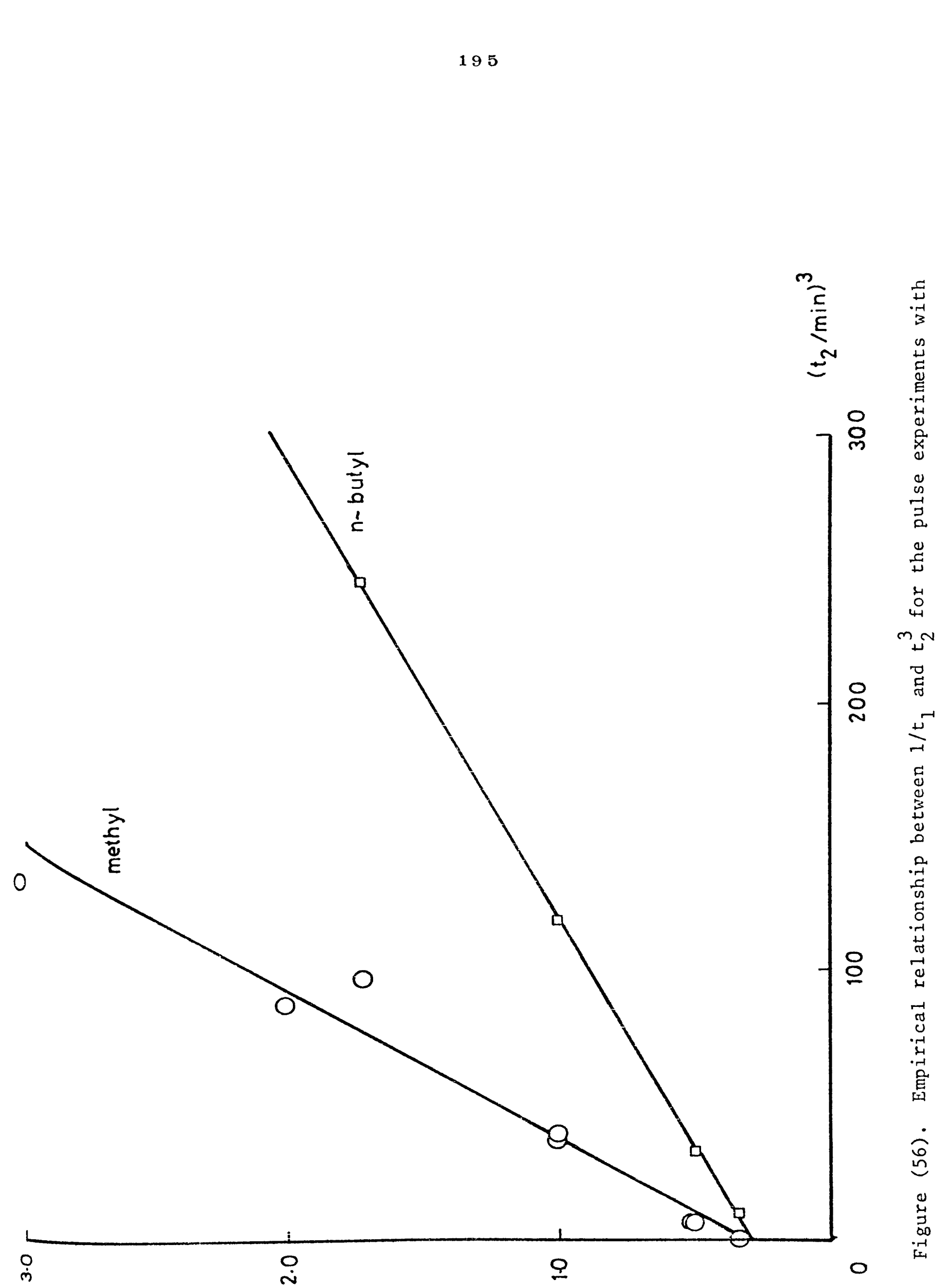

Figure (56). Empirical relationship between $1/t_1$ and t_2^3 for the pulse experiments with methyl and butyl nicotinate.

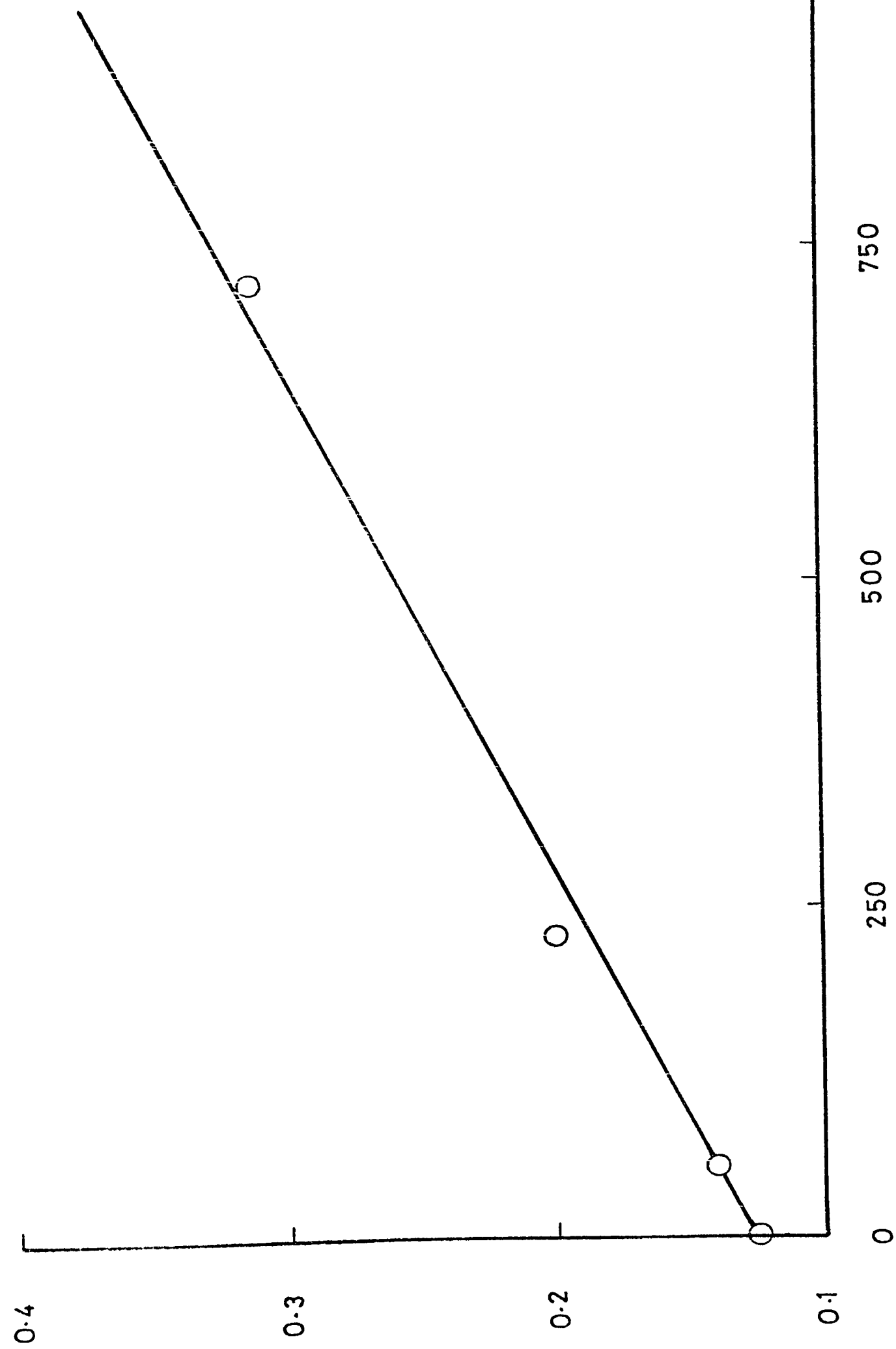

Figure (57). Empirical relationship between $1/t_1$ and $t_2^{1.91}$ for the pulse experiments with hexyl nicotinate.

of κ, κ_R and κ_T for transport round and through the cells will be obtained. The values are given in Table (24).

Table (24). Values of the normalised interfacial rate constants for methyl, butyl and hexyl nicotinate.

	Methyl	n-butyl[1]	n-hexyl[1]
$k_{-I}/m.Ms^{-1}$	46	223	17
K	3.05	38.5	71.3
$D_T/m^2\ Ts^{-1}$	0.053	0.044	0.041
$D_R/m^2\ Gs^{-1}$	0.026	0.022	0.02
κ_T	4309	1961	86.6
κ_R	195	88.7	4.01

---

[1] D values for n-butyl and n-hexyl nicotinate calculated by the ratio method (page 51).

Depletion correction ($K/\sqrt{p}$). The depletion correction $K/\sqrt{p}$ will also be dependent on the route of penetration and values for the two functions are given in Table (25).

Table (25). Value of the depletion correction $K/\sqrt{p}$ for the different nicotinates.

	Methyl	n-butyl[1]	n-hexyl[1]
K	3.05	38.5	71.3
D_{aq}/m^2Gs^{-1}	0.29	0.24	0.22
$\sqrt{p_T}$	74.32	73.6	73.1
$\sqrt{p_R}$	3.34	3.30	3.33
$K/\sqrt{p_T}$	0.041	0.423	0.977
$K/\sqrt{p_R}$	0.91	11.67	21.42

---

[1] D values for n-butyl and n-hexyl nicotinate calculated by the ratio method (page 51).

(c) Calculation of the values of u'.

Methyl nicotinate. Experimentally, the relationship between t_1 and t_2 was found to be:

$$\frac{1}{t_1} = 0.018\ t_2^3 + 0.329 \qquad (5.58)$$

or

$$3.04 = t_1(5.47 \times 10^{-2}\ t_2^3 + 1) \qquad (5.61)$$

In terms of the normalized time function $\tau(\tau = tD/\ell^2 = t\theta)$

$$3.04.\theta = \tau_1\left(1 + \frac{5.47 \times 10^{-2}\ \tau_2^3}{\theta^3}\right) \qquad (5.62)$$

which may be expressed

$$A' = \tau_1(1 + B'\ \tau_2^3) \qquad (5.63)$$

Taking Laplace transforms,

$$\frac{A'}{s_1 s_2} = \frac{1}{s_1^2}\left(\frac{1}{s_2} + \frac{6B'}{s_2^4}\right) \qquad (5.64)$$

$$s_1 = \frac{1}{A'} + \frac{6B'}{s_2^3} \qquad (5.65)$$

where $A' = 3.04 \times D/\ell^2 = 4.26 \times 10^{-2}$

$B' = 5.47 \times 10^{-2}/(D/\ell^2)^3 = 1.99 \times 10^4$.

The results in Table (23) show that the ratio t_1/t_2 varies from 7×10^{-2} to 3 and thus the range of values of s_1/s_2 for which equation (5.57) should remain constant is ~ 15 to 0.3.

Table (26) shows values of s_1 and s_2 which obey equation (5.65); values of u' are given which have been calculated using the computer program in Appendix (4).

Table (26)

s_1	s_2	s_1/s_2	$u' \times 10^3$ (κ_R =195, $K/\sqrt{p_R}$=0.91)	$u' \times 10^3$ (κ_T=4309, $K/\sqrt{p_T}$=0.041)
26.3	100	0.26	4.8	9.15
27.3	90	0.3	4.52	8.60
29	80	0.36	4.05	7.72
31.7	70	0.45	3.46	6.61
36.5	60	0.61	2.73	5.22
46	50	0.92	1.97	3.79
67.4	40	1.69	1.48	2.85
78.95	37	2.13	1.42	2.74
101.66	33	3.08	1.41	2.73
127.5	30	4.25	1.46	2.82
151.46	28	5.41	1.51	2.93
226.69	24	9.45	1.66	3.23
374.6	20	18.73	1.85	3.63

Table (26) shows values of s_1, s_2 and u' for methyl nicotinate.

For transport both through and round the cells, the value of u' remains within a factor of four over a large s_1/s_2 range. In biological models this sort of deviation is expected.

n-butyl nicotinate. A similar treatment is adopted with this ester. Equation (5.65) is still applicable but the values of A' and B' are different:

$$s_1 = \frac{1}{A'} + \frac{6B'}{s_2^3} \qquad (5.65)$$

where $A' = 3.356 \times D/\ell^{2*} = 3.96 \times 10^{-2}$

$B' = 1.956 \times 10^{-2}/(D/\ell^2)^3 = 1.19 \times 10^4$

The results of the pulse experiments show a variation in the t_1/t_2 ratio from 9.5×10^{-2} to 1.5 and thus the chosen range of s_1/s_2 values has been taken to be from 11 to 0.7.

Table (27) shows values of s_1 and s_2 calculated using equation (5.65). Values of u' are also given for values of κ and $K/\sqrt{p}$ corresponding to the two different penetration mechanisms.

---

* D/ℓ^2 for butyl nicotinate has been estimated

$$(D/\ell^2)_{butyl} = (D/\ell^2)_{methyl} \times \frac{D_{butyl,IPM}}{D_{methyl,IPM}}$$

$$= 0.012 \quad .$$

Table (27)

s_1	s_2	s_1/s_2	$u' \times 10^3$ $K_R = 38.5$ $K/\sqrt{p_R} = 11.67$	$u' \times 10^2$ $K_T = 1961$ $K/\sqrt{p_T} = 0.523$
33.6	60	0.56	6.23	5.5
39.7	50	0.79	5.07	4.5
45.04	45	1	4.48	3.98
53.4	40	1.34	3.98	3.54
92	30	3.07	3.65	3.23
116.85	27	4.33	3.79	3.34
173.44	23	7.54	4.12	3.63
250.6	20	12.53	4.47	3.93

Table (27) shows values of s_1, s_2 and u' for n-butyl nicotinate.

Over the range of s_1/s_2 chosen the function u' remains essentially constant for both proposed routes of penetration.

n-hexyl nicotinate. For this ester a slightly different analysis is needed since the relationship between $1/t_1$ and t_2 is not cubic as before.

The equation best fitting the data was found to be:

$$\frac{1}{t_1} = 0.127 + 2.85 \times 10^{-3} \, t_2^{1.91} \qquad (5.60)$$

which is of the form

$$\frac{1}{t_1} = A + Bt_2^{1.91} \qquad (5.61)$$

Normalizing the time variables (using $D/\ell^2 = \theta$):

$$1 = \frac{\tau_1}{\theta}\left(A + \frac{B\tau_2^{1.91}}{\theta^{1.91}} \right) \qquad (5.66)$$

which may be transformed:

$$\frac{1}{s_1 s_2} = \frac{1}{s_1^2 \theta}\left(\frac{A}{s_2} + \frac{B\Gamma(2.91)}{\theta^{1.91} s_2^{2.91}} \right) \qquad (5.67)$$

Therefore

$$s_1 = \frac{A}{\theta} + \frac{B\Gamma(2.91)}{\theta^{2.91} s_2^{1.91}} \qquad (5.68)$$

where

$$A = 0.127$$

$$B = 2.88 \times 10^{-3}$$

$$\Gamma(2.91) = 1.91\Gamma(1.91) = 1.844 .$$

In this set of experiments the range of s_1/s_2 has been taken to be from 3 to 0.1. The values of s_1 and s_2 which fit equation (5.64) are given in Table (28) with the corresponding u' values for both penetration routes.

Table (28). Values of s_1, s_2 and u' for n-hexyl nicotinate.

s_1	s_2	s_1/s_2	$u' \times 10^2$ $\kappa_R=4.01$ $K/\sqrt{p_R}=21.42$	$u' \times 10$ $\kappa_T= 86.6$ $K/\sqrt{p_T}= 0.977$
11.91	100	0.119	3.44	7.1
13.01	50	0.26	3.26	6.85
15.48	30	0.516	2.87	6.19
20.12	20	1.006	2.54	5.53
23.298	17	1.37	2.47	5.34
34.36	12	2.863	2.57	5.34
43.88	10	4.388	2.73	5.52

For both diffusion round and through the cells, the function is essentially constant over the desired range.

Summary

Values of log u' are plotted against log s_1/s_2 in Figure (58). The reasonably horizontal lines show that over the appropriate ranges of s_1 and s_2 the function u' remains constant. For further analysis of the results mean values of u' have been estimated. These are given in Table (29).

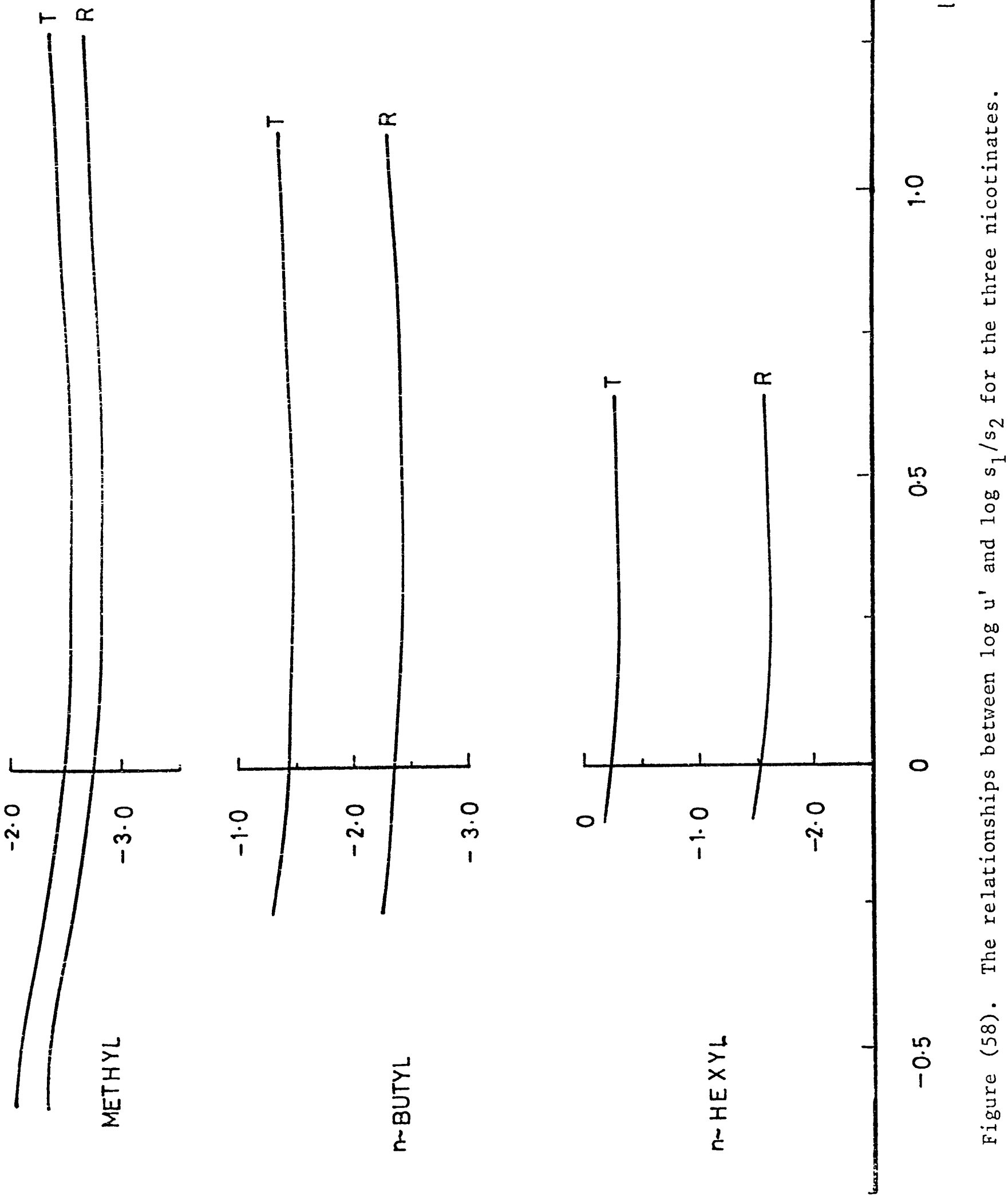

Figure (58). The relationships between log u' and log s_1/s_2 for the three nicotinates.

(d) Calculation of the triggering concentration n'_E.

The concentration of nicotinate required to produce erythema (n'_E) should be independent of the alkyl group[121]. It is possible to calculate the values of n'_E as before from the values of u'. Since u' does vary slightly with s_1/s_2 a mean value of u' is estimated which is substituted into equation (5.29) to give a value for n'_E

$$n'_E = \ell \cdot c_\infty \cdot u' \qquad (5.29)$$

Table (29). The mean values of u' and corresponding n'_E for the two different routes of penetration.

	Methyl	n-butyl	n-hexyl
c_∞/mol.cm^{-3}	75×10^{-6}	5.3×10^{-6}	0.92×10^{-6}
$\bar{u}_R$	2.08×10^{-3}	4.31×10^{-3}	2.7×10^{-2}
$\bar{u}_T$	4.03×10^{-3}	3.81×10^{-2}	0.57
$n'_{E,R}$/mol.cm^{-2}	5.26×10^{-9}	0.77×10^{-9}	0.84×10^{-9}
$n'_{E,T}$/mol.cm^{-2}	4.53×10^{-10}	3.03×10^{-10}	7.87×10^{-10}

The triggering concentrations obtained from the non pulsed experiments were:-

$$n'_{E,R} = 3.47 \times 10^{-9} \text{ mol. cm}^{-2}$$

$$n'_{E,T} = 3.7 \times 10^{-10} \text{ mol. cm}^{-2} .$$

Since the values should be independent of the alkyl group a mean triggering concentration may be calculated:

$$\bar{n}'_{E,R} = 2.6 \times 10^{-9} \text{ mol. cm}^{-2} \qquad (\sigma = 2.2 \times 10^{-9})$$

$$\bar{n}'_{E,T} = 4.8 \times 10^{-10} \text{ mol.cm}^{-2} \qquad (\sigma = 2.1 \times 10^{-10}) .$$

Thus for both proposed routes of penetration a fairly constant value has been obtained for the triggering concentrations.

CHAPTER VI

GENERAL DISCUSSION

The research conducted in this thesis may be divided into two complementary sections. Primarily the work was performed to gain a better understanding of the physical chemistry involved in percutaneous absorption. However, in pursuing this aim, interesting discoveries were made concerning the general transport of species between two liquid phases.

A novel piece of apparatus was developed to extend the range over which interfacial transfer reactions had previously been studied. The technique involved the measurement of transport rates between two compartments separated by a Millipore filter. The construction of the diffusion cell allowed rotation of the Millipore filter and hence controlled convective flow patterns to its surfaces.

Initially experiments were conducted to test that the hydrodynamics produced in the cell were those predicted by the Levich equation[92]. The first sets of data were obtained using a single phase throughout the cell. The diffusion of acetic acid was studied as this carboxylic acid has well documented aqueous diffusion coefficients[103]. Non-reproducible results were obtained since hydrostatic pressure differences in the two compartments caused mass flow through the filter. Equations were derived which showed that transfer by mass flow was far more

efficient than diffusional transport. It became apparent that the experimental technique had to be modified to prevent mass transfer between the two compartments.

Various different techniques were developed to try and equalize the hydrostatic pressure in the inner and outer compartment; however none were successful and no further experiments were conducted on single phase systems.

Two Phase Studies

In order to characterize the hydrodynamics on both sides of the filter several sets of two phase experiments were conducted. The theory for the transport process was developed and flux equations derived. The basic form of the different flux equations is very similar. Slight modifications to the terms depend on the location of the organic/aqueous interface(s). The general equation given in Chapter 3 is:

$$J = \vec{k} A c_I$$

where

$$\frac{1}{\vec{k}} = \frac{Z_{D,I}}{D_I} + \frac{1}{\alpha k_1} + \frac{\ell}{\alpha D_F K_F} + \frac{1}{\alpha k_2 K_F} + \frac{Z_{D,o}}{D_o K_o}$$

with notation as used previously.

In experiments where the diffusants were carboxylic acids there was possible dimerisation of the acids in the organic phase. This possibility complicates the general flux equation and the modifications have been reported.

The three different types of experiment conducted were:

1) a single interface located at the outside surface of the filter;
2) a single interface located at the inside surface of the filter;
3) a sandwich with two interfaces and the same phase in both inner and outer compartments.

In all these preliminary experiments the outer phase was aqueous.

The stability of the interface was found to be dependent on the pore size of the filter and also on the nature of its pretreatment. The optimum pore size was found to be ~ 1.0 μm. When the filter was impregnated with an organic solvent, the most stable interfaces were created if the filter had been pretreated with repelcote. The experimental results showed that the interfaces were very stable and would remain intact for several days.

By changing the substrate/phase systems it was possible to alter the partition coefficient and thus control the compartment in which the convective diffusion was rate determining. Consequently the hydrodynamics in either compartment could be studied independently. In experiments where an organic sandwich is formed between aqueous phases in the inner and outer compartments the diffusion layers on both sides of the filter contribute significantly to the overall transport process.

The first set of experiments tested the hydrodynamics in the inner compartment. Good agreement between the theoretical and experimental results showed that reproducible hydrodynamic flow patterns were established in the inner compartment. Experiments

using hexoic acid as the diffusant and hexane as the organic phase proved that the Levich equation predicted the diffusion layer thickness in the outer compartment. Sandwich experiments with acetic acid, hexoic acid and methyl nicotinate confirmed that the geometry of the rotating diffusion cell imposed known reproducible hydrodynamics to both surfaces of the filter.

Interfacial Transfer Terms

The intercepts of the graphs of $\vec{k}^{-1}$ against $W^{-\frac{1}{2}}$ correspond to an infinite rotation speed ($W^{-\frac{1}{2}} \rightarrow 0$). At this point there are no contributions to the overall flux from the diffusion layers and the remaining terms correspond to diffusion through the filter and to interfacial transfer reactions. The contribution from diffusion through the filter can be calculated from known values of the diffusion coefficient, partition coefficient and filter characteristics. Where necessary,diffusion coefficients have been measured in the conventional Stokes Cell.

A comprehensive list of all the systems studied has been given previously (Tables (10) and (13)). The values of the interfacial rate constants, together with values measured by other workers, are given in Tables (30) and (31).

Table (30). Systems studied in which appreciable interfacial rate constants have been detected.

System No.	Diffusant	Organic Phase	Aqueous Phase
1	acetic acid	IPM	Water
4	hexoic acid	hexane	Water
6	p-methyl benzyl chloride	IPM	Water
7	methyl nicotinate	IPM	Water
8	methyl nicotinate	IPM	60% glycerol
9	methyl nicotinate	IPM	80% glycerol
10	butyl nicotinate	IPM	Water
11	hexyl nicotinate	IPM	Water
12	betamethasone-17-valerate	IPM	Water
13	p-methyl benzyl chloride	CCl_4	Water

The values obtained for the interfacial rate constants for system 6 show that there is good agreement between the two experimental techniques employed, the rotating cell and the Stokes Cell. It seems unlikely that both methods would suffer from the same experimental errors and the good agreement confirms the existence of the interfacial term and the reliability of the new technique.

Table (31). A comprehensive list of interfacial rate constants*, together with the corresponding free energy change.

System	T/^{o}K	k_I/m. Ms^{-1}	k_{-I}/m. Ms^{-1}	$\Delta G^{\theta}_{I,\dagger}$/ kJ.mol^{-1}	$\Delta G^{\theta}_{-I,\dagger}$/ kJ.mol^{-1}
1	298	7.18	0.28	41	49
4	298	2.7	28	43	37
6[†107]	298	0.025	24	55	38
6 [117]	281.5	0.003	-	57	-
	298	0.017	26	56	38
	316.7	0.04	-	57	-
7	284	18.2	32	37	55
	294	9.3	20	40	38
	310	18	46	40	38
8	310	34	66	38	37
9	310	3.5	5.9	44	43
10	310	5.8	223	43	33
11	310	0.24	17	51	40
12	310	2.6	344	45	32
13[† 31]	298	0.016	32	56	37

* Values superscripted (†) were measured in the conventional Stokes diffusion cell.

Table (32) shows values of ΔG associated with the rate constants. These have been calculated from equation (6.1).

$$k_{\pm I} = Z \exp(-\Delta G^{\theta}_{\pm I}/RT) \qquad (6.1)$$

The frequency factor, Z, has been taken to be 10^2 $m.s^{-1}$ [127]; the actual size of $\Delta G^{\theta}_{\pm I}$ thus depends on the value of Z chosen but a frequency factor of 10^{-4} $m.s^{-1}$, which would make ΔG^{θ}_{-I} zero, seems too small.

There are no apparent correlations between the values of ΔG calculated and the nature of either the substrates or the solvents used. However it can be seen that the value of $\Delta G_{\downarrow}$, the free energy of activation in the thermodynamically favoured direction, is remarkably constant. For seven different substrates, three different organic solvents, and three different aqueous mixtures

$$\Delta G^{\theta}_{\downarrow}/kJ\ mol^{-1} = 38 \qquad (6.2)$$

with a standard deviation of

$$\sigma/kJ\ mol^{-1} = 3 \ .$$

Alternatively this may be expressed as $\log k_{\downarrow,I}$, which then does not depend on the choice of frequency factor:

$$\log(k_{\downarrow,I}/m.s^{-1}) = -4.7 \quad \sigma = 0.5 \qquad (6.3)$$

This magnitude of interfacial barrier has been found for all systems studied. The choice of substrates and solvents used cover a wide range of partition coefficients and the diffusants are neutral organic molecules of varying size and character. For these types of molecules equations (6.2) and (6.3) give some guidance to the size of the interfacial transfer barrier.

Since the value found for the rate constant is relatively constant, it seems likely that there exists a fundamental process common to all the systems. On the molecular scale this could be an interfacial restructuring which is necessary to permit solute transfer. A type of gate mechanism could be envisaged. Electric field gradients could be involved; however, there is no apparent variation in the magnitude of the kinetic term with dipole moment.

At the moment not enough information is available to predict the cause of the free energy barrier and further studies are required to gain a less empirical understanding of the phenomenon.

An *in vitro* model for percutaneous absorption

Isopropyl myristate has been used as the organic phase in the rotating diffusion cell since it has been suggested as a good model for skin lipids. A more complex solution containing phospholipids and sterols could have been used but initially the systems studied were kept as simple as possible. This greatly facilitates the interpretation of the results by reducing the number of possible interactions.

Some esters of nicotinic acid were used as the diffusants. These have been studied since their rate of penetration *in vivo* is easily measured[121]. By combining the *in vivo* and *in vitro* results it was hoped to gain a better understanding of the fundamental processes involved in percutaneous absorption.

From Table (30), the systems relevant in this section are: 7, 8, 9, 10, 11 (and 12). The three nicotinate esters cover a wide range of partition coefficients and, in the case of methyl nicotinate the partition coefficient has been modified by addition of glycerol to the aqueous phase.

No apparent pattern emerges from the results, however for all these systems interfacial barriers have been measured and the rate constants have been used to interpret *in vivo* results.

When the diffusion of the steroid, betamethasone-17-valerate was studied it was found that the steroid partitioned very favourably into the filter saturated with IPM. Since the steroid arriving in the outer compartment was not removed a steady state with no diffusive flux was quickly established. This effect is very similar to the reservoir effect found *in vivo* in which corticosteroids form a depot in the epidermis. When the steroid is applied to skin vasoconstriction occurs and if the site is left unoccluded the associated pallor gradually disappears. If the same areas are reoccluded at intervals up to 14 days after the initial application, vaso-constriction reappears. Clinical and radiobiological data

indicates that the reservoir is located in the lower regions of the stratum corneum[128]. This may be attributed to very favourable partitioning into the skin lipids associated with slow release into the lower aqueous environment. The slow release could be due to a combination of the adverse partition coefficient and slow interfacial transfer.

In vivo Results

Two distinct types of experiment were conducted. The more simple type was the continuous application of methyl nicotinate to the skin. The nicotinate was applied in different concentrations and in different aqueous glycerol mixtures. A mathematical model describing the diffusion process was developed and the results analyzed.

For the continuous application of solutions of methyl nicotinate in water, the data was found to be best described by the mathematical model Class IA (page 163). In this model the triggering concentration of the nicotinate is given by equation (5.52); steady state conditions have not been established and interfacial transport is rapid. It has thus been established that for methyl nicotinate any corrections due to interfacial effects will be small.

Using this mathematical model and equation (5.52) a value for D/ℓ^2 for methyl nicotinate was calculated. The value was found to be 1.4×10^{-2} min^{-1}. The diffusional path length, ℓ, depends on the route of penetration. The average thickness of

the stratum corneum has been taken to be 15 μm[126] and this value has been used in calculations where the route of penetration has been assumed to be straight through the cells. A value of 337 μm has been taken as the diffusional path length round the cells. This thickness has been calculated on the basis of an idealized skin structure developed by Michaels et al.[124].

Using these two values for ℓ the diffusion coefficient of methyl nicotinate through (D_T) and round (D_R) the cells can be estimated. The two values are:-

$$D_T/m^2\ s^{-1} = 8.25 \times 10^{-14}$$

$$D_R/m^2\ s^{-1} = 2.65 \times 10^{-11}$$

The value of D_T seems very low whereas the value of D_R is similar in magnitude to penetrant diffusion coefficients calculated for lipid viscosities of 10 to 100 centipoise[124]. It is, however, a factor of ten lower than isopropyl myristate, the solvent chosen as the lipid model. This may be attributed to the presence of phospholipids and sterols in the natural skin lipids which increase the viscosity and hence decrease the diffusion coefficient.

The more reasonable diffusion coefficient is D_R for transport round the cells and from a consideration of the magnitudes of the diffusion coefficients the more likely route of penetration is via the lipid rich intercellular channels.

Further investigations were conducted in which glycerol was added to the aqueous solutions of methyl nicotinate. The results for these experiments were treated with the same Class IA solution but corrections were included to allow for concentration depletion in the applied phase. As the percentage of glycerol was increased so the correcting factor increased (Table (25)).

The correction depends on the route of penetration since it includes a term with the ratio of the diffusion coefficient in the applied solution and in the skin. It also includes the value of the vehicle/skin partition coefficient which has been taken to be approximated by the vehicle/isopropyl myristate partition coefficient. The results were treated 1) without any correction; 2) correcting for an intercellular route; 3) correcting for an intracellular route. The straight lines obtained by these three distinct methods were analyzed statistically. It was found that the least scatter was obtained when the data was treated by assuming an intracellular route i.e. when the depletion correction was largest.

Again the implication is that the route of penetration is via the intercellular channels, however no firm evidence can be obtained to substantiate this.

The mathematical treatment also allows calculation of the concentration of methyl nicotinate at the epidermal/dermal junction required to trigger erythema (n'_E). This value is dependent on the route of penetration and both figures have

been estimated, $n'_{E,R}$ for round the cells, and $n'_{E,T}$ for through the cells:-

$$n'_{E,R}/\text{mol.cm}^{-2} = 3.5 \times 10^{-9}$$

$$n'_{E,T}/\text{mol.cm}^{-2} = 3.7 \times 10^{-10} .$$

The second type of *in vivo* experiments were of the pulse variety in which the solution containing the nicotinate is removed before erythema develops. Three esters were studied by this technique, methyl, n-butyl, and n-hexyl. The effect of concentration on the time of onset of erythema for the last two esters could not be studied since they are very insoluble and at almost saturated concentrations the erythema takes quite a long time to develop. Thus by performing the pulse experiments a different variable is introduced which may be analyzed mathematically.

A more complex mathematical model was developed for the analysis of these results. Simplifications possible in the previous type of analysis could not be applied and for the treatment of the results, terms for depletion ($K/\sqrt{p}$), interfacial transfer (κ), and partitioning had to be included. Since absolute measurement of the interfacial transfer coefficients and partition coefficients is not possible, estimates have been used which are based on the *in vitro* findings for the rotating diffusion cell. In this way the *in vivo* results have been linked with the *in vitro* results obtained from the model system.

The mathematical model describes the variation in triggering concentration (u') with the Laplace time variables s_1 and s_2 (equation (5.57)).

$$u' = \frac{2Ks_2 e^{-\sqrt{s_1}}}{s_1^{\frac{1}{2}}[1+\sqrt{s_1}/K][1+\sqrt{s_1}/K + K/\sqrt{p}]} \cdot \frac{1}{(s_2-s_1)} \left(1 - \frac{s_1(e^{\sqrt{s_1}} + \sqrt{s_1}e^{\sqrt{s_1}/K})}{s_2(e^{\sqrt{s_2}} + \sqrt{s_2}e^{\sqrt{s_2}/K})}\right) \qquad (5.57)$$

This equation cannot be inverted to give u' in terms of s_1 and s_2. The experimental results are converted from relationships between t_1 and t_2 to s_1 and s_2 and substituted into equation (5.57). Constant values of u' then give a measure of the triggering concentration for the three esters.

The values of the depletion terms and the interfacial terms vary with the route of penetration. Both mechanisms have been considered and the results for both are given. The normalized interfacial terms (K) and the depletion correction terms ($K/\sqrt{p}$) are given in Table (33).

Table (33). Terms used for interfacial transfer correction and depletion correction in the mathematical analysis.

	Methyl	n-butyl	n-hexyl
K_T	4309	1961	86.6
K_R	195	88.7	4.01
$K/\sqrt{p}_T$	0.041	0.523	0.977
$K/\sqrt{p}_R$	0.91	11.67	21.42

Table (33) shows that the interfacial terms and the depletion terms have more effect on the results for the intracellular route. This would be expected since the diffusion coefficient for the intercellular route is very small.

In the final analysis constant triggering concentrations are found when both routes are considered. The results are given in Table (34).

Table (34). The concentrations of the nicotinates required to trigger erythema.

		PULSE EXPERIMENTS		
	Methyl	Methyl	Butyl	Hexyl
$n'_{E,R}$/mol.cm^{-2}	3.5×10^{-9}	5.3×10^{-9}	0.8×10^{-9}	0.8×10^{-9}
$n'_{E,T}$/mol.cm^{-2}	3.7×10^{-10}	4.5×10^{-10}	3.0×10^{-10}	7.9×10^{-10}

Stoughton et al.[121] achieved results which showed that when the different nicotinates were injected to the dermal-epidermal junction, erythema was induced by equimolar concentrations (to within a factor of 10). The results above confirm this finding and the scatter of the results is reasonable considering the assumptions made. The main assumptions introduced are:-

(i) the skin/water partition coefficient is the same as the IPM/water partition coefficient.

(ii) the skin/water interfacial transfer term is the same as the IPM/water interfacial transfer term.

Since such good results are obtained for the different nicotinates it seems likely that the choice of isopropyl myristate as a model for skin lipids is satisfactory. Consequently the Millipore filter impregnated with isopropyl myristate can be regarded as a good *in vitro* system for testing the transport of drugs across the epidermis.

The Final Model

In a recent review article[129] it was stated that: 'The role of intercellular spaces in cutaneous permeability has been pondered, but no one has seriously proposed these canals as an avenue for percolation of materials through the epidermis ..... Few studies of the significance of this pathway have been attempted. It has been assumed that the principal route of entry is directly through the cells rather than between them'.

From the results of the continuous application experiments there are three main reasons to suggest that the route of penetration of methyl nicotinate is via the intercellular channels.

1) The value of the diffusion coefficient for transport round the cells is of the correct magnitude.

2) The treatment of the results for aqueous glycerol mixtures gives the best correlation when the route of transport is via the intercellular channels.

3) Isopropyl myristate is found to be a satisfactory model. The nature of isopropyl myristate is much more like the natural skin lipids found in the intercellular channels than the solid proteinaceous epidermal cells.

A more absolute method of determining the route of penetration would be to measure the transport rate of methyl nicotinate across excised human skin. From the steady state flux it is possible to calculate aD/ℓ where a is the fractional area across which diffusion is occurring. With no assumptions the work conducted here gives a value of D/ℓ^2. Combining these two values the quantity $a\ell$ is calculated and can be compared to values of $a\ell$ predicted by the two models.

Further experimental evidence suggesting the pathway of penetration to be round the cells has been reported. If excised human skin is treated with a chloroform/methanol mixture, a substantial fraction of the skin lipids is removed. The removal is not accompanied by mechanical or morphological alteration to the membrane. When the tissue is rehydrated the permeability of the delipidized skin is very much greater than that of normal skin[130,131]. Furthermore the barrier function is restored when the extracted lipids are returned to the skin[132]. This suggests that the route of penetration is via the lipids in the epidermis which are mainly located in the intercellular channels. Additionally, experiments show there to be marked changes in skin permeability over narrow temperature ranges. The temperatures coincide with reversible thermal transitions detected by differential scanning calorimetry[133],

which have been explained by reversible structural changes in the lipid. Species which partition very unfavourably into lipids e.g. electrolytes do not penetrate the intact stratum corneum suggesting a lipid route. If the lipids are removed the penetration of electrolytes is possible[134].

The chosen idealized model is thus one in which there are proteinaceous plates of dimensions 25 x 25 x 0.5 μm separated by a lipid rich phase of thickness 8×10^{-2} μm and area fraction (at the skin surface) 6.8×10^{-3}. Transport is via these lipid rich intercellular channels which have an effective path length of 337 μm. The diffusion coefficient of methyl nicotinate in the lipid is 0.026 $m^2\ Gs^{-1}$. The partitioning of drug into the lipid phase is well modelled if the organic material is considered to be isopropyl myristate. The magnitude of any interfacial barriers encountered in the transport of drug from the vehicle to the dermis is of the order of 10^{-5} ms^{-1}.

Application of the Model

Having established a model it may be applied to interpret other researchers' data. The steady state fluxes of a wide range of drugs across excised human skin have been measured[124]. In these experiments the skin is in a fully hydrated state and consequently the permeability will be increased about five fold. Thus in the model a diffusion coefficient of $5 \times 0.026\ m^2\ Gs^{-1}$

has been used. Diffusion coefficients of many low molecular weight compounds in the hydrated epidermis are approximately the same[135], and thus a fixed value for the diffusion coefficient has been taken.

The concentration and area normalized flux ($\bar{j}$) is given by

$$\frac{1}{\bar{j}} = \frac{2}{ak_{-I}} + \frac{\ell}{aDK_p} \qquad (6.4)$$

where a is the area fraction of the intercellular channels (6.8×10^{-3});

k_{-I} is the interfacial rate constant (10^{-5} m s^{-1});

ℓ is the diffusional path length (337 μm);

D is the average diffusion coefficient (0.13 m^2 Gs^{-1});

K_p is the oil water partition coefficient.

Equation (6.4) has been used to construct Figure (59) in which log $\bar{j}$ is shown as a function of log K_p. For low values of K_p there is a linear relationship between log $\bar{j}$ and log K_p but as the partition coefficient approaches unity the interfacial term begins to dominate. A limiting flux is reached and no increase in K_p will increase it. Also included in Figure (59) are values of log $\bar{j}$ and log K_p from Michaels et al.[124]. There is good correlation between the theoretical line and the experimental points. The broken line has been calculated for a model in which transport is through the cells. The correlation between the experimental points and this theoretical line is not so good. The values obtained in reference 124 thus support the

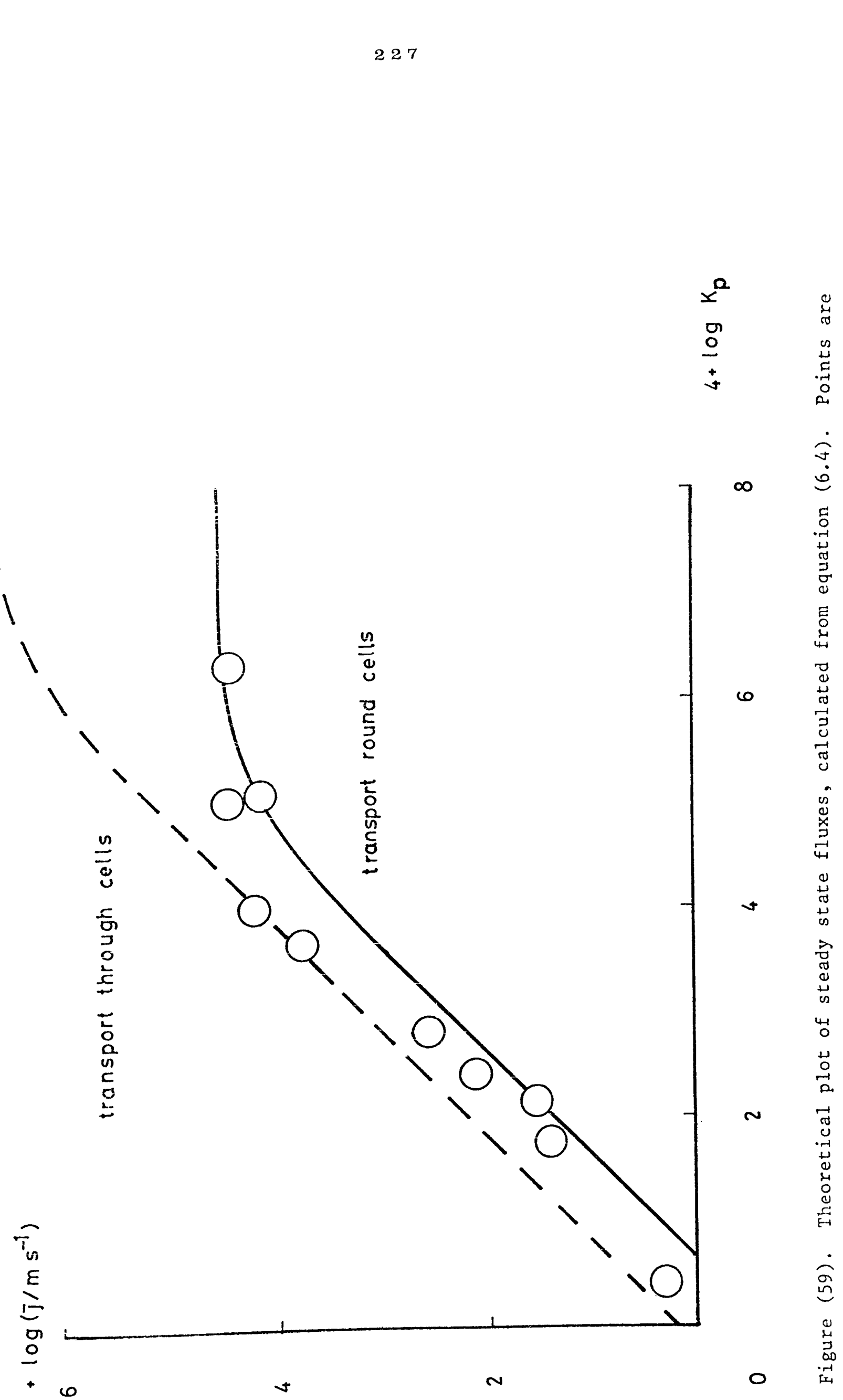

Figure (59). Theoretical plot of steady state fluxes, calculated from equation (6.4). Points are experimental data from reference

postulated model when transport is via the intercellular channels and involves an interfacial transfer term.

Other researchers have studied the penetration of nicotinate esters and measured the time of onset of erythema. It is possible to see if these results are in agreement with the model. Barrett et al.[76] measured the effect of concentration of methyl nicotinate on the times of onset of erythema. They applied the nicotinate in aqueous cream B.P. and altered the aqueous phase with varying amounts of glycerol. Expressing the glycerol as a percentage of the total aqueous phase, a value for the depletion correction F_R can be calculated. Figure (60) shows the straight line (from the experimental section) relating $\log(F_R.c_\infty t^{3/2})$ to 10/t and the circles are experimental points from reference 76. The reasonable scatter around the line shows the model is satisfactory in explaining the release of methyl nicotinate from aqueous cream B.P.

General Model for Structure-Activity Relationships

Much research has been conducted into understanding the change of drug activity with molecular structure. One of the easiest means of studying this problem is to choose a physiologically active homologous series. It is then assumed that the ability of each member of the homologous series to reach the receptor sites is equated to the permeability of the biological barrier (the biomembrane and contiguous aqueous layers)[136].

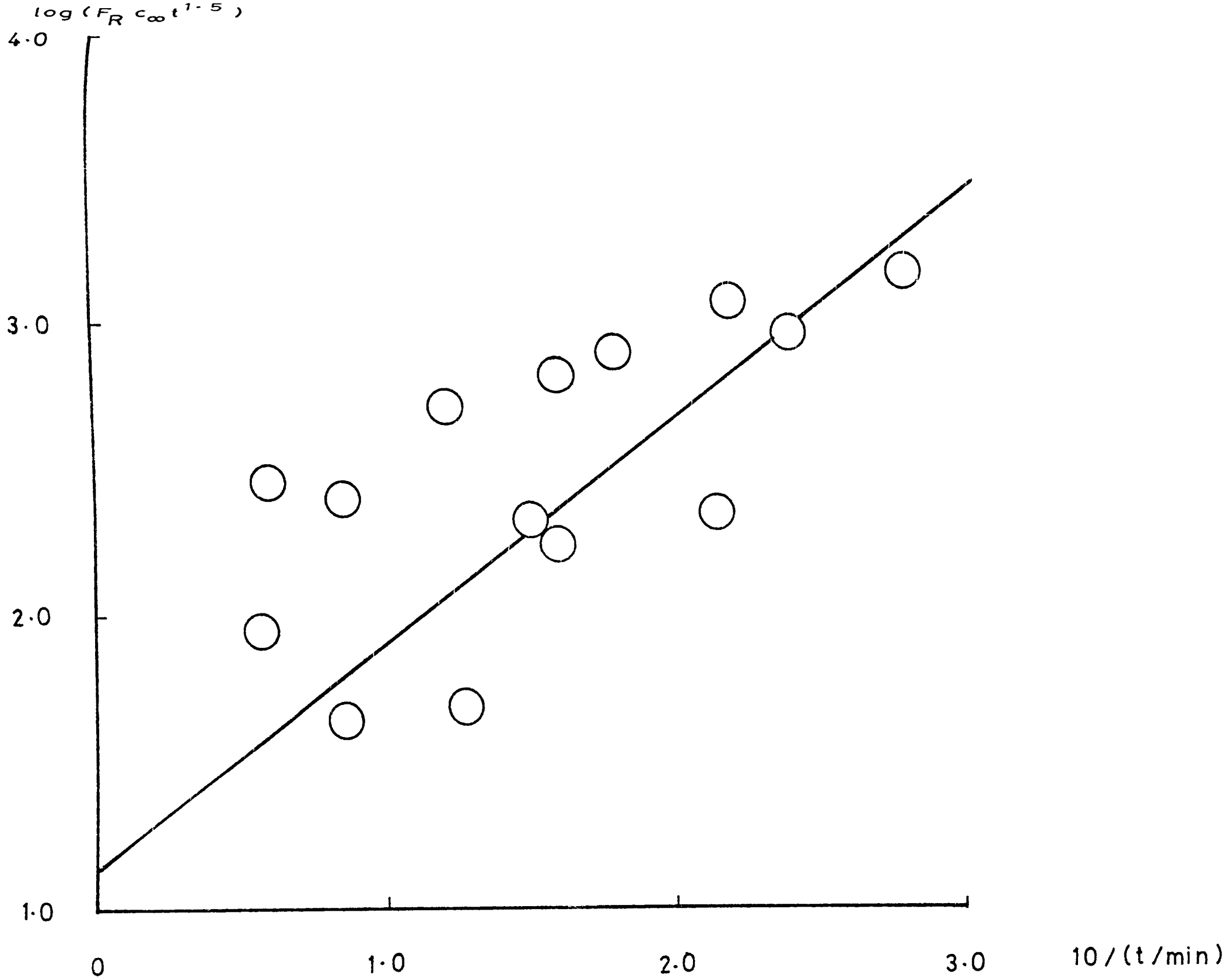

Figure (60). Theoretical line for the relation between $\log(F_R\ c_\infty t^{1.5})$ and 10/t for aqueous solutions of methyl nicotinate. The points are experimental data from reference (76).

Many equimolar structure-activity curves show a levelling off of activity with increasing chain length. This plateauing effect has been observed for various systems and by different workers. It has been found for both steady state fluxes[137,138] and biological activity[139-143]. Yalkowsky and Flynn[136] have explained this plateauing by considering a transition from membrane control to diffusion layer control of transport. They have not considered the possibility of slow interfacial transport which also produces a plateauing effect (figure (59)). Since both hypotheses are plausible and could be complementary it is necessary to conduct more work into the problem and not ignore the possibility of slow interfacial transfer.

Future Developments

Much more data needs to be accumulated in order to try and find any correlation between solvent/solute nature and the magnitudes of the interfacial term. The temperature dependence of the rate constants would provide insight into whether the barrier was primarily entropic or enthalpic. Measurement of the solvent isotope effect would determine whether structural changes in the lipid or the aqueous phase were important. Studies into the nature of the interface with for example a ring viscometer might provide more insight into the cause of the phenomena.

Whatever the outcome of the work outlined above, account needs to be taken, in future studies, of the possibility of slow

interfacial transport. There are many two phase industrial processes in which transfer between organic and aqueous liquids occurs and usually it has been assumed to be rapid. Additionally in transport in biological systems where passive diffusion occurs, a term in the flux equation describing the possibility of slow interfacial transfer should be included.

In Vitro Model

The estimated diffusion coefficient of methyl nicotinate in the skin lipids was found to be a factor of ten lower than the diffusion coefficient in isopropyl myristate. In order to lower the diffusion coefficient in the model lipid,esters of cholesterol could be added together with small concentrations of phospholipids. However at this stage it is impossible to predict what effect this might have on the interfacial transfer coefficient; hopefully these and the partition coefficients would be little affected. More work needs to be conducted to discover suitable solvent systems to model biological processes.

Another obvious application of this cell is in the modelling of gastro-intestinal diffusion which is also thought to be a passive process. The *in vitro* model is useful in testing the absorption of new drugs and the effect of formulation on their rates of release.

The results discussed in this thesis may have a wider application in the general field of membrane transfer since a leading researcher writes[144]:

"An understanding of the diffusion mechanism through the skin may have even wider significance to the mechanism of membrane transport in general. The stratum corneum is an aggregate of tightly adherent cells, densely packed with lipid enriched keratin fibrils and presents a unique system for studying the chemical influence of naturally occurring protein-lipids on membrane transport. This is particularly significant when it is realized that many cell membranes are chemically quite similar to the stratum corneum and transport through them is believed to be governed in large part by a lipid-penetrant interaction. In this restricted sense the stratum corneum is a macroscopic analogue of the unit cellular membrane."

APPENDIX 1

The following program was used to calculate the value of the cell constant β in the single phase experiments.

```
      GLOBAL, CELLCONSTANTJH]
C     THE DATA TAPE MUST READ, N:- THE NUMBER OF DATA
C     POINTS, HAINF:- THE BULK ACID CONC., COH:- THE ALKALI
C     CONC., VTOP:- THE VOL. OF THE INNER COMPARTMENT, CAC:-
C     THE ACETATE CONCENTRATION, NR:- THE RUN NO.. THEN READ
C     IN VALUES OF ALKALI ADDED, VOH, AT TIME T.

      READ(1) N.HAINF,COH,VTOP,CAC,NR
      WRITE(2,3) NR
      X=0.01
      Y=0.01
      DO 2 M=1,N
      READ(1) VOH,T
      FLUX=(VOH-X)*COH/(T-Y)/60000.0
      Z=VOH+((VOH-X)/2)
      HASLOPE=HAINF-((Z*COH)/VTOP)
      CH=2.75*HASLOPE/(CAC*100000.0)
      CHAC=HASLOPE-CH
      DHAC=(1.201-(0.55*CHAC))/100000.0
      DH=9.31/100000.0
      B=FLUX*1000/((CHAC*DHAC)+(CH*DH))
      FLUX=FLUX*1000000000.0
      WRITE(2,4)VOH,X,T,Y,FLUX,B
      X=VOH
      Y=T
  2   CONTINUE
  3   FORMAT(/7HRUN NO·,I9,
  $   //56H      VOH          X          T          Y     10**9FLUX     B
  4   FORMAT(2F 11.3,2F8.2,F13.4,F8.2)
END
```

APPENDIX 2

The following Fortran Computer Program was used to calculate gradients and intercepts using a least squares analysis.

```
      GLOBAL, LMS, SQRT,ABS]
C     DATA TAPE MUST READ:- N, NUMBER OF POINTS; XI, VALUE OF X
C     FOR WHICH INTERCEPT IS REQUIRED; CH. CHUCK POINT IF DEVIATION
C     >CH*PROBABLE ERROR;     PAIRS OF READINGS ,
C     X1  Y1       X2   Y2     .........   XN     YN.
      DIMENSION V(100),W(100)
      READ (1) N,XI, CH
      NS=0
      DO 3 M=1,N
      READ(1) X,Y
      V(M)=X
3     W(M)=Y
7     NR=0
      EN=N
      SEA=0.0
      SX=0.0
      SY=0.0
      SXY=0.0
      SX2=0.0
      SY2=0.0

      DO 8 M=1,N
      SX=SX+V(M)
8     SY=SY+W(M)
      AX=SX/EN
      AY=SY/EN
      XJ=XI-AX
      DO 1 M=1,N
      X=V(M)-AX
      Y=W(M)-AY
      SXY=SXY+X*Y
      SEA=(X-XJ)**2+SEA
      SX2=SX2+X**2
1     SY2=SY2+Y**2
      C=EN*SX2
      B=SXY/SX2
      A=B*XJ+AY
      D=SY2-B*SXY
      Z=D/(EN-2.0)/C
      EA =0.6745*SQRT(Z*SEA)
      EB=0.6745*SQRT(Z*EN)
      R=0.6745*SQRT(Z*C)*CH
      AZ=AY-B*AX
```

```
      M=0
22    M=M+1
25    IF(M-N) 26,26,27
26    Z=ABS(AZ+B*V(M)-W(M))
      IF(Z-R) 22,22,23
23    DO 24 L=M,N-1
      V(L)=V(L+1)
24    W(L)=W(L+1)
      N=N-1
      NR=NR+1
      GO TO 25
27    WRITE (2,33) NS,CH
33    FORMAT( /15HREJECTED POINTS, I4, 5H CH= ,F7.3)
      WRITE (2,2) B,EB,XI,A,EA
2     FORMAT(11HGRADIENT IS , E14.5, 5H +/- , E10.4, 18H (PROBABLE ERROR) /
$     17HVALUE OF Y AT X= ,E14.5,4H IS , E14.5,5H +/- , E10.4)
      NS=NS +NR
      IF(NR) 28,28,29
29    IF(N-2) 30,30,7
30    WRITE(2,32) V(1),W(1),V(2),W(2)
32    FORMAT(6HONLY (,E10.4, 1H.,E10.4,7H) AND (,E10.4, 1H.,E10.4,  ,
$     6H) LEFT/23HBACK TO THE TEST TUBES!)
28    END
```

APPENDIX 3

Solution of the differential equation describing the concentration profile for the 'pulse' experiments

$$s_2\bar{\bar{u}} - \bar{u}_+ = \left(\frac{\partial^2\bar{\bar{u}}}{\partial\chi^2}\right) \qquad (1)$$

$\bar{u}$ is the value of $\bar{u}$ at $\tau' = 0$ or $\tau = \tau_1$.

At the internal interface

$$-\left(\frac{\partial\bar{\bar{u}}}{\partial\chi}\right)_1 = \kappa u_1 \qquad (2)$$

and at the external interface

$$\left(\frac{\partial\bar{\bar{u}}}{\partial\chi}\right)_o = 0 \qquad (3)$$

But

$$\bar{u}_+ = A\cosh\sqrt{s_1}\chi + B\sinh\sqrt{s_1}\chi \qquad (4)$$

$$\bar{\bar{u}} = A'\cosh\sqrt{s_1}\chi + B'\sinh\sqrt{s_1}\chi + C'\cosh\sqrt{s_2}\chi + D'\sinh\sqrt{s_2}\chi \qquad (5)$$

Differentiating equation (5)

$$\left(\frac{\partial\bar{\bar{u}}}{\partial\chi}\right) = \sqrt{s_1}A'\sinh\sqrt{s_1}\chi + \sqrt{s_1}B'\cosh\sqrt{s_1}\chi + \sqrt{s_2}C'\sinh\sqrt{s_2}\chi + \sqrt{s_2}D'\cosh\sqrt{s_2}\chi \qquad (6)$$

Using the condition in equation (3)

$$\sqrt{s_1}B' + \sqrt{s_2}D' = 0 \qquad (7)$$

Differentiating equation (5) twice:

$$\left(\frac{\partial^2 \bar{\bar{u}}}{\partial \chi^2}\right) = s_1 A' \cosh\sqrt{s_1}\chi + s_1 B' \sinh\sqrt{s_1}\chi + s_2 C' \cosh\sqrt{s_2}\chi + s_2 D' \sinh\sqrt{s_2}\chi \qquad (8)$$

Substitution of equations (4), (5), (8) into equation (1) and equating coefficients in $\cosh\sqrt{s_1}\chi$ and $\sinh\sqrt{s_1}\chi$ gives:

$$A = A'(s_2 - s_1) \qquad (9)$$

$$B = B'(s_2 - s_1) \qquad (10)$$

Thus from equation (7)

$$D' = \frac{-B\sqrt{s_1}}{\sqrt{s_2}(s_2 - s_1)} \qquad (11)$$

Thus from equations (2) and (6)

$$\left(\frac{\partial \bar{\bar{u}}}{\partial \chi}\right)_1 = \frac{1}{(s_2 - s_1)} \{ A\sqrt{s_1}\sinh\sqrt{s_1} + B\sqrt{s_1}(\cosh\sqrt{s_1} - \cosh\sqrt{s_2}) + C''\sqrt{s_2}\sinh\sqrt{s_2} \}$$

$$= -\kappa \bar{\bar{u}}_1 \qquad (12)$$

where $C'' = C'(s_2 - s_1)$.

Hence by substituting equation (5) for $\bar{\bar{u}}_1$, C'' can be written in terms of A and B:-

$$C'' = \frac{B\left(\frac{\sqrt{s_1}}{\sqrt{s_2}}\kappa\sinh\sqrt{s_2}+\sqrt{s_1}\cosh\sqrt{s_2}-\kappa\sinh\sqrt{s_1}-\sqrt{s_1}\cosh\sqrt{s_1}\right)-A\left(\kappa\cosh\sqrt{s_1}+\sqrt{s_1}\sinh\sqrt{s_1}\right)}{\sqrt{s_2}\sinh\sqrt{s_2}+\kappa\cosh\sqrt{s_2}} \qquad (13)$$

Turning to the coefficients A and B. From equation (4), when $\chi = 1$

$$\bar{u}_{\dagger,1} = A\cosh\sqrt{s_1} + B\sinh\sqrt{s_1}$$

But $\bar{u}_1$ is also given by equation (27) (page 161)

$$\bar{u}_1 = \frac{K/s_1\left[\left(1+\frac{\sqrt{s_1}}{\kappa\tanh\sqrt{s_1}}\right)\cosh\sqrt{s_1}-\left(1+\frac{\sqrt{s_1}\tanh\sqrt{s_1}}{\kappa}\right)\frac{\sinh\sqrt{s_1}}{\tanh\sqrt{s_1}}\right]}{\left(1+\frac{2\sqrt{s_1}}{\kappa\tanh\sqrt{s_1}}+\frac{s_1}{\kappa^2}+\frac{K}{\sqrt{p}\tanh\sqrt{s_1}}+\frac{\sqrt{s_1}K}{\sqrt{p}\kappa}\right)} \qquad (14)$$

$$= \sqrt{s_1}\bar{f}\sinh\sqrt{s_1}\left\{\left(1+\frac{\sqrt{s_1}}{\kappa\tanh\sqrt{s_1}}\right)\cosh\sqrt{s_1}-\left(1+\frac{\sqrt{s_1}\tanh\sqrt{s_1}}{\kappa}\right)\frac{\sinh\sqrt{s_1}}{\tanh\sqrt{s_1}}\right\} \qquad (15)$$

where $\bar{f}$ is given by equation (32) (page 162)

Comparing terms gives

$$A = \sqrt{s_1}\,\bar{f}\,\sinh\sqrt{s_1}\,\left(1 + \frac{\sqrt{s_1}}{\kappa\tanh\sqrt{s_1}}\right) \quad (16)$$

$$B = -\left(1 + \frac{\sqrt{s_1}\tanh\sqrt{s_1}}{\kappa}\right)\frac{\sqrt{s_1}\,\bar{f}\sinh\sqrt{s_1}}{\tanh\sqrt{s_1}} \quad (17)$$

Therefore

$$B = -\bar{f}\left(\sqrt{s_1}\cosh\sqrt{s_1} + \frac{s_1\sinh\sqrt{s_1}}{\kappa}\right) \quad (18)$$

Substitution of the coefficients A', B', C', D' into equation (6) gives

$$\frac{\kappa\bar{\bar{u}}_1}{s_2} = \frac{f\,s_1}{(s_2-s_1)s_2}\left\{1 - \frac{\cosh\sqrt{s_1}+\sqrt{s_1}\sinh\sqrt{s_1}/\kappa}{\frac{\sqrt{s_2}}{\kappa}\sinh\sqrt{s_2}+\cosh\sqrt{s_2}}\right\} \quad (19)$$

But

$$\bar{\bar{u}}' = \frac{\bar{f}}{s_2} + \frac{\kappa\bar{\bar{u}}_1}{s_2} \quad (20)$$

therefore

$$\bar{\bar{u}}' = \bar{f}\,\bar{\bar{g}} \quad (21)$$

where

$$\bar{\bar{g}} = \frac{1}{s_2-s_1}\left[1 - \frac{s_1}{s_2}\left\{\frac{\cosh\sqrt{s_1}+\sqrt{s_1}\sinh\sqrt{s_1}/\kappa}{\cosh\sqrt{s_2}+\sqrt{s_2}\sinh\sqrt{s_2}/\kappa}\right\}\right] \quad (22)$$

APPENDIX 4

The following program was used to calculate the function

$$\bar{\bar{u}}_1 = \frac{2Ks_2\, e^{-\sqrt{s_1}}}{s_1^{\frac{1}{2}}\left[1+\frac{\sqrt{s_1}}{K}\right]\left[1+\frac{\sqrt{s_1}}{K}+\frac{K}{\sqrt{p}}\right]} \cdot \frac{1}{(s_2-s_1)}\left\{1-\left(\frac{s_1(e^{\sqrt{s_1}}+\sqrt{s_1}e^{\sqrt{s_1}/K})}{s_2(e^{\sqrt{s_2}}+\sqrt{s_2}\,e^{\sqrt{s_2}/K})}\right)\right. \tag{5.57}$$

```
      PROGRAM S1S2 (INPUT,OUTPUT,TAPE1=INPUT,TAPE2=OUTPUT)
      DIMENSION S1(100),S2(100)
      WRITE(2,90)
90    FORMAT(1X,22HPARTITION COEFFICIENT=)
      READ(1,)AK
      WRITE(2,91)
91    FORMAT(1X,6HKAPPA=)
      READ(1,)BKAP
      WRITE(2,92)
92    FORMAT(1X,9HK/P**0.5=)
      READ(1,)CKRP
      WRITE(2,93)
93    FORMAT(1X,22HNUMBER OF DATA POINTS=)
      READ(1,)N
      WRITE(2,94)
94    FORMAT(1X,20HREAD VALUES OF S1 S2)
      READ(1,)(S1(M),S2(M),M=1,N)
      WRITE(2,95)
95    FORMAT(1X,2HS1,5X,2HS2,5X,4HCONC)
      DO 3 M=1,N
      R1=SQRT(S1(M))
      R2=SQRT(S2(M))
      Z=S1(M)*((R1*EXP(R1)/BKAP)+EXP(R1))
      Y=S2(M)*((R2*EXP(R2)/BKAP)+EXP(R2))
      U=(1.-Z/Y)/(S2(M)-S1(M))
      T=S2(M)*2.*AK/(R1*EXP(R1))
      S=(1.+R1/BKAP)*(1.+R1/BKAP+CKRP)
      ANS=U*T/S
      WRITE(2,6)S1(M),S2(M),ANS
6     FORMAT(2F7.2,E12.5)
3     CONTINUE
      STOP
      END
```

REFERENCES

General

J.T. Davies, E.K. Rideal, Interfacial Phenomena, Academic Press, London (1961).

An Introduction to the Biology of the Skin (R.H. Champion, T. Gillman, A.J. Rook, R.T. Sims, eds.), Blackwell Scientific Publications, Oxford (1970).

R.T. Tregear, Physical Functions of Skin, Academic Press, London (1966).

1. J.H. Wills, *In* Advances in Biology of Skin, Vol.12, Pharmacology and the Skin. (W. Montagna, R.B. Stoughton, and E.J. Van Scott, eds.) Meredith Corporation, New York (1972).
2. R.D. Mussey, Philadelphia Med. Phys. J. 1899, 3, 288.
3. T.F. Reilly, J. Amer. Med. Ass. 1901, 56, 250.
4. I.H. Blank, R.D. Griesemer, E. Gould, J. invest. Derm., 1957, 29, 299.
5. *Ibid.*, 1958, 30, 187.
6. C.D. Calnan, Brit. J. Derm., 1970, 82, Suppl. 6, 43.
7. J.J. O'Neill and E.D. Goddard, J. Colloid Interface Sci., 1967, 25, 57.
8. M.J. Busse, P. Hunt, K.A. Lees, P.N.D. Maggs, T.M. McCarthy, Br. J. Derm., 1969, 81, Suppl. 4, 103.
9. D.H.O. Gemmell and J.C. Morrison, J. Pharm. Pharmacol., 1957, 9, 641.
10. T.J. Franz, J. invest. Derm., 1975, 64, 190.
11. H. Pinkus, *In* Physiology and Biochemistry of the Skin (S. Rothman, ed.) Chicago University Press (1954).
12. P. Flesch, J. invest. Derm., 1958, 31, 63.

13. H.W. Spier and G. Pascher, Hautarzt, 1956, 7, 55.

14. V.R. Wheatley and R.P. Reinartson, J. invest. Derm., 1959, 32, 49.

15. R.T. Tregear, Physical Functions of Skin, New York: Academic Press, Inc. (1966).

16. R.J. Scheuplein, J. invest. Derm., 1967, 48, 79.

17. F. Hermann and P.H. Prose, *ibid.*, 1951, 16, 217.

18. A.M. Kligman, Brit. J. Derm., 1963, 75, 307.

19. J.S. Strauss and P.E. Pochi, J. invest. Derm., 1961, 36, 293.

20. R.E. Kellum, Arch. Derm., 1967, 95, 218.

21. V.R. Wheatley, N.Y. Acad. Med. Bull., 1965, 41, 353.

22. N. Nicolaides, H.C. Fu, G.R. Rice, J. invest. Derm., 1968, 51, 83.

23. M. Katz and B.J. Poulson, *In* Handbook of Experimental Pharmacology, Vol.28, (B.B. Brodie and J. Gillette, eds.) Springer-Verlag, Berlin (1971).

24. R.J. Scheuplein, I.H. Blank, G.J. Braunn, D.J. MacFarlane, J. invest. Derm., 52, 63.

25. T. Higuchi and W.J. Tillmann, *ibid.*, 1961, 37, 87.

26. I.H. Blank and R.J. Scheuplein, *In* Progress in the Biological Sciences in Relation to Dermatology, 2nd ed. (A.J. Rook and R.H. Champion, eds.), Vol.2. Cambridge University Press, London (1964).

27. I.H. Blank, J. invest. Derm., 1953, 21, 259.

28. D.E. Loveday, J. Soc. cosmet. Chem., 1961, 12,224.

29. F.D. Malkinson and M.B. Kirschenbaum, Arch. Derm., 1963, 88, 427.

30. S. Monash and I.D. Blank, *ibid.*, 1958, 78, 710.

31. W.J. Albery, A.M. Couper, J. Hadgraft, C. Ryan, J.C.S. Faraday Trans. I, 1974, 70, 1124.

32. G.E. Burch and N.P. de Pasquale, Hot Climates, Man and his Heart. Thomas, Springfield (1962).

33. D.E. Wurster and S.F. Kramer, J. Pharm. Sci., 1961, 50, 288.

34. E. Cronin and R.B. Stoughton, Arch. Derm., 1963, 87, 445.

35. D.R. Harris, C.M. Papa, R. Stanton, Brit. J. Derm., 1974, 91, 27.

36. T.H. Sternberg, P. Levan, E.T. Wright, Curr. ther. Res., 1961, 3, 469.

37. R.F. Doerge, *In* Textbook of Organic Medicinal and Pharmaceutical Chemistry (C.O. Wilson, O. Gisvold, R.F. Doerge, eds). Lippincott Co., Philadelphia, (1966).

38. C.A. Schlagel, J. Pharm. Sci., 1965, 54, 335.

39. T. Fredriksson, Acta derm-venereol., 1961, 41, 353.

40. T. Fredriksson, J. invest. Derm., 1964, 42, 37.

41. D.E. Wurster and R.E. Dempski, J. Amer. pharm. Ass., Sci. Ed., 1960, 49, 305.

42. B. Idson, J. Soc. cosmet. Chem., 1967, 18, 91.

43. F.D. Malkinson and E.H. Ferguson , J. invest. Derm., 1955, 25, 281.

44. C.F.H. Vickers, Arch. Derm., 1963, 88, 20.

45. R.B. Stoughton, *ibid.*, 1965, 91, 657.

46. R.D. Carr and R.G. Wieland, *ibid.*, 1966, 94, 81.

47. D.H. Powers and C. Fox, J. Soc. cosmet. Chem., 1959, 10, 109.

48. R.E. Dempski, J.D. Demarco, A.D. Marcus, J. invest. Derm., 1965, 44, 361.

49. R.B. Fountain, B.S. Baker, J.W. Hadgraft, I. Sarkany, Brit. J. Derm., 1969, 81, 202.

50. A.M. Kligman, J. Amer. med. Ass., 1965, 193, 140 and *ibid.*, 1965, 193, 151.

51. G.E. Schumacher, Drug. Intell., 1967, 1, 188.

52. J. Crank. The Mathematics of Diffusion. Oxford University Press, London (1956).

53. B.J. Poulson, E. Young, V. Coquilla, M. Katz, J. Pharm. Sci., 1968, 57, 928.

54. T. Higuchi, J. Soc. cosmet. Chem., 1960, 11, 85.

55. Z.T. Chowhan and R. Pritchard, J. Pharm. Sci., 1975, 64, 754.

56. W.I. Higuchi and T. Higuchi, J. Amer. pharm. Ass., Sci. Ed., 1960, 49, 598.

57. C.W. Barrett, J.W. Hadgraft, G.A. Caron, I. Sarkany, Brit. J. Derm., 1965, 77, 576.

58. R.E. Hasmani, M. Sc. Thesis, London (1973).

59. M.F. Coldman, B.J. Poulsen, T. Higuchi, J. Pharm. Sci., 1969, 58, 1098.

60. C.W. Barrett, M. Pharm. Thesis, London (1966).

61. E.G. Lovering and D.B. Black, *ibid.*, 1974, 63, 1399.

62. E.R. Garrett and P.B. Chemburkar, *ibid.*, 1968, 57, 944.

63. *Ibid.*, 1968, 57, 949.

64. G.L. Flynn and E.W. Smith, *ibid.*, 1971, 60, 1713.

65. G.L. Flynn and T.J. Roseman, *ibid.*, 1971, 60, 1788.

66. G.L. Flynn and E.W. Smith, *ibid.*, 1972, 61, 61.

67. A.M. Agostini and J.H. Schulmann, *In* Surface Activity and the Microbial Cell, Gordon and Breach, New York, N.Y., (1965).

68. M.A. Augustine and J. Swarbrick, J. Pharm. Sci., 1970, 59, 314.

69. J. Ostrenga, J. Haleblian, B. Poulsen, B. Farrell, N. Mueller, S. Shastri, J. invest. Derm., 1971, 56, 392.

70. T. Malone, J.K. Haleblian, B.J. Poulsen, K.H. Burdick, Brit. J. Derm., 1974, 90, 187.

71. I. Sarkany and J.W. Hadgraft, *ibid.*, 1969, 81, Suppl. 4, 98.

72. I.H. Blank, J. Soc. cosmet. Chem., 1960, 11, 59.

73. W. Weiss, Amer. J. Med. Sci., 1956, 231, 13.

74. G.P. Fulton, E.M. Farber and A.P. Moreci, J. invest. Derm., 1959, 33, 317.

75. V. Henschel, F. Jaminet, J. Pharm. Belg., 1972, 27, 743.

76. C.W. Barrett, J.W. Hadgraft, I. Sarkany, J. Pharm. Pharmacol., 1964, 16, 104T.

77. J. Hadgraft, J.W. Hadgraft, I. Sarkany, Brit. J. Derm., 1972, 87, 30.

78. J. Hadgraft, J.W. Hadgraft, I. Sarkany, J. Pharm. Pharmacol., 1973, Suppl. 25, 122P.

79. C.W. Barrett, J. Soc. cosmet. Chem., 1969, 20, 487.

80. B.J. Poulsen, Brit. J. Derm., 1970, 82, Suppl. 6, 49.

81. D.R. Cowsar, *In* Controlled Release of Biologically Active Agents, (A.C. Tanquary, R.E. Lacey, eds.), Plenum Press, New York, (1974).

82. J.E. Shaw, S.K. Chandrasekaran, L. Taskovich, Pharm. J., 1975, 25, 325.

83. A.H. Goldberg, W.I. Higuchi, N.F.H. Ho, G. Zografi, J. Pharm. Sci., 1967, 56, 1432.

84. W.I. Higuchi, *ibid.*, 1967, 56, 315.

85. S.A. Howard, A. Suzuki, M.A. Farvar, W.I. Higuchi, *ibid.*, 1969, 58, 1325.

86. T. Yotsuyanagi, W.I. Higuchi, J. Pharm. Pharmacol., 1972, 24, 934.

87. A. Ghanem, W.I. Higuchi, A.P. Simonelli, J. Pharm. Sci., 1969, 58, 165.

88. W.J. Albery, A.R. Greenwood, R.F. Kibble, Trans. Faraday Soc., 1967, 63, 360.

89. G.L. Flynn, O.S. Carpenter, S.H. Yalkowsky, J. Pharm. Sci., 1972, 61, 312.

90. W.J. Albery, J.F. Burke, E.B. Leffler, J. Hadgraft, J.C.S. Faraday Trans. I., 1976, 72, 1618.

91. W.J. Albery, J. Hadgraft, Patent Specification 13455/75, (1975).

92. V.G. Levich, Physicochemical Hydrodynamics, Prentice Hall, Englewood Cliffs, N.J. (1962).

93. B.J. Poulsen, *In* Symposium on the Biology of Skin, Gleneden Beach, Oregon Regional Primate Center, (1970).

94. M. Katz, Z.I. Shaikh, J. Pharm. Sci., 1965, 54, 591.

95. E.J. Lien, G.L. Tong, J. Soc. cosmet. Chem., 1973, 24, 371.

96. M.R. Charonnat, J.V. Harispe, L. Chevillard, Bull. Soc. chim. France, 1948, 1014.

97. A.I. Vogel, A Textbook of Practical Organic Chemistry, Longmans, Green & Co., London, (1951).

98. C.O. Bagdett, R.C. Provost, C.L. Ogg, C.F. Woodward, J. Amer. Chem. Soc., 1945, 67, 1135.

99. The Merck Index, Merck, 8th Edn. (1968).

100. British Pharmaceutical Codex, The Pharmaceutical Press, London (1973).

101. A.N. Kost, L.A. Golovleva, P.B. Terentlev, M. Islam, J. Analyt. Chem. of Russia, 1966, 21, 765.

102. A.R. Greenwood, Hons. School Chemistry, Pt.II Thesis, Oxford (1965).

103. V. Vitagliano, P.A. Lyons, J. Amer. Chem. Soc., 1956, 78, 4538.

104. H.S. Harned, B.B. Owen, Physical Chemistry of Electrolyte Solutions. Reinhold, N.Y. 3rd Edn., (1958).

105. Handbook of Electrochemical Constants (R. Parsons), Butterworths, London, (1959).

106. C. Ryan, D. Phil. Thesis, Oxford (1969).

107. J. Hadgraft, Hons. School Chemistry, Pt. II Thesis, Oxford (1973).

108. D.E. Bidstrup, C.J. Geankóplis, J. Chem. Eng. Data, 1963, 8, 170.

109. G.L. Flynn, S.H. Yalkowsky, T.J. Roseman, J. Pharm. Sci., 1974, 63, 479.

110. Handbook of Chemistry and Physics, Chemical Rubber Publishing Co., Cleveland,(1959).

111. A.C. Riddiford, Adv. in Electrochemistry and Electrochem. Eng., 1966, 4, 47.

112. W.J. Albery, M.L. Hitchman, Ring Disc Electrodes, Clarendon Press, Oxford (1971).

113. T. von Karman, Z. angew. Math. Mech., 1921, 1, 233.

114. W.G. Cochran, Proc. Camb. Phil. Soc. math. phys. Sci., 1934, 30, 365.

115. Millipore Literature, ADM 60, Millipore Corporation, Bedford, Mass.,

116. Y.W. Chien, C.L. Olson, T.D. Sokolowski, J. Pharm. Sci., 1973, 62, 435.

117. J.F. Burke, Hons. School Chemistry, Pt II Thesis, Oxford (1974).

118. J.F.C. Brown, Millipore (U.K.) Ltd. , personal communication.

119. M. Grinter, Millipore (U.K.) Ltd., personal communication.

120. W.A. Akers, F. Leonard, D.K. Ousterhout, T.A. Cortese, Arch. Derm., 1973, 107, 544.

121. R.B. Stoughton, W.E. Clendenning, D. Kruse, J. invest. Derm., 1960, 35, 337.

122. L.S. Rao, Glaxo Research Laboratories, personal communication.

123. C.W. Barrett, J.W. Hadgraft, I. Sarkany, Brit. J. Derm., 1964, 76, 479.

124. A.S. Michaels, S.K. Chandrasekaran, J.E. Shaw, A.I.Ch.E., 1975, 21, 985.

125. Handbook of Mathematical Functions, (M. Abramowitz, I.A. Stegun, eds.), Dover Publs. Inc. New York, (1972).

126. K.A. Holbrook, G.F. Odland, Brit. J. Derm., 1969, 81, 47.

127. R.A. Marcus, J. Phys. Chem., 1963, 67, 853.

128. B. Idson, *In* Absorption Phenomena, (J.L. Rabinowitz, R.M. Myerson eds.), Wiley, N.Y.(1971).

129. B. Idson, J. Pharm. Sci., 1975, 64, 901.

130. R.K. Winkelmann, Brit. J. Derm., 1969, 81, Suppl. 4, 11.

131. R.J. Scheuplein, I.H. Blank, Physiol. Rev., 1971, 51, 702.

132. H.D. Onken, C.A. Moyer, Arch. Derm., 1963, 87, 584.

133. I.H. Blank, R.J. Scheuplein, D.J. MacFarlane, J. invest. Derm., 1967, 49, 582.

134. J.D. Middleton, Brit. J. Derm., 1969, 81, Suppl. 4, 56.

135. R.J. Scheuplein, I.H. Blank, G.J. Brauner, D.J. MacFarlane, J. invest. Derm., 1969, 52, 63.

136. S.H. Yalkowsky, G.L. Flynn, J. Pharm. Sci., 1973, 62, 210.

137. R.G. Stehle, W.I. Higuchi, *ibid.*, 1967, 56, 1367.

138. *Ibid.*, 1972, 61, 1922.

139. H. Rosen, A. Leaf, W.B. Schwartz, J. Gen. Physiol., 1964, 48, 379.

140. A.H. Beckett, A.C. Moffat, J. Pharm. Pharmacol., 1968, Suppl. 20, 239S.

141. N.F.H. Ho, W.I. Higuchi, J. Pharm. Sci., 1971, 60, 537.

142. R. Adams, E.K. Rideal, W.B. Burnett, R.L. Jenkins, E.E. Dreger, J. Amer. Chem. Soc., 1926, 48, 1758.

143. J. Buchi and X. Perlia, Arzneim.-Forsch., 1960, 10, 465.

144. R.J. Scheuplein, J. invest. Derm., 1965, 45, 334.